Environmental
Studies
Research
Funds

088 Wave Hindcast Sensitivity

Canada

April 1987

Environmental Studies Revolving Funds
Report No. 088

April 1987

WAVE HINDCAST SENSITIVITY

Frank X. Penicka

Newfoundland Marine Sciences
13 Pumphrey Avenue
Mount Pearl, Newfoundland, A1N 2V4

Scientific Advisers: J.R. Buckley and V.R. Swail

The correct citation for this report is:

Penicka, F.X. 1987. Wave Hindcast Sensitivity. Environmental Studies Research Funds Report 088. Ottawa. 114 p.

Published under the auspices
of the Environmental Studies
Research Funds
ISBN 0-920783-87-2

TABLE OF CONTENTS

LIST OF TABLES

LIST OF FIGURES

ACKNOWLEDGEMENTS

All wave hindcasts for this study were prepared by the Marine Environmental Data Service in Ottawa. We are particularly grateful for assistance given by Mr. J. Taylor who processed the input wind fields and by Mr. S. Yuen who ran the wave model. Dr. J.R. Wilson, J.R. Keeley, J. Taylor and S. Yuen also reviewed the milestone 1 report for this study and provided many helpful comments and suggestions.

Atmospheric input data were provided by the Canadian Meteorological Centre in Montreal and by the Atlantic Weather Centre in Bedford, N.S.

Wave measurement data for comparison with the test hindcasts were provided by Seakem Oceanography Ltd. and by the Marine Environmental Data Service.

Dr. D.T. Resio reviewed the milestone 1 report. We are grateful for his constructive criticism and suggestions and for several alternative interpretations of the test results. However, the responsibility for any possible errors and misinterpretations rests entirely with us.

Dr. W. Perrie reviewed parts of the final report and noticed certain inaccuracies which escaped the attention of the author.

Finally, thanks are extended to Dr. J.R. Buckley and Dr. V.R. Swail, the study's Scientific Advisers for their help and advice, and to Mr. P.M. Wood and Mr. D. Milburn for the services they provided as Program Officers for the study.

SUMMARY

Numerical wave model developed by D.T. Resio was acquired by the Marine Environmental Data Service in Ottawa for wave climate hindcasting in Canadian offshore areas. The purpose of this study was to evaluate the sensitivity of the model to a number of factors which may affect the accuracy of the wave hindcasts.

In the first set of tests the sensitivity of the model to errors in input wind fields was determined using synthetic input. On the basis of published information typical errors in wind speed were assumed to have a bias in the range of 2 to 6 knots and root mean square (RMS) error in the range of 4 to 10 knots. Errors in wind direction were assumed to have a bias of 25 to 40 degrees and RMS errors in the range of 25 to 50 degrees. Uniform stationary wind field with a random perturbation in speed and direction was used to drive the wave model and the fluctuations in the hindcast significant wave heights, peak periods and mean directions were compared against the input perturbations. Site specific correlation was found to have a large scatter due to advection of energy from neighbouring grid points. Where local input predominates, the error in significant wave height, expressed as per-

centage of the mean, was found to be approximately equal to the percent error in wind speed in accordance with empirical relationships for growing windseas.

Comparison of two sets of weather maps prepared by different weather offices suggested that a common source of errors in hindcast wind fields based on surface pressure analysis may be errors in storm track and errors in central pressures. Accordingly, tests were made with synthetic storm input subjected to a random perturbation in central pressure and in storm centre velocity. As would be expected the increase or decrease in central pressure leads to intensification or weakening of the storm and a corresponding increase or decrease in the attained maximum significant wave height. The errors in storm track lead to a shift in time of the wave evolution pattern as well as to changes in the maximum significant wave height.

In the second set of tests sensitivity of the model to grid spacing and time step was evaluated. Synthetic and real event inputs were employed in these tests. The model was found to be relatively insensitive to a decrease in grid spacing from the grid presently used by MEDS; increase in grid spacing leads to a larger change in the hindcast wave

parameters. The model results are quite sensitive to time step, with a shorter time step leading to higher estimates of the significant wave height, particularly at the peak of the storm. It is suggested that a decrease of the time step from the present 3 h to 2 h would improve the accuracy of the hindcasts, however, the model would require recalibration.

The input wind fields used to drive numerical wave models are determined from surface atmospheric pressure distributions, using a planetary boundary layer model, and/or from observed wind speeds and directions, using the technique of kinematic analysis. The input to the wave model may be a blend of pressure based winds and kinematic analysis winds. In the third set of tests hindcasts using various percentages of pressure based winds and kinematic analysis winds were compared using two storm events. In the case of one storm the hindcast accuracy increased with increasing proportion of pressure based winds while the opposite was true in the case of the second storm. This test is not objective and the results cannot be generalized because they depend on the relative accuracy of the pressure based winds and the kinematic winds which in turn are affected by the amount of available data, meteorological conditions and skill of the analysts.

In the MEDS hindcast procedure wind fields are initially specified on a 2.5° latitude x 2.5° longitude grid. For the use by the wave model they have to be interpolated onto the wave model spherical orthogonal grid. In the forth set of tests quadratic interpolation was compared with the presently used bi-linear interpolation. The differences in the hindcast wave parameters were found to be negligible.

Two events from the ESRF list of severe storms were hindcast in order to test the performance of the model. The results of one hindcast compared well with measured wave parameters while in the second case the correspondence was unsatisfactory. It is suggested that the poor results of the second hindcast were not caused by a failure of the wave model itself but by a poor resolution of pressure fields which did not adequately represent rather complex conditions occurring during the storm.

RÉSUMÉ

Le Service des Données sur l'Environnement Marin à Ottawa a acquis le simulateur numérique de vagues développé par D.T. Resio pour prévoir à postériori les vagues dans les régions extracôtières canadiennes. Le but de cette étude était d'évaluer la sensibilité du simulateur à un certain nombre de facteurs qui pourraient affecter l'exactitude de la rétroprévision des vagues.

Dans la première série d'expériences, la sensibilité du simulateur aux erreurs d'input pour les vents a été déterminée à l'aide de données synthétiques. Si l'on se base sur les résultats déjà publiés, on peut dire que les erreurs typiques dans la vitesse du vent se situaient entre 2 et 6 noeuds et l'erreur de moyenne quadratique (MQ) se situait entre 4 et 10 noeuds. On admet que les erreurs dans la direction du vent ont tendance à varier entre 25 et 40 degrés et l'erreur des MQ entre 25 et 50 degrés. Pour faire fonctionner le simulateur de vagues, on s'est servi d'un vent uniforme et stationnaire que l'on a soumis à des perturbations de vitesse et de direction (au hasard), on a ensuite comparé les fluctuations de la hauteur des vagues

importantes, des périodes maxima et des directions moyennes aux perturbations données. On a trouvé que la corrélation spécifique au site était très dispersée à cause de l'advection d'énergie des zones voisines de la grille. Lorsque les données locales dominent, l'erreur de la hauteur des vagues importantes, exprimée en pourcentages de la moyenne, était à peu près égale au pourcentage d'erreur de la vitesse du vent conformément aux relations empiriques de formation des vagues de mer.

La comparaison de deux cartes préparées par deux centres météorologiques a permis de supposer qu'il y avait une source commune d'erreur dans la rétroprévision des vents, cette erreur étant basée sur l'analyse de la pression à la surface et pouvant se trouver dans la trajectoire de la dépression ou dans les pressions centrales. On a par conséquent effectué des essais selon des données synthétiques de dépression soumise à des perturbations au hasard dans la pression centrale et dans la vitesse du centre de dépression. Comme prévu, l'augmentation ou la diminution de la pression centrale provoque l'intensification ou l'affaiblissement de la dépression et une augmentation ou une diminution conrrespondante de la hauteur maximum des vagues importantes. Les erreurs dans la trajectoire de la dépression amènent une

variation temporelle du modèle d'évolution de la vague ainsi qu'un changement dans la hauteur maximum des vagues importantes.

Dans la deuxième série d'expériences, on a évalué la sensibilité du simulateur à l'espacement de la grille et à l'espacement temporel. Pour ces expériences, on a employé des données artificielles et des données réelles. On a trouvé que le simulateur était relativement insensible à la réduction de l'espacement de la grille par rapport à la grille utilisée par SDEM; une augmentation de l'espacement de la grille résulte en un changement plus marqué des paramètres de la rétroprévision des vagues. Les résultats sont assez sensibles à l'espacement temporel et démontrent qu'un espacement plus court a pour résultat des prévisions plus élevées de la hauteur des vagues importantes, surtout lorsque la dépression atteint son ampleur maximum. On suggère de diminuer le temps écoulé de 3 heures à 2 heures pour améliorer l'exactitude des rétroprévisions; il faudrait toutefois recalibrer le simulateur.

L'input des conditions de vent, qui a été utilisé pour former des simulations numériques de vagues, est déterminé par la distribution de la pression atmosphérique en surface, à

l'aide d'un modèle en couches des limites planétaires et/ou par la vitesse et la direction des vents observés, au moyen de l'analyse cinétique. On peut utiliser pour l'input du simulateur de vagues un mélange de vents formés à partir de la pression atmosphérique et de l'analyse cinétique. Dans la troisième série de tests, on comparé les rétroprévisions de deux dépressions en utilisant divers pourcentages basés sur des vents résultant d'analyse cinétique. Dans l'un des cas, l'exactitude des prévisions augmentait en proportion avec les vens de pression tandis que le contraire se passait dans l'autres cas. Ce test n'est pas objectif et on ne peut donc pas en généraliser les résultats puisqu'ils dépendent de l'exactitude relative des vents de pression atmosphérique et des vents d'analyse cinétique qui, à leur tour, sont affectés par la quantité des données disponibles, les conditions météorologiques et la qualité des analyses.

Dans le processus de rétroprévision du SDEM, les vents sont d'abord marqués sur une grille de 2.5° de latitude et 2.5° de longitude. Pour les utiliser dans le simulateur de vagues, il faut les interpoler sur la grille orthogonale sphérique du simulateur. Dans la quatrième série d'expériences, on a comparé l'interpolation quadratique avec l'interpolation bi-linéaire utilisée actuellement. On a trouvé que les

différences entre les paramètres de rétroprévision des vagues étaient négligeables.

On a choisi d'effectuer des rétroprévisions à partir de deux dépressions importantes faisant partie de la liste de FRÉE afin de mesurer le taux de performance du simulateur. Dans l'un des cas, les résultats de la rétroprévision se comparaient favorablement aux paramètres des vagues mais dans le deuxième cas, la comparaison n'était pas satisfaisante. On suggère que les résultats peu satisfaisants des deuxième prévisions n'ont pas été causées par une malfonction du simulateur mais plutôt par une faible résolution des champs de pression qui ne représentaient pas d'une manière adéquate les conditions plutôt complexes qui prévalaient durant la tempête.

1. INTRODUCTION

1.1 BACKGROUND

This report presents the results of hindcast sensitivity tests of the wave directional spectrum model developed by D.T. Resio and implemented for hindcasting in the Canadian East Coast waters by the Marine Environmental Data Service in Ottawa. (In the following the model is referred to as the "Resio model"). The objective of the study was to evaluate the sensitivity of the model to variations in input wind fields and to factors such as model time step and grid spacing. Variations in the wind fields were to include errors in wind estimates, variation of the percentage of pressure based winds versus kinematic analysis winds and linear versus nonlinear interpolation of the input wind fields. An indication of the performance of the model under various storm conditions was to be provided by hindcasting several storms from the ESRF list of severe storms.

The actual hindcasting for this study was done by the Marine Environmental Data Service (MEDS). According to the terms under which MEDS acquired the model, Newfoundland

Marine Sciences (NMS) did not have access to the computer code and to the full documentation of the hindcast procedures. This presented certain restrictions on the design of the tests and complicated interpretation of the results. The tests had to be performed in such a way that none or minimum changes in the model code were required. This was achieved by accessing the hindcast procedure at various stages using an appropriate input and, in the case of quadratic interpolation test, by replacing the original bi-linear interpolation program with a new program supplied by the NMS. The test results were interpreted in terms of published information and on the basis of personal experience.

In all the sensitivity tests the present MEDS system was taken as a standard and the assumption was made that no a priori changes need to be made. For example, the present grid and time step were employed for testing the sensitivity to input errors and the sensitivity to variable percentage of pressure based versus kinematic analysis winds. It is believed that the general conclusions are valid even if the grid spacing or the time step are changed in the future.

While all wave model simulations described in this report are referred to as hindcasts the results are equally

applicable to model simulations in the forecast mode. In that case, however, the errors in the input wind fields are likely to be greater than those assumed in this study.

1.2 WIND INPUTS

Two types of input were used in the sensitivity tests:

(a) synthetic wind fields, and

(b) wind input data prepared for wave hindcasting in support of the ESRF Directional Wave Spectrum Intercomparison Study.

The synthetic input consisted of a uniform stationary wind to which a small perturbation, an "error", was applied, and from a hypothetical cyclonic weather system moving across the model grid. By using a simple synthetic input the errors could be controlled and the resulting wave parameter errors could be compared with theory.

The wind fields from the ESRF Directional Wave Spectrum Intercomparison Study provided realistic cases for testing

the effect, on the hindcast wave parameters, of varying the proportion of pressure based winds and kinematic analysis winds, and the effect of quadratic interpolation of the wind fields as compared to the bi-linear interpolation presently used by MEDS. Directional wave observations were available for comparison with the hindcasts. In addition, wave hindcasts prepared for the intercomparison study by the Offshore and Coastal Technologies Inc. (Penicka et al., 1985), which showed a very good agreement with the observations (Juszko, 1985), were also available for comparison in the sensitivity tests. Their use provided a means of reducing subjectivity inherent in testing the sensitivity to variable percentage of pressure based winds and kinematic analysis winds.

1.3 OUTPUT VARIABLES

A large amount of data is generated in a discrete spectrum hindcast. In the present case, at each grid point and each time step the sea state is represented by a discrete directional spectrum consisting of 320 energy density values (in 20 frequency bands and 16 direction bands). Clearly it is desirable, for the purpose of intercomparison, to reduce the number of variables to a few parameters describing only

the essential characteristics of the sea state. The parameters most often used in practical applications are significant (or characteristic) wave height, H_s, defined as four times the square root of the total variance of the wave spectrum; peak period, T_p, that is a period at which the spectral density reaches its maximum; and mean direction at peak period, θ, which is computed as a weighted sum of the directional distribution of energy density at the peak period. These are the parameters chosen for comparison in the following sensitivity tests.

It should be noted that restricting the comparison to these parameters does not necessarily mean a loss of information. The shape of the windsea spectrum is essentially controlled by nonlinear wave-wave interaction. For practical reasons this interaction is not solved exactly; in the Resio model (Resio, 1981) it is parameterized in terms of the peak frequency, $f_p = 1/T_p$, and the Phillips equilibrium coefficient, α, (a measure of energy in the equilibrium range of the spectrum). Thus the number of degrees of freedom representing the non-directional windsea spectrum is equal 2 rather than 20 (corresponding to the 20 frequency bands). Some loss of detailed information may occur only in the swell region of the spectrum which is not represented in terms of few parame-

ters. However, the evolution of swell is controlled primarily by advection and thus, in the sensitivity tests described here, could be affected only by the changes in grid spacing and time step.

With few exceptions the results of the sensitivity tests are presented for specific sites. It is assumed that the main application of the model will be in coastal areas subject to hydrocarbon exploration. Since the MEDS version of the model does not include any shallow water effects it is not, in its present form, suitable for hindcasting waves on the Scotian Shelf. The model grid is also not optimized for the Labrador Shelf, and therefore it is assumed that the primary application area for the model is on the Grand Banks. The comparison sites are selected accordingly. However, the results are believed to be generally applicable to any location to which the model itself is applicable.

1.4 MEDS HINDCAST PROCEDURE

The hindcast procedure employed by MEDS consists of four steps, schematically shown in Figure 1.1. The input to the wave model is a blend of winds derived from sea-level pressure fields and winds obtained through kinematic analysis. The sea-level pressure fields are digitized on a 2.5° latitude x 2.5° longitude grid extending from 30°N to 70°N and from 20°W to 70°W. A planetary boundary layer (PBL) model is applied to the pressure fields to obtain wind velocity vectors at 20m reference level. Into these are blended wind vectors obtained through kinematic analysis and the result is interpolated onto the spherical orthogonal grid (SOG) required by the wave model. For the synthetic input tests, the first three steps in the MEDS hindcast procedure were bypassed, and the input wind speeds and directions were fed directly into the interpolation routine as shown in Figure 1.1 by the entry point 1.

The wind interpolation is accompanied by a rotation of the wind velocity vectors, in order to account for the curvature (in terms of the geographical coordinates) of the SOG. A corresponding reverse rotation is applied to the computed wave directions. It was found, after the completion

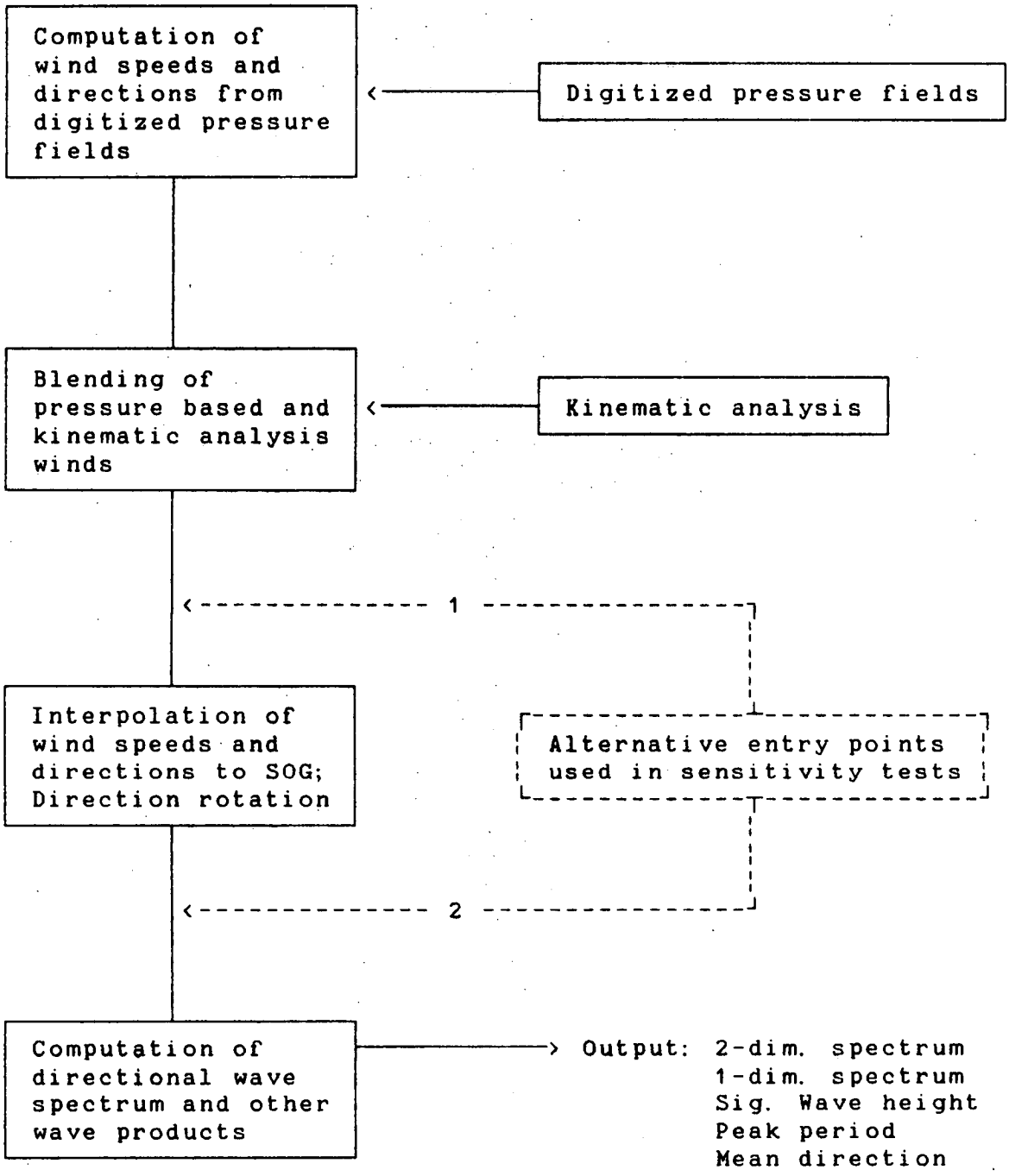

FIGURE 1.1 MEDS WAVE HINDCAST PROCEDURE

of the tests, that the code for the reverse rotation was missing in the model. The wave directions were subsequently corrected at grid points other than those on the central meridian (49° W or j=8, see Figure 1.2). Site specific hindcasts at grid points in the vicinity of Hibernia (i=7, j=8 in Figure 1.2) did not require any correction since the missing rotation was less than the resolution of the plots (the rotation is zero at the Hibernia grid point).

The wind rotation is done separately of the wave model, in the wind interpolation program. NMS learnt this only after most sensitivity tests had been completed. In some of the tests the wind interpolation was bypassed as shown by the entry point 2 in Figure 1.1. In these tests the input wind directions were not rotated. Where appropriate in the following text, this is mentioned and the effect on the test results is discussed.

The relationship between the input 2.5° x 2.5° grid and the standard MEDS SOG is shown in Figure 1.2. Only the active grid points of the SOG which fall within the area covered by the input grid are shown in the figure. Several active SOG grid points are located east of the 20°W boundary. These grid points are retained in the wave computation but

since they are outside the input region, the wave energy at these points contains only a swell component which propagated there from the forced region. Wave data at these outside grid points were not included in the sensitivity analyses described in this report.

The sequence of input wind fields is at 6 hour intervals corresponding to the regular synoptic weather analysis times. The wave model time step is, however, 3 hours. The required time interpolation of the input winds is done internally in the wave model program. It is believed that the space- and time-wise interpolation affects the sensitivity tests to some extent by smoothing the input wind fields and decreasing their RMS error. However, this effect is also present when processing real wind data.

As part of this study the sensitivity of the Resio model to grid spacing and time step were also tested. The modified SOG grids had spacing approximately 20% smaller and 20% larger than the grid shown in Figure 1.2. The non-standard time steps were 2 hours and 4 hours. In order to avoid the need for changes in the time-wise interpolation routines in the MEDS computer programs, the input wind fields were modified to correspond to intervals of 4 and 8 hours.

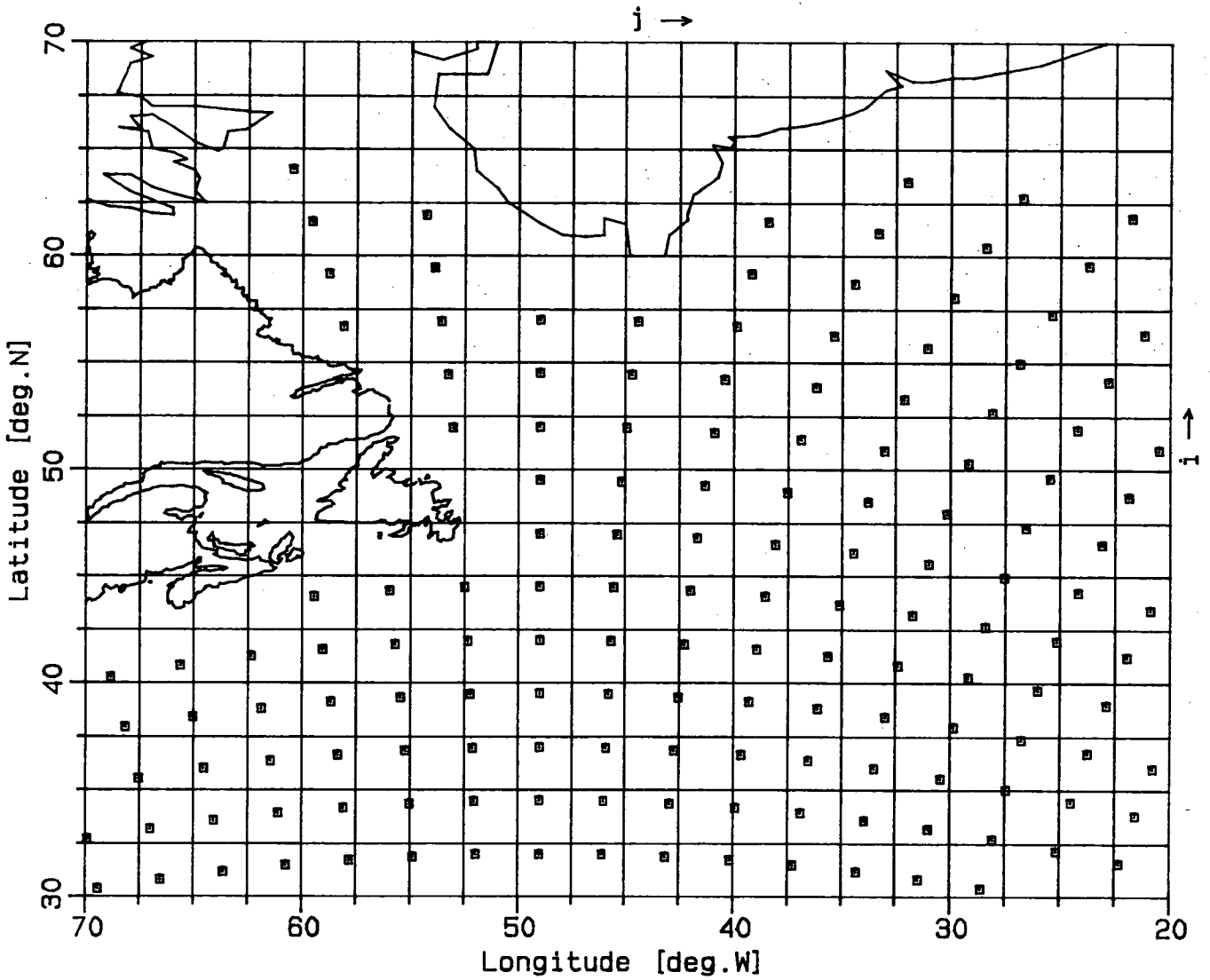

FIGURE 1.2 COMPARISON BETWEEN INPUT WIND FIELD GRID AND WAVE MODEL SPHERICAL ORTHOGONAL GRID (ACTIVE REGION).

The primary output from the wave model is a sequence of discrete two-dimensional spectra represented by 20 frequency bands (0.03 Hz to 0.22 Hz in 0.01 Hz increments) and 16 direction bands (0° to 360°, measured counter-clockwise from the east, in 22.5° increments). The secondary wave products provided by MEDS include one-dimensional spectra, significant wave heights, peak periods and mean wave directions, as well as swell heights, periods and directions.

2. SENSITIVITY TO ERRORS IN INPUT WIND FIELDS

2.1 ERROR CHARACTERISTICS OF INPUT WIND FIELDS

Marine surface wind fields used as input in wave simulations are usually derived from sea-level atmospheric pressure fields (available either in a digitized form or scaled off sea-level analysis charts) and from surface wind observations reported by ships. The accuracy of such wind fields depends on the amount and quality of the pressure and wind data and on the technique which is used to synthesize these data into the continuous wind fields.

Routine weather analyses rely on a limited number of ship reports which were transmitted to shore by radio in real time. Improved pressure and wind fields can be specified from enhanced data bases which include all ship reports (real and non-real time) and which are carefully analyzed to take into account a whole development (prior and subsequent to each synoptic time) of the weather system. Ultimately, however, the accuracy of hindcast wind estimates is limited by the accuracy of the ship and other observations from which they were derived. The quality of these observations is varied, and there are inconsistencies in observation level and method. According to Cardone et al. (1979) the accuracy of ships' wind reports is at best ±5 knots in speed and ±20° in direction. Resio et al. (1982) approximate the error variance, e^2, of ships' wind observations, determined from comparisons with buoy measurements, by

$$e^2 = 1.5 + 0.18\bar{u}$$

where $\bar{u}$ is the sample mean of the wind speeds. For a 20 m/s (39 knot) wind e is about 2.3 m/s or 4.5 knots. Since these errors are random, it can be expected that if carefully synthesized into continuous wind fields more accurate wind

estimates can be obtained than indicated by the above numbers.

The procedures used in preparation of wind fields range from a fully computerized analysis of digitized pressure fields to a manual reconstruction of the wind fields from ships' wind observations through the technique of kinematic analysis. The accuracy of these methods varies, and it is closely related to the amount of effort and time which can be expended in preparation of the wind fields.

Planetary boundary layer (PBL) models such as the one described by Cardone (1969) or by Resio et al. (1982) are used to relate quasi-geostrophic winds, determined from sea-level pressure gradients, and the distribution of air-sea temperature differences (as a measure of atmospheric stability) to winds at a suitable reference level. Overland and Gemill (1977) found the Cardone (1969) PBL model to have root-mean-square (RMS) errors of 2.92 m/s, 3.49 m/s and 2.93 m/s for $u<5$, $5<u<10$, and $u>12.5$ m/s wind speed classes, respectively, while Resio et al. (1982) reported their model to have a standard deviation of the error distribution approximately linearly dependent on the mean wind speed, $\bar{u}$,

$$e = 1.7 + 0.11\tilde{u}$$

In an objective analysis, the wind estimates are further improved by blending in ships' observations of wind speed, which are observations made independent of pressure. Resio et al. (1982) made an extensive comparison between winds predicted by an objective analysis and independent buoy and ship's observations (before the information from these observations was blended into the wind fields). Figures 2.1 and 2.2, reproduced from Resio et al. (1982), show the bias and RMS errors of wind speed and wind direction estimates stratified according to a season. The statistics were computed for 10 years of ships' data for each month. The years were selected randomly from 20 years of information.

The errors in wind speed have a negative bias between 0.5 and 1.3 m/s and a RMS error of about 2 to 3 m/s. The bias in wind direction is between -5° and +5° while the RMS error in wind direction is about 20° for wind speeds greater than 18 m/s and increasing markedly at lower wind speeds. According to Resio et al. (1982) much of the deviation between observed and predicted wind speeds and directions is due to differences in storm locations.

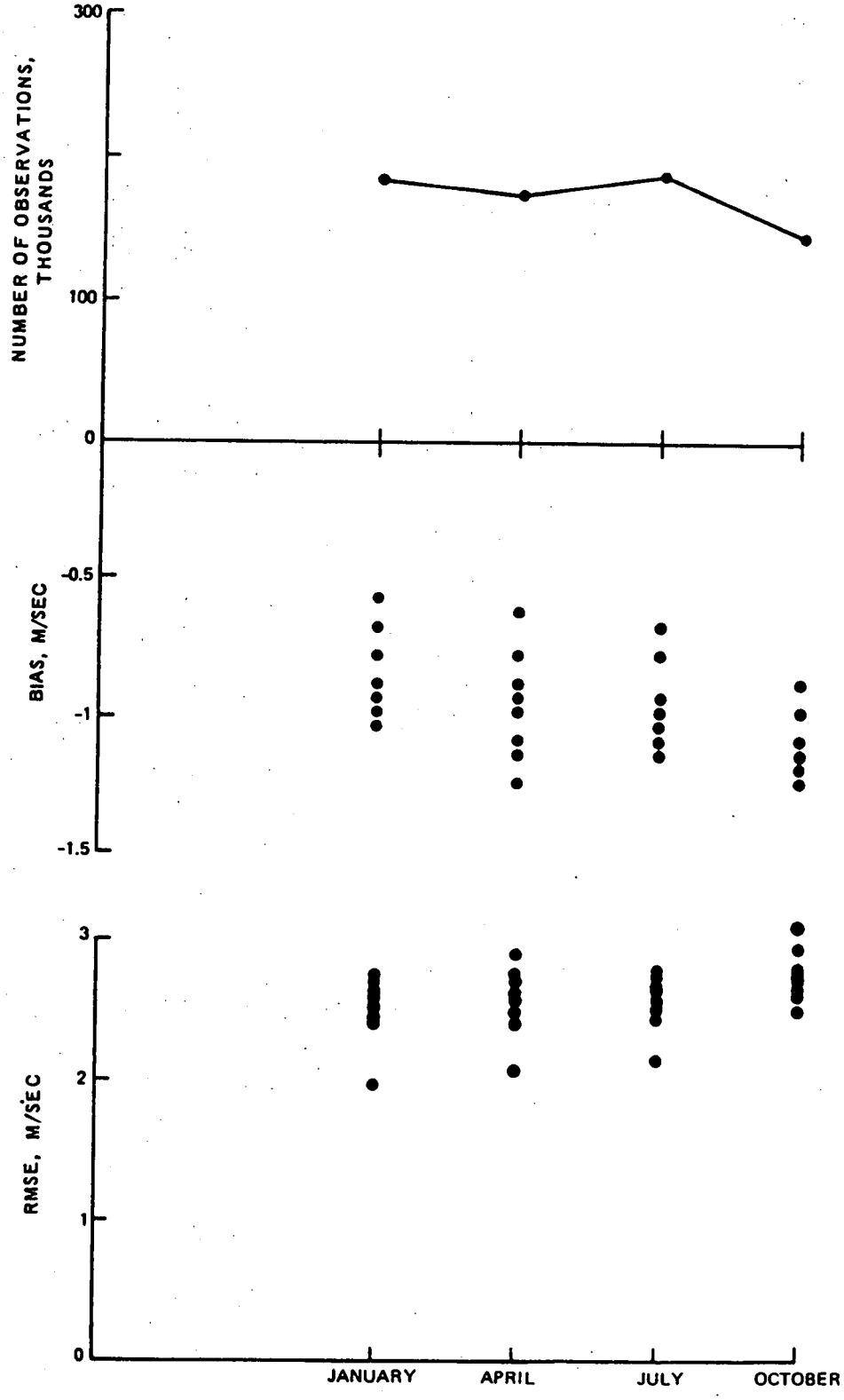

FIGURE 2.1 BIAS AND RMS ERROR OF WIND SPEED FOR THE MONTHS INDICATED. INFORMATION WAS COMPUTED FOR TEN YEARS OF EACH MONTH. (FROM RESIO ET AL., 1982).

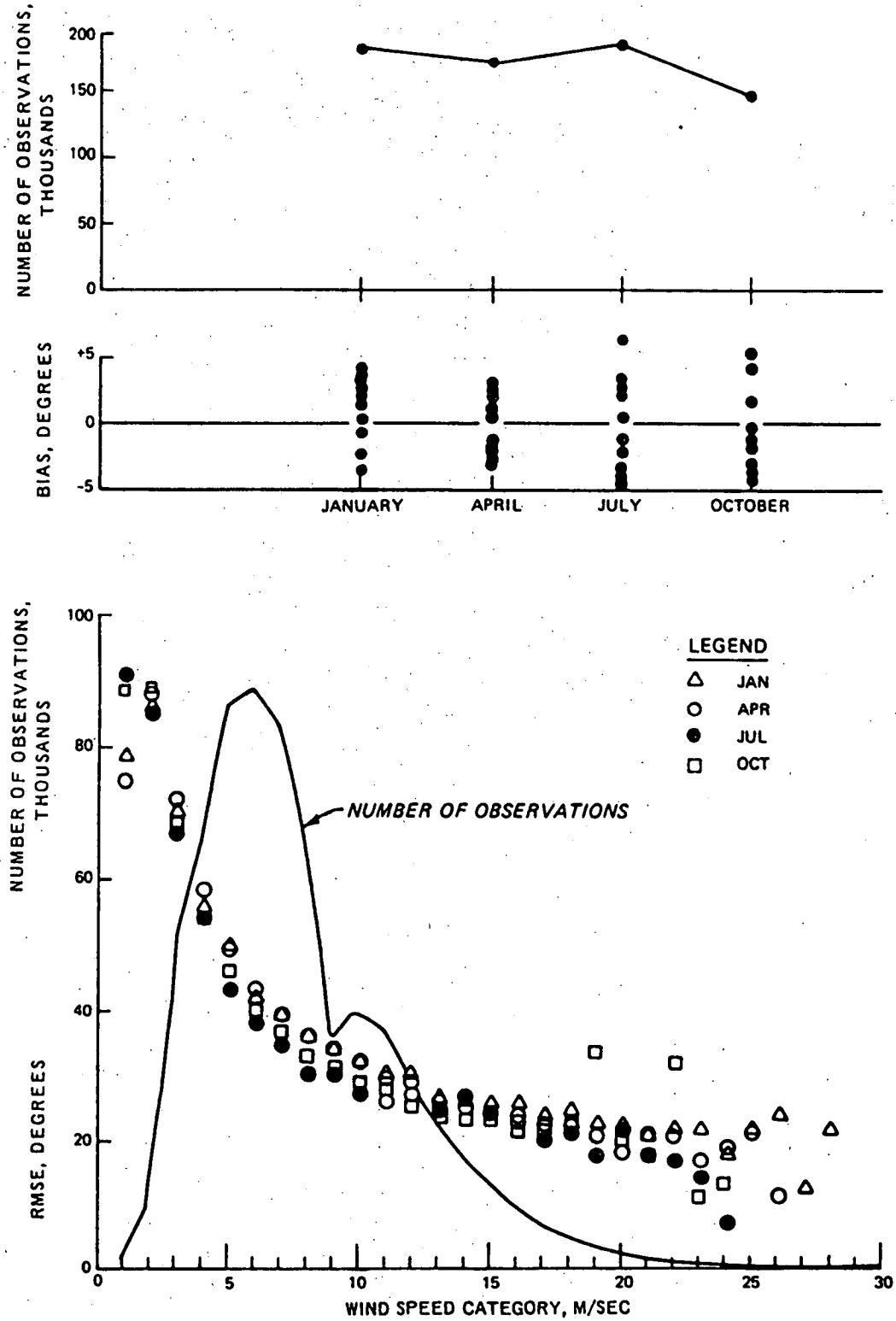

FIGURE 2.2 BIAS AND RMS ERROR OF PREDICTED WIND DIRECTION. INFORMATION WAS SELECTED AS IN FIGURE 2.1. (FROM RESIO ET AL., 1982).

Figure 2.3 shows the comparison of the same hindcast set with buoy wind measurements which, unlike the ships' reports are time- and site-specific, and have a lower observational error. The bias of the hindcast wind speeds varies with the month but on average it approaches zero. The RMS error is between 2 and 4 m/s.

Where a sufficient number of ships' wind observations is available, the method of kinematic analysis can be applied to reconstruct continuous wind fields by fitting the set of observations with a coherent pattern of streamlines (lines parallel to the wind) and isotachs (lines of constant wind speed) in accordance with fundamental meteorological principles. A sequence of such maps represents the evolution of meteorological systems, and since the flow must be continuous in both space and time, additional information can be inferred by time-wise interpolation where data are sparse, or erroneous data can be corrected where the maps show inconsistency. Kinematic analysis is a time consuming procedure that requires experienced analysts to execute. Thus, in a particular hindcast effort, it is sometimes limited only to the immediate area of interest or to selected times of most intense wave generation during the peak of a storm. Where wind observations are sparse, the most stable wind estimates

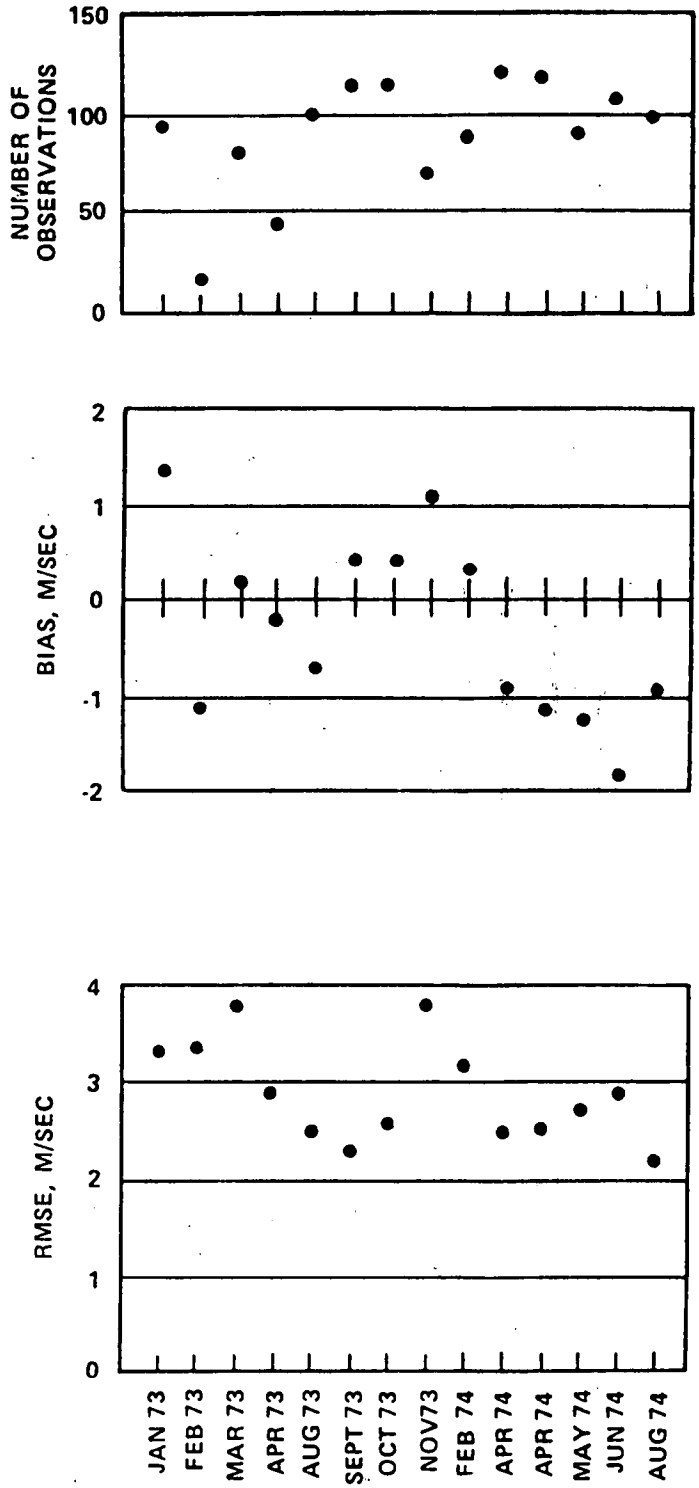

FIGURE 2.3 COMPARATIVE STATISTICS FOR HINDCAST WIND DATA AND CORRESPONDING BUOY DATA. (FROM RESIO ET AL., 1982).

are obtained from a weighted average of the pressure based and kinematic analysis based estimates (Resio, 1982). Typical weighting factors are 0.8 on the kinematic analysis and 0.2 on the pressure based winds.

Cardone et al. (1979) investigated error characteristics of extratropical wind fields obtained by three different methods of analysis:

(a) manual scaling of winds from surface weather charts, using a planetary boundary layer model;

(b) computer-based objective analysis of gridded pressure data and wind observations; and

(c) construction of streamlines and isotachs through manual kinematic analysis.

Table 2.1, adapted form Cardone et al. (1979), shows the results of the comparison of the three hindcast wind fields with winds reported from ships. The comparison is based on three storms in the eastern north Pacific Ocean.

TABLE 2.1

COMPARISON OF WIND FIELDS AND SHIP REPORTS
Adapted from Cardone et al. (1979)

	VBIAS [m/s]	VRMS [m/s]	DRMS [deg]	Number of Comparisons
PBL winds - all ships	-1.6	4.5	47.9	1805
Objective winds - all ships	-1.6	3.6	40.6	1299
Kinematic winds - all ships	0.3	2.7	30.4	1805

The most accurate method, the kinematic analysis, provided wind speed estimates with very low bias (0.3 m/s) and RMS error of 2.7 m/s. The PBL winds and the objective winds, both derived from sea-level pressure gradients, had a negative bias (-1.6 m/s). The RMS error of the PBL wind speeds (4.5 m/s) was somewhat greater than that of the objective winds (3.6 m/s) and so was the wind direction error (47.9° vs. 40.6°).

It is not obvious to what extent these errors depend on the magnitude of the mean wind speed. Cardone et al. (1979) provide only absolute values and only in the discussion of bias in the PBL and objective analysis estimates they express them as percentage (10% to 15%) of the wind speed.

The negative bias in the PBL and objective winds is due to a limited resolution and smoothing of sharp pressure gradients in intense storms, particularly the small ones. The smoothing depends on coarseness of the grid on which the pressure fields are defined. Lazanoff and Stevenson (1977) reported that hindcast winds based on pressures defined on a 63x63 point Northern Hemisphere grid had an approximate RMS error in wind speed of 7 m/s and bias of 3 m/s. The winds were consistently low above speeds of 15 m/s. For most wave hindcasts this accuracy would not be considered adequate and the wind estimates would be improved at least in central areas of major storms, as was done in a Waterways Experiment Station (WES) wave hindcast in the Northwest Atlantic Ocean (Vincent and Resio, 1979).

For the purposes of the present study, it is assumed that a typical RMS error is in the range of 4 to 10 knots (about 2 to 5 m/s) in wind speed, and 25° to 50° in wind direction. The bias is assumed to be up to 15% in wind speed and 40° in wind direction.

2.2 INPUT ERROR PROPAGATION IN THE WAVE MODEL

The Resio model is a discrete spectrum model in which the spectrum is resolved into a finite number of frequency and direction bands. A spatial grid is overlaid over the wave generation area, and at each grid point and each time step the discrete directional spectrum is computed from input wind fields by numerically solving the energy balance equation:

$$\frac{\partial F}{\partial t} = G + \mathbf{c}_g \cdot \nabla F \qquad (1)$$

Here $F = F(f, \theta, \mathbf{x}, t)$ is the energy density of the wave field as a function of frequency, f, direction of propagation, θ, position, $\mathbf{x}$, and time, t; G is the source function which represents the physical processes that add energy to, or subtract energy from, the spectrum; and $\mathbf{c}_g = \mathbf{c}_g(f, \theta)$ is the wave group velocity (bold characters indicate vectors). The last term in Equation (1) represents the propagation of wave energy across the model grid.

The source function

$$G = G_{in} + G_{nl} + G_{ds} \qquad (2)$$

in general is a sum of three terms: the energy input from the atmosphere, G_{in}, the transfer of energy across the spectrum due to conservative non linear wave-wave interaction, G_{nl}, and wave energy dissipation term G_{ds}. In the Resio model, G_{ds} is included only implicitly by forcing the tail of the wave spectrum to conform to a f^{-5} dependence.

The wave model consists of two domains, a local (non-propagating) parametric domain which initializes wave growth from zero energy, and the main, discrete spectrum, domain which takes over once the peak period reached certain threshold value. A detailed description of the model can be found in Resio (1981).

Errors in input wind fields that enter the computation at a particular time step and grid point through the source term G_{in} propagate across the grid with a speed equal to a mean value of the group velocity $\mathbf{c}_g$. They also affect the subsequent error at the same grid point through the non linear wave-wave interaction term G_{nl}. Thus, at each time step at any individual grid point, the error in wave energy is a combination of an energy error input into the wave field locally at that time step and some fraction of errors input into the same grid point and into surrounding grid points at

earlier times. Even if the wind velocity is known at some location exactly (e.g. from nearby wind measurements) the hindcast waves at that point still are contaminated by errors which propagated there from the rest of the grid. This interplay of local input and advection makes it difficult to quantify the effects of the input errors.

The largest contribution to the total error is expected to be due to local input. For fully developed seas the one-dimensional wave spectrum, S(f), approaches a model spectrum proposed by Pierson and Moskowitz (1964):

$$S_{PM}(f) = \int F(f,\theta)\, d\theta = \alpha g^2 (2\pi)^{-4} f^{-5} \exp\{-5/4(f_p/f)^4\} \quad (3)$$

where $\alpha = 0.0081$, and g is the gravitational acceleration.

The frequency of the spectral peak, f_p, is inversely proportional to wind speed, $u = u_{19.5}$ (assumed here at a reference level of 19.5 m)

$$f_p = 0.14g/u \quad (4)$$

The total energy of the fully developed wave field is obtained by integrating the spectrum over all frequencies

$$E = \int S_{PM}(f)\, df \sim u^4 \qquad (5)$$

and the significant wave height is

$$H_s = 4\sqrt{E} \sim u^2 \qquad (6)$$

For a wind speed with a small fractional error, δ_u, the corresponding significant wave height and peak period are given by

$$H_s(1 + \delta_H) \sim \{u(1 + \delta_u)\}^2 \approx u^2(1 + 2\delta_u) \qquad (7)$$

$$f_p(1 + \delta_f) \sim \{u(1 + \delta_u)\}^{-1} \approx u^{-1}(1 - \delta_u) \qquad (8)$$

Thus, as a first approximation for the fully developed seas, it is expected that for small errors in the input winds the fractional (or percent) error in significant wave height, δ_H, and that in peak frequency, δ_f, will be approximately proportional to the corresponding fractional errors in wind speed with the proportionality constant equal 2 for the significant wave height and -1 for the peak frequency.

In the ocean the fully developed wave fields are typical only of low to moderate wind speeds and therefore the above error characteristics would not apply to storm conditions. In growing seas the relationship between wind speed and wave height or period depends on fetch, duration, changes in wind direction etc., and the relationship between input and output errors is more complex.

The Resio model was developed to be consistent with fetch limited wave growth rates observed during the JONSWAP experiment. Therefore, as a first approximation, the windsea significant wave height and peak period under the fetch limited conditions should follow empirical relationships proposed by Hasselmann et al. (1973)

$$H_s \sim u \tag{9}$$

$$T_p \sim u^{0.33} \tag{10}$$

From this the corresponding fractional errors in significant wave height and in peak period are estimated to be $\delta_H \approx \delta_u$, and $\delta_T \approx 0.33\delta_u$ respectively.

Similarly, for duration limited waves which are more typical in open ocean situations, the relationships for the significant wave height and the peak period can be derived from (9) and (10) using an approximate relationship between fetch and duration (Carter, 1982) as

$$H_s \sim u^{9/7} \tag{11}$$

$$T_p \sim u^{4/7} \tag{12}$$

Under these conditions, the fractional errors in significant wave height and in peak period are expected to be, respectively, $\delta_H \approx 1.3\delta_u$ and $\delta T \approx 0.6\delta_u$.

2.3 UNIFORM STATIONARY WIND INPUT

2.3.1 Test description

In order to evaluate the sensitivity of the model to errors in input wind fields, it is desirable to control the distribution and magnitude of these errors, and to isolate specific aspects of the problem. This is most conveniently achieved using a synthetic wind input with a preset bias and

RMS error. All tests employing synthetic input, which are described here, consist of a reference hindcast with a simplified error-free input, and a set of hindcasts in which the reference input is modified by a random perturbation (in the following referred to as "error") with a preset bias and RMS. In these tests the wind fields were specified on the 2.5° latitude x 2.5° longitude grid and entered directly into the wind interpolation program (entry point 1 in Figure 1.1).

The first set of tests employs the simplest possible input: a uniform stationary wind blowing from the west. Westerly (i.e. off shore) winds were selected in order to test to what extent errors in wind direction affect the hindcast waves through changes in fetch. After certain time (144 hours), sufficient to bring the wave field from zero energy into balance with the input wind field, a sequence of unbiased and biased random perturbations in speed and direction is applied to the uniform wind field. The reference wind has a speed of 40 knots (20 m/s) and the perturbation is random (in space) and normally distributed. The sequence of the perturbations is shown in Figure 2.4, the RMS and bias values are listed in Table 2.2.

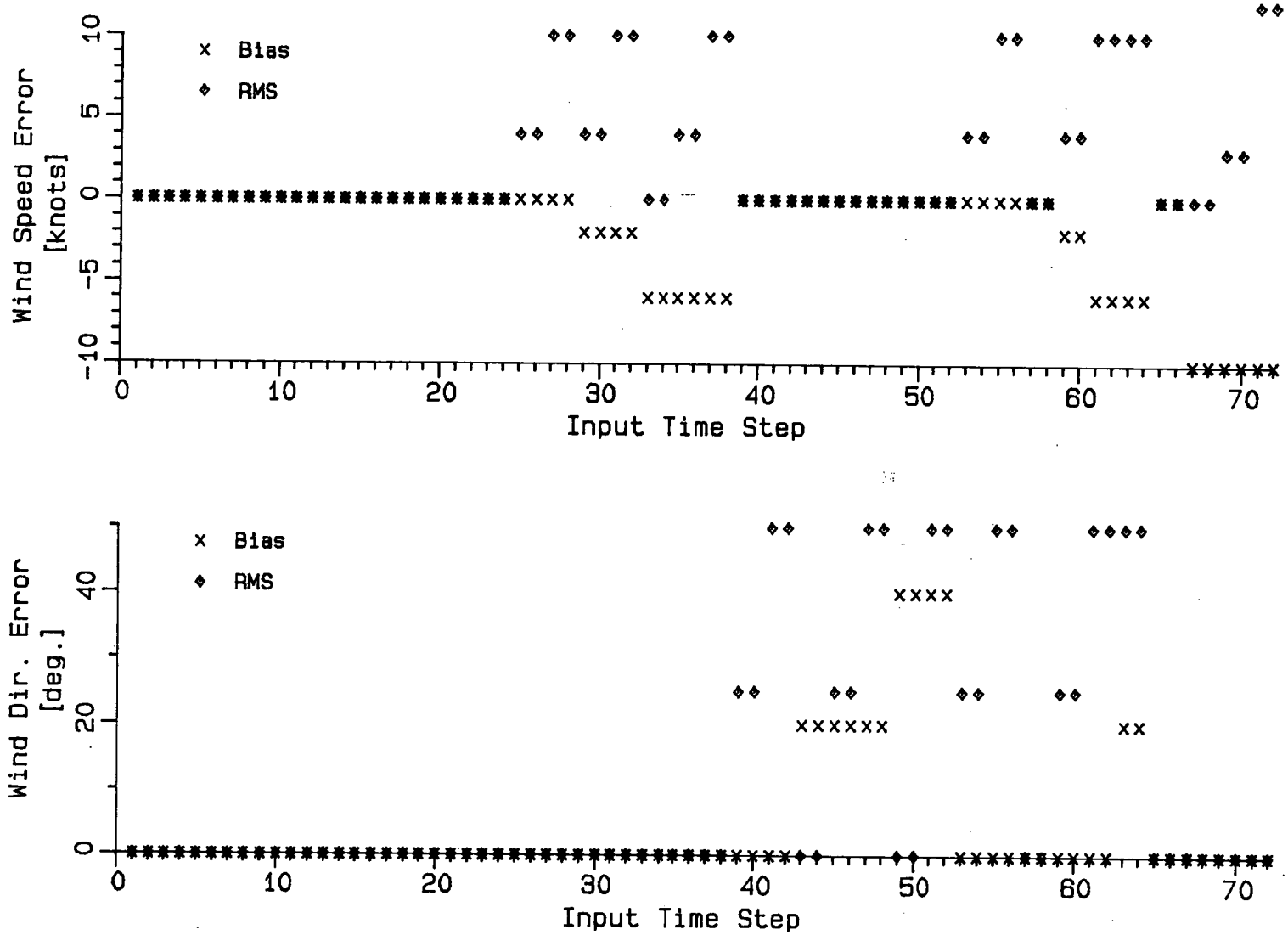

FIGURE 2.4 SEQUENCE OF BIAS AND RMS ERRORS IN THE FIRST SYNTHETIC INPUT TEST.

TABLE 2.2

VALUES OF BIAS AND RMS ERRORS IN THE FIRST TEST SEQUENCE
(Figure 2.4)

			Min.	Max.
Wind Speed (knots)	RMS	0	4	10
	Bias	0	-2	-6
Wind Direction (degrees)	RMS	0	25	50
	Bias	0	25	40

Each test consists of two six-hour (input) time steps. The RMS and bias at the two time steps are the same but the actual perturbations at each grid point differ randomly (two different random sets were used for the two time steps). This is believed to best represent errors in actual wind estimates which may be random in both time and space. The constant change of the perturbation is also believed to make the test representative of wave growth situation which is typical of storm conditions. The various combinations of RMS and bias in speed and direction are shown in Figure 2.4.

As noted in Section 1.4 the 6 hourly input is interpolated, as part of the MEDS hindcast procedure, to 3 hour intervals required by the wave model. This interpolation, as well as the spatial interpolation to the SOG, does not affect the

bias of the input errors but it tends to smooth them and decrease their RMS.

2.3.2 Model Spin-up

A hindcast of a discrete event starts with the model initialized with zero energy at all grid points. Certain amount of time, usually termed "spin-up" or "warm-up" period, is required to bring the wave field into balance with the input wind field; the appropriate spin-up period depends on fetch and on the wind speed. After a sufficient time, the wave field should reach an equilibrium state in which the significant wave height and peak period are functions of only the fetch and wind speed, and the mean wave direction away from the boundaries is in the direction of the wind. According to Equation (4) for long fetches the peak period should be proportional to the wind speed while the significant wave height should be proportional to the square of the wind speed (Equation 6).

Figure 2.5 shows the evolution of the significant wave height, peak period and mean direction at three grid points after a uniform stationary wind, blowing from the west (0°)

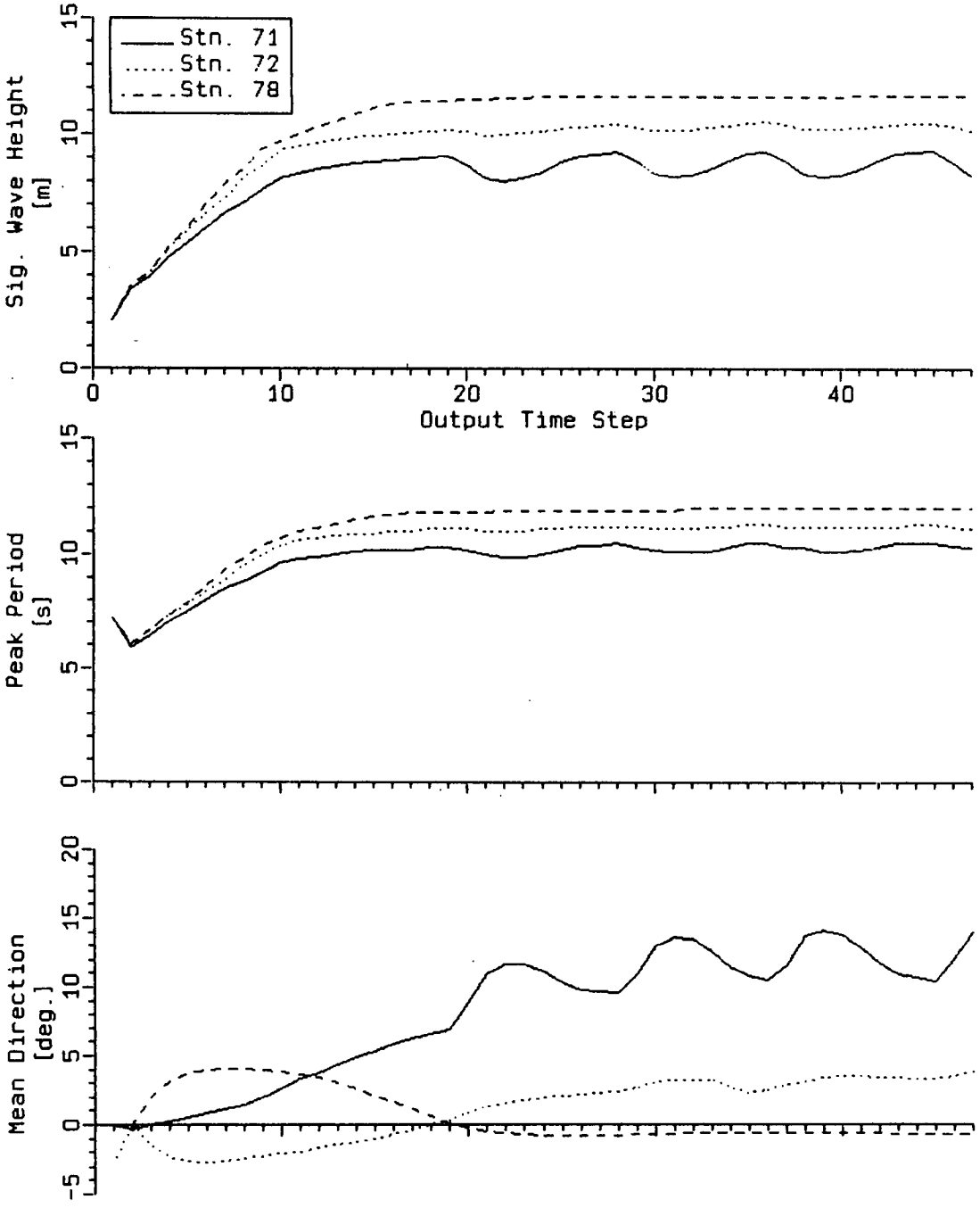

FIGURE 2.5 EVOLUTION OF WAVE PARAMETERS IN RESPONSE TO A SUDDEN APPLICATION OF A UNIFORM STATIONARY WIND.

with a speed of 40 knots, was switched on at time zero. Station 71 is located close to the upwind boundary in the vicinity of Hibernia, Station 72 is one grid spacing to the east of 71 while Station 78 is exposed to the longest fetch, across eight grid spacings (Figure 2.6). The plot for Station 78 (large fetch) illustrates the duration-limited wave growth in the model.

The most noticeable features of the plots, which are of relevance for the sensitivity tests described here, are the ripple in the curves and the deviation of the mean wave direction from the wind direction.

The fluctuation in the curves in Figure 2.5 is most pronounced at Station 71 which is the closest to the western boundary of the model (i.e. subject to the shortest fetch). Table 2.3 presents a sequence of H_s at the end of three time steps (45, 46, and 47), corresponding to hours 135, 138, and 141 of the spin-up, for a portion of the grid adjacent to the western boundary. Comparison with Figure 2.5 shows that this is long after the wave field reached full development. Changes of over 9% occur at grid points at, or close to, the upwind boundary. These are the grid points where most of the energy is input locally through the G_{in} and G_{nl} terms and

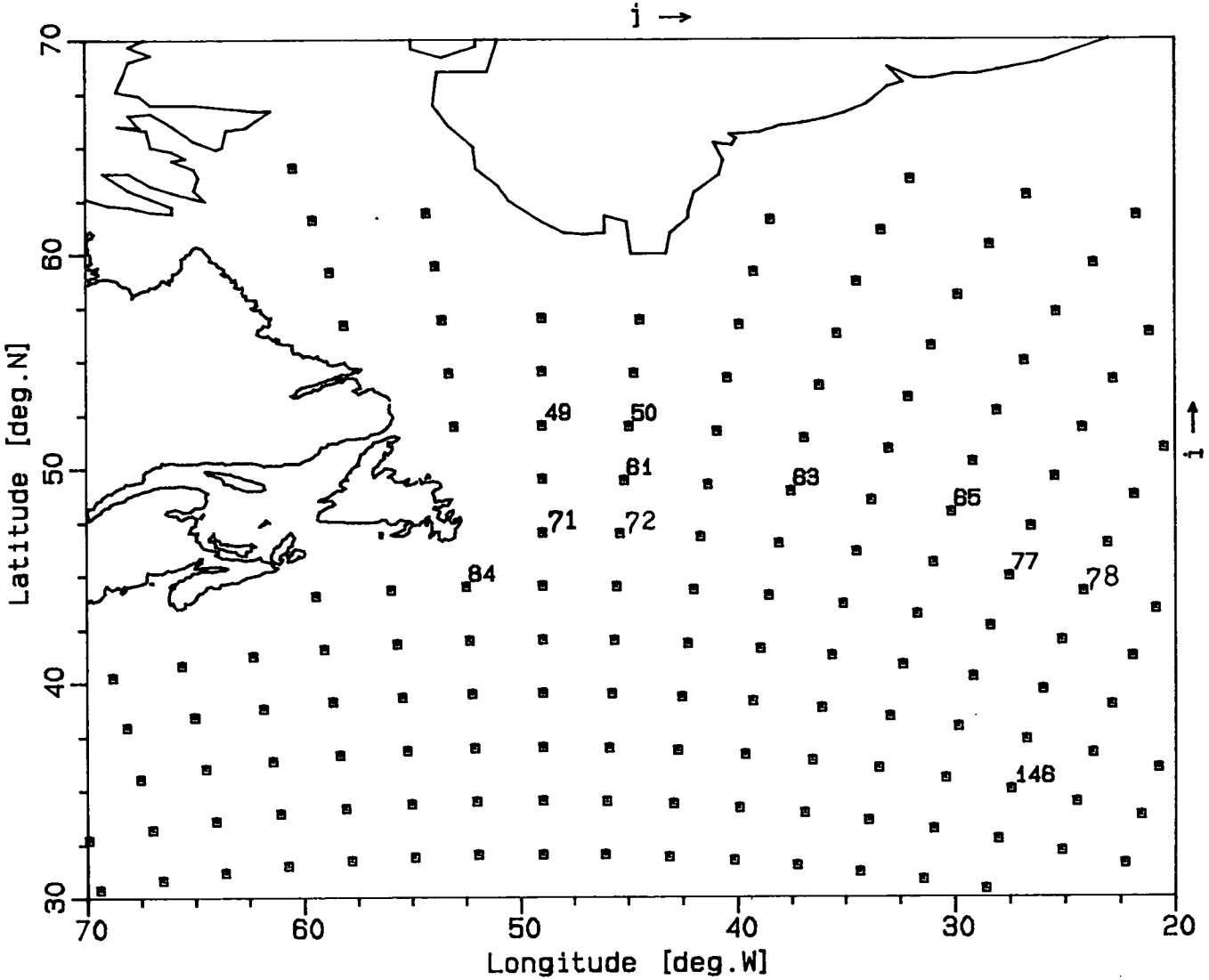

FIGURE 2.6 LOCATION OF SELECTED STATIONS IN STANDARD MEDS SOG.

TABLE 2.3

DISTRIBUTION OF SIGNIFICANT WAVE HEIGHT [m] AND PERCENT CHANGE FROM PREVIOUS TIME STEP (IN BRACKETS) IN RESPONSE TO A UNIFORM STATIONARY WIND. CHANGE LESS THAN 1% IS INDICATED BY SIGN (+/-) ONLY.

Time Step No. 45

14	.	.	7.7(-6)	.	.	.
13	.	.	8.1(+5)	9.5(+)	.	.
12	.	.	8.1(+5)	9.5(+)	.	.
11	.	.	7.7(-6)	9.4(-1)	10.1(+)	10.5(+)
10	.	.	.	8.5(+)	9.8(+)	10.5(-)
9	.	.	.	8.0(+5)	9.5(+)	10.3(+)
8	.	.	.	.	8.6(+)	10.5(-)
7	.	.	.	.	9.3(+)	10.5(+)
6	.	7.6(+1)	9.7(+1)	10.6(-)	11.1(-)	11.4
5	9.8	10.4(-)	11.0(-)	11.4(-)	11.4	11.5
i/j	4	5	6	7	8	9

Time Step No. 46

14	.	.	6.9(-10)	.	.	.
13	.	.	8.1(+)	9.5(+)	.	.
12	.	.	8.1(+)	9.6(+)	.	.
11	.	.	6.9(-10)	9.1(-3)	10.1(-)	10.6(+)
10	.	.	.	8.5(-)	9.8	10.5(-)
9	.	.	.	8.1(+2)	9.6(+)	10.4(+)
8	.	.	.	.	8.6(+)	10.5(-)
7	.	.	.	.	8.8(-5)	10.4(-1)
6	.	7.9(+4)	9.8(+1)	10.6(-)	11.1(-)	11.4(-)
5	9.8	10.4	11.0(-)	11.4(-)	11.4(-)	11.5(-)
i/j	4	5	6	7	8	9

Time Step No. 47

14	.	.	6.9(+)	.	.	.
13	.	.	8.2(+)	9.6(+)	.	.
12	.	.	8.2(+)	9.6(+)	.	.
11	.	.	6.9(+)	9.2(+1)	10.0(-)	10.5(-)
10	.	.	.	8.5(-)	9.8(-)	10.5(-)
9	.	.	.	8.2(+)	9.6(+)	10.4(+)
8	.	.	.	.	8.6(+)	10.5(+)
7	.	.	.	.	8.3(-6)	10.2(-2)
6	.	8.3(+5)	9.9(+)	10.6(+)	11.1(-)	11.4(-)
5	9.8	10.4	11.0	11.4	11.4(-)	11.5
i/j	4	5	6	7	8	9

practically no energy through the advection term $\mathbf{c}_g \cdot \nabla F$. Similar fluctuation is evident in the results of some of the tests described by Perrie and Toulany (1985). According to D.T. Resio (personal communication) this fluctuation is caused by the non linear source term included in the governing equation. A rigorous numerical solution of the non linear wave-wave interaction requires evaluation of quadruple Boltzman integrals at each grid point. This is impractical to do in a wave model and instead, in the Resio model, the G_{nl} term is only approximated in terms of two parameters: the peak frequency and the Phillips' equilibrium coefficient. According to Hasselmann et al. (1985) this behaviour is common to all high resolution discrete spectral models in which the nonlinear source function is represented by fewer degrees of freedom than the spectrum itself. The difference in the number of degrees of freedom means that for some spectral shapes the nonlinear transfer cannot balance the remaining source terms which leads to unstable growth of the spectrum.

The variability described above indicates a limit on the accuracy of the sensitivity tests presented in this report. It is also a measure of the minimum error (i.e. for a perfect input) that can be expected in actual hindcasts for the

standard grid spacing and time step. Station 71 (i=7, j=8 in Table 2.3) is the grid point closest to the Hibernia oil field. The error at Station 71 for the 40 knot wind reaches over 1/2 m (over 6%). This error would not seriously affect hindcasts of design wave conditions since the most severe sea states are not likely to occur for winds blowing off shore, but it would somewhat contaminate normal wave statistics. It is likely that this error could be minimized by decreasing the model time step and grid spacing. Station 71 is the first active grid point adjacent to the land boundary. Since the advection term appears to provide an effective damping at grid points further downwind from the boundary, it seems desirable to separate the grid points for which a hindcast is required from the land boundary by an additional line of grid points. This, however, would require the use of a finer grid than the one employed at present.

The unstable growth described above is also evident, in Figure 2.5, in the curves representing the evolution of the mean wave direction at Station 71 and, to a much lesser degree, at Station 72. In addition, at full development the mean wave directions differ from the wind direction. Table 2.4 shows the distribution of the mean wave direction over the whole grid at hour 141 (output time step 47). In order

TABLE 2.4

DISTRIBUTION OF MEAN WAVE DIRECTION (IN DEGREES) AT TIME STEP NO. 47 (HOUR 141) IN RESPONSE TO UNIFORM STATIONARY WIND FROM WEST.

i/j	1	2	3	4	5	6	7	8	9	10	11	12	13	14	15	16
14	.	.	.	.	.	11.7	.	.	.	.	11.6	7.0	2.2	.	.	.
13	.	.	.	.	.	9.3	5.7	.	.	-7.4	8.2	5.9	1.9	.	.	.
12	.	.	.	.	.	7.8	3.8	.	.	-.9	5.8	5.0	3.2	-1.0	.	.
11	.	.	.	.	.	5.4	1.0	-.1	.4	-3.5	-7.1	1.9	.6	-1.5	.	.
10	.	.	.	.	.	.	.1	-1.8	-4.2	-5.1	-4.6	.0	1.3	-.4	-2.7	.
9	.	.	.	.	.	.	1.5	-3.5	-4.2	-2.4	-6.2	.1	.9	-.2	-1.9	.
8	.	.	.	.	.	.	.	-2.7	2.1	-2.6	-6.7	-.5	.3	-.2	-1.3	.
7	.	.	.	.	.	.	.	14.1	3.8	-1.6	-6.6	-9.4	-1.4	.0	-.8	-1.8
6	.	.	.	.	16.9	13.1	10.4	6.9	2.4	-2.2	-6.1	-9.4	-3.3	-1.4	-1.1	-1.7
5	.	-1.3	12.1	12.6	11.4	9.1	6.1	3.0	.3	-2.7	-5.6	-8.9	-11.1	-3.8	-1.6	-1.9
4	.	9.0	12.7	10.2	8.4	6.5	3.9	1.2	-1.2	-3.4	-5.6	-8.0	-11.0	-4.6	-3.2	-2.3
3	.	33.9	15.3	9.7	6.5	4.1	2.0	-.3	-2.5	-4.6	-6.5	-8.4	-10.5	-12.9	-5.4	-3.9
2	13.1	12.9	10.5	7.3	4.3	1.7	-.4	-2.2	-4.0	-5.9	-7.7	-9.5	-11.3	-13.0	-7.3	-6.7
1	9.5	6.3	4.5	2.5	.3	-2.1	-4.0	-5.5	-7.0	-8.7	-10.2	-11.9	-13.4	-14.9	-16.3	.

to separate the fluctuations from the trend the mean wave directions were averaged between time steps 30 and 47, and the average values are presented in Table 2.5 and Figure 2.7. Comparison between Tables 2.4 and 2.5 indicates that the fluctuations, believed to be caused by the nonlinear source term as described above, represent only a small fraction of the total deviation from the wind direction. The larger part of the deviation is approximately constant over the time steps 30 to 47. In general the values in Table 2.5 are the largest close to the grid boundaries and they diminish towards the interior. This suggests that the deviation of the mean wave direction from the wind direction may be connected with the presence of boundaries in the model.

Energy input from the atmosphere into the wave field is distributed within the model spectrum in proportion to the square of the cosine of the angle from the wind direction $\theta - \theta_w$:

$$E \sim \cos^2(\theta - \theta_w)$$

Since some of the wave energy propagates at an angle to the wind, a grid point which, for a given wind direction, is located asymmetrically with respect to the boundaries is

TABLE 2.5

DISTRIBUTION OF MEAN WAVE DIRECTION (IN DEGREES), AVERAGED OVER TIME STEPS 30 TO 47, IN RESPONSE TO UNIFORM STATIONARY WIND FROM WEST.

i/j	1	2	3	4	5	6	7	8	9	10	11	12	13	14	15	16
14	.	.	.	.	.	11.5	.	.	.	.	11.3	6.9	2.2	.	.	.
13	.	.	.	.	.	9.2	5.8	.	.	-6.8	8.8	5.9	1.6	.	.	.
12	.	.	.	.	.	7.9	3.8	.	.	-1.2	5.7	4.7	2.5	-1.2	.	.
11	.	.	.	.	.	5.8	1.0	-.2	-.1	-3.8	-7.7	.9	.3	-1.7	.	.
10	.	.	.	.	.	.	-.1	-2.1	-4.3	-5.2	-5.5	-.6	.9	-.6	-2.7	.
9	.	.	.	.	.	.	.7	-4.0	-.7	-2.0	-6.7	-.5	.7	-.3	-1.9	.
8	.	.	.	.	.	.	.	-2.6	7.1	-3.0	-7.1	-.9	.0	-.1	-.9	.
7	.	.	.	.	.	.	.	12.3	3.2	-2.4	-6.9	-9.7	-1.6	-.1	-.7	-1.7
6	.	.	.	.	17.1	12.7	10.2	6.9	2.5	-2.2	-6.5	-9.5	-3.3	-1.3	-1.1	-1.6
5	.	-1.1	12.1	12.6	11.3	8.9	6.0	2.9	.3	-2.7	-5.6	-8.8	-11.0	-3.8	-1.5	-1.8
4	.	8.7	12.6	10.2	8.4	6.5	3.9	1.2	-1.2	-3.4	-5.7	-8.1	-10.7	-4.5	-3.0	-2.1
3	.	33.8	15.4	9.7	6.5	4.1	2.0	-.3	-2.5	-4.6	-6.5	-8.5	-10.5	-12.5	-5.2	-3.7
2	12.6	12.5	10.4	7.3	4.3	1.8	-.4	-2.2	-4.0	-5.9	-7.7	-9.5	-11.3	-13.0	-7.0	-6.5
1	9.4	6.1	4.4	2.5	.3	-2.1	-4.0	-5.6	-7.1	-8.6	-10.3	-11.9	-13.4	-15.0	-16.3	.

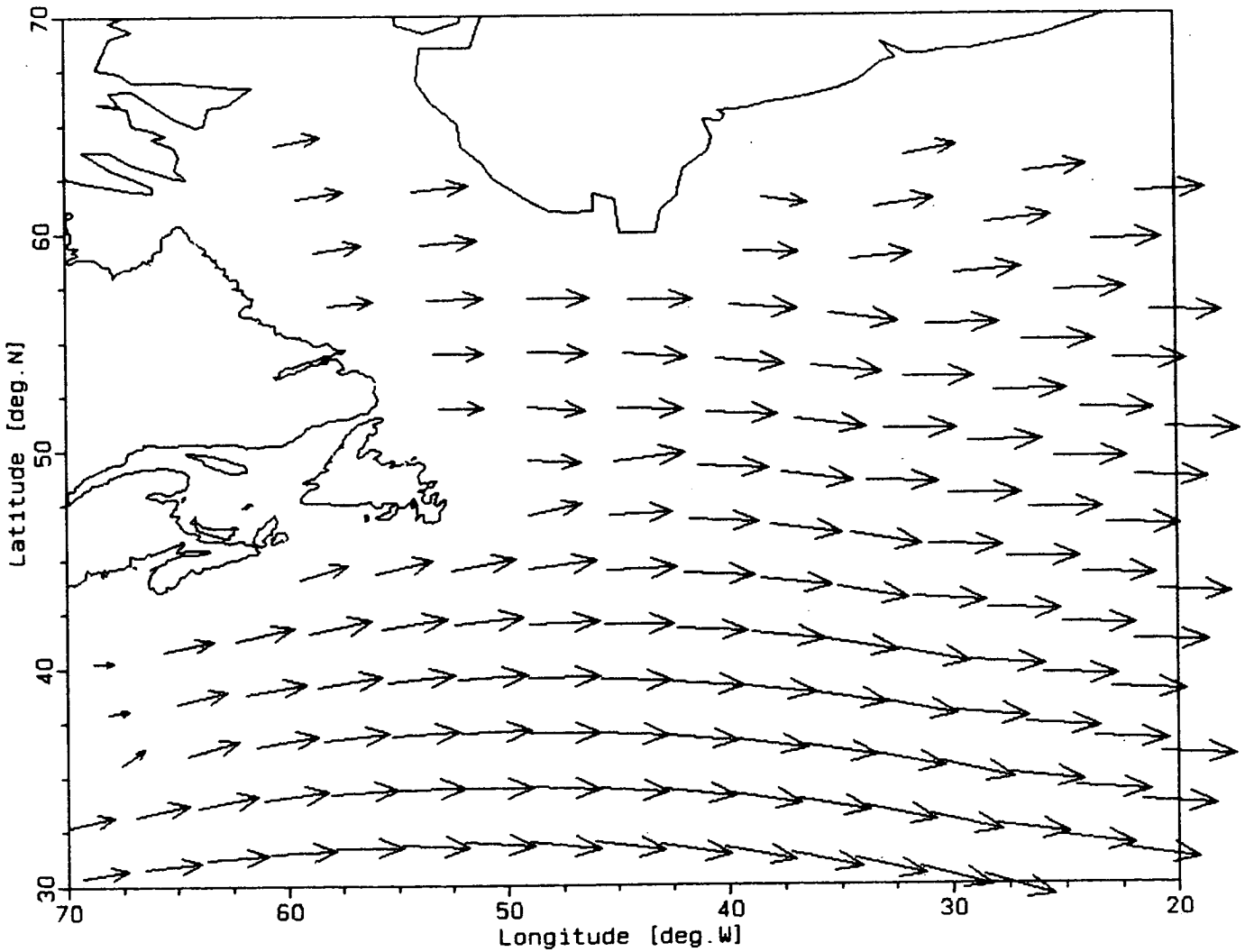

FIGURE 2.7 DISTRIBUTION OF SIGNIFICANT WAVE HEIGHT AND MEAN DIRECTION AVERAGED OVER TIME STEPS 30 TO 47 OF SPIN-UP. (VECTOR OF LENGTH 0.5 INCHES CORRESPONDS TO H_s = 10 M)

expected to receive smaller amounts of advected wave energy from the side of the boundary than from the interior side. Thus it follows that the mean direction should be deflected away from the interior and towards the boundary. The effect of asymmetrical fetch on wave directions is observed in nature (Donelan et al., 1985) and therefore it would represent an artifice of the model only along the oceanic boundaries of the model.

The pattern in Figure 2.7 and Table 2.5 seems to be only partially consistent with the above argument, namely in the western half of the grid. There is no other obvious reason, in the physical processes represented in the model, for the differences shown in Table 2.5. It should be noted that, with only one exception (grid point i=3, j=2), at all the grid points the difference between the mean wave direction and the input wind direction is less than the directional bandwidth (22.5°) of the discrete wave spectrum. This suggests that the values in Table 2.5 most likely reflect the numerical accuracy achievable for the given resolution rather than errors in representing the modelled physical processes. It is believed that this accuracy in the computed wave directions would be adequate for most practical applications of the model.

2.3.3 Perturbed Uniform Stationary Wind Field

Figure 2.8 shows the time series of RMS and bias of wave parameter errors in relation to the RMS and bias of the input errors. "Error" is here a difference between a value of the parameter at a given time step and a value at the same grid point at the end of spin-up (output time step 47, i.e. after 141 hours). "Bias" is the mean of the difference computed over all active grid points within the forced region, while "RMS" is the corresponding root-mean-square difference. The slight non-zero values at time step 47 were computed from the differences between H_s, T_p, and θ at steps 47 and 46. They are shown here for comparison with the effect of input errors. Averaged over the whole grid, these differences are small; however, as noted in the previous section, they may be much larger at individual grid points.

A number of observations can be made on the basis of this plot:

(1) An unbiased error in the input (step 49-50) results in a positive bias in H_s and T_p.

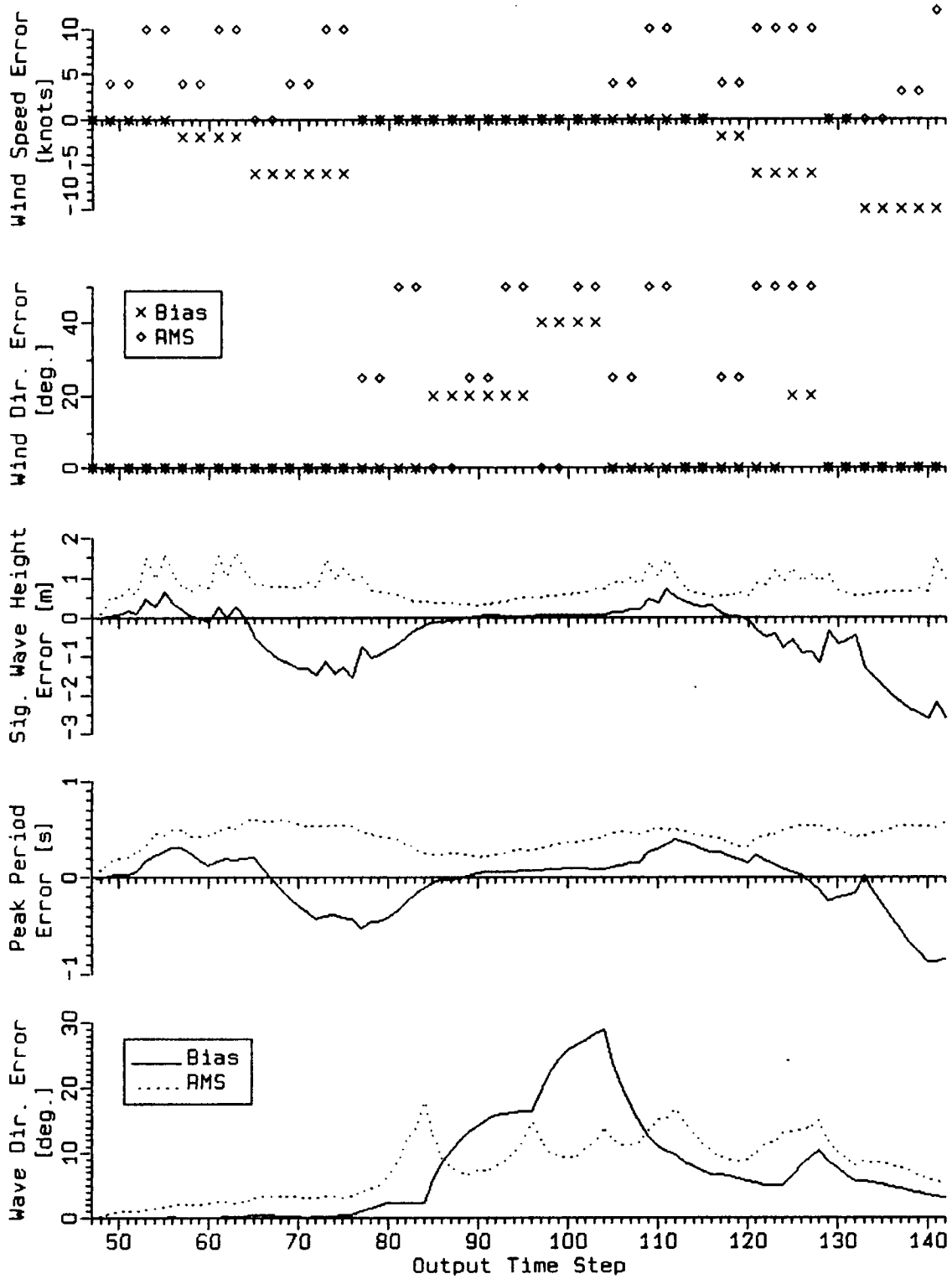

FIGURE 2.8 WAVE MODEL RESPONSE TO A PERTURBED UNIFORM STATIONARY WIND FIELD. BIAS AND RMS ERRORS OVER ENTIRE GRID.

(2) Errors in wind direction do not have any appreciable effect on the bias in the wave height errors and only a small effect on the bias in peak period errors. They have a greater effect on the RMS of H_s and T_p errors, most likely through changing the fetch.

(3) Errors in wind speed produce only small and virtually unbiased errors in the wave direction.

(4) Unbiased errors in wind direction result in somewhat biased errors in wave direction. According to D.T. Resio (personal communication) the magnitude of this bias depends on the particular sequence of the input errors.

(5) There is a considerable persistance in the errors past the 12 h duration of each test. This makes difficult correlating the input and output errors.

(6) Time-wise interpolation leads to a decrease in the RMS error in the input and a corresponding decrease in the RMS error in H_s as evidenced by the presence of double peaks in a number of tests.

The correlations between input errors at a single grid point and the corresponding errors in H_s, T_p, and θ at that grid point are shown in Figures 2.9 to 2.22. Each set of plots consists of a time series of input and output parameters and scatter plots of various combinations of these parameters. Only errors at the 6 hourly input time steps are shown in the scatter plots. The circles correspond to the situation where the overall wind error has a bias. The station numbering conforms to the system used by MEDS: stations are counted along each grid row starting in the upper left corner. The locations of the stations in the SOG are shown in Figure 2.6. The results are presented for stations at, or close to, a single point in the 2.5° x 2.5° input grid so that the smoothing effect of the space-wise interpolation is minimized.

Station 49 is surrounded by input grid points at which the wind speed error and the wind direction error are set to zero. The interpolated local input error at Station 49 is thus zero (up to step 131) and the errors in the output parameters demonstrate the effect of advection from the surrounding area. The error in H_s and T_p reached its peak at step 77, after the overall wind speed error dropped to zero (see Figure 2.8), and it remained noticeable another 8 to 9

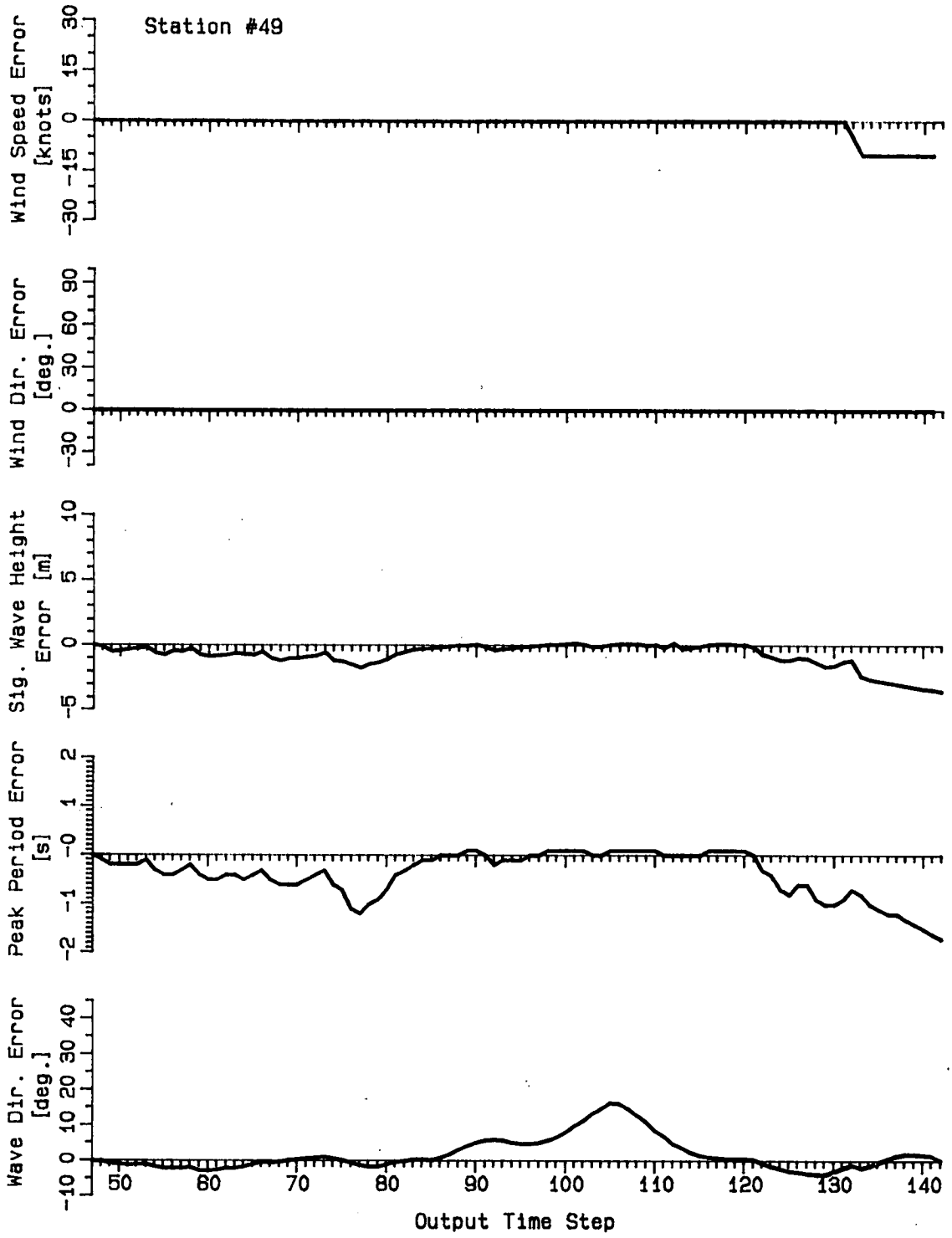

FIGURE 2.9 WAVE MODEL RESPONSE TO A PERTURBED UNIFORM STATIONARY WIND FIELD. ERRORS AT STATION 49.

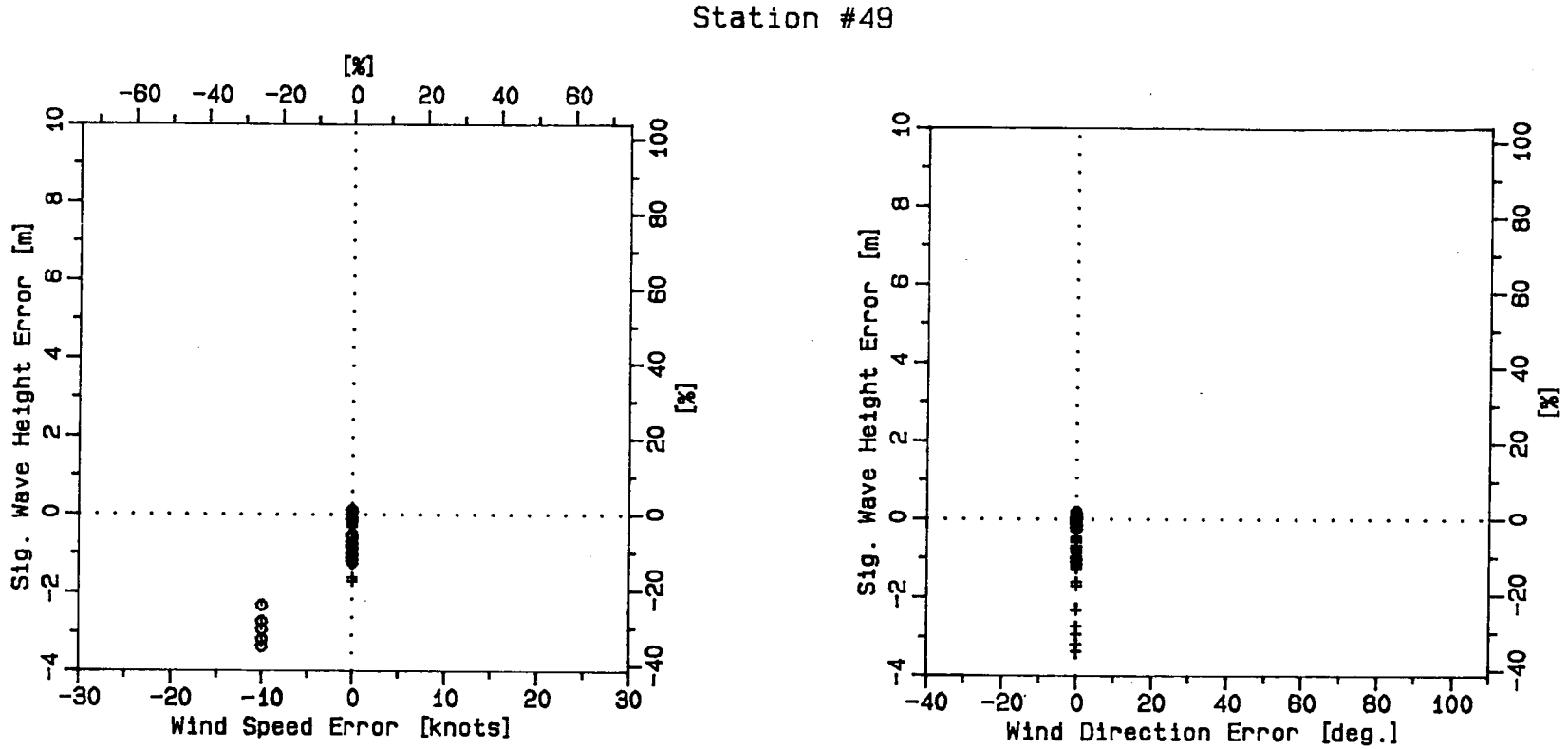

FIGURE 2.10 CORRELATION BETWEEN INPUT AND OUTPUT ERRORS AT STATION 49.

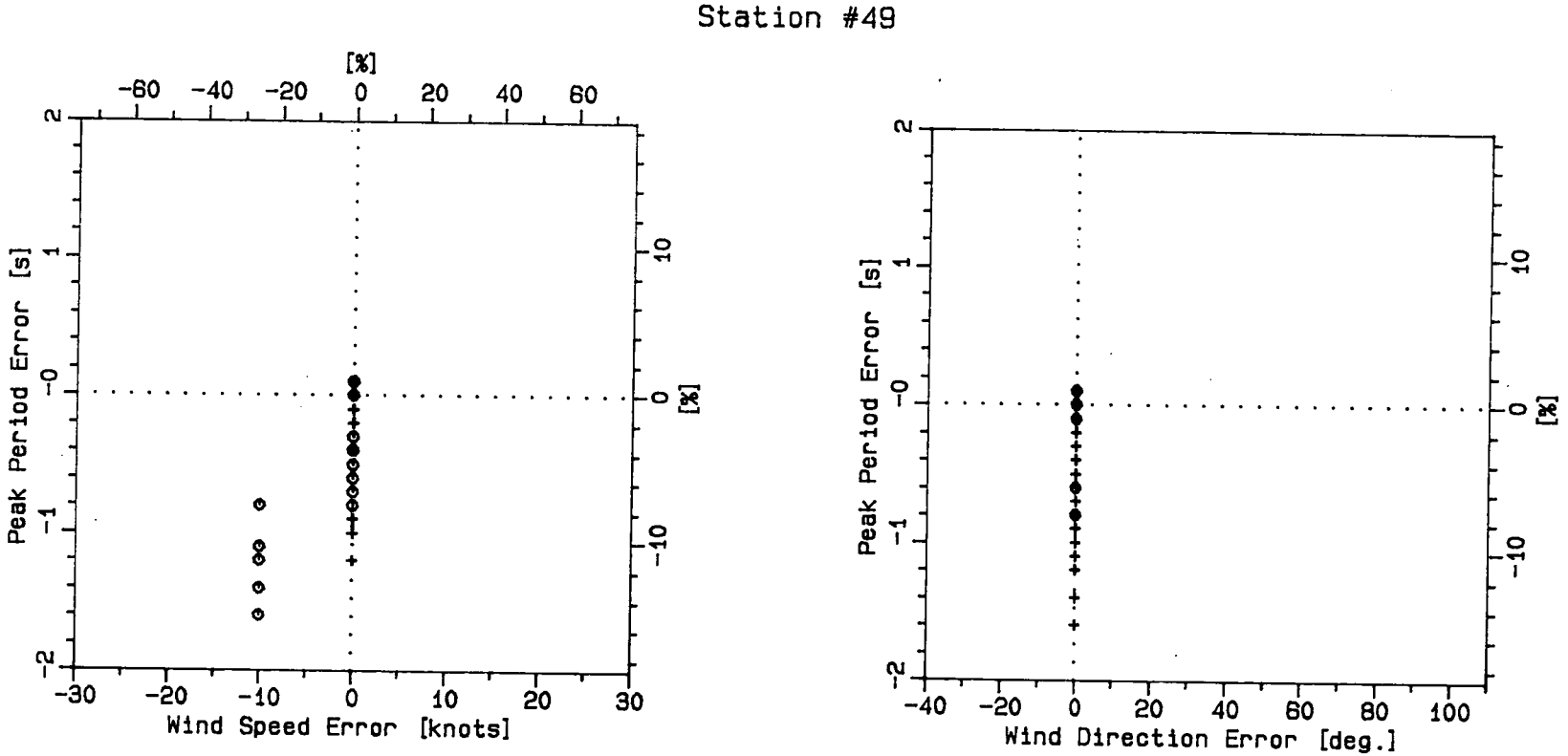

FIGURE 2.10 CONTINUED...

Station #49

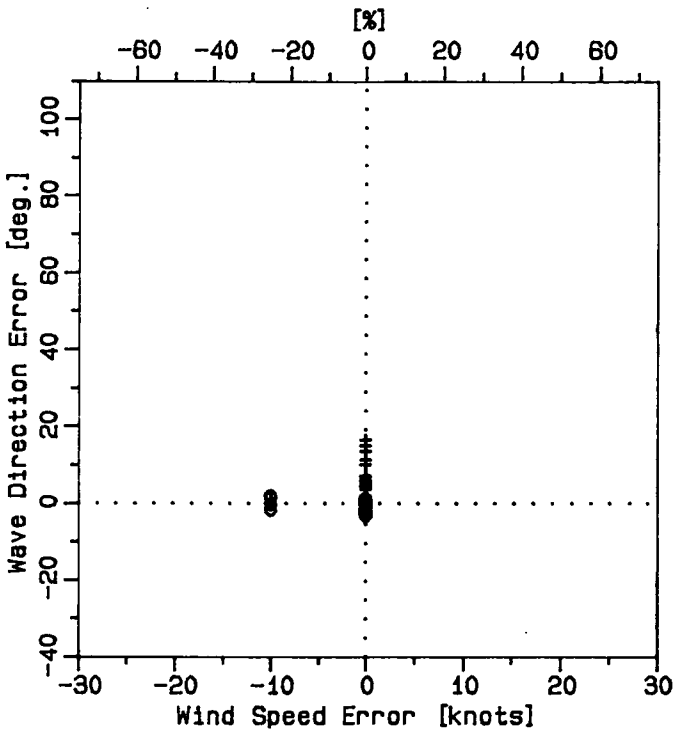

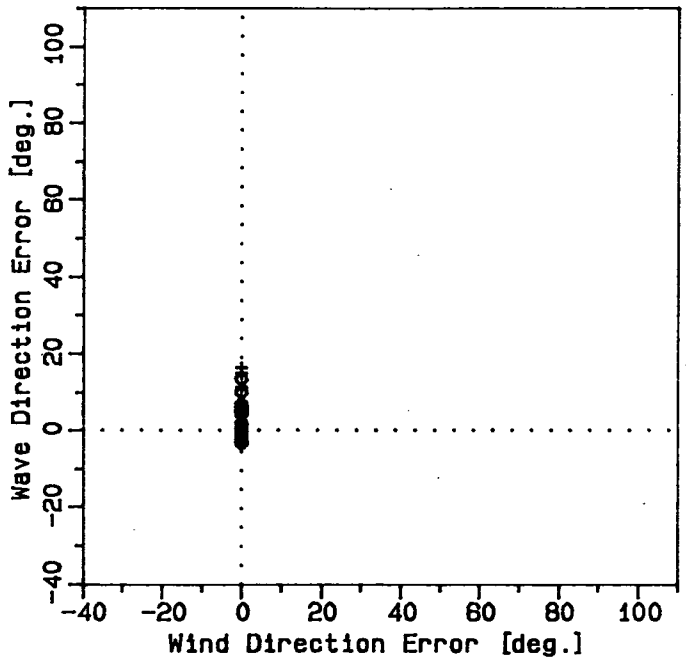

FIGURE 2.10 CONTINUED...

time steps. The magnitude of the error is relatively large, almost 2 m or 20% in H_s and 1 s or 10% in T_p. The fact that the error is negative suggests that the bias in the input error has a dominant effect on the advected output error, as would be expected.

Station 50 is directly downwind from Station 49. Therefore, the output errors should be primarily of local origin and closely correlated with the local input errors. Figures 2.11 and 2.12 confirm this. There is a small amount of scatter in the H_s error versus wind speed error plot and the points can be fitted well with a straight line of slope 1 (%/%). A slope of approximately 2 would be expected according to Equation (7) for fully developed seas while for fetch and duration limited waves the slope should be 1 and 9/7 respectively (Equations (9) and (11)). For a westerly wind the fetch at Station 50 is two grid spacings or approximately 150 nautical miles. Empirical wave forecasting diagrams (e.g. WMO, 1976) indicate that at this fetch and 40 knot winds the seas are fetch limited for wind duration greater than approximately 9 hours and duration limited for duration less than 9 hours. In this test the wind changes every 6 hours but the change is only small and therefore it is more likely that the sea state is limited by fetch and the

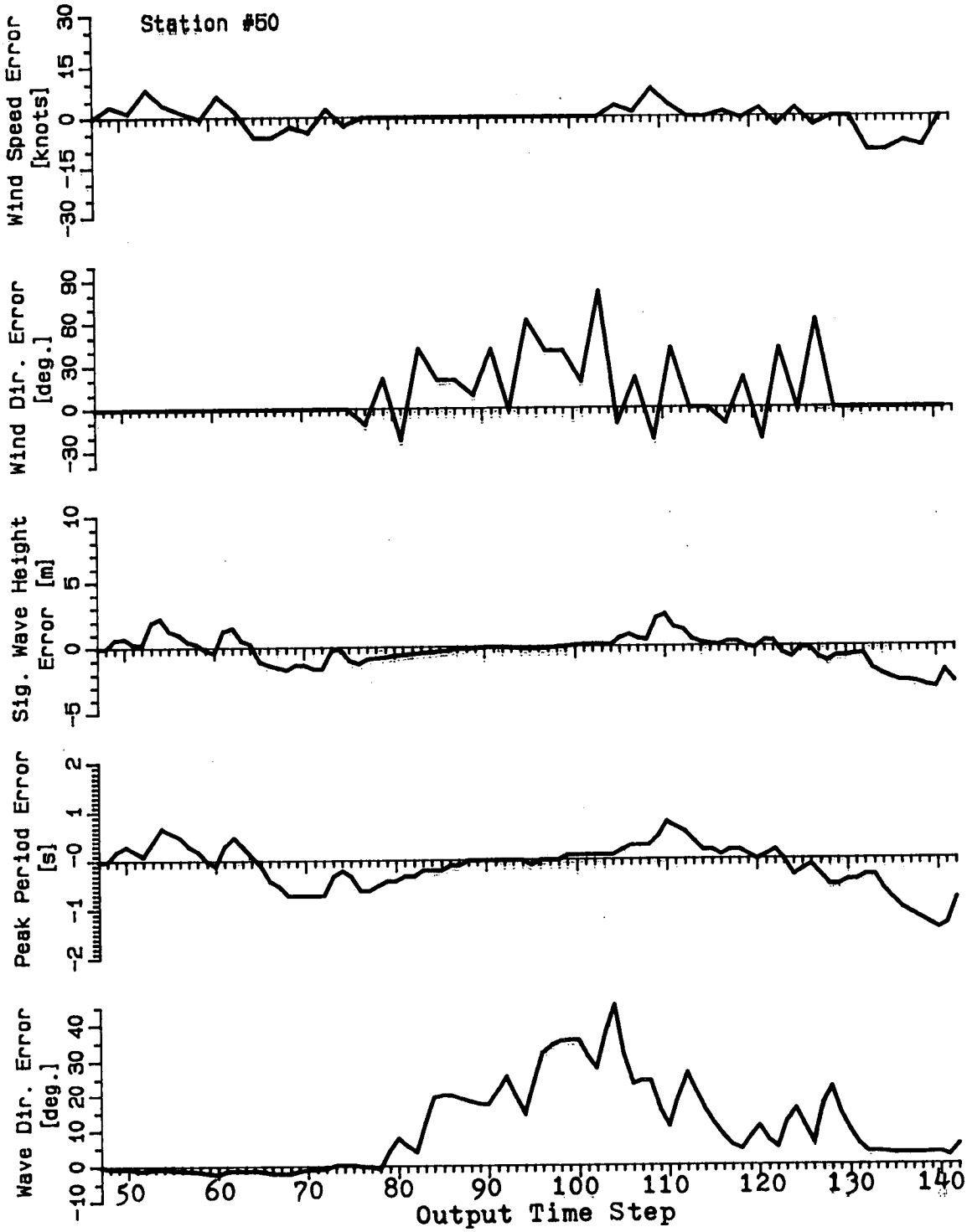

FIGURE 2.11 WAVE MODEL RESPONSE TO A PERTURBED UNIFORM STATIONARY WIND FIELD. ERRORS AT STATION 50.

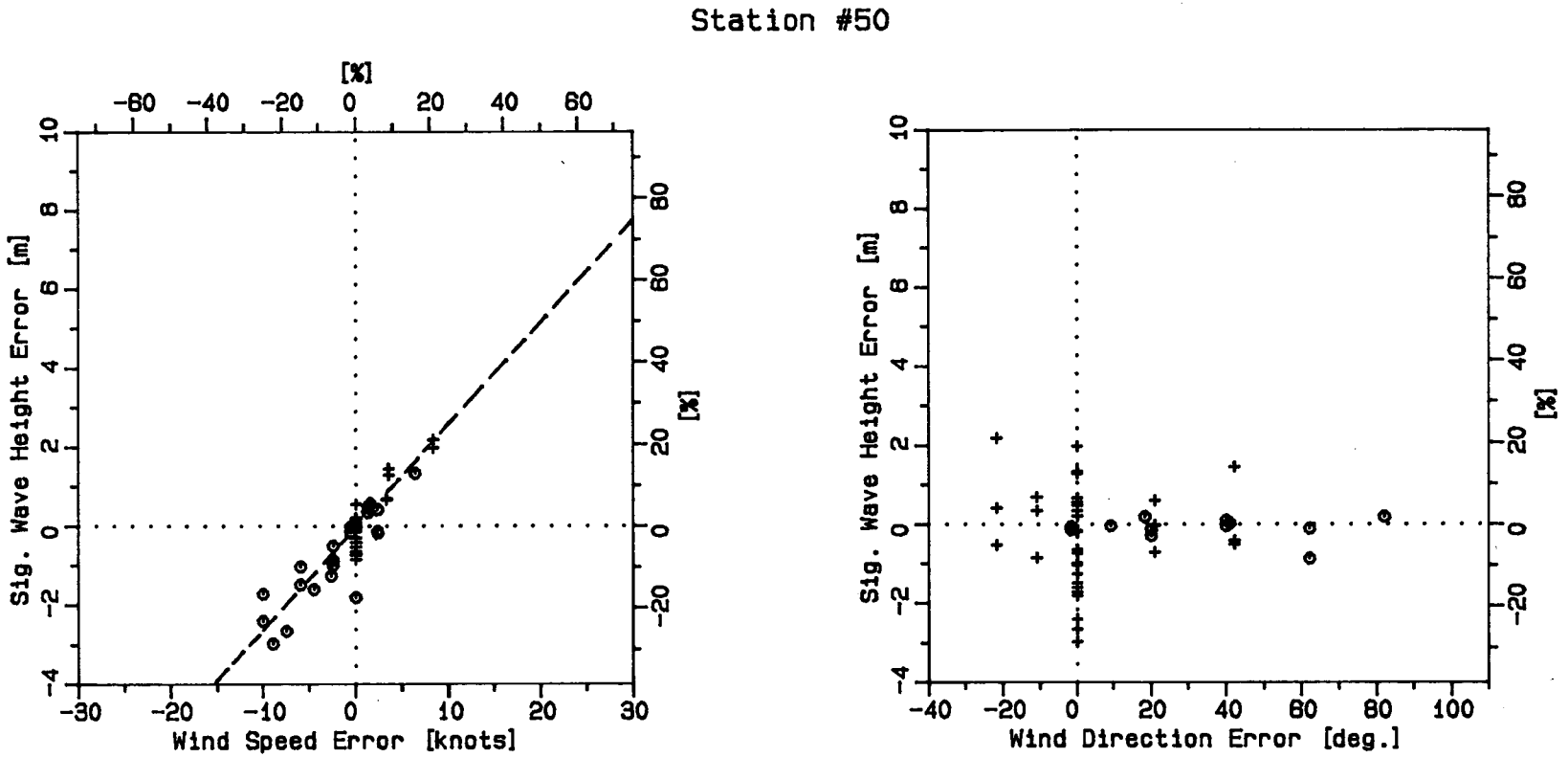

FIGURE 2.12 CORRELATION BETWEEN INPUT AND OUTPUT ERRORS AT STATION 50.

Station #50

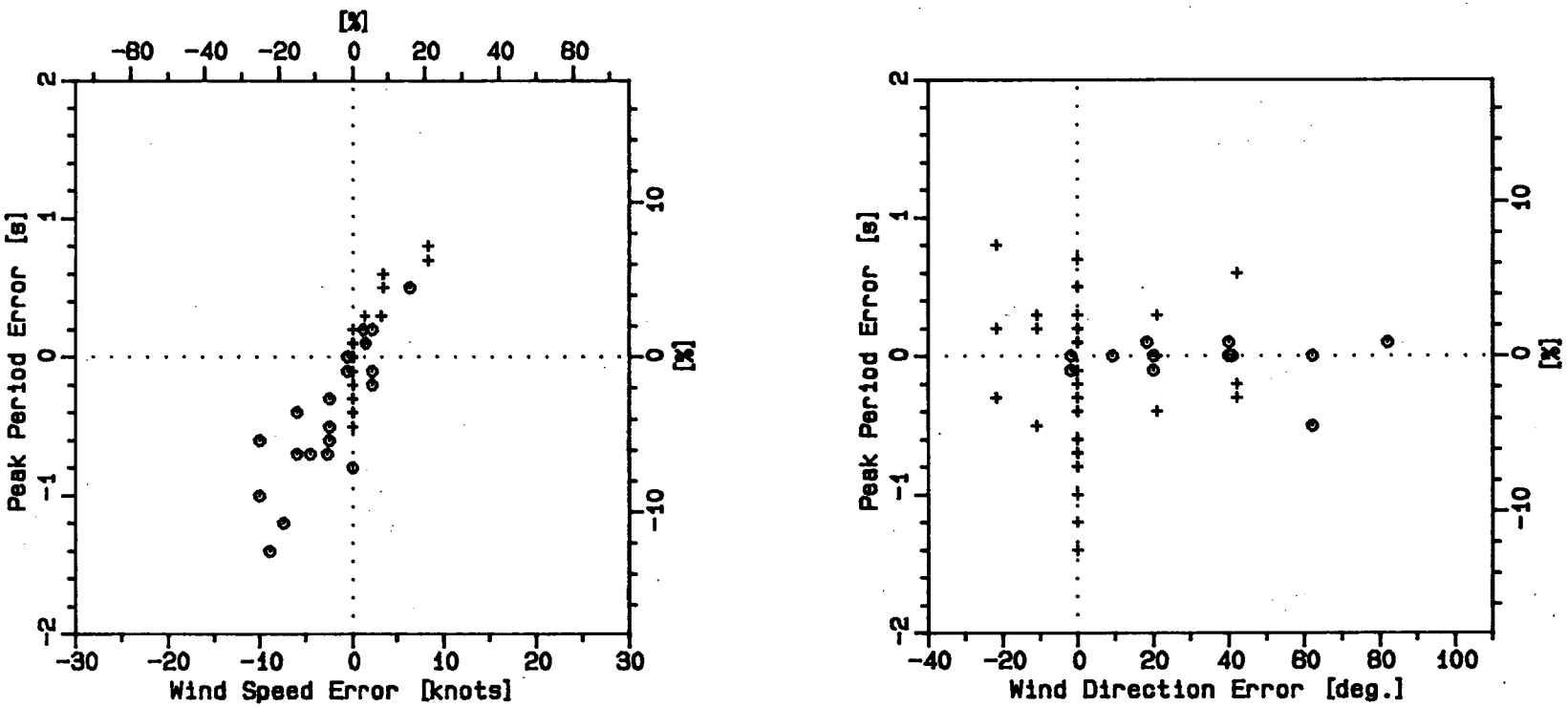

FIGURE 2.12 CONTINUED...

Station #50

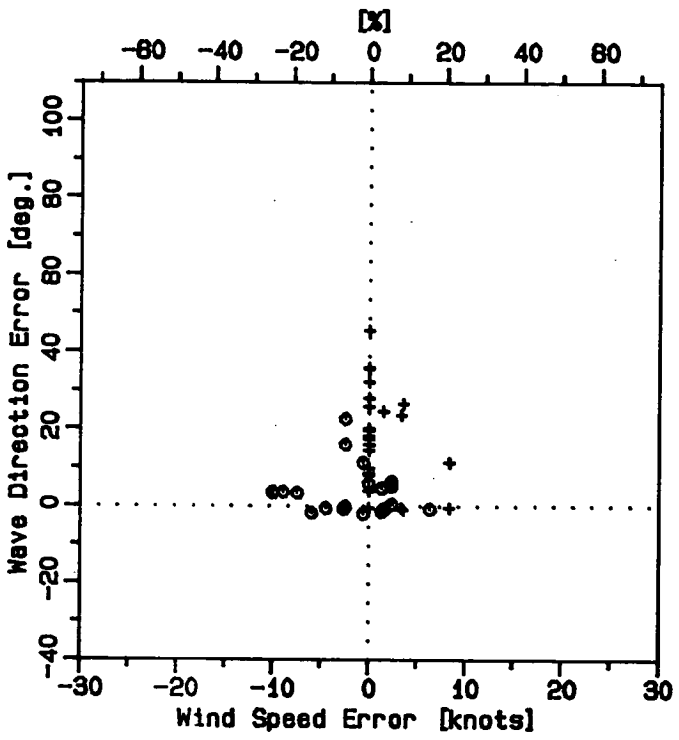

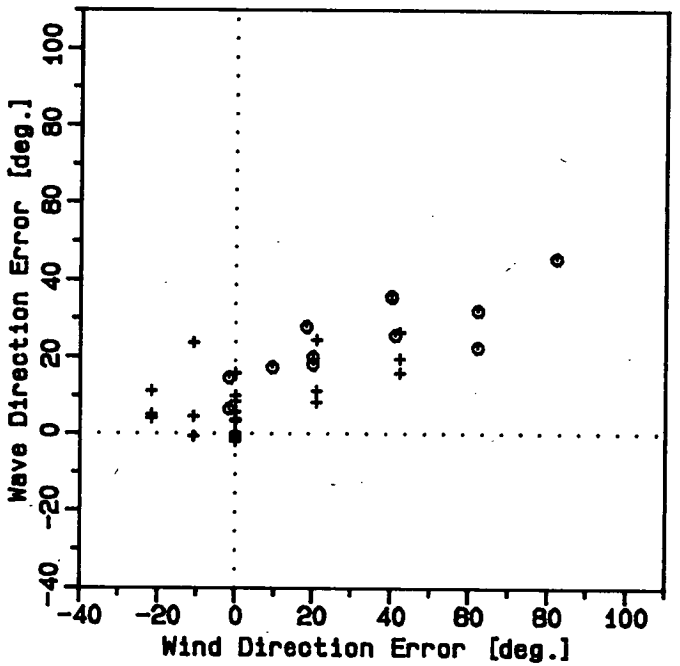

FIGURE 2.12 CONTINUED...

duration effect only contributes to the scatter in Figures 2.7 and 2.8. Thus the results shown in the scatter diagram are consistent with what would be expected on the basis of theoretical considerations.

The peak period errors show far greater scatter than the H_s errors but this is not unexpected since only discrete values of the peak period are resolved. At a mean period of 10 s the period increment is approximately 1 s which is of the same magnitude as the T_p errors shown in Figure 2.12. Neither the H_s errors nor the T_p errors are correlated with the errors in wind direction.

Large scatter is apparent in the wave direction error versus wind direction error plot. There are two possible reasons for this: first, the wave field does not respond to a change in wind direction immediately but rather after certain delay; second, the mean wave direction is a parameter more sensitive to advective errors than for example H_s. This is because the significant wave height is a function of the integral (zeroth moment) of the directional spectrum, while θ is a function of the directional distribution of energy within the spectrum (first directional moment).

Stations 61, 63, and 65 are affected by both local errors in the input as well as advected errors. These stations are exposed to a differing amount of fetch with Station 65 being the farthest. The correlation between the H_s error and the local wind speed error appears to decrease with increasing fetch as the number of upwind grid points increases. Peak period errors appear virtually uncorrelated with wind speed errors. The correlation between wind and wave direction errors is the closest for the middle station (#63).

Station 84 is adjacent to a boundary parallel to the wind direction. This should lead to a correlation between wind direction on the one hand and H_s or T_p on the other since a small change in wind direction leads to a large change in fetch. There seems to be some correlation between the H_s and T_p errors and the wind direction errors in the case of biased wind fields (circles in Figure 2.20) but not significantly greater than that for the other stations. The bias in the wind direction errors was chosen to be positive (towards the north) and thus its effect on the fetch is not as great as it would be in the case of a negative bias. For a positive bias the change in fetch is greater at Station 146 where a 40° change in bias (steps 97 to 103) leads to about

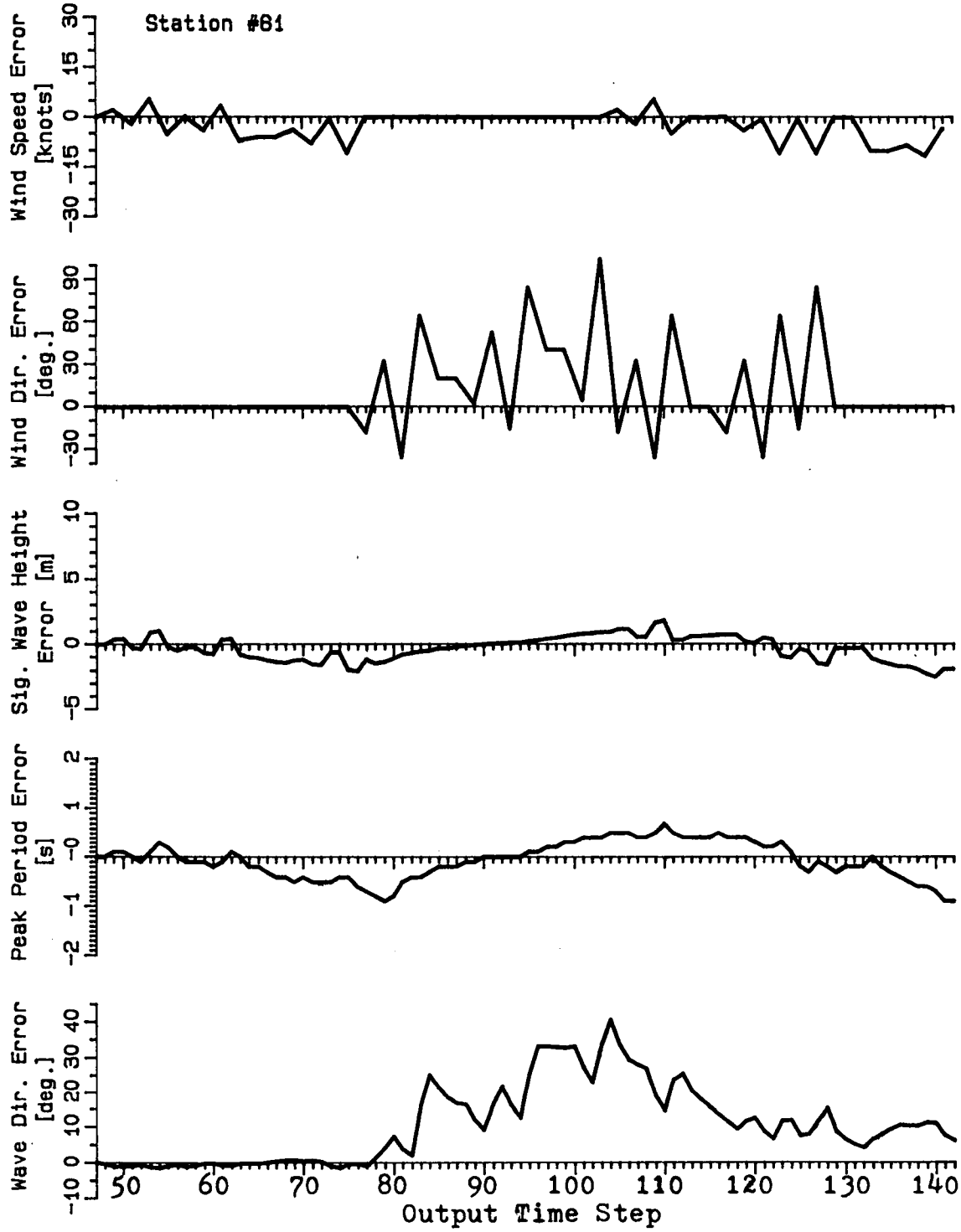

FIGURE 2.13 WAVE MODEL RESPONSE TO A PERTURBED UNIFORM STATIONARY WIND FIELD. ERRORS AT STATION 61.

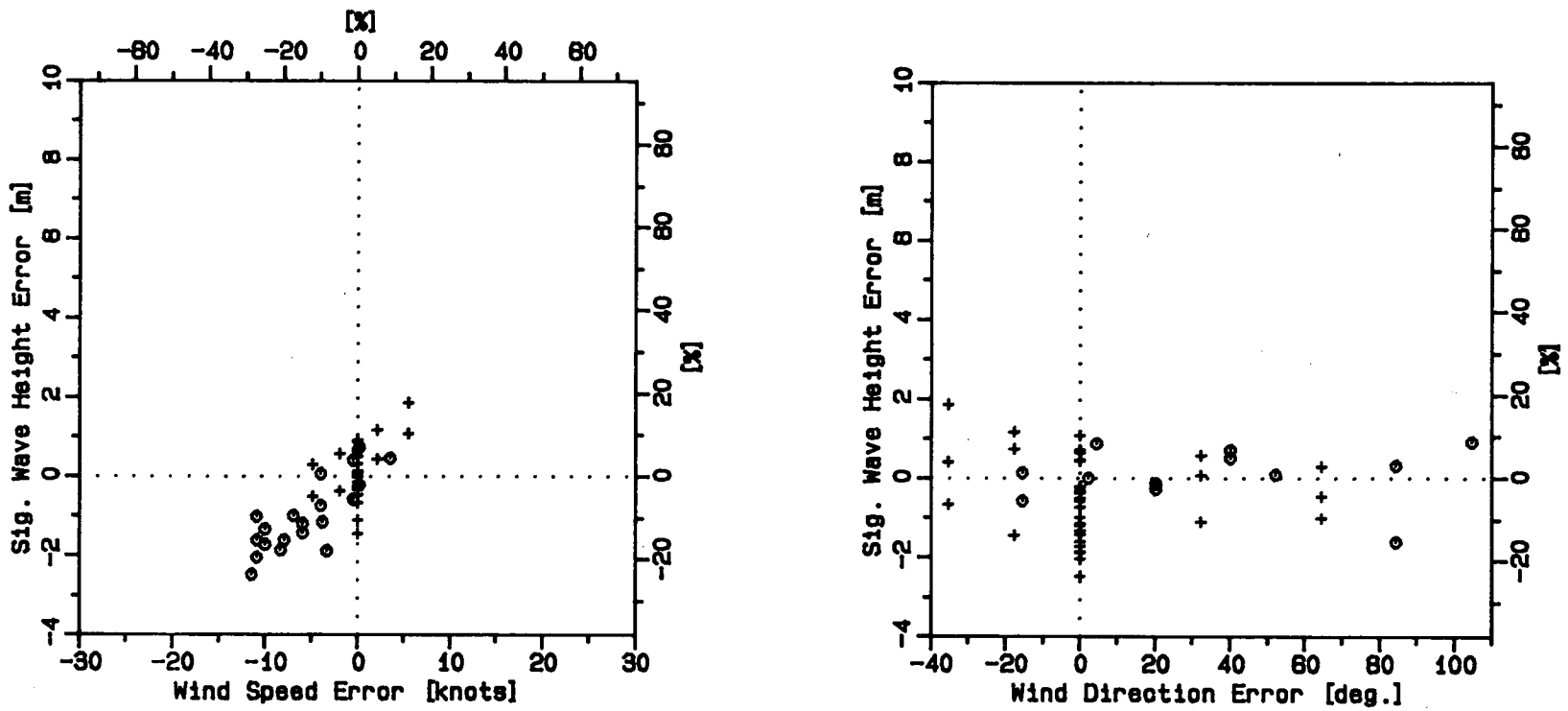

FIGURE 2.14 CORRELATION BETWEEN INPUT AND OUTPUT ERRORS AT STATION 61.

Station #61

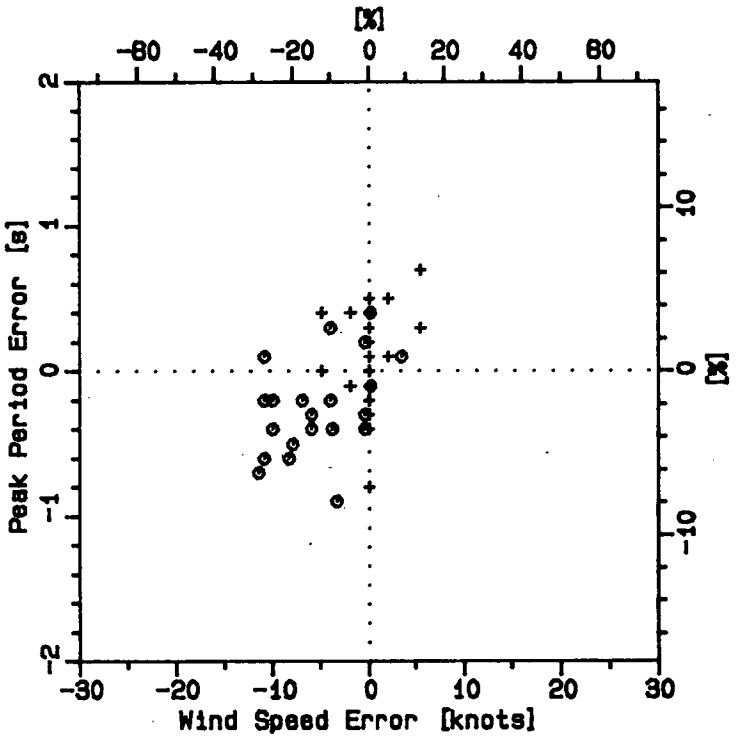

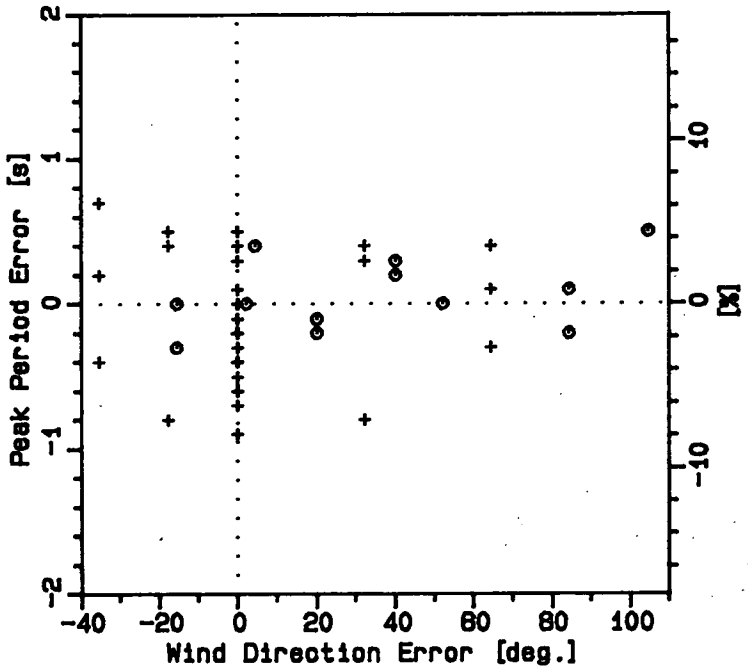

FIGURE 2.14 CONTINUED...

Station #61

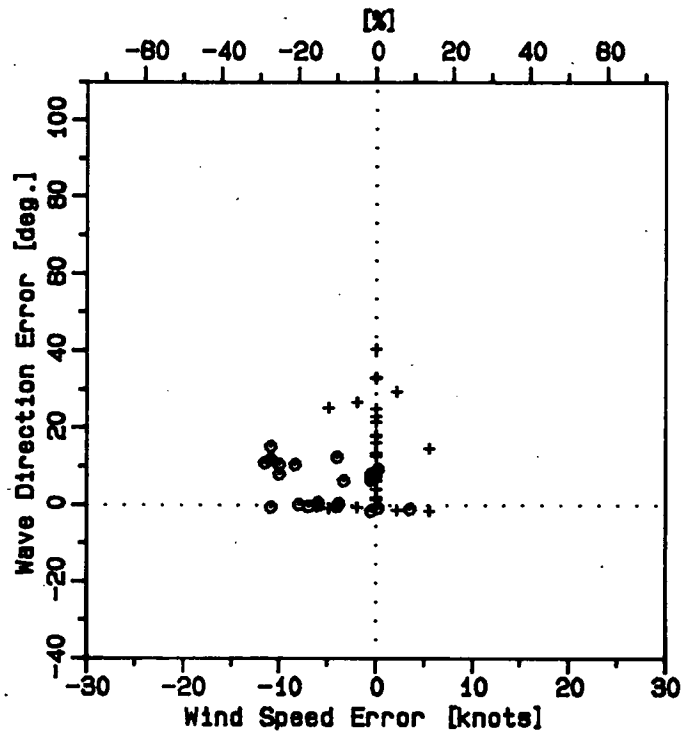

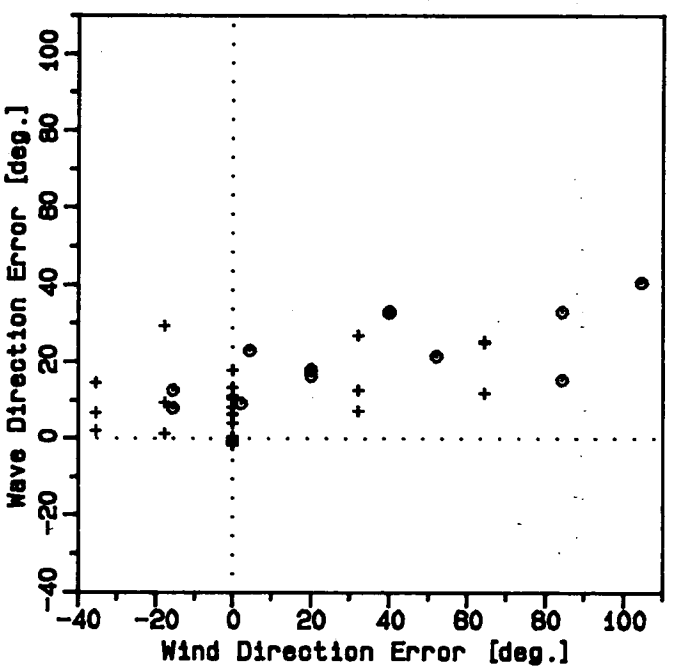

FIGURE 2.14 CONTINUED...

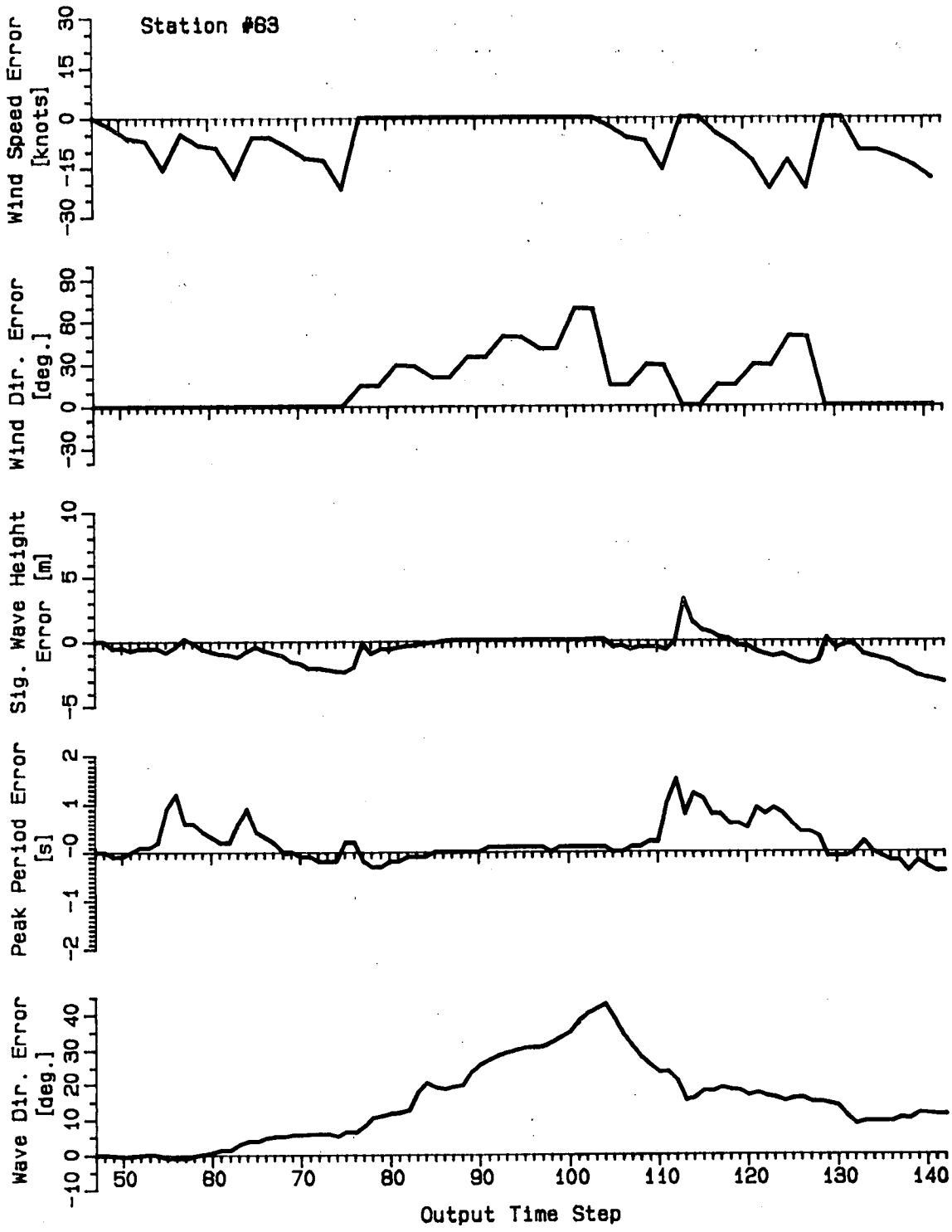

FIGURE 2.15 WAVE MODEL RESPONSE TO A PERTURBED UNIFORM STATIONARY WIND FIELD. ERRORS AT STATION 63.

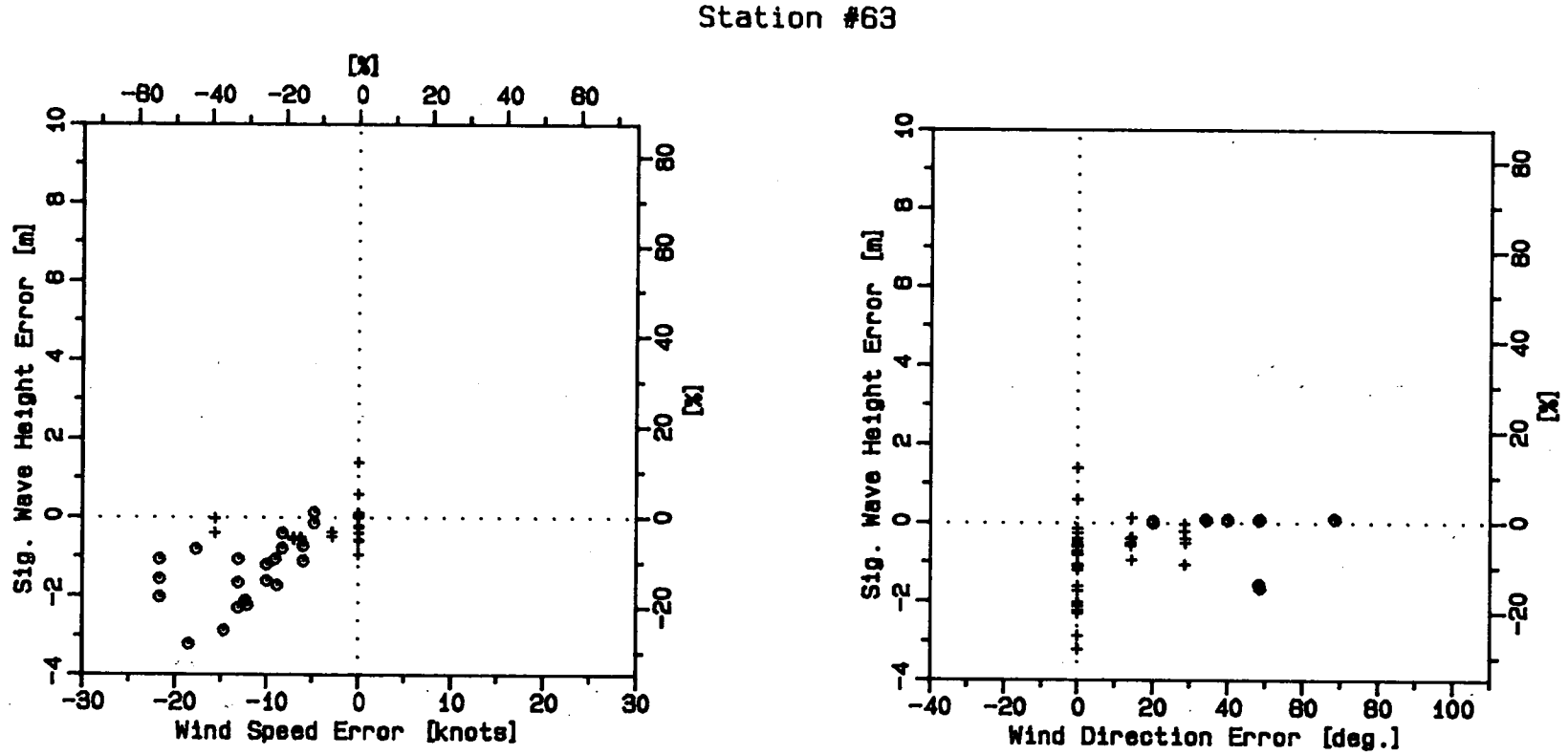

FIGURE 2.16 CORRELATION BETWEEN INPUT AND OUTPUT ERRORS AT STATION 63.

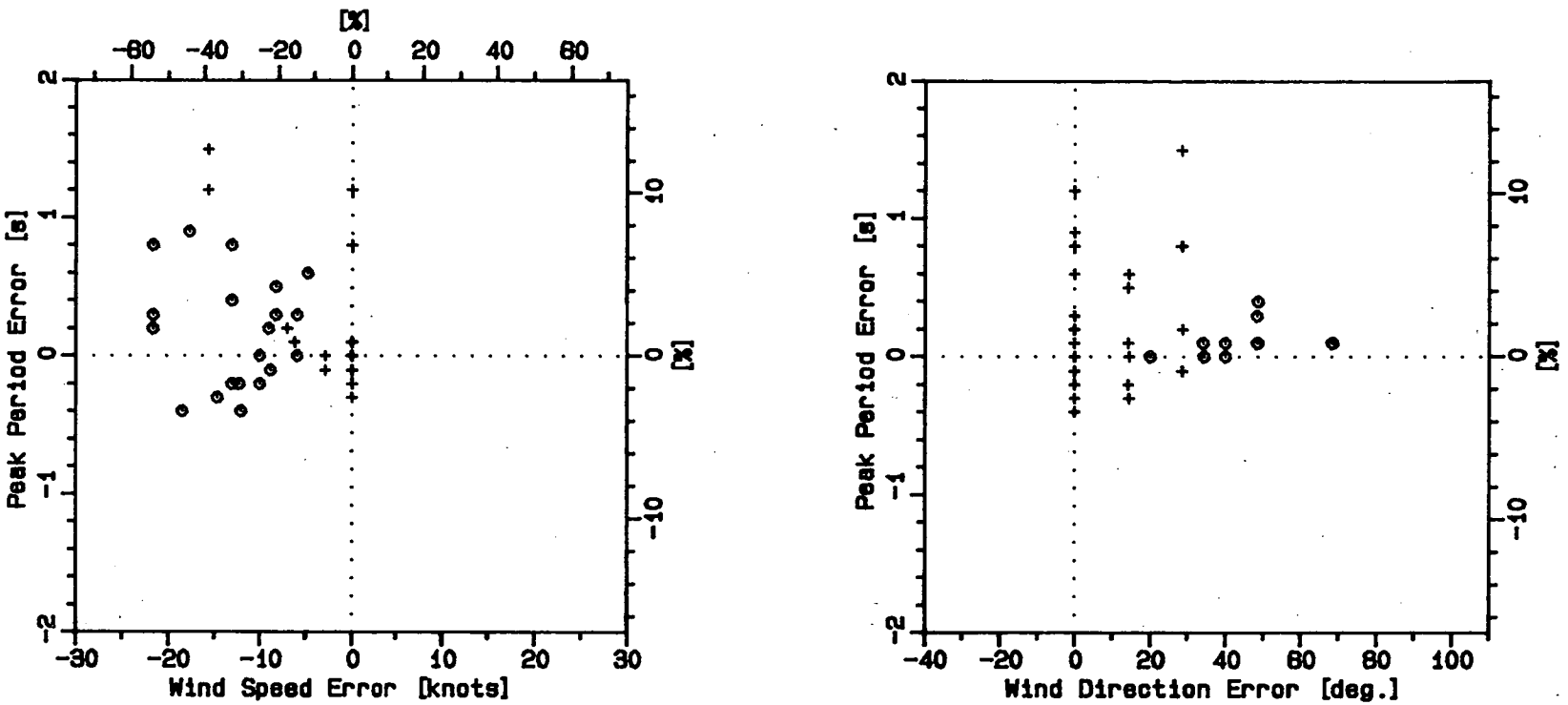

FIGURE 2.16 CONTINUED...

Station #63

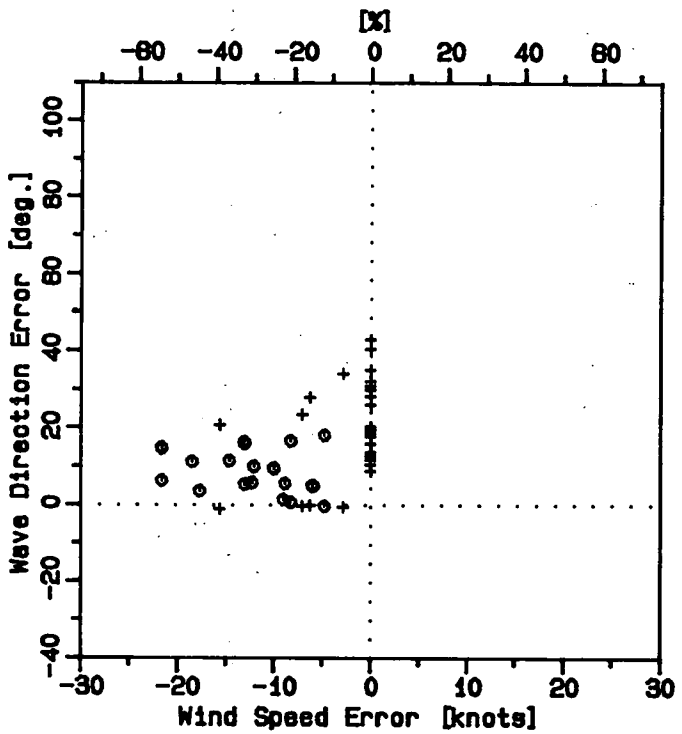

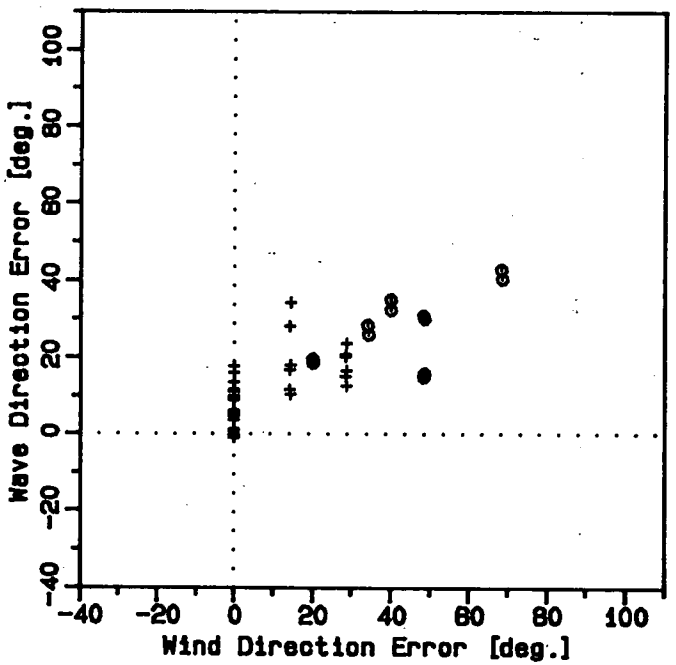

FIGURE 2.16 CONTINUED...

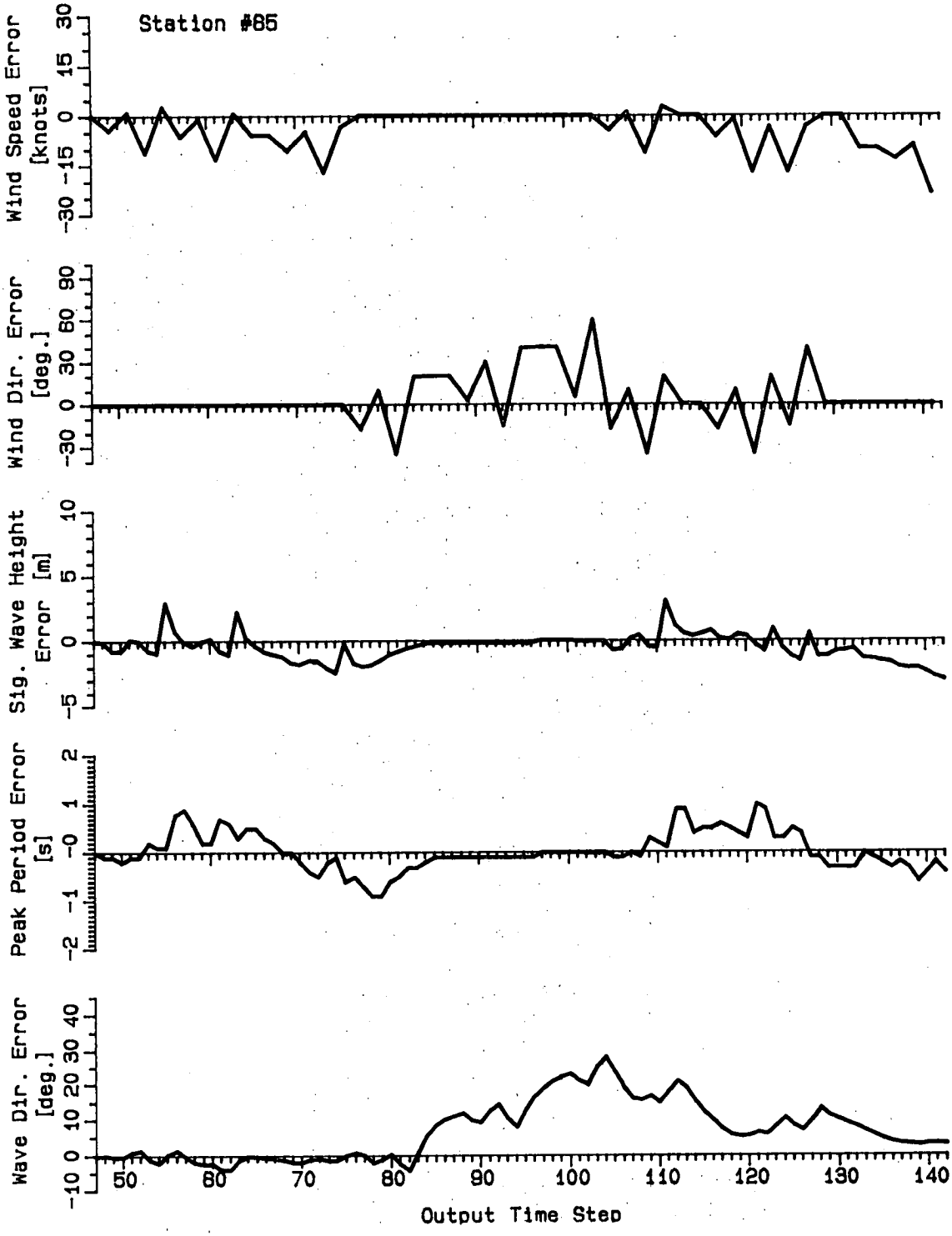

FIGURE 2.17 WAVE MODEL RESPONSE TO A PERTURBED UNIFORM STATIONARY WIND FIELD. ERRORS AT STATION 65.

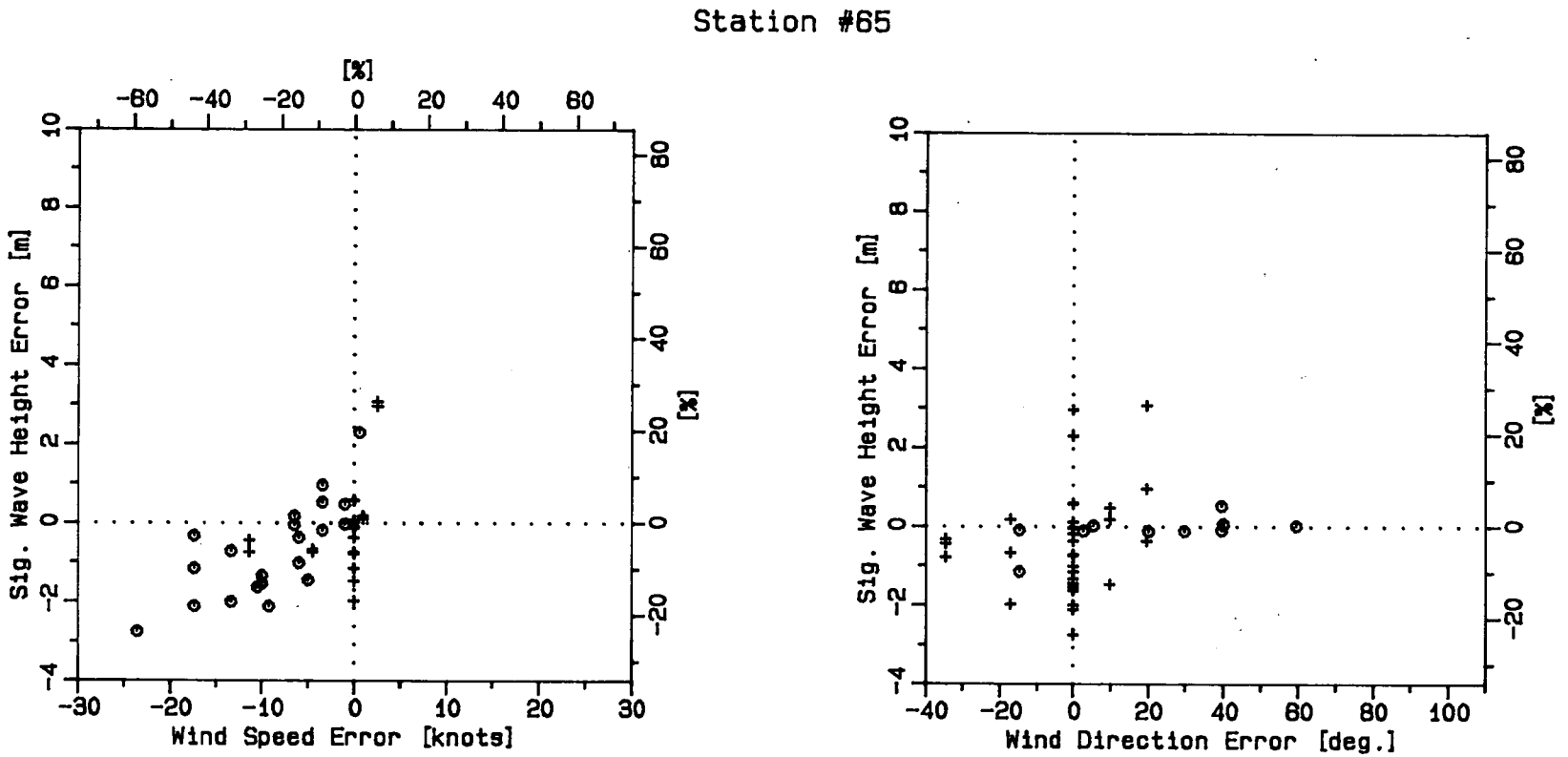

FIGURE 2.18 CORRELATION BETWEEN INPUT AND OUTPUT ERRORS AT STATION 65.

Station #65

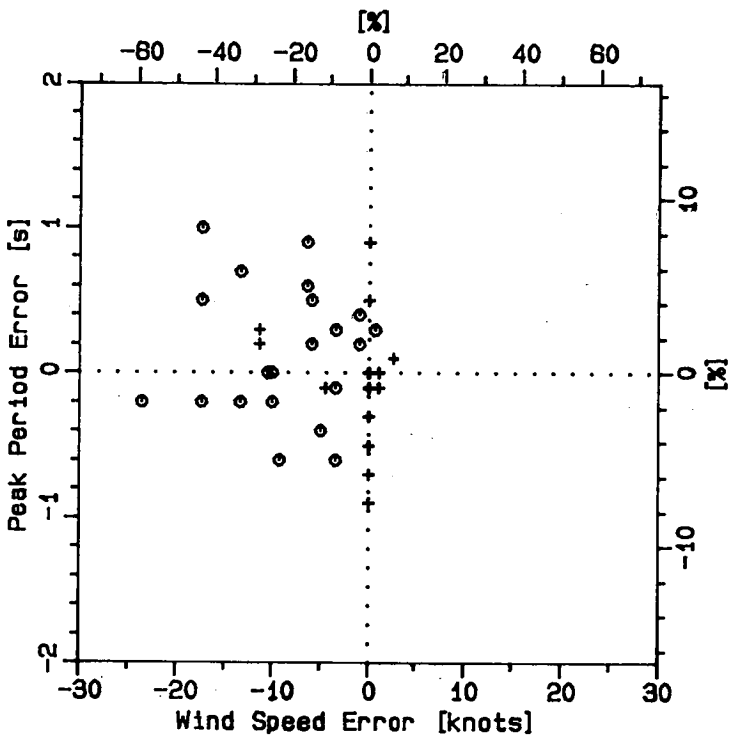

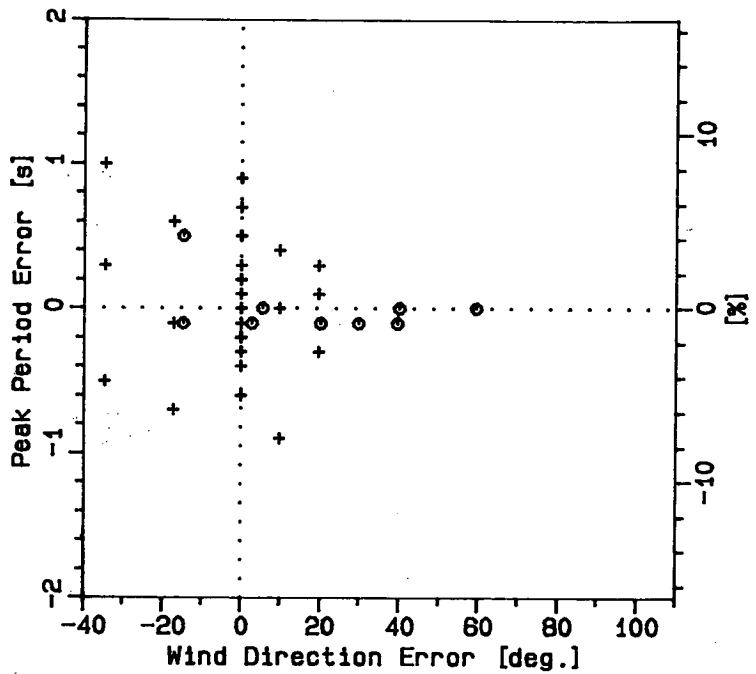

FIGURE 2.18 CONTINUED...

Station #65

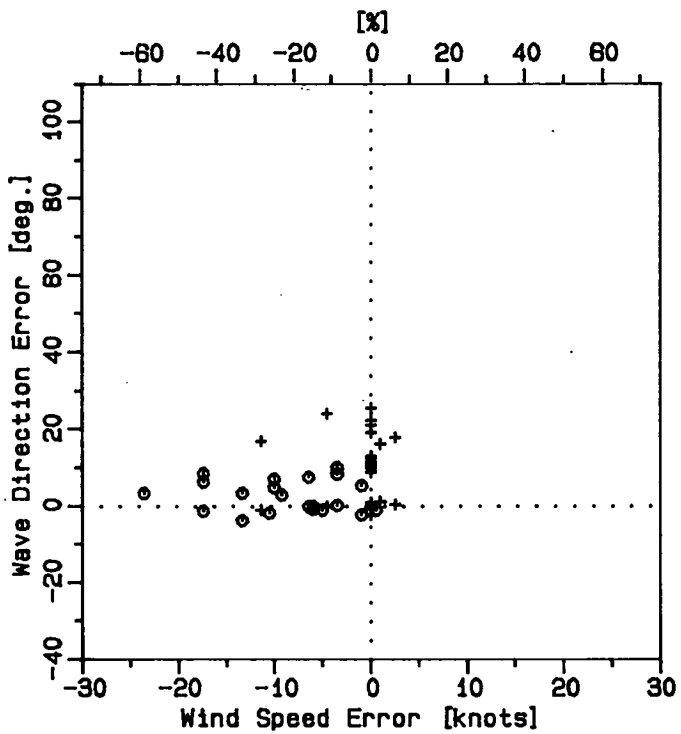

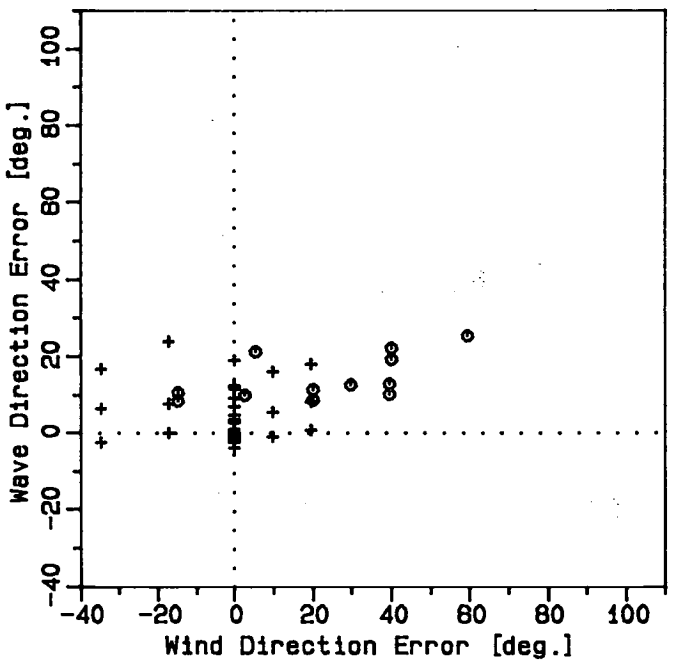

FIGURE 2.18 CONTINUED...

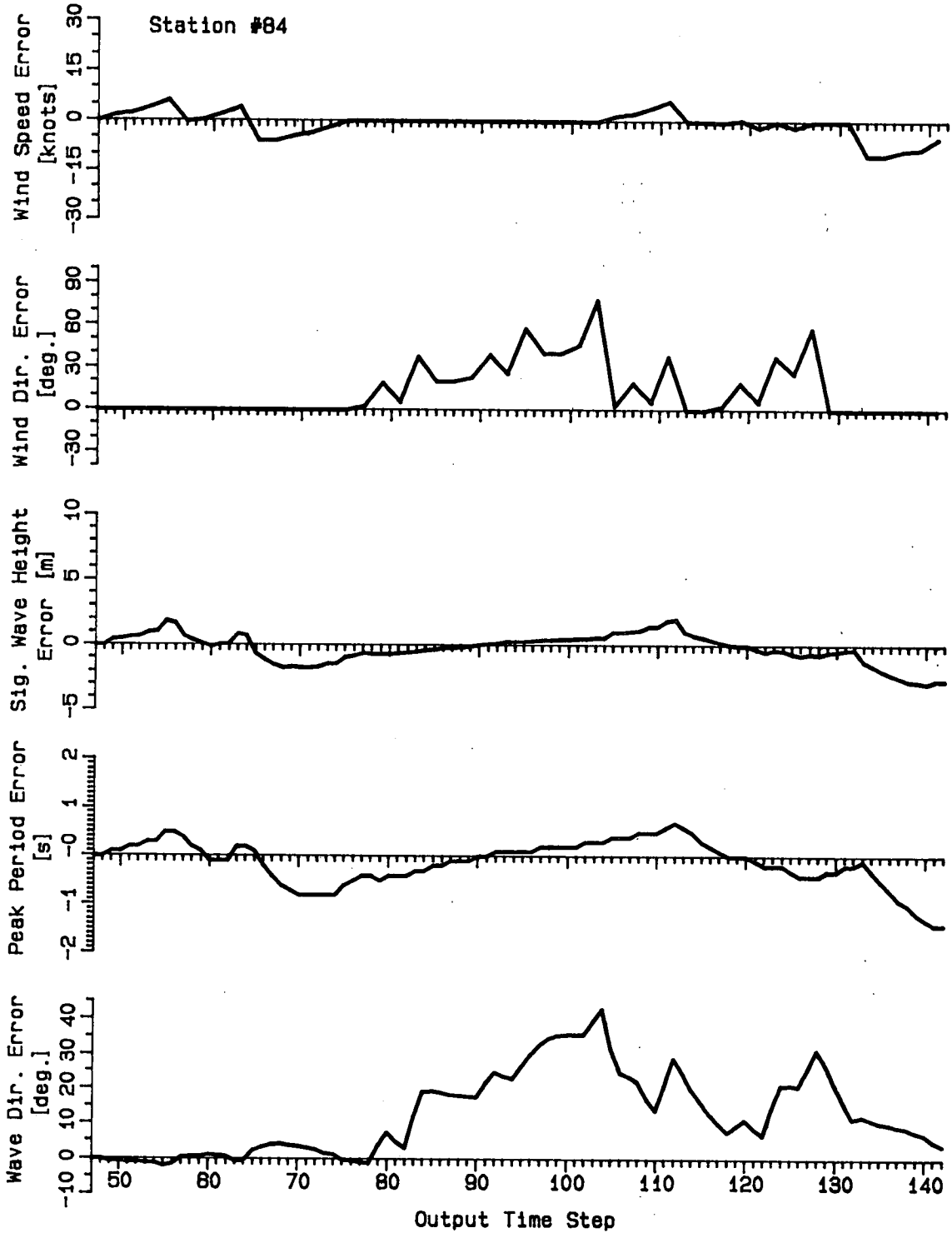

FIGURE 2.19 WAVE MODEL RESPONSE TO A PERTURBED UNIFORM STATIONARY WIND FIELD. ERRORS AT STATION 84.

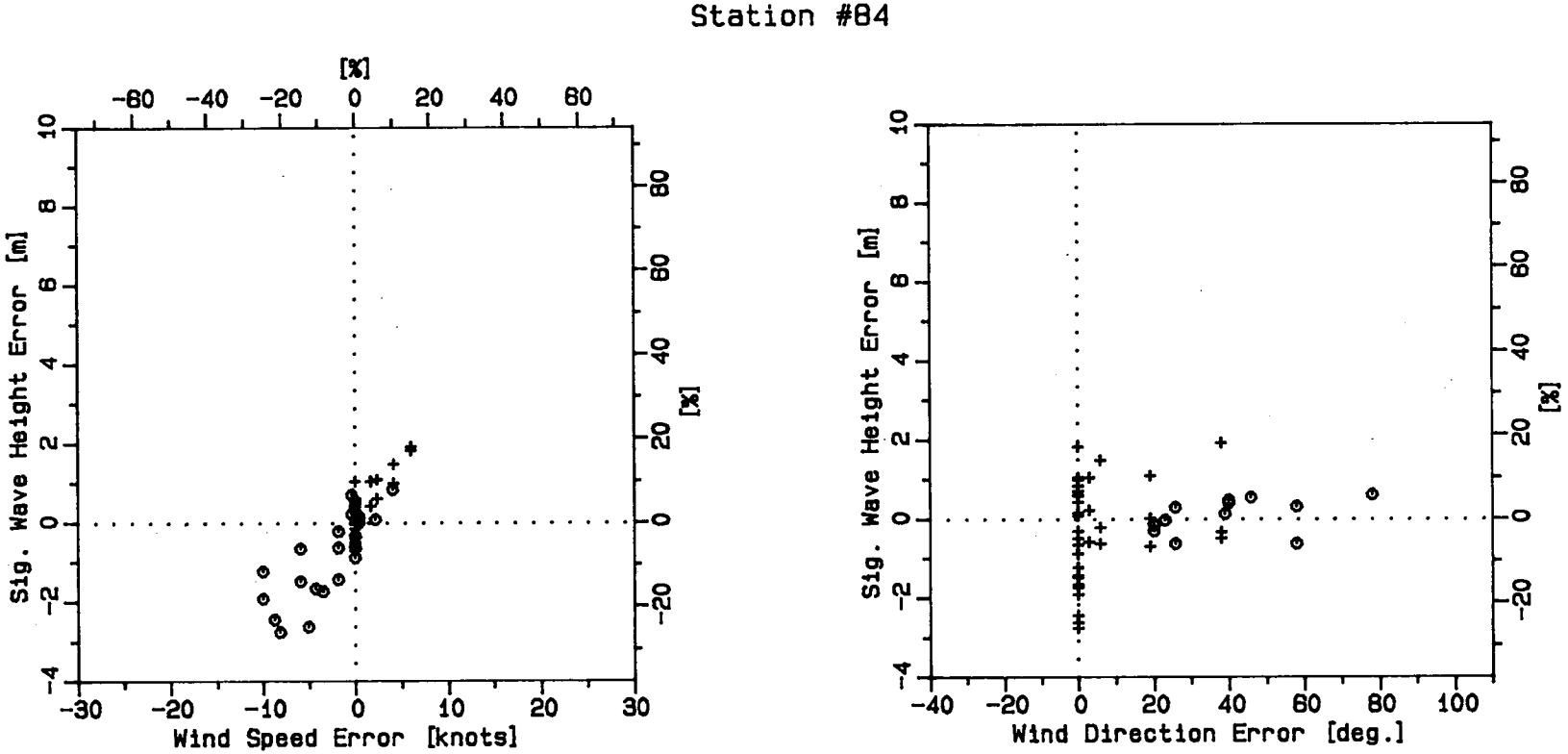

FIGURE 2.20 CORRELATION BETWEEN INPUT AND OUTPUT ERRORS AT STATION 84.

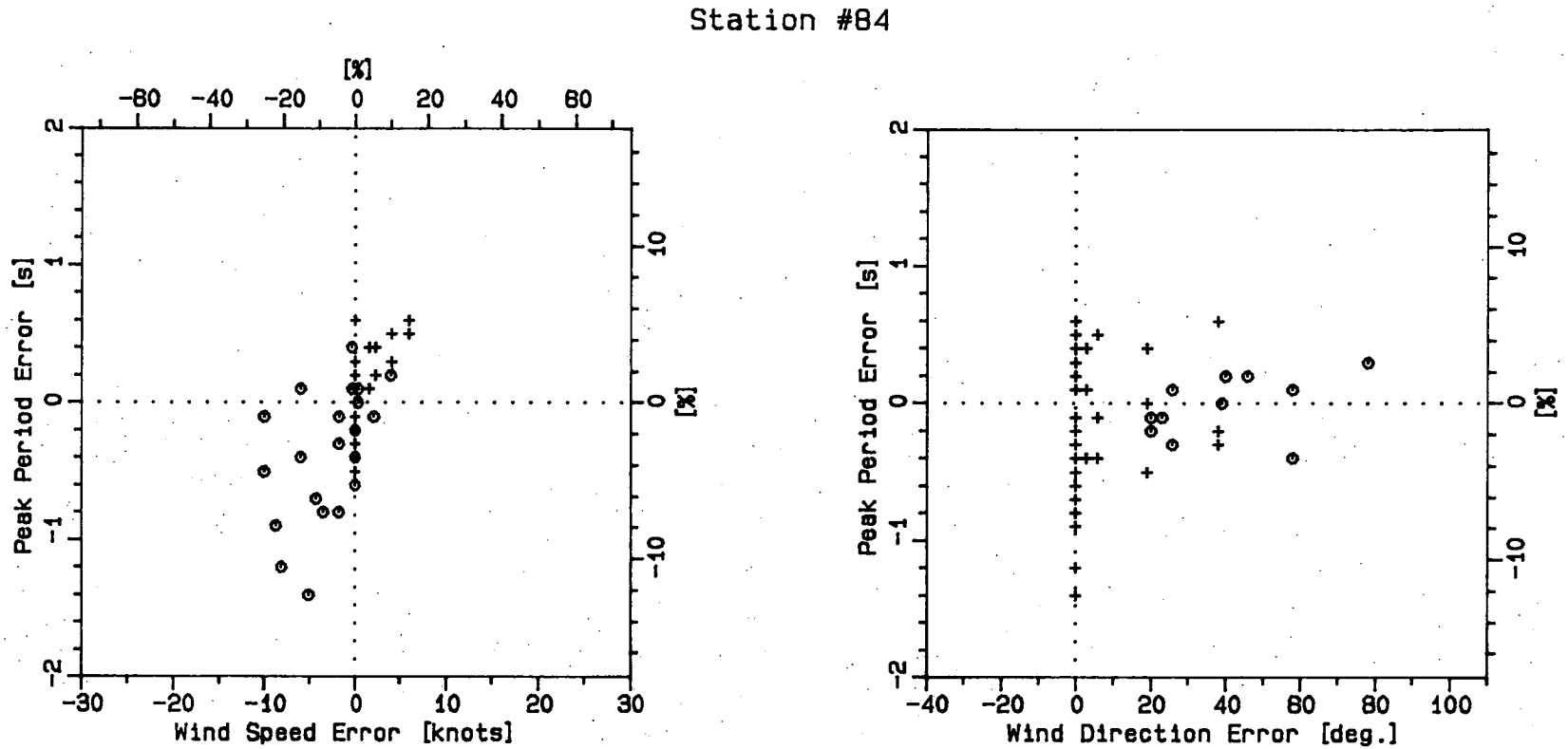

FIGURE 2.20 CONTINUED...

Station #84

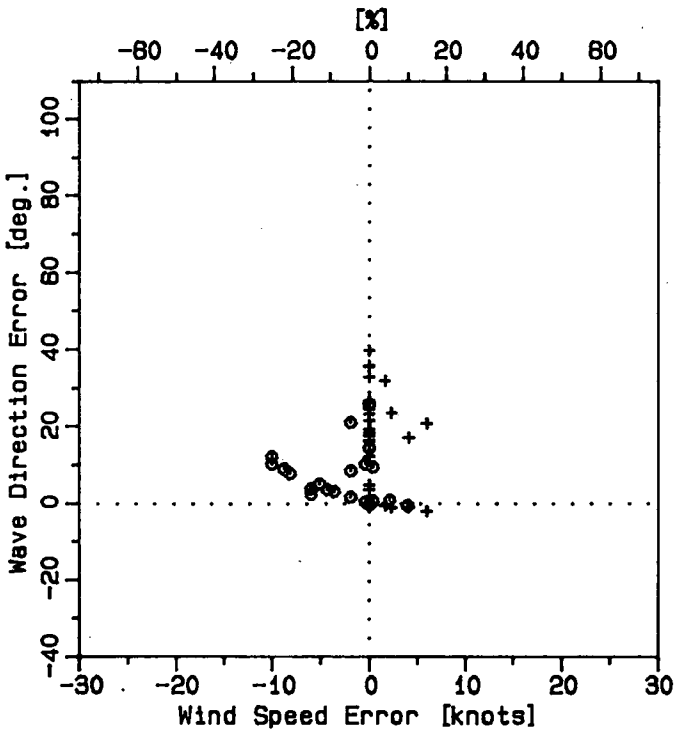

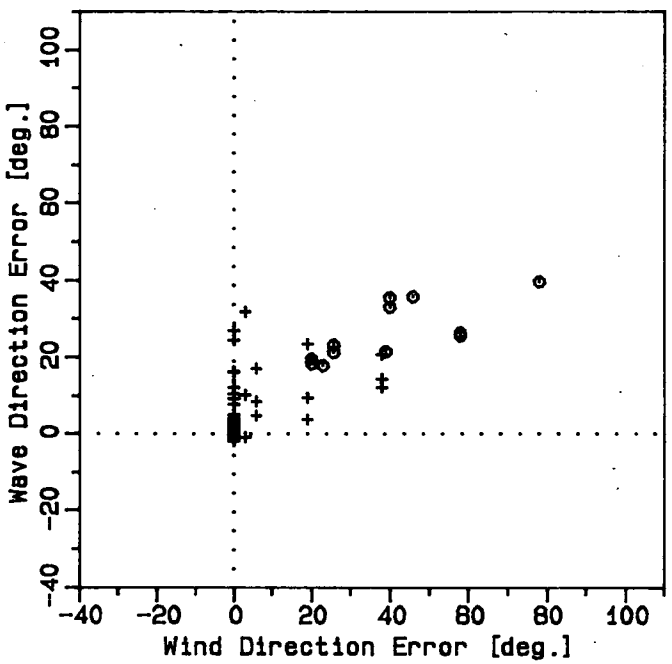

FIGURE 2.20 CONTINUED...

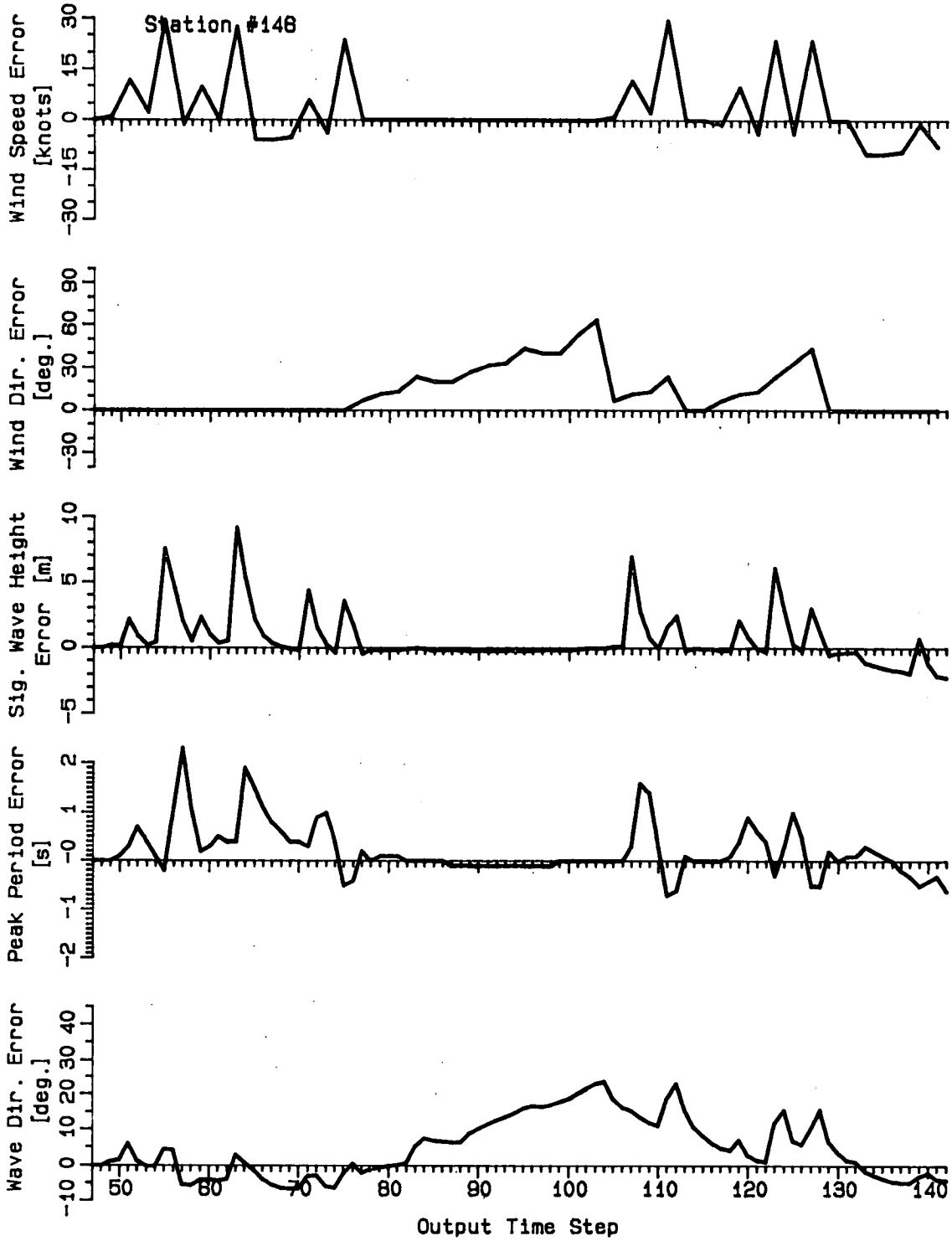

FIGURE 2.21 WAVE MODEL RESPONSE TO A PERTURBED UNIFORM STATIONARY WIND FIELD. ERRORS AT STATION 146.

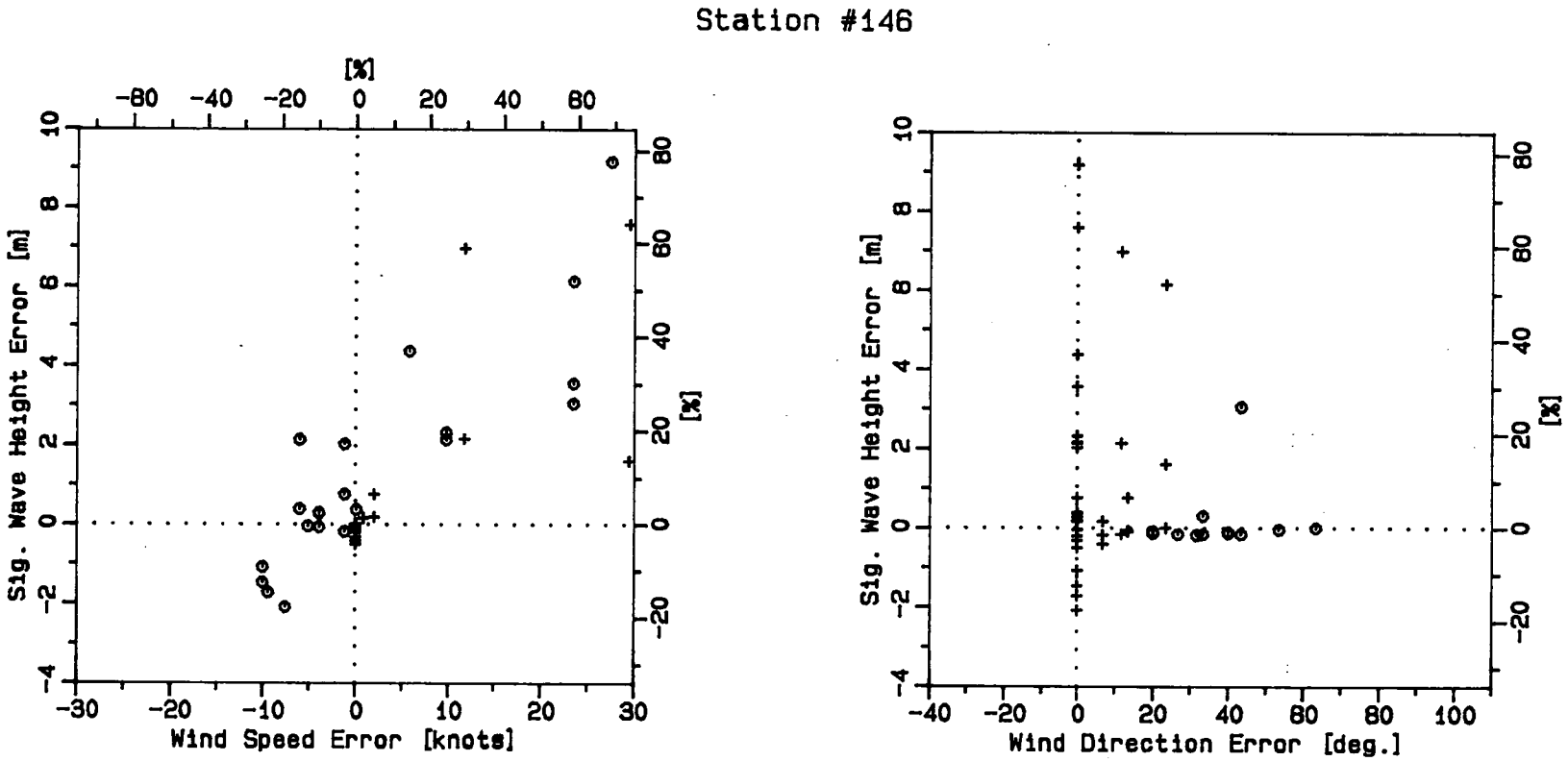

FIGURE 2.22 CORRELATION BETWEEN INPUT AND OUTPUT ERRORS AT STATION 146.

Station #146

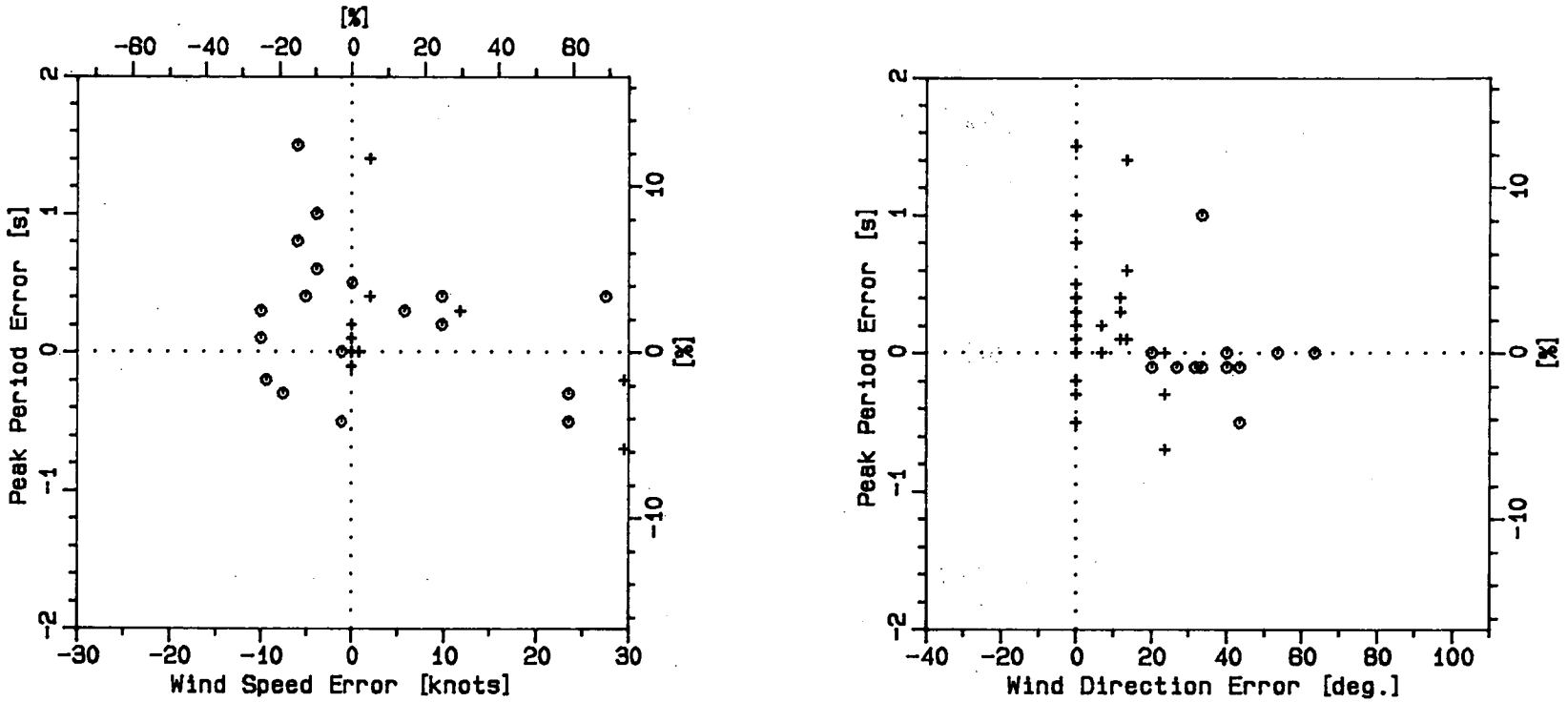

FIGURE 2.22 CONTINUED...

Station #146

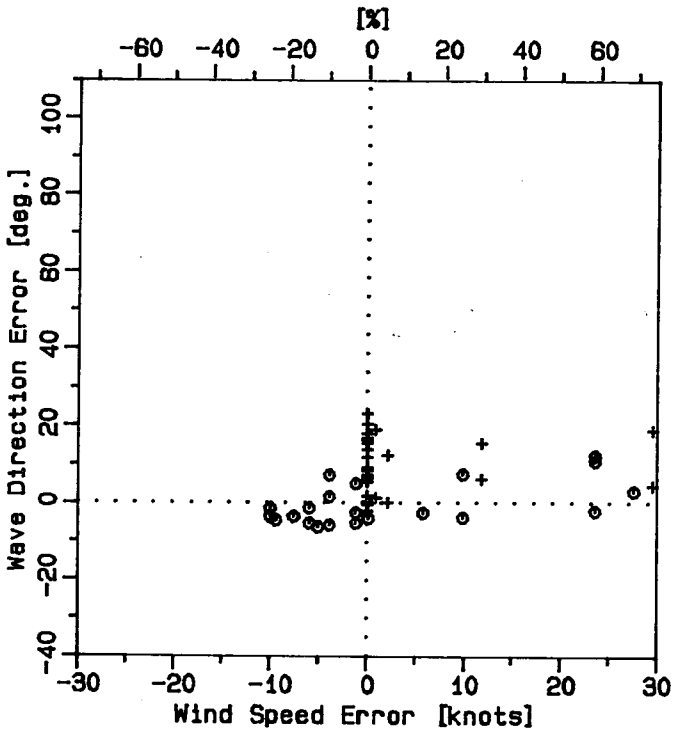

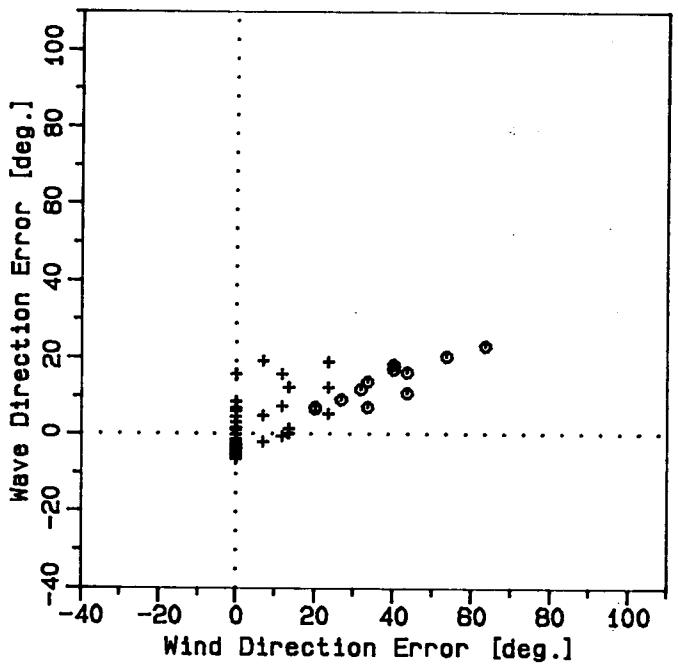

FIGURE 2.22 CONTINUED...

86% reduction in fetch. However, in this case H_s and T_p appear to be even less correlated with the error in wind direction than at Station 84. The error in H_s and T_p at that time is virtually zero. The effect of fetch on sea state can be seen in Figure 2.5. After the seas stop growing, the difference in H_s at Stations 71 and 78 (seven grid spacings along the fetch apart) is approximately 2.5 m while the difference in T_p is about 2 s. The differences are smaller when the seas are growing and this may explain the lack of correlation with the wind direction error noted above.

It should be also noted that the effect of changing fetch is rather subtle and not immediate. The amount of energy, input into the wave field locally, is not affected, only the amount of energy advected from upwind grid points. This energy propagates with the finite wave group velocity and thus arrives at the given grid point with a delay. When the error in wind direction is random and unbiased, its effect on wave height and period is minimized. At Station 84 (Figure 2.19) there is a gradual increase in H_s and T_p between time steps 80 and 105 which may be due to the increase in fetch after the wind direction turned towards the north-east (positive angle).

2.4 SYNTHETIC STORM

The unperturbed wind field, used in the previous set of tests, was independent of time and space. Real weather systems are dynamic and a realistic sensitivity test should take into consideration the time and space scales of real weather systems.

Errors in wind estimates are also not entirely random, as assumed in the previous test. In a real event hindcast the winds are determined from patterns (isobars or streamlines and isotachs) and, therefore, there will be some relationship between errors at adjacent grid points. Inspection of two sets of weather maps (for the same storm) prepared by two different weather offices indicated that there may be considerable differences between weather maps prepared by different analysts, in central pressures of a storm and in its track. For example, central pressures in a low pressure system which affected the wave conditions off the Canadian East Coast between March 9 and March 12, 1984, as given by the Canadian Meteorological Centre (CMC) surface analysis maps, differ by 0 to 11 mb from those indicated on the Atlantic Weather Centre (AWC) maps. Lower differences (0 to 2 mb) are typical south of and over the Grand Banks while

greater differences occur more frequently north of the Great Banks, most likely due to scarcity of ship reports. The positions of the low pressure centres differ by 0° to 2° in latitude and 0° to 1° in longitude. In another example, for a storm which occurred during March 26 to 29, 1984 the differences between the CMC and the AWC surface analyses were 0 to 5 mb in pressures at the centre of the low and 0° to 2° latitude, 0° to 6° longitude in the position of the centre. Figure 6.9 in Section 6.4 (page 174) shows another example of the differences in storm track between two sets of weather maps.

The effect of these errors is expected to differ from that due to completely random errors. In the case of an error in central pressure the storm track and the flow pattern are unchanged but the storm may be weakened or intensified. In the case of an error in the location of the storm centre the flow pattern is again unchanged but shifted with respect to the unperturbed position. Thus neighbouring grid points are affected in a similar way and the total effect is likely to be greater.

The set of tests described in this section is intended to investigate the sensitivity of the Resio model to these

two types of non-random errors. A synthetic input was again used for the sake of simplicity.

The synthetic storm is caused by a low pressure system travelling in a north-easterly direction across the model grid (Figure 2.23). The storm deepens as it moves along its track until it reaches about half way across the grid. After that the central pressure increases again as the storm moves out of the generating area (Figure 2.24). The linear variation of the pressure drop at the storm centre is intended to simulate, in the simplest way, the growth and decay of the storm.

On square projection the pressure distribution as a function of distance from the centre of the storm, r (in degrees latitude/longitude), is given by

$$P(r) = 1016. - \delta P \exp\{-\frac{1}{a}(\frac{r}{b})^{a}\} \qquad (12)$$

where δP is the pressure drop at the centre of the storm and the constants are a = 1.25 and b = 4.0 degrees. The isobars are circles on the square projection but not on the spherical earth. The flow is counter-clockwise around the centre with

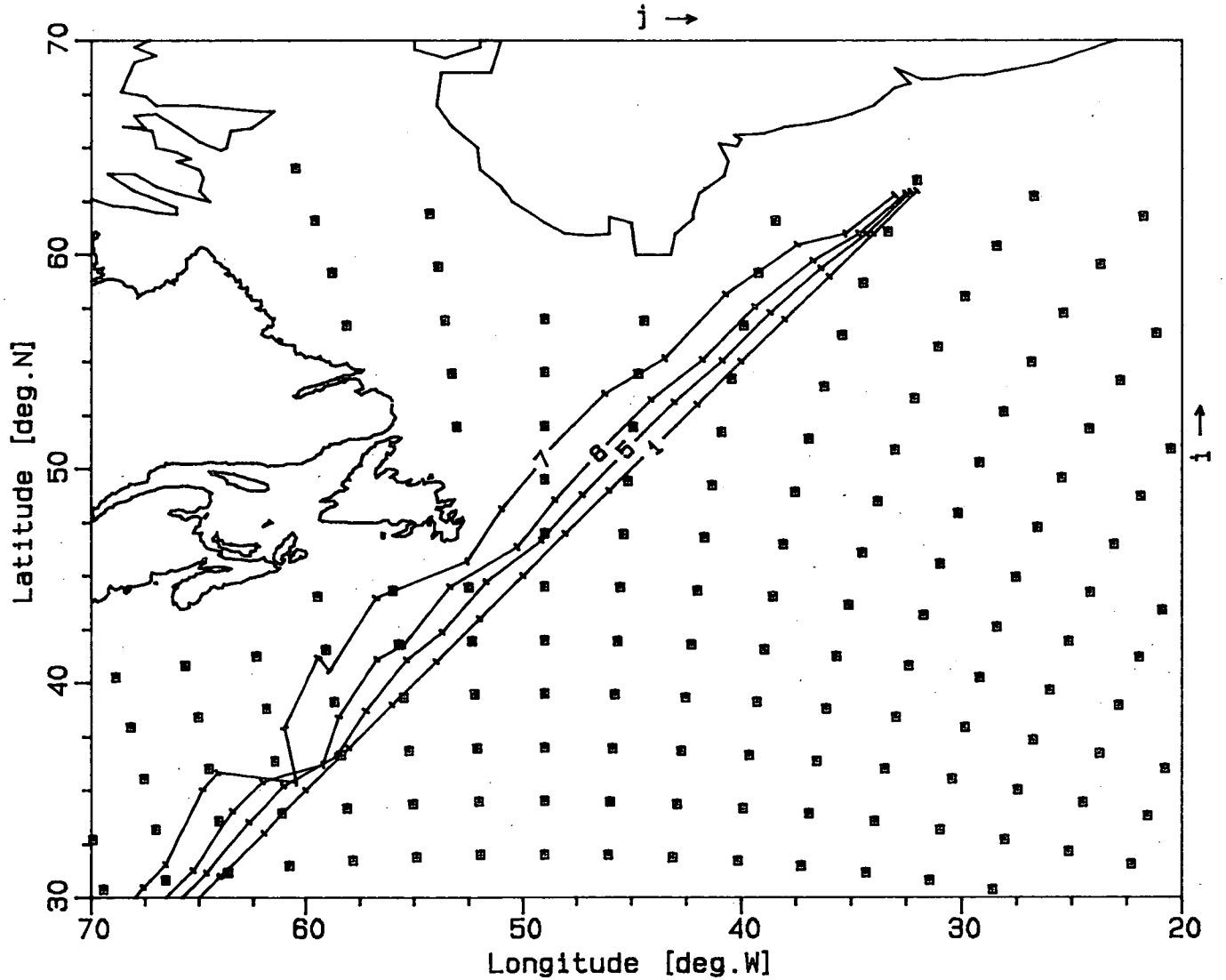

FIGURE 2.23 SYNTHETIC STORM TRACKS. (1 UNPERTURBED; 5 TO 7 PERTURBED)

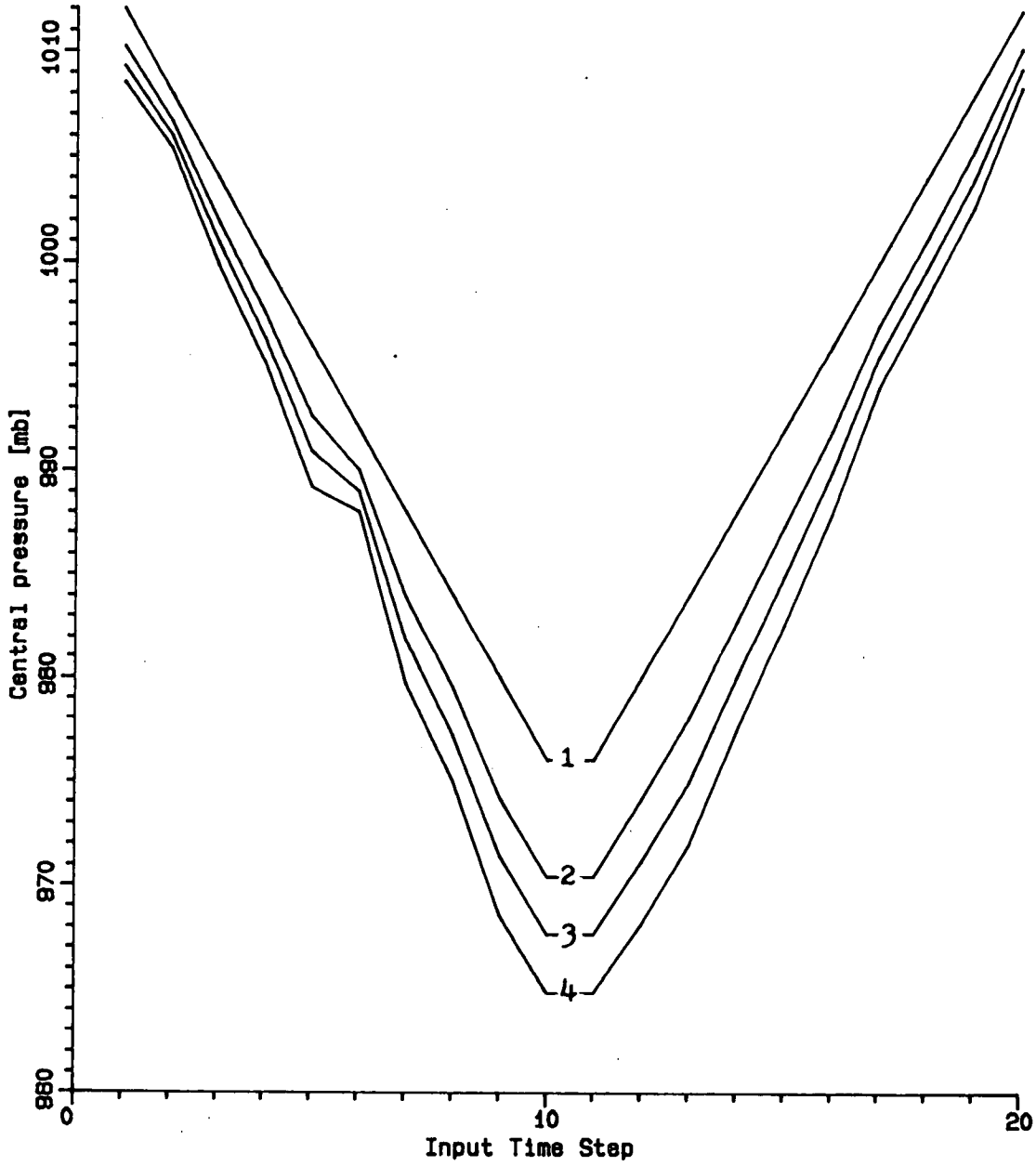

FIGURE 2.24 EVOLUTION OF CENTRAL PRESSURE IN SYNTHETIC STORM. (1 UNPERTURBED; 2 TO 4 PERTURBED)

the wind vectors deflected 15° from along the isobars towards the centre. Wind speed is given by

$$u(r) = C\, u_g = C \frac{1}{\rho_a f} \frac{dP}{dr} \qquad (13)$$

where ρ_a is the air density taken at 0°C and at pressure P, and f is the Coriolis parameter varying with latitude. Constant C relates the surface wind speed, u, to the geostrophic wind, u_g. According to the U.S. Army Coastal Engineering Research Center's Shore Protection Manual (1977), for neutral air mass stability the average surface wind speed over water is about 60% of the free air value which, in turn, when corrected for isobar curvature, is about 90% of the geostrophic wind speed. For the present application the value of C is not critical; $C \approx 0.57$ was selected as giving reasonable wind speeds. Including units conversion in equation (13), it becomes

$$u(r) = \frac{2800}{f\ P} \frac{dP}{dr}$$

where P is in millibars, r in degrees latitude and u in knots.

The straight track of the reference storm together with three tracks of storms in which the storm centre velocity is

perturbed by a random error are shown in Figure 2.23. (Note that the reference track is straight only on the square projection shown; on the spherical Earth the track is curved towards the north). Only that part of the tracks which lies within the grid area is shown; each track starts at 25°N and 70°W. Ticks mark the distance travelled during one 6 h interval. The RMS error of the storm speed for tracks 5, 6 and 7 is 0.3, 0.6, and 1.2 degrees/time step, respectively. (For comparison see also Figure 6.9 in Section 6.4 which was prepared after the tests described here had been completed. It shows differences in storm track possibly larger than those assumed here.)

The central pressure drop δP varies along the storm track as shown in Figure 2.24 (the spin-up portion of the simulation is not included in the time step count). Curve 1 corresponds to the reference storm while curves 2, 3 and 4 correspond to storms in which the central pressure is perturbed by a random amount. The RMS of this perturbation is 1.0 mb for storm 2, 1.5 mb for storm 3 and 2.0 mb for storm 4. These perturbations are comparable to the differences between the two sets of real event surface analyses discussed at the beginning of this section. All four storms

move along the same track. The resulting wind field has a random biased error in speed but no error in direction.

2.4.1 Errors in Central Pressure

The time series of wind speed and direction, significant wave height, peak period and mean wave direction for selected grid points are shown in Figures 2.25 to 2.27. In order to clearly show trends the time series are represented by continuous lines even though the model inputs and outputs are given at discrete time steps. The lines representing directions are interrupted where the directions change more than 180° in one step. The storm develops very rapidly, and as a consequence the development of the seas is limited by duration. During the growth stages the evolution of the significant wave height and peak period lags the evolution of the wind speed. As follows from equation (1), at each time step the wave parameters are determined not only by the wind speed and direction at that time step but also by the past history of the wind field. Therefore no attempt has been made to correlate time specific input and output errors, more meaningful comparison is made between error statistics pertaining to the whole storm.

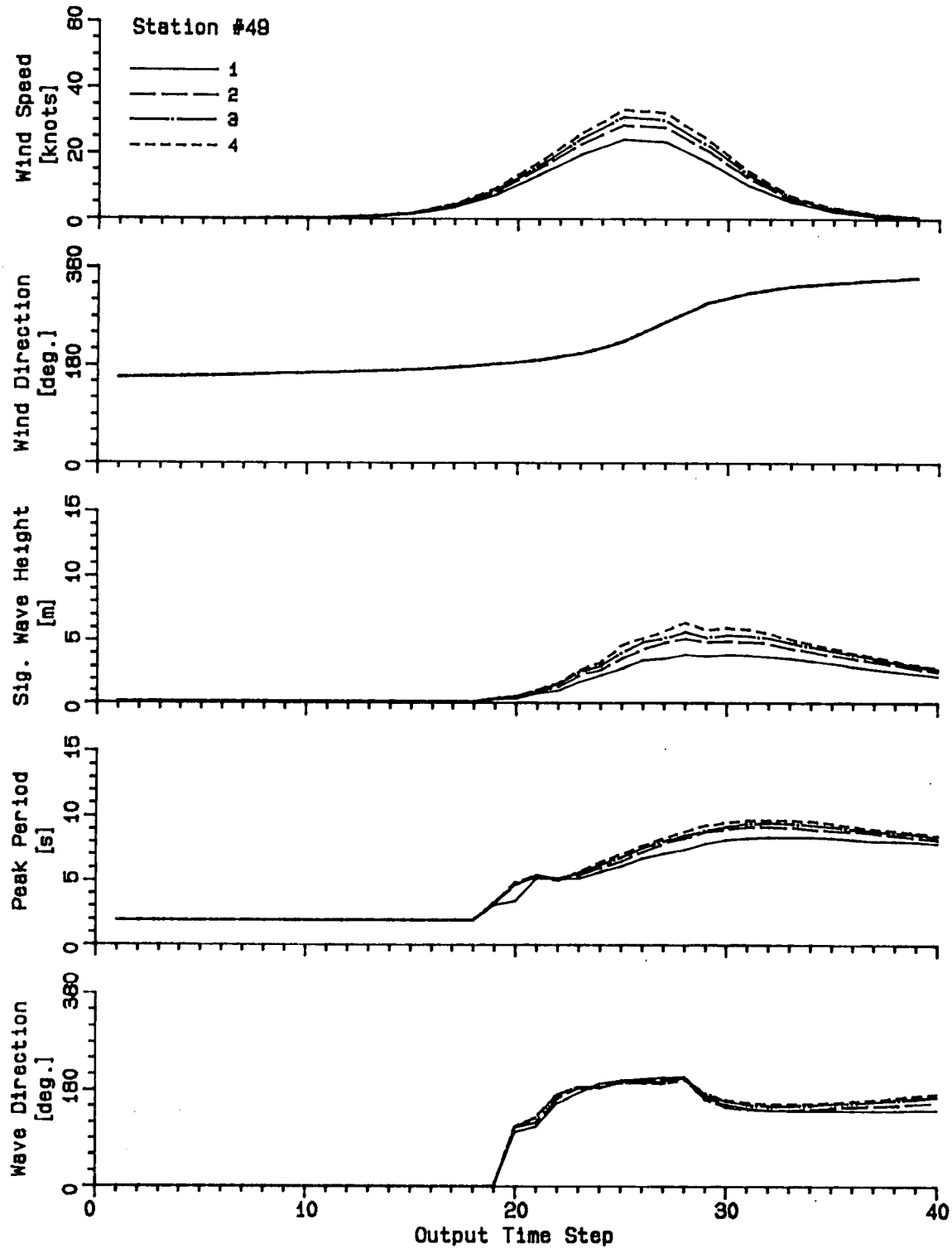

FIGURE 2.25 WAVE MODEL SENSITIVITY TO ERRORS IN CENTRAL PRESSURE. RESPONSE AT STATION 49.

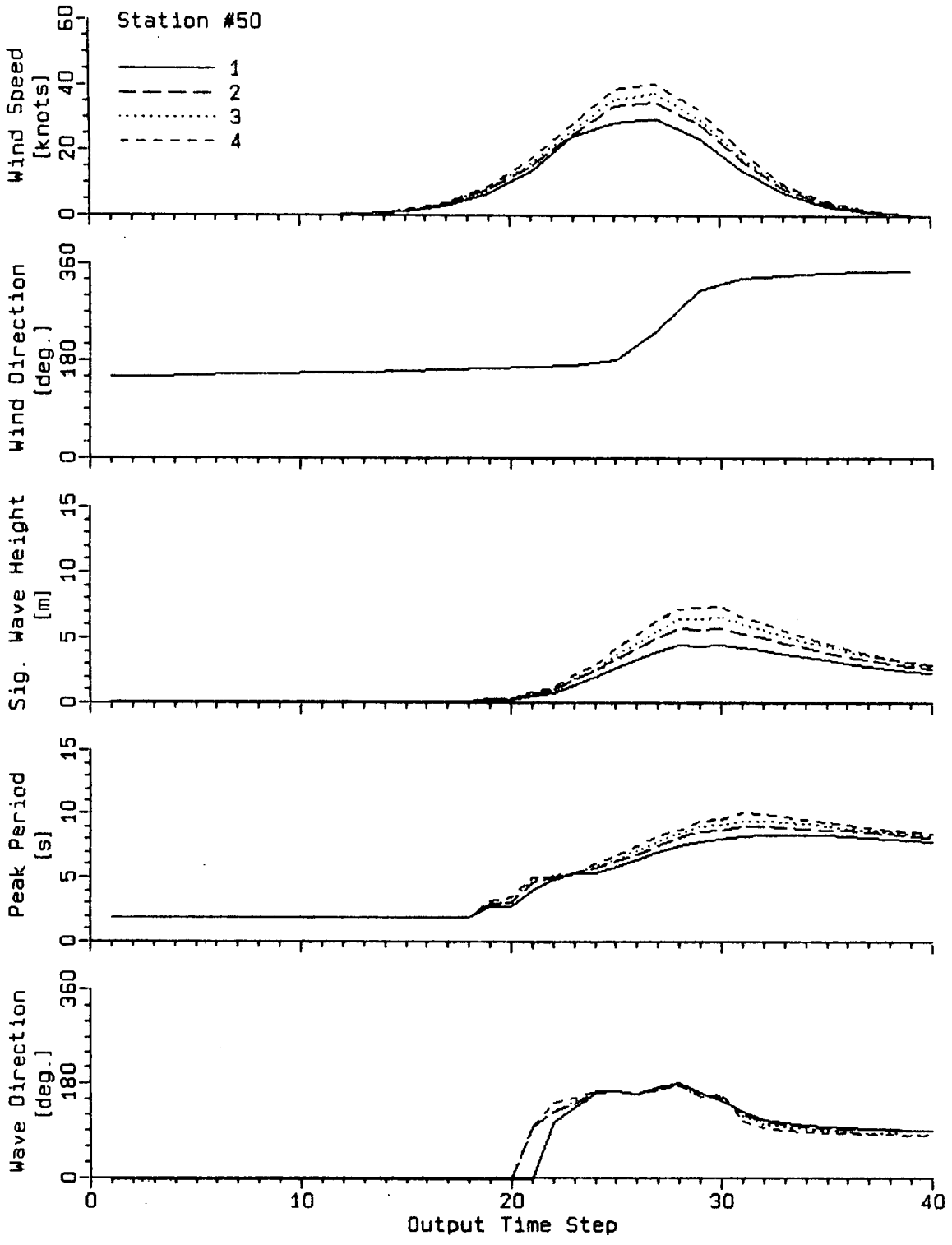

FIGURE 2.26 WAVE MODEL SENSITIVITY TO ERRORS IN CENTRAL PRESSURE. RESPONSE AT STATION 50.

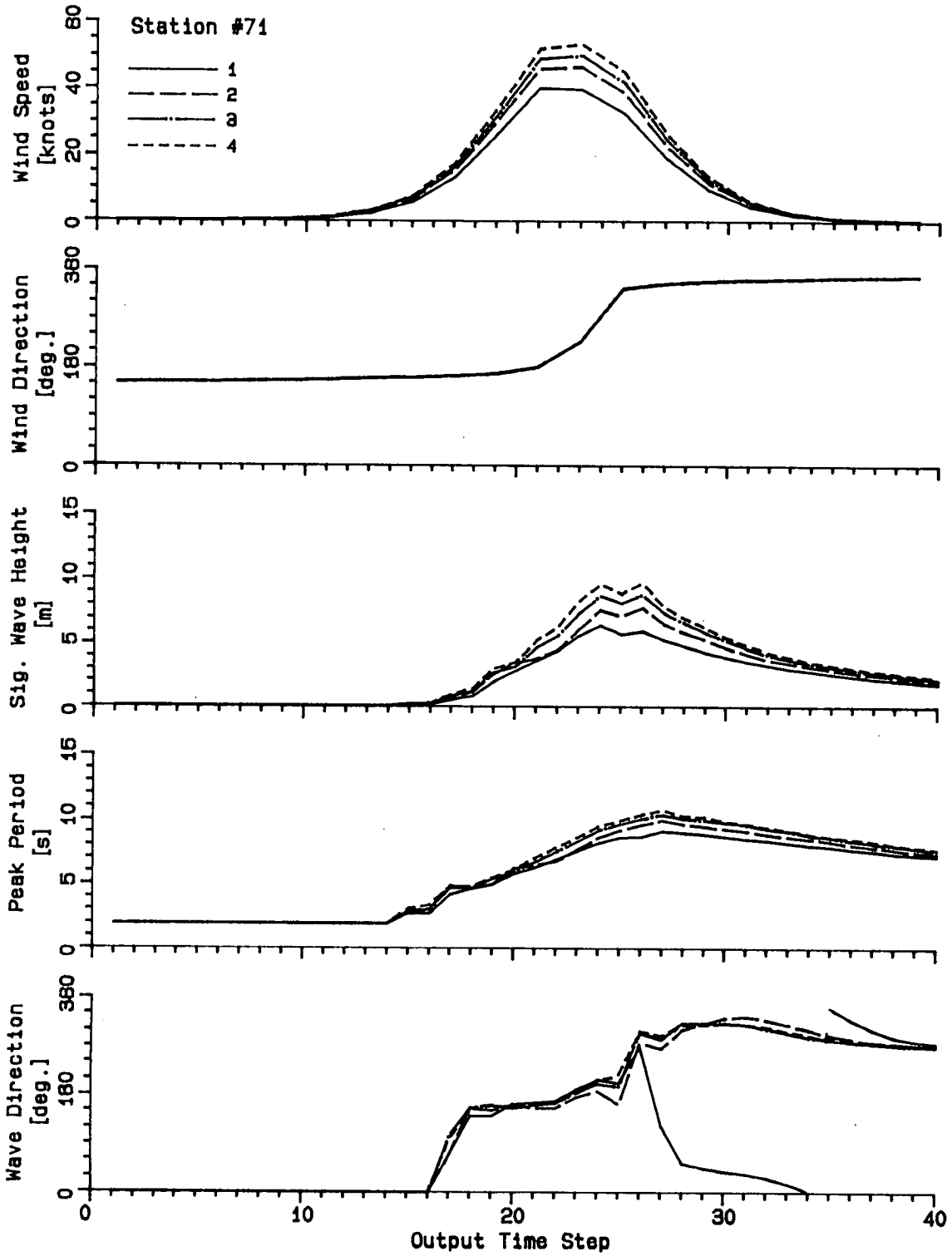

FIGURE 2.27 WAVE MODEL SENSITIVITY TO ERRORS IN CENTRAL PRESSURE. RESPONSE AT STATION 71.

Table 2.6 shows the relationship between the bias and RMS errors of input and output parameters at the selected stations. The errors are expressed as a fraction of the unperturbed value, for example:

$$\text{Bias}(H) = \frac{1}{n - m} \sum (\delta H_i / H_i)$$

$$\text{RMS}(H) = \left\{\frac{1}{n-m-1} \sum (\delta H_i / H_i - \text{Bias})^2\right\}^{1/2}$$

where δH_i is the error in the parameter H_i at time step i; m and n are, respectively, the first and last time step where wind speed (for input) or H_s (for output) reach certain threshold. For wind speed the threshold is 2 knots while for H_s and T_p the threshold is H_s = 1 m. Summation is from i = m to i = n.

Direction parameters are not included in the table. It appears from Figures 2.25 to 2.27 that the mean wave direction is only loosely related to the local wind direction. The most likely explanation for this lies in the relatively small size of the synthetic storm and in its track which passes directly over some of the stations. Outside the small area of the cyclonic system the winds, and initially the waves, are almost zero. At a particular grid point (see for example

TABLE 2.6. ERROR STATISTICS FOR PERTURBED CENTRAL PRESSURE TEST

	Relative Error														
	Wind Speed					Sig.Wave Height					Peak Period				
	Bias	RMS	Min.	Max.	Steps	Bias	RMS	Min.	Max.	Steps	Bias	RMS	Min.	Max.	Steps
Stn. 49 Test 2	.18	.03	.00	.25	20	.24	.05	.00	.33	19	.07	.03	.00	.12	19
Test 3	.27	.04	.00	.36	20	.36	.08	.00	.49	19	.10	.03	.00	.15	19
Test 4	.36	.05	.00	.47	20	.46	.12	.00	.64	19	.13	.05	-.02	.19	19
Stn. 50 Test 2	.18	.03	.00	.26	21	.22	.06	.00	.32	18	.07	.03	.00	.11	18
Test 3	.28	.05	.00	.40	21	.36	.08	.00	.49	18	.10	.04	.00	.17	18
Test 4	.37	.07	.00	.54	21	.48	.13	.00	.67	18	.14	.06	-.02	.23	18
Stn. 61 Test 2	.18	.02	.00	.20	20	.22	.03	.00	.28	20	.06	.02	.00	.11	20
Test 3	.26	.03	.00	.31	20	.34	.05	.00	.44	20	.09	.02	.00	.16	20
Test 4	.35	.05	.00	.41	20	.46	.10	.00	.62	20	.13	.04	.00	.22	20
Stn. 63 Test 2	.18	.03	.00	.25	18	.30	.06	.00	.43	16	.06	.08	-.22	.10	16
Test 3	.27	.04	.00	.37	18	.46	.07	.00	.62	16	.12	.08	-.19	.17	16
Test 4	.37	.06	.00	.49	18	.66	.11	.00	.83	16	.16	.09	-.16	.22	16
Stn. 84 Test 2	.16	.03	.00	.20	21	.20	.11	.00	.42	25	.08	.04	.00	.16	25
Test 3	.24	.04	.00	.29	21	.33	.15	.00	.57	25	.12	.05	.00	.19	25
Test 4	.32	.06	.00	.40	21	.35	.18	.00	.67	25	.13	.05	.00	.20	25
Stn. 71 Test 2	.17	.03	.00	.21	20	.17	.07	.00	.31	22	.05	.03	-.01	.10	22
Test 3	.26	.04	.00	.31	20	.29	.09	.00	.47	22	.10	.03	.00	.16	22
Test 4	.34	.05	.00	.41	20	.38	.11	.00	.63	22	.12	.04	.00	.20	22

Station 50 in Figure 2.26) the waves start noticeably growing only after the storm centre approached sufficiently close. After a few time steps the wave direction approximately matches the local wind direction, however, as the storm centre passes over the area of the grid point and the storm peaks there, the local wind direction rapidly changes by 180°. At that time most of the wave energy still propagates in the old direction but new energy is input with the opposite direction. The result is a change in the mean wave direction but since the winds quickly abate the new wave direction never approaches the new wind direction. Similar behaviour can be seen in all plots for stations close to the storm centre track. The wave direction varies somewhat from one test to another even though the wind direction is the same for all the tests. This is because the proportion of energy input into the wave field during the intensification and during the abatement of the storm differs between tests.

The input relative errors are approximately the same at all grid points since only δP in Equation (12) is perturbed. The small differences in Table 2.6 are most likely due to numerical rounding errors. The input errors are strongly biased, their RMS is only about 11 to 19% of the bias. The corresponding significant wave height and peak period errors

are also biased but the ratio between the RMS and the bias is greater (0.14 to 0.15 for H_s and 0.22 to 1.33 for T_p).

The ratio between the H_s bias and the wind speed bias appears to be related mainly to the strength of the mean wind. It is the largest (1.64 to 1.80) at Station 63 which is the farthest away from the storm track and has the largest proportion of swell. It is the smallest (0.99 to 1.14) at Station 71 which was exposed to the strongest winds. Typical ratios at the remaining stations are between 1.20 and 1.35. This result is not surprising since in the area along the storm track the wave energy is mainly of local origin and therefore it is affected primarily by the bias in the local winds. Away from the track the contribution due to advected energy is more important and the effect of wind speed bias becomes cumulative.

The ratios between the RMS errors of H_s and the RMS errors of wind speed exhibit a different behavior. At Station 71 this ratio ranges between 2.4 and 2.9 while at Station 63 it is only between 1.6 and 1.9. The ratio is the largest at Station 84 (3.0 and 3.7). Both Station 71 and Station 84 are grid points adjacent to the boundary while Station 63 is an interior point. Thus it seems possible that a large portion of the RMS error at the boundary points is

not due to the input errors but rather to numerical errors which were discussed in Section 2.3.2.

No clear pattern can be recognized in the ratio between bias in peak period errors and bias in wind speed errors or in the ratios between the corresponding RMS errors. The former vary between 0.30 and 0.53, and they are the largest at Station 84, the latter vary between 1.1 and 2.5, and are the largest at Station 63.

2.4.2 Errors in Storm Track

In this sensitivity test the pressure at the centre of the storm varies according to curve 1 in Figure 2.24, identically for all four test storms. The storm track, however, is subject to a random unbiased perturbation with a RMS error of 0.3, 0.6, and 1.2 degrees per 6 hour time step for track 5, 6, and 7 respectively. As a result, both the wind speed and the wind direction have a biased random error. The errors in wind direction can be substantial even for a small deviation from the correct track where the perturbed storm centre passes on the opposite side, compared with the reference storm, of a particular grid point (for example Stations 71 or 84). The error in wind speed can also be disproportionate,

for example when the storm track passes directly over a grid point. This, however, is not apparent in the present test. The synthetic storm employed in the test has a relatively sharp centre and even though track 5 passes almost exactly over Station 71, the wind speed does not drop there. This is probably due to the discretization of the wind fields in time and space and the subsequent interpolations.

Time series plots of the input and output variables at the selected grid points are shown in Figures 2.28 to 2.32. As would be expected the effect of the track perturbation on the wind speed at a particular point is mainly a shift in time of the storm evolution pattern but there is also a difference in the maximum speed attained during the storm. The effect on the evolution of significant wave height is similar: a shift in time and possibly a change in the maximum H_s. The peak period plots show an unexpected behaviour in the initial stages of wave growth. This is most likely due to switching between the parametric and discrete domains of the model. The relationship between the wind and wave directions is again determined by the relative amounts of energy input into the wave field during the growth and decay stages of the storm, as described in the previous section. However, since not only the wind speed changes

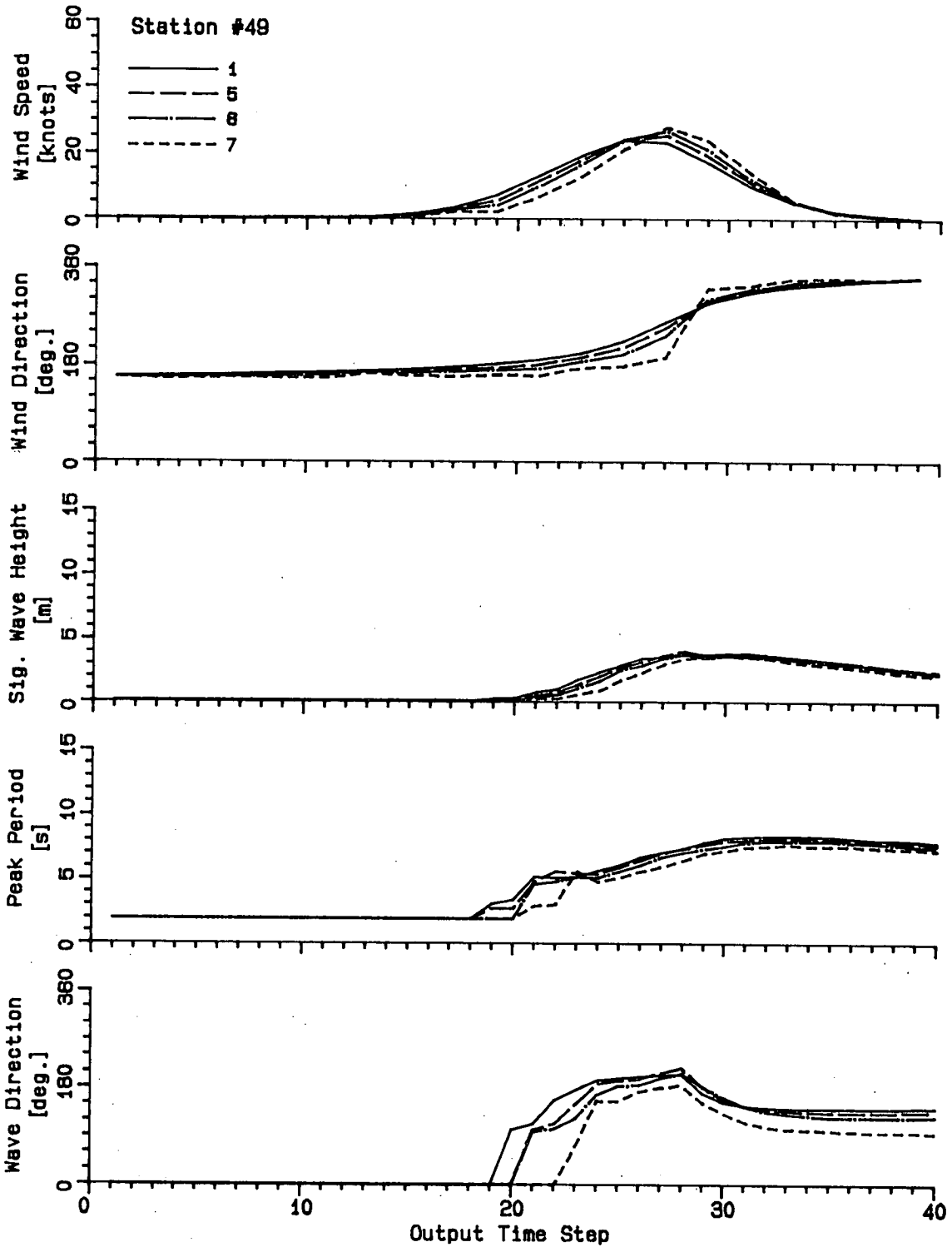

FIGURE 2.28 WAVE MODEL SENSITIVITY TO ERRORS IN STORM TRACK. RESPONSE AT STATION 49.

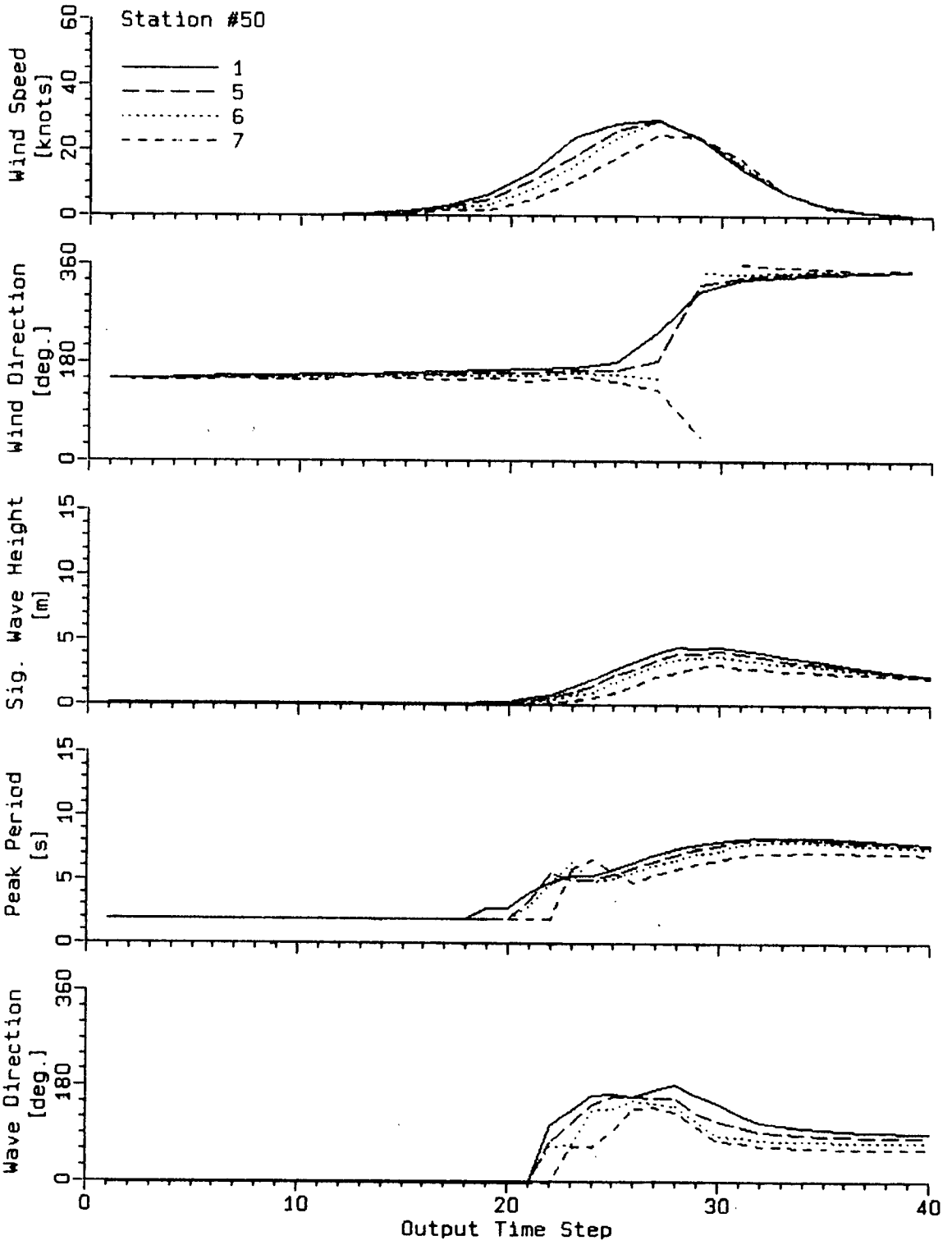

FIGURE 2.29 WAVE MODEL SENSITIVITY TO ERRORS IN STORM TRACK. RESPONSE AT STATION 50.

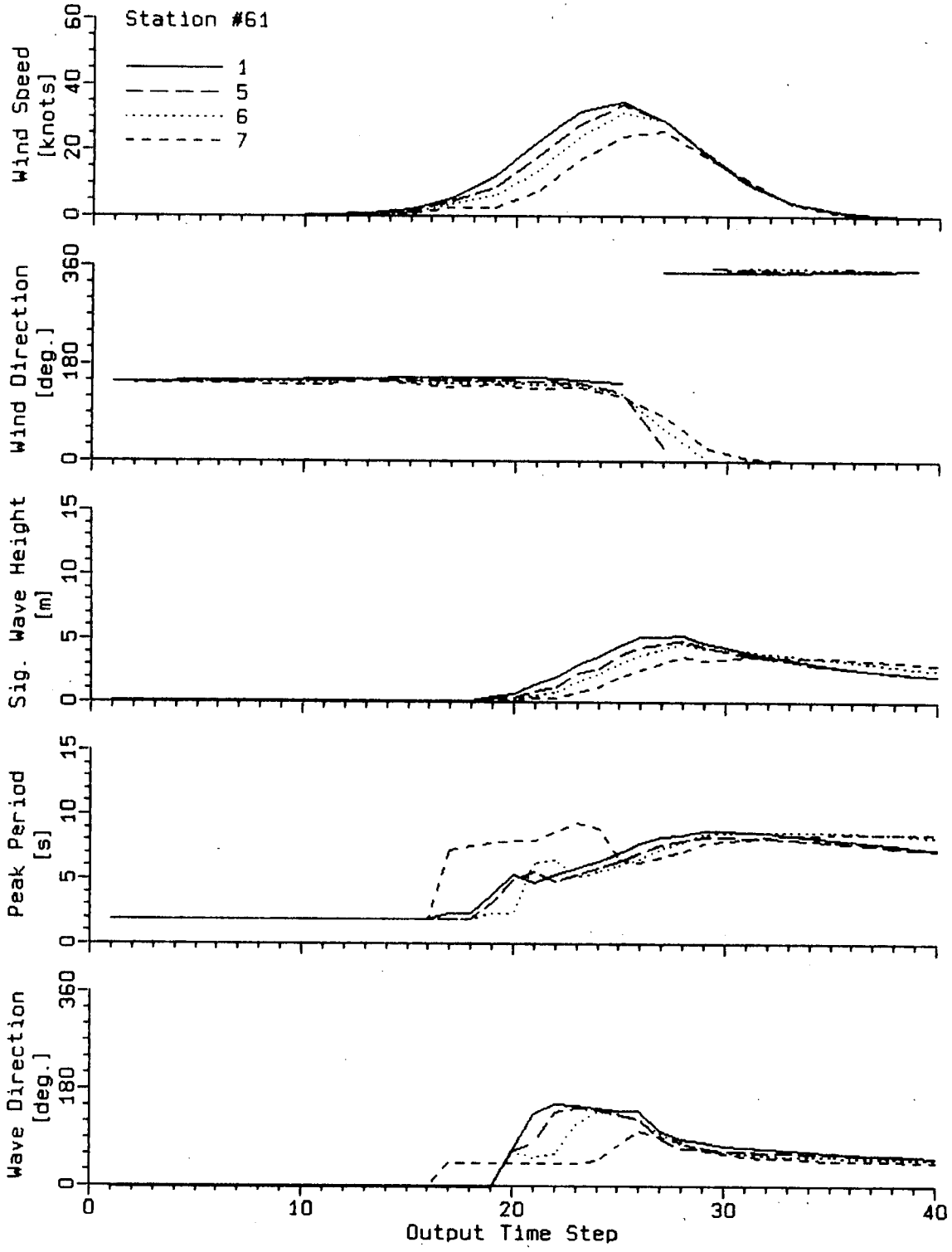

FIGURE 2.30 WAVE MODEL SENSITIVITY TO ERRORS IN STORM TRACK. RESPONSE AT STATION 61.

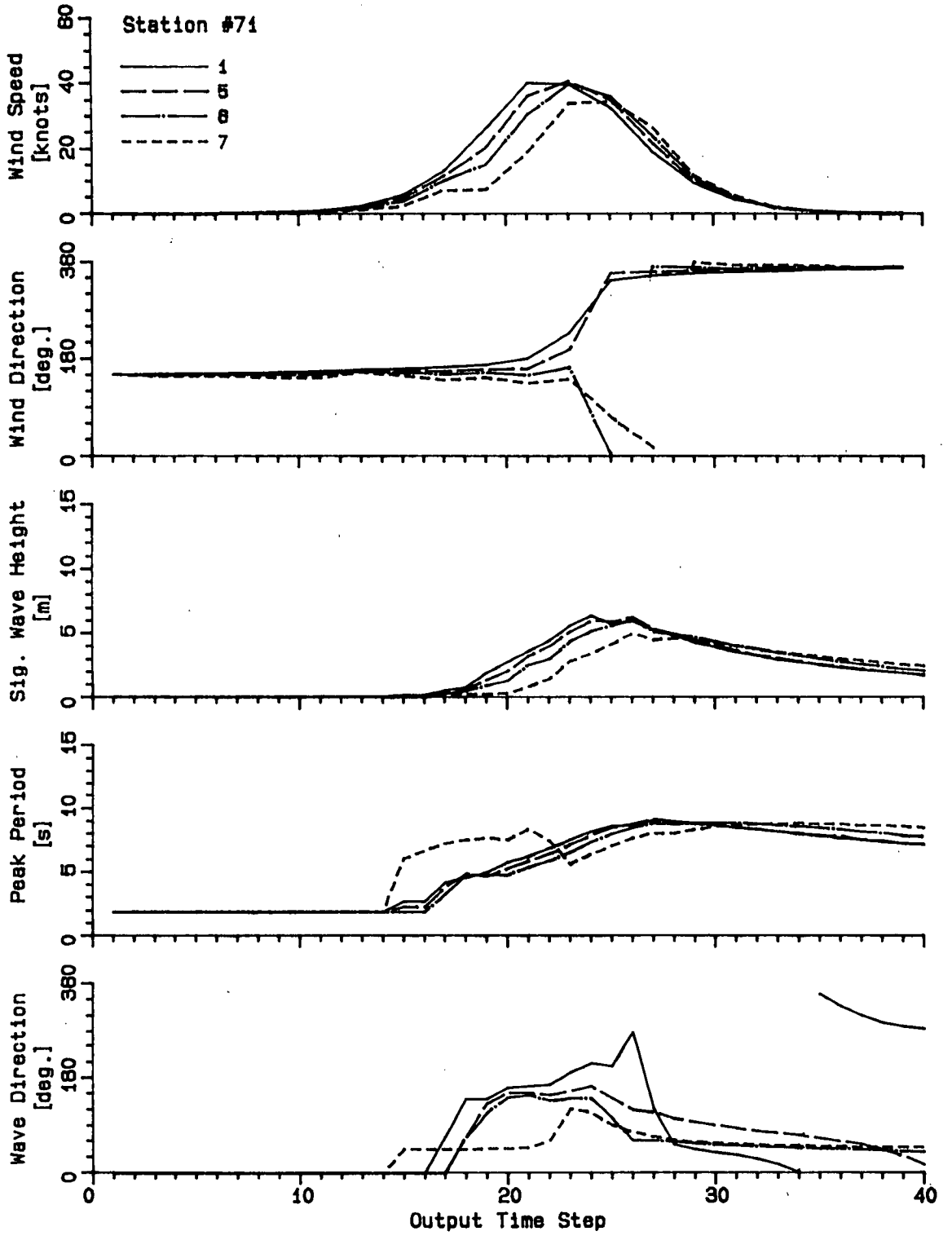

FIGURE 2.31 WAVE MODEL SENSITIVITY TO ERRORS IN STORM TRACK. RESPONSE AT STATION 71.

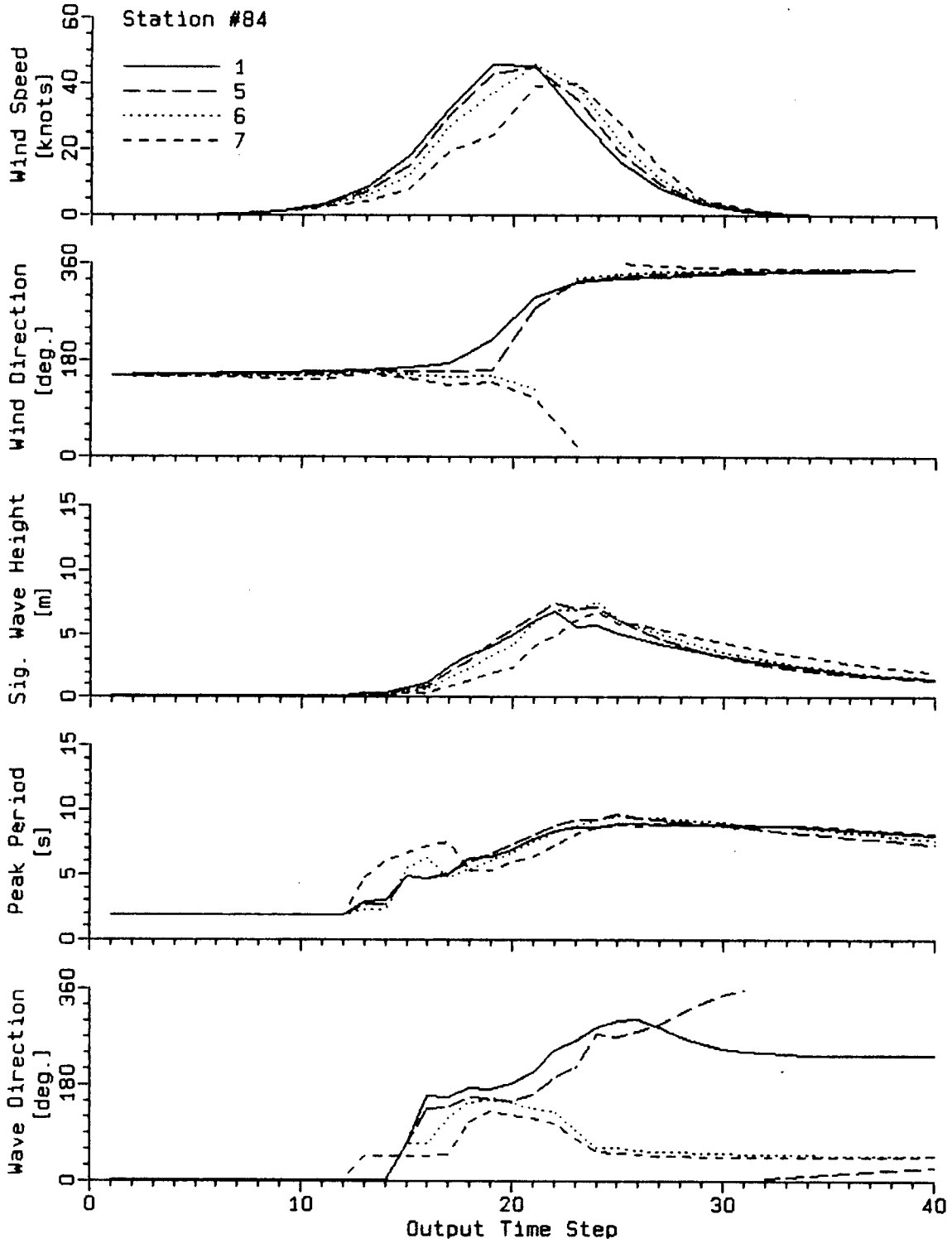

FIGURE 2.32 WAVE MODEL SENSITIVITY TO ERRORS IN STORM TRACK. RESPONSE AT STATION 84.

between the tests runs but also its direction, the differences in the wave directions between the test runs are more dramatic.

An attempt has been made to relate the local wind speed bias and RMS errors with the bias and RMS errors in the significant wave height and the peak period. However, this was not successful. This could be expected since the sea state at one point is a combination of energy input locally, and energy advected from other grid points. The change in the wind forcing at a particular grid point depends on the position of that grid point with respect to the perturbed storm track. Thus the local input and the advected wave energy are not affected by the perturbation in the same way and consequently the errors in the wave parameters cannot be correlated with errors in the local wind forcing.

2.5 CONCLUSIONS AND RECOMMENDATIONS

The purpose of the tests presented in this section was to provide information on the response of the wave model to errors in input wind fields. Due to the number of factors involved in this response the results are primarily qualita-

tive and only a few quantitative conclusions may be drawn.

The first test provides an indication of the basic accuracy of the model simulation assuming zero error in the input wind fields. The errors in significant wave height appear to be the largest at grid points adjacent to the upwind boundary where they are of the order of 1/2 m for the test wind of 40 knots and they diminish rapidly with distance away from the boundary. It is therefore recommended that the model grid should be designed in such a way that the grid points for which a hindcast is required should not be immediately adjacent to the boundary. The errors in peak period in this test are small and less then the period resolution of the discrete spectrum. The errors in mean wave direction are in general the largest close to the model boundaries and they diminish towards the interior. In the Grand Banks area this error reaches 14° for the 40 knot westerly wind which, however, is smaller than the directional resolution of the discrete spectrum.

Three types of errors in the input wind fields were considered in this study: errors in wind speed and wind direction random in space and in time; errors in pressure at the centre of a low pressure system which cause weakening or

intensification of the storm; and errors in storm track which result in a displacement of the storm from its correct location.

In the first case there is a large scatter in the correlation between local input errors and the errors in the resulting wave parameters due to advection from surrounding grid points. Where the advected errors are small the correlation between the input and output percent errors is closer and consistent with relationships following from the JONSWAP results. Errors in wind direction have only a small effect on the errors in wave parameters.

Errors in central pressure result in a bias in the input wind speeds and consequently in a bias in the computed wave parameters. The relative bias in the significant wave height is larger than the relative bias in the wind speed, their ratio ranging approximately 1 in areas of strong winds to 1.8 in areas further away from the storm track which contain a large proportion of swell.

Errors in the position of the storm track lead to errors in both wind speed and wind direction. The response of the model is therefore more complex. In general there is

shift in the time evolution of the wave parameters as well as an increase or decrease in their magnitude. The response depends strongly on the relative position of the hindcast site with respect to the unperturbed and perturbed storm track with the greatest differences occurring when the track passes close to the hindcast site.

3. SENSITIVITY TO GRID SPACING AND TIME STEP

3.1 INTRODUCTION

In order to numerically solve the energy balance equation (1) the space and time variables must be discretized. It can be expected that the resolution with which this discretization is achieved affects the accuracy and stability of the numerical solution. The grid spacing determines the resolution of land boundaries, and of the spatial structure of the input wind fields, as represented in the model. The grid spacing may also limit how well a grid point can be matched with a location for which a hindcast is required. Obviously it is preferable to use as small a grid spacing and

time step as allowed by the available computer resources.

Hodgins et al.(1985) suggest that in order to model variations in wind on either side of and along fronts embedded in large-scale winter storms occurring on the East Coast, the model grid should be capable of resolving features as small as 50 km. Moreover, to properly delineate fetch and resolve coastline features or marginal sea ice zones would require resolution of about 20 km. These requirements seem to be rather extreme and impractical in the context of a single grid model. The technique of wind analysis presently in use at MEDS is not likely to resolve features of scale smaller than about 150 nautical miles (278 km). Thus little advantage would be gained by substantially decreasing the wave model grid spacing except in areas close to the coast. Because of this, only the sensitivity to moderate (20%) changes in grid spacing has been tested in this study.

The standard spherical orthogonal grid employed by MEDS has a nominal spacing of 150 nautical miles (278 km). In the following sensitivity tests two non-standard grids were used: a coarse grid with a nominal spacing 20% larger than the standard (180 nautical miles or 333 km) and a fine grid with a nominal spacing 20% smaller (120 nautical miles or 222 km).

Figures 3.1 and 3.2 show, respectively, the coarse and the fine grids superimposed on the regular grid. Additional tests were made with the standard and the fine grids modified by including additional sea grid points along the western boundary. This provided an indication of the model sensitivity to a change in fetch. In Section 2.3.2 it was pointed out that some of the grid points of potential interest are the first active grid points adjacent to the land boundary, and that this may have a detrimental effect on the hindcast results. By inserting additional grid points along the boundary this effect could be evaluated for real case hindcasts.

The temporal resolution of the input is usually determined by the synoptic times of weather analysis maps (or the temporal resolution of other available atmospheric data) and not by the wave model time step. However, for a given grid spacing, δs, the model time step, δt, is limited by the Courant stability condition (Resio et al., 1978)

$$c_g \frac{\delta t}{\delta s} \leq 2$$

The non-standard time steps tested here were 4 hours and 2 hours respectively which represent about ±33% change from the standard time step. All the resulting combinations of

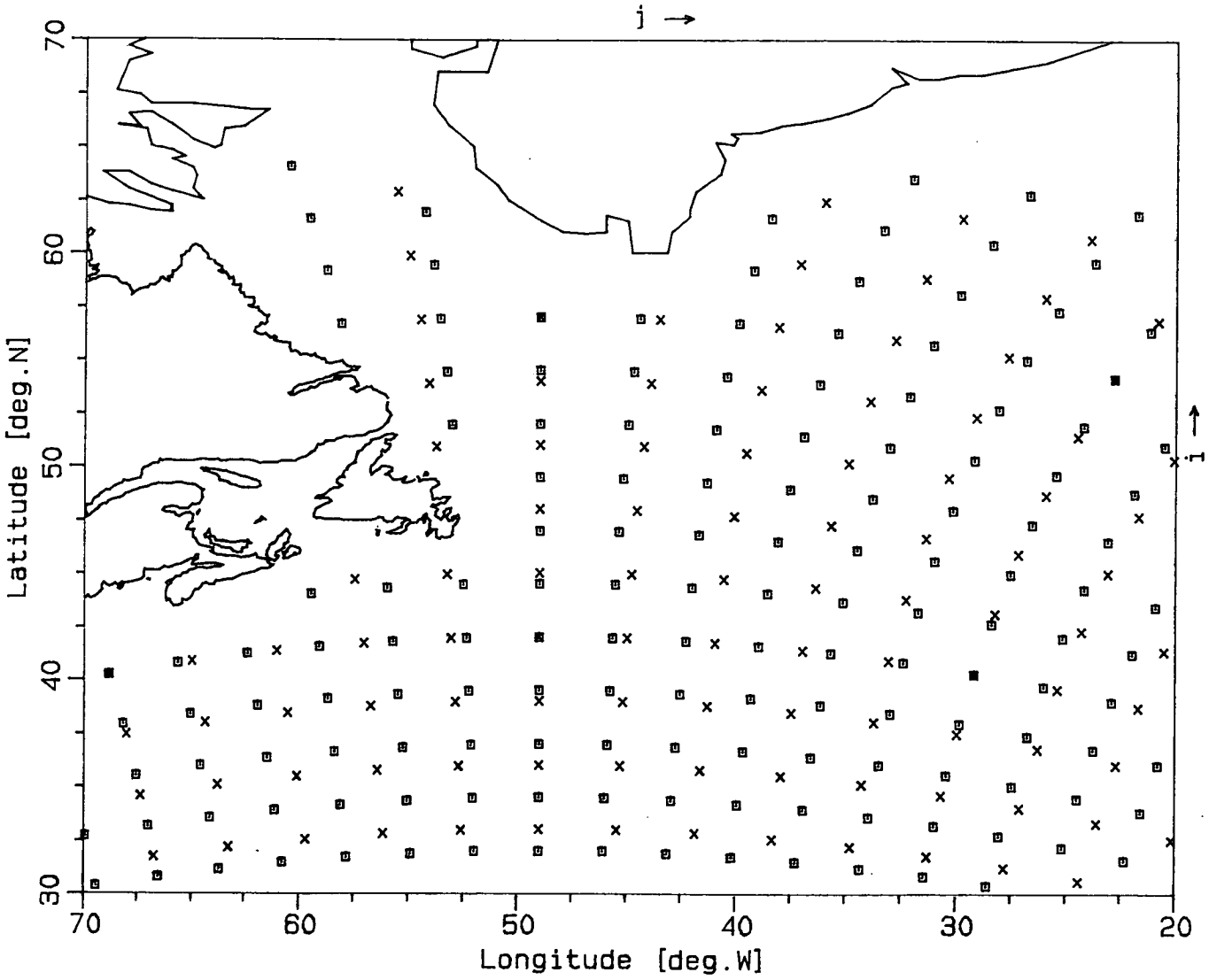

FIGURE 3.1 COMPARISON BETWEEN COARSE AND STANDARD SOG.

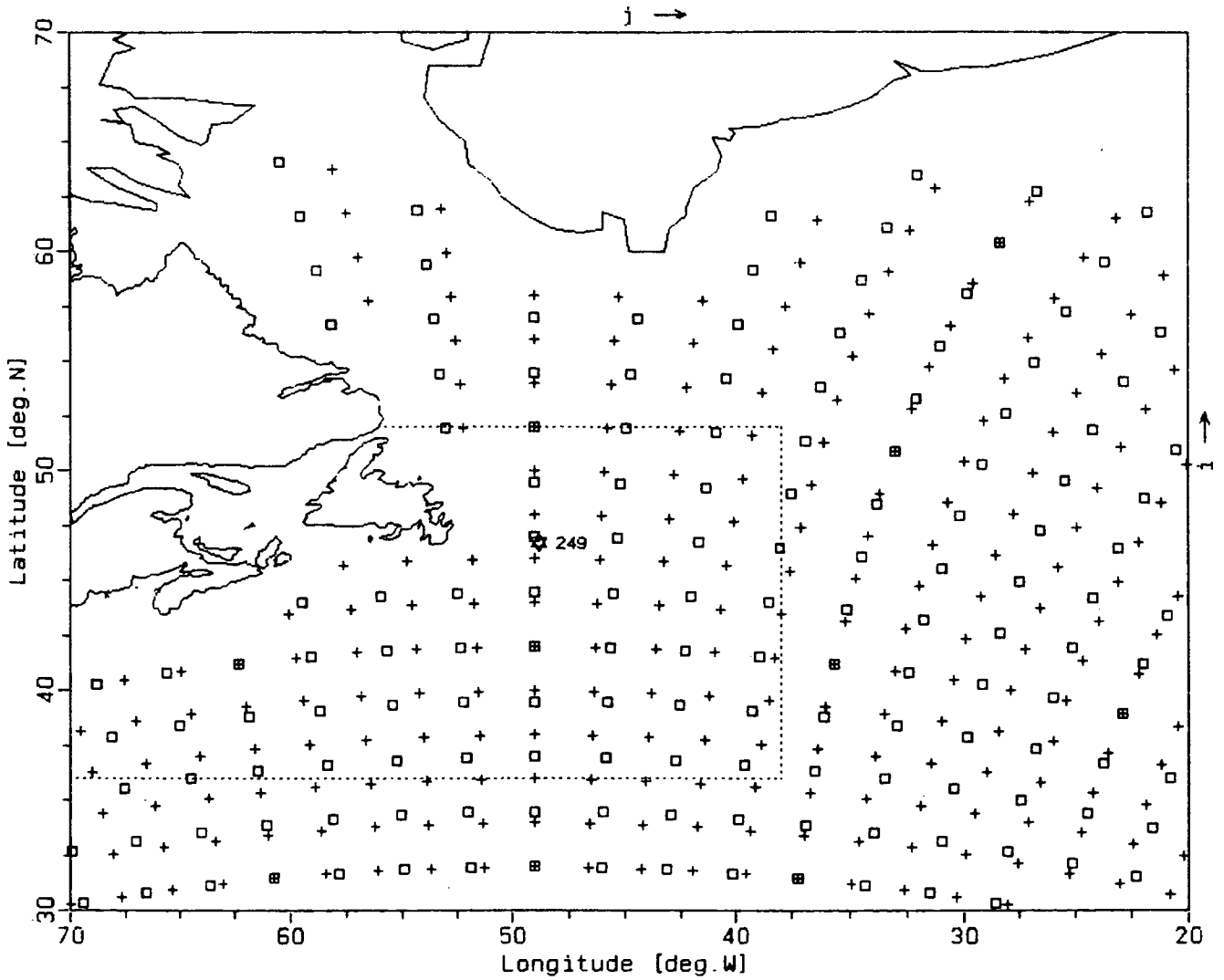

FIGURE 3.2 COMPARISON BETWEEN FINE AND STANDARD SOG.
DOTTED LINE INDICATES EXTENT OF OCTI GRID.

grid spacing and time step satisfy the stability condition. In order to avoid the need for making changes in the time-wise interpolation routines included in the wave model, the input wind fields supplied to MEDS were digitized at 8 and 4 hourly intervals respectively.

Two types of wind input were employed in the tests:

(a) synthetic storm winds described in Section 2.4 (the unperturbed, reference winds);

(b) wind fields prepared for the ESRF Wave Intercomparison Study (Penicka et al., 1985) which represented two storms of a somewhat differing character. For these storms wave observations were available for comparison, as well as wave hindcasts prepared by the Offshore and Coastal Technologies, Inc. (OCTI).

The wind fields used in the intercomparison study were digitized on a 2° latitude x 2° longitude grid. These fields were interpolated to the spherical orthogonal grids by NMS, since the MEDS interpolation routine accepts only winds defined on a 2.5° x 2.5° grid. As a consequence the interpo-

lated wind directions were not corrected for the curvature of the SOG which is normally done as part of the MEDS interpolation. It is believed that this omission has only a negligible effect on the results presented here, since the comparison grid points for the real storm tests lie on a central line that coincides with a meridian (j = 8 in Figure 2.6). This means that the local wind direction requires no rotation while at the surrounding grid points the required correction is only slight. Only swell arriving from greater distances could be noticeably affected.

The area of the original OCTI grid is smaller than the active area of the MEDS grids. Therefore, for the real storm tests, the active region of both the standard and fine grids was modified as marked in Figure 3.2 by the dashed line, to make it the same as for the OCTI runs. No real storm tests have been made using the coarse grid. For the synthetic storm tests the active region of the MEDS grids was left unmodified.

3.2 SENSITIVITY TO GRID SPACING

Figures 3.3 to 3.11 show the time series of input and output variables and scatter diagrams from runs using synthetic input and various grids. The comparisons are made for stations at which the compared grids coincide. For the coarse grid this is only at Station 103 (station numbering is based on the standard grid) while the fine grid coincides with the regular grid at Stations 49 and 103. In addition, the non-standard grid runs were linearly interpolated to Station 71 (which is the station closest to Hibernia) from the two closest grid points. Interpolation, however, may lead to smoothing of the data and contamination of the tests (see the differences in wind speeds and in wind directions).

In all cases the differences between the hindcast wave parameters for the various grid spacings are small particularly during the growth stage. For hindcasts using the standard and fine grids the wave height reaches virtually the same maximum while the use of the coarse grid leads to a slightly lower peak. The difference in the significant wave height is the largest during the abatement of the storm which may indicate that the change in grid spacing affects mainly

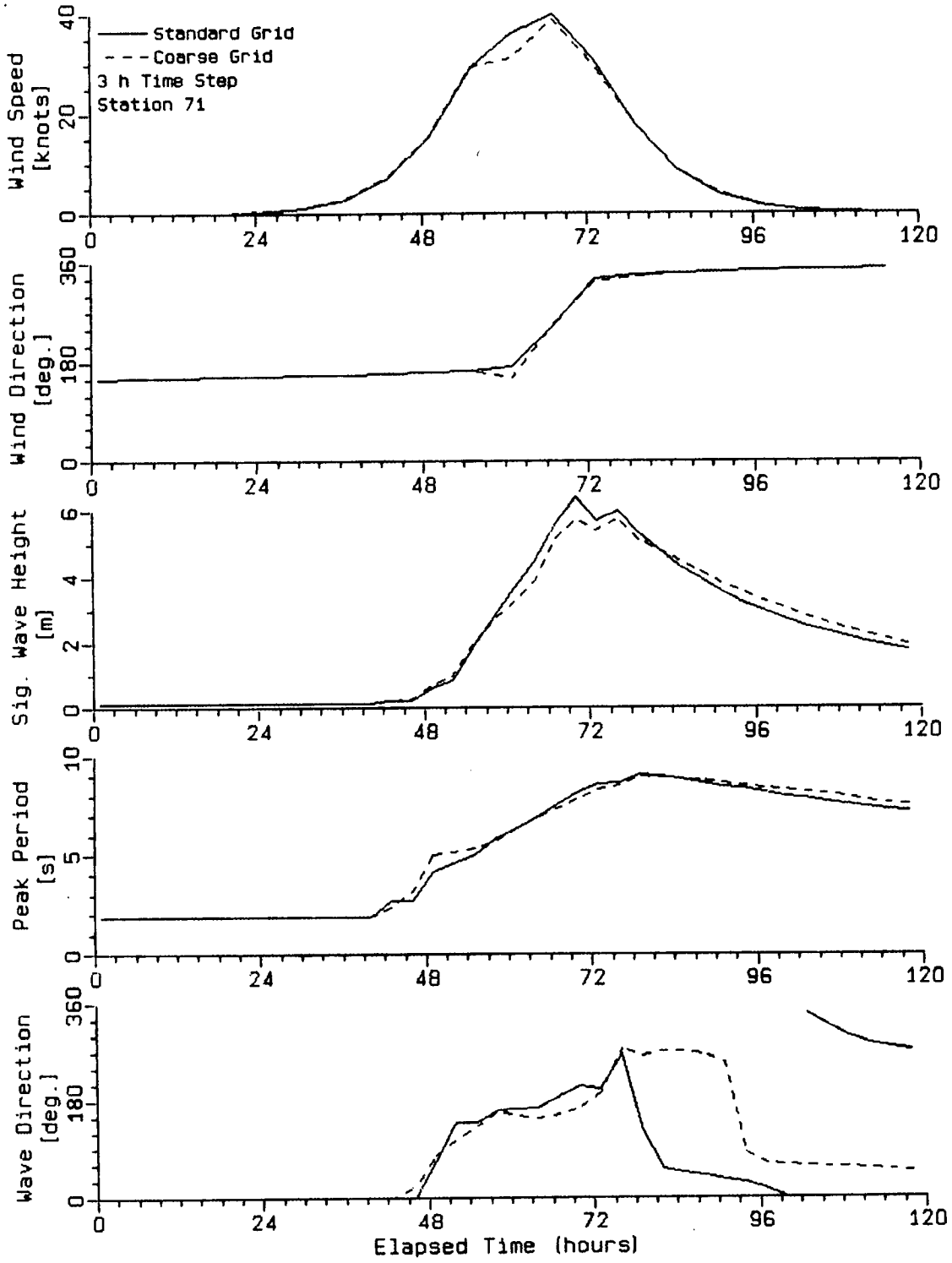

FIGURE 3.3 SENSITIVITY TO GRID SPACING. SYNTHETIC INPUT HINDCASTS AT STATION 71.

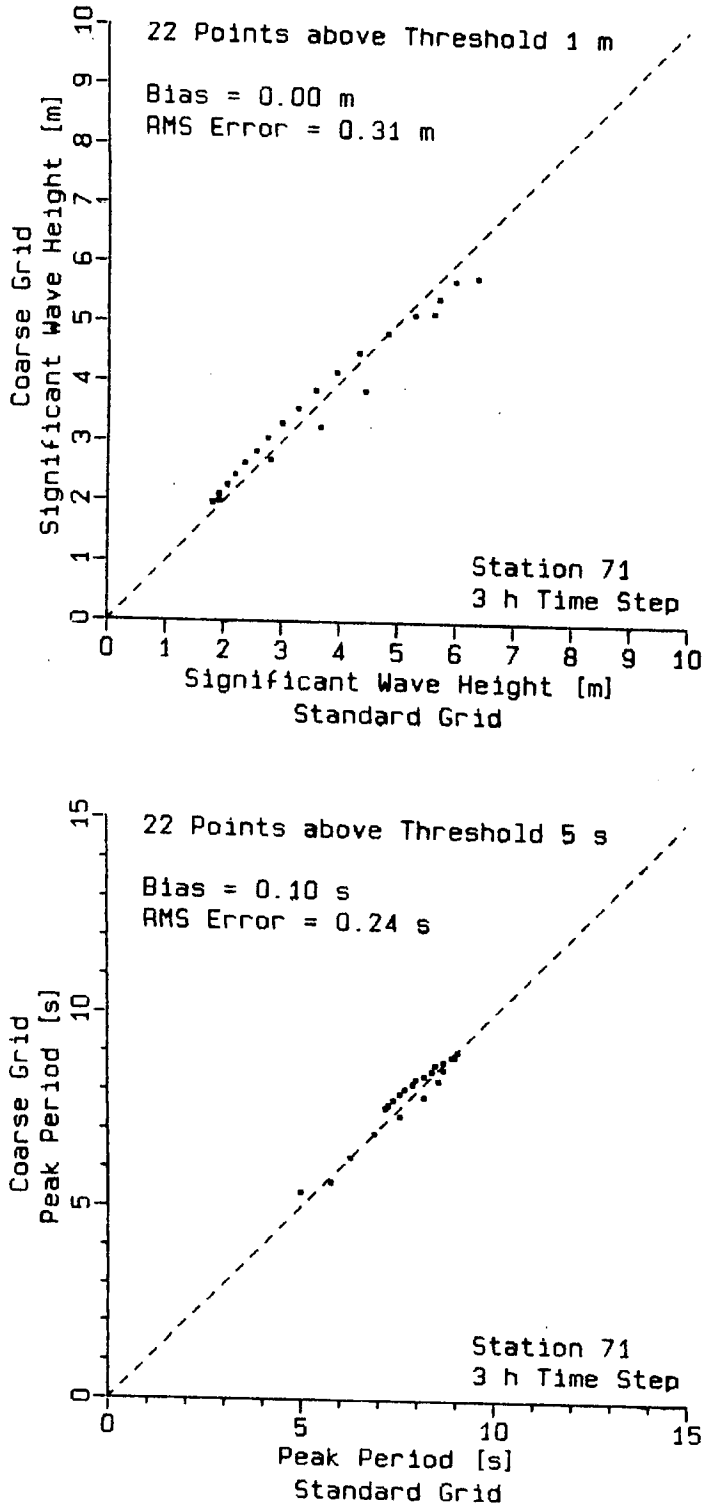

FIGURE 3.4 COMPARISON OF HINDCAST WAVE PARAMETERS AT STATION 71: COARSE VERSUS STANDARD GRID.

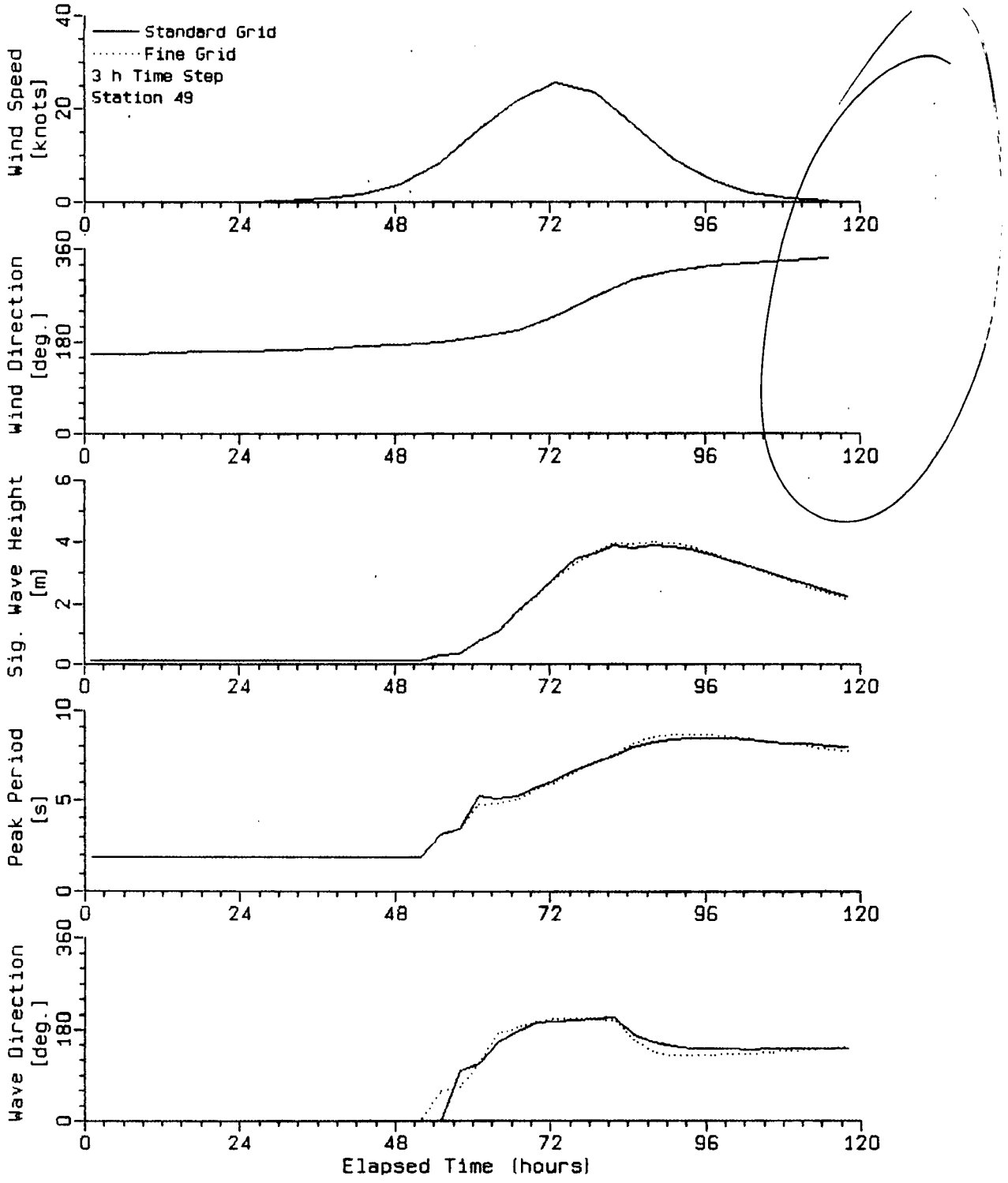

FIGURE 3.5 SENSITIVITY TO GRID SPACING. SYNTHETIC INPUT HINDCASTS AT STATION 49.

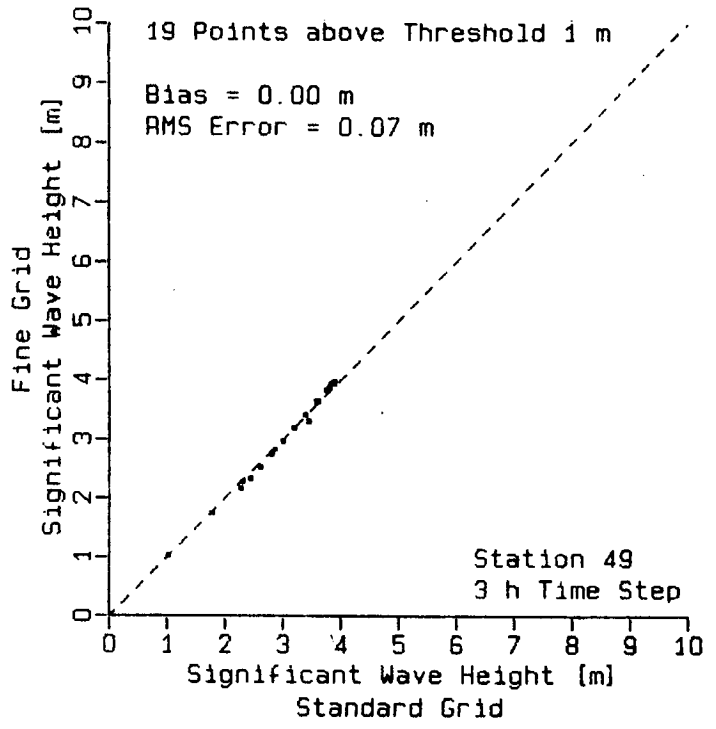

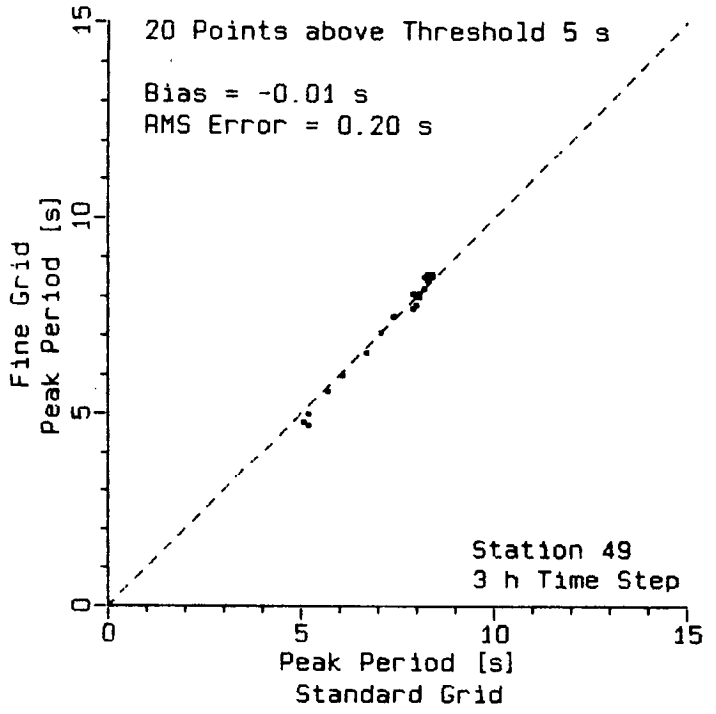

FIGURE 3.6 COMPARISON OF HINDCAST WAVE PARAMETERS AT STATION 49: FINE VERSUS STANDARD GRID.

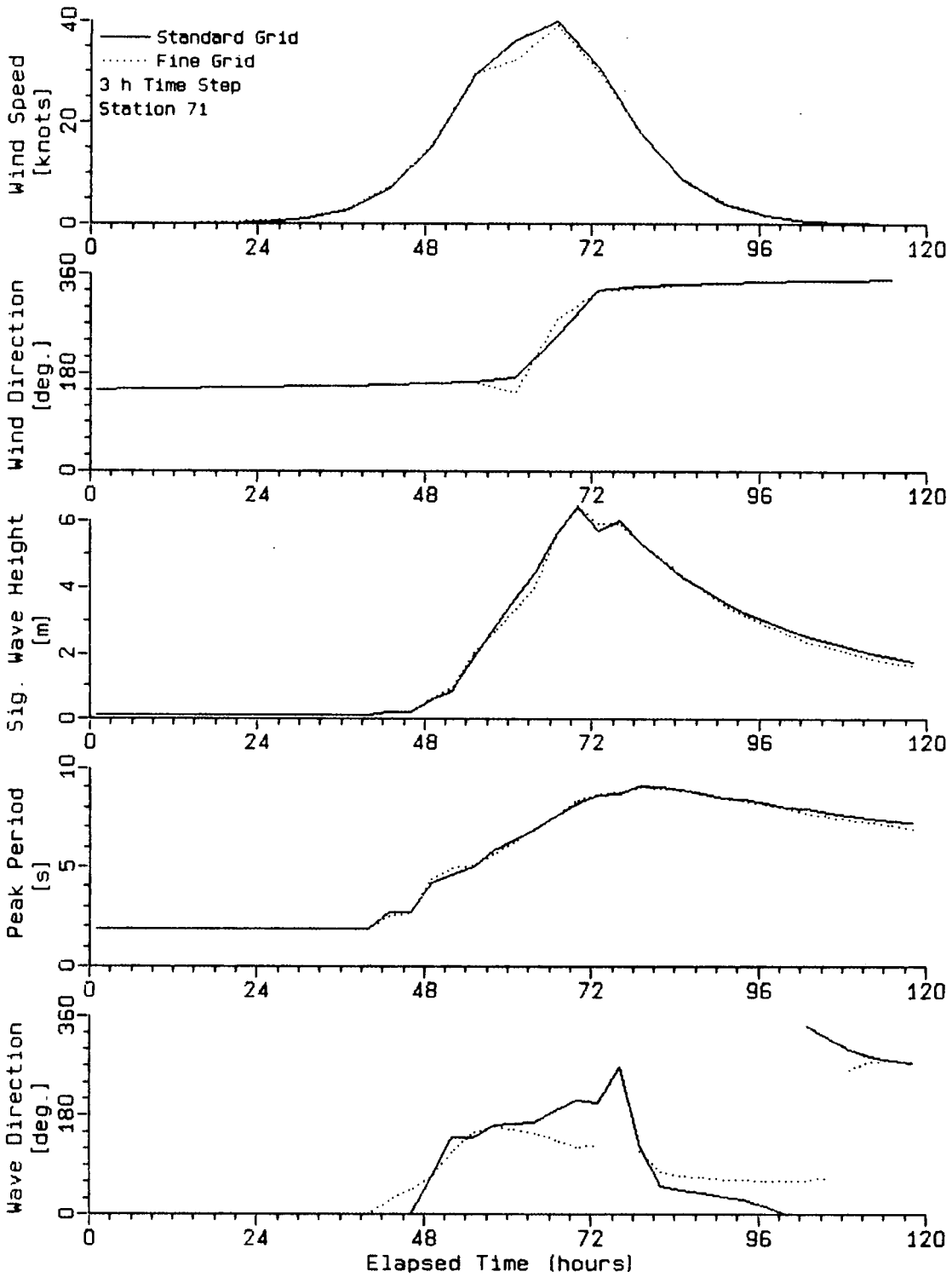

FIGURE 3.7 SENSITIVITY TO GRID SPACING. HINDCASTS INTERPOLATED TO STATION 71.

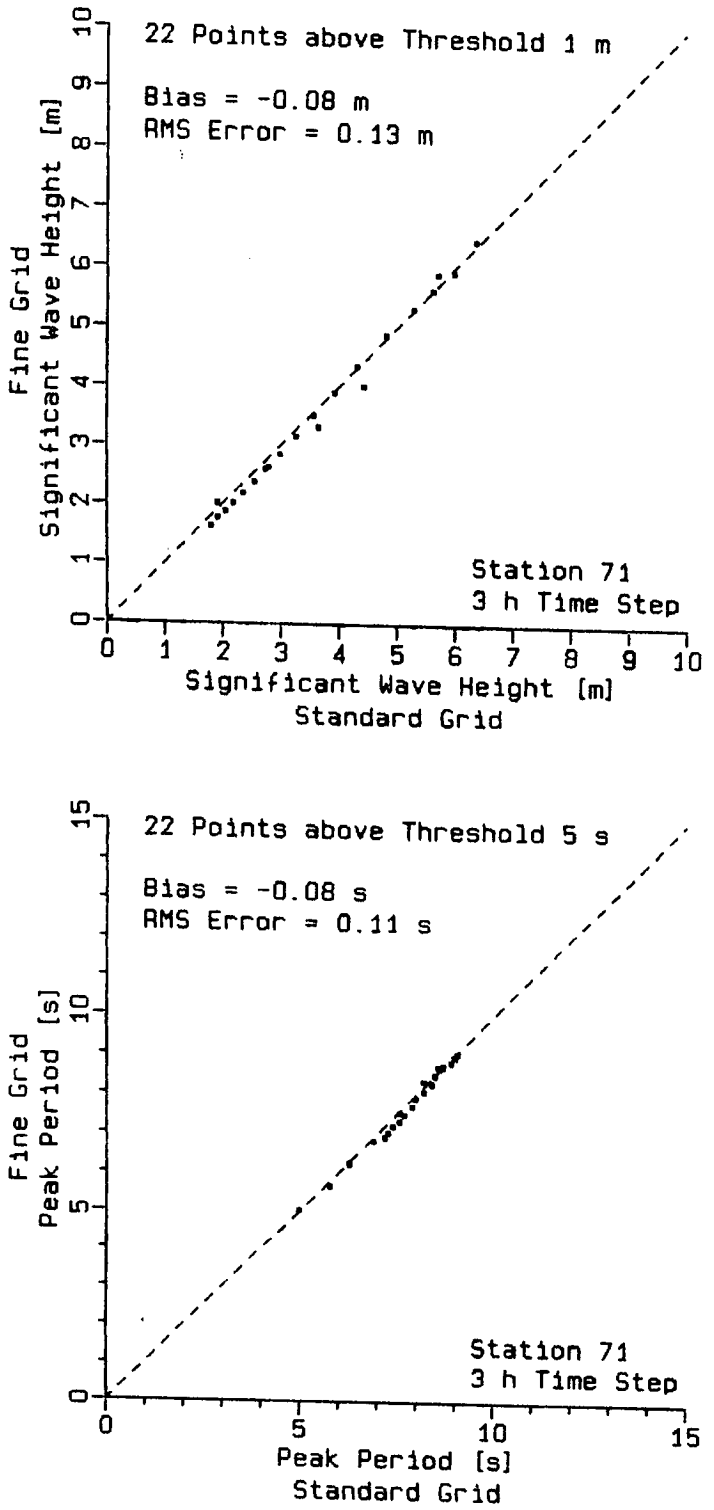

FIGURE 3.8 COMPARISON OF HINDCAST WAVE PARAMETERS INTERPOLATED TO STATION 71: FINE VERSUS STANDARD GRID.

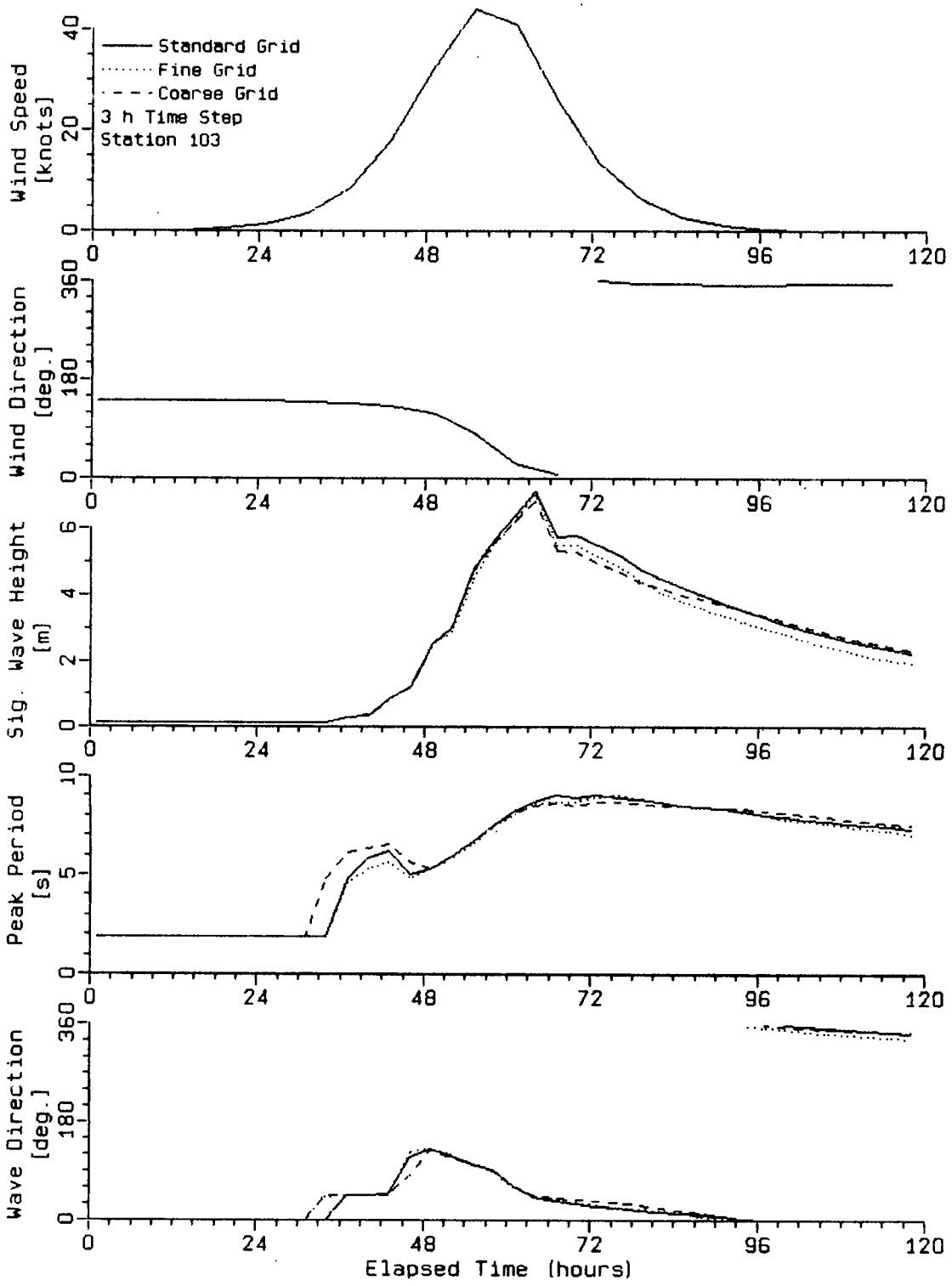

FIGURE 3.9 SENSITIVITY TO GRID SPACING. SYNTHETIC INPUT HINDCASTS AT STATION 103.

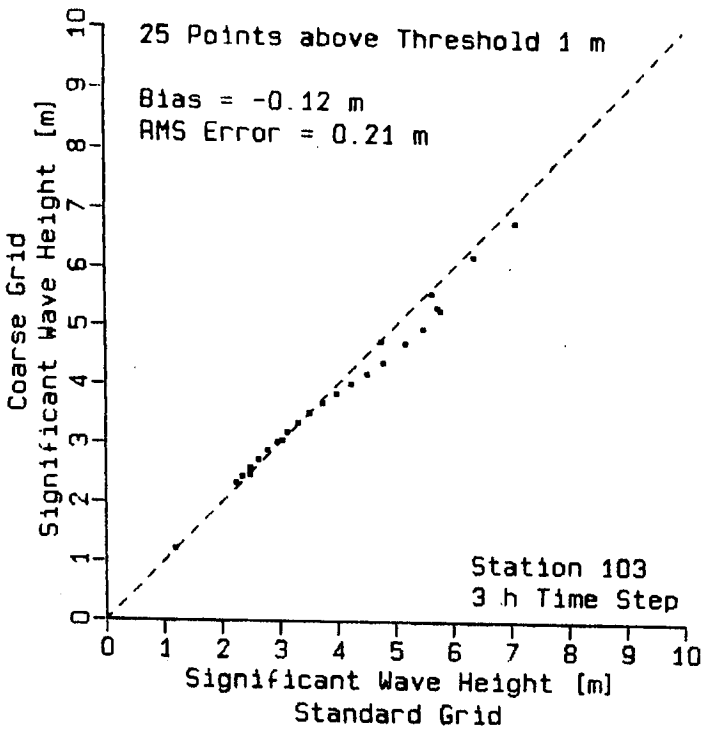

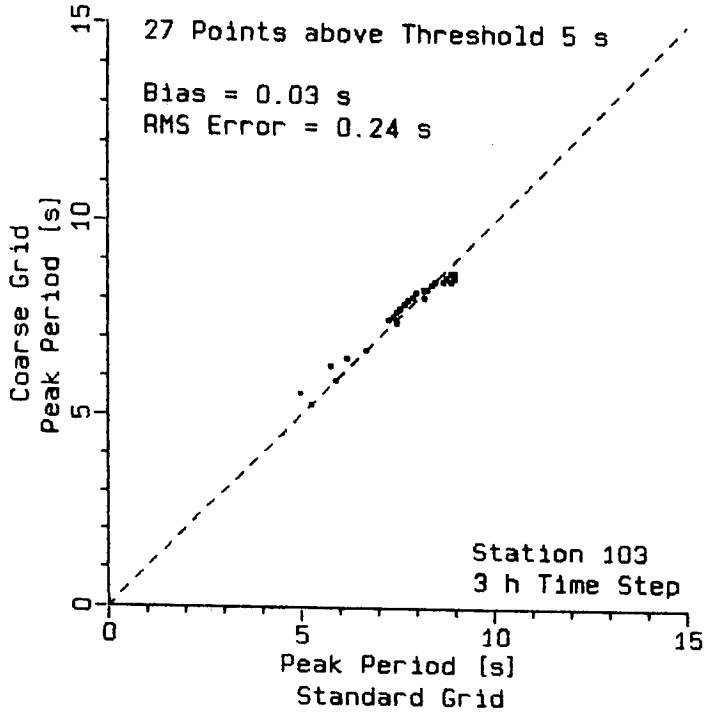

FIGURE 3.10 COMPARISON OF HINDCAST WAVE PARAMETERS AT STATION 103: COARSE VERSUS STANDARD GRID.

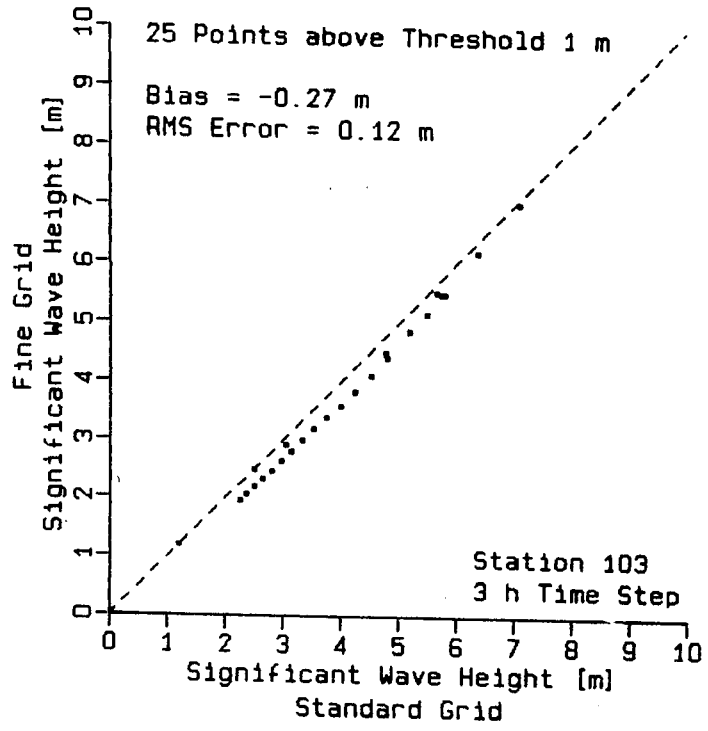

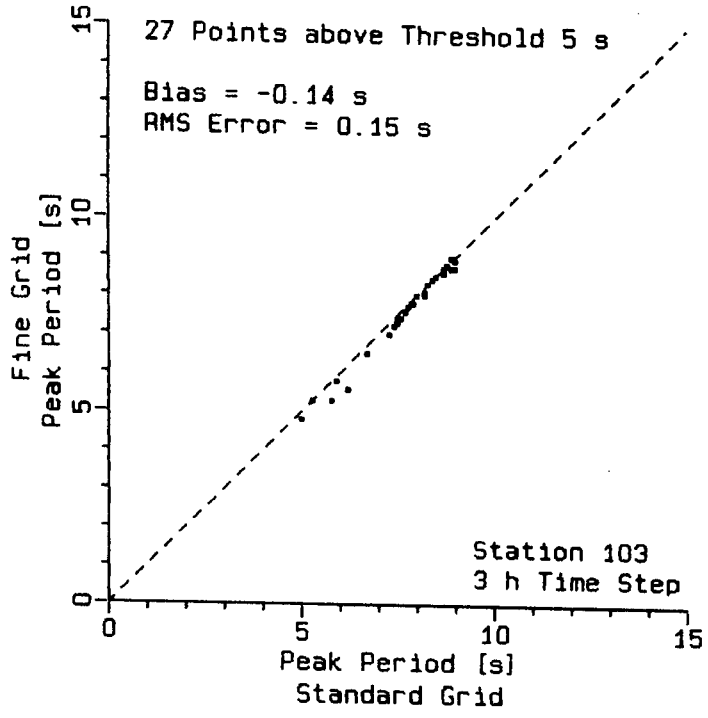

FIGURE 3.11 COMPARISON OF HINDCAST WAVE PARAMETERS AT STATION 103: FINE VERSUS STANDARD GRID.

the wave propagation term. However, it may be also due to a change in fetch (note that during this stage the winds are from the west). On average, the differences in significant wave height are negligible for the 20% decrease in grid spacing (bias 0 m to -0.27 m, RMS difference 0.07 m to 0.13 m); the RMS difference is somewhat larger for the 20% increase in grid spacing (bias 0 m and -0.12 m, RMS difference 0.21 m and 0.31 m). The larger bias for the decrease in grid spacing is due to a more rapid wave decay after the storm reached its peak and in view of the tests that follow it may be beneficial. The bias and RMS differences in peak period are smaller than the period resolution in all cases. A possible effect of a change in fetch is not clear in these tests. At Station 103 there is virtually no difference between the three grids in fetch available for all wind directions. The fetch for westerly winds (during the abatement of the storm) at Station 49 is somewhat shorter in the fine grid than in the regular grid but the corresponding difference in the significant wave height (Figures 3.7 and 3.8) is negligible.

Comparisons between the standard and the fine grids for the real event hindcasts are shown in Figures 3.12 to 3.17. In the first storm hindcasts (Figures 3.12 to 3.14) there

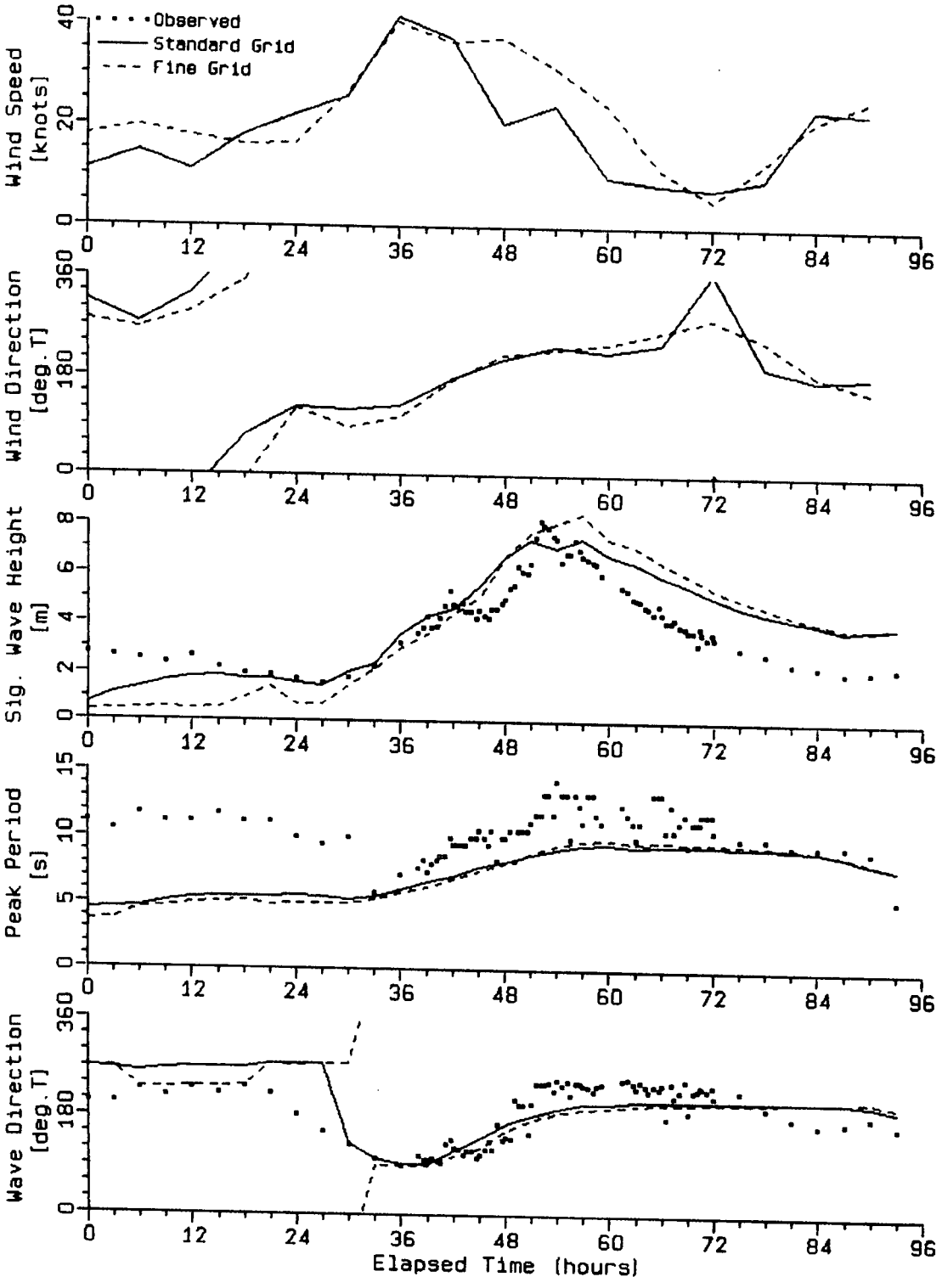

FIGURE 3.12 SENSITIVITY TO GRID SPACING. REAL EVENT HINDCAST: STORM 1.

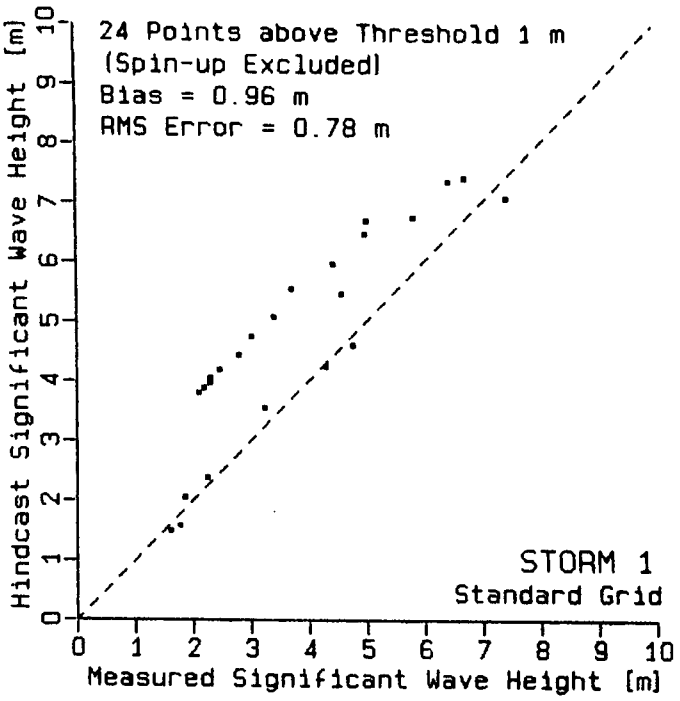

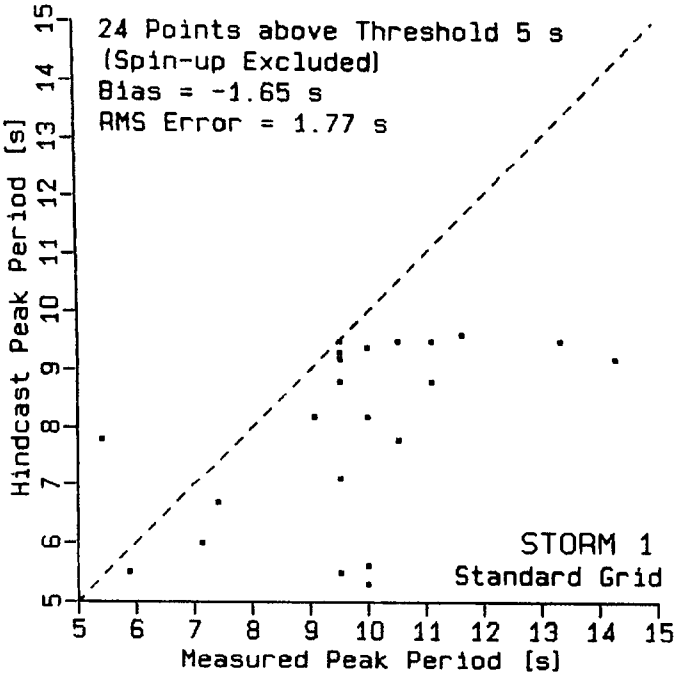

FIGURE 3.13 COMPARISON OF HINDCAST VERSUS MEASURED WAVE PARAMETERS FOR STANDARD GRID - STORM 1.

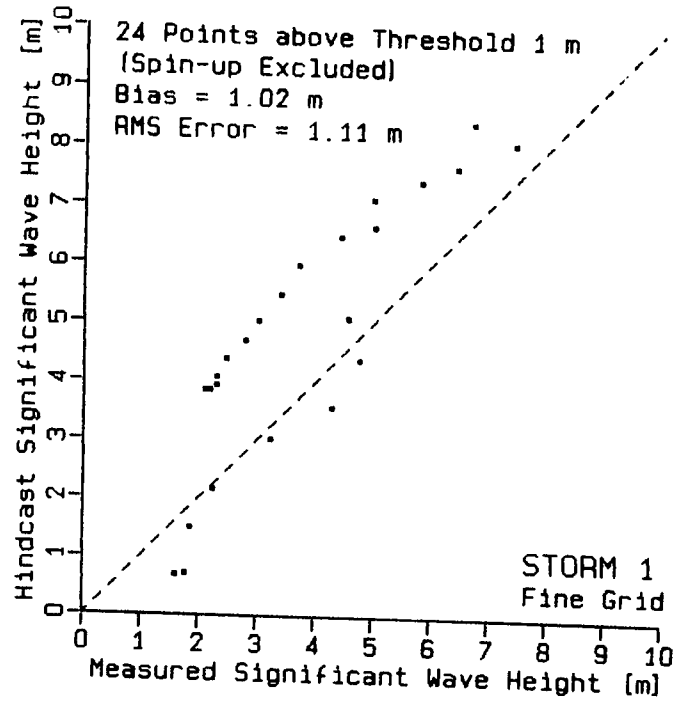

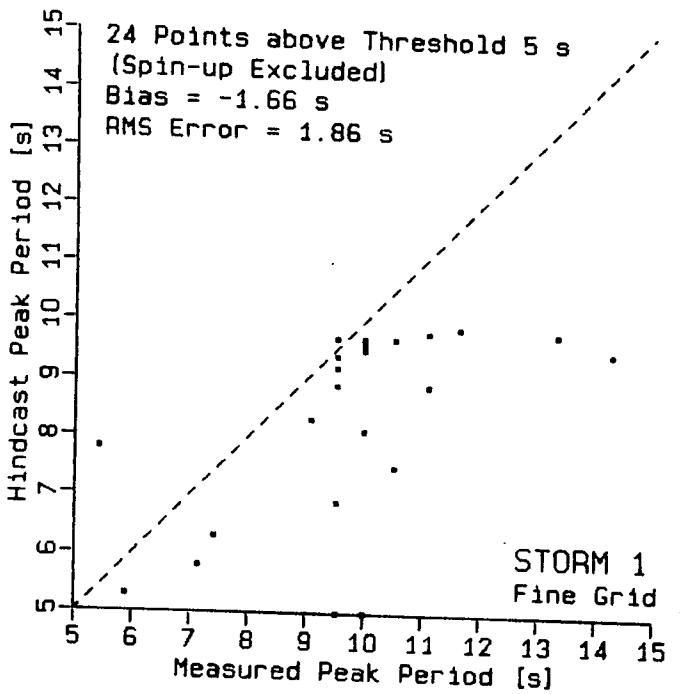

FIGURE 3.14 COMPARISON OF HINDCAST VERSUS MEASURED WAVE PARAMETERS FOR FINE GRID - STORM 1.

are only slight differences in peak periods and in mean directions but the differences in significant wave heights are much larger. The fine grid hindcast over-estimates the maximum significant wave height, unlike the standard grid hindcast in which the peak is underestimated. In both cases the peak is shifted and the wave decay is inadequate.

The comparisons were made for grid points closest to the observation site (Figure 3.2) which do not coincide for the two grids. This may explain the relatively large differences in the significant wave heights. The local winds also differ between the two grids but it is interesting to note that while the local wind speed drops more rapidly (from about the same peak) in the fine grid case, the significant wave height during the abatement of the storm is lower in the standard grid hindcast (note that this is due to its higher peak and not due to a lower rate of decrease). On average, the use of the fine grid leads to a somewhat greater error, compared to the measurement, (bias 1.02 m, RMS error 1.11 m in the significant wave height, -1.66 s and 1.86 s in the peak period) than the use of the standard grid (0.96 m and 0.78 m in H_s, -1.65 s and 1.77 s in T_p). Figure 3.2 shows that the fine grid comparison point is further away from the measurement site than the standard grid point and

this is most likely the reason for the worse error statistics. No other explanation is apparent, why a finer grid spacing should lead to a greater error in the hindcast. This storm was relatively compact and it moved rapidly, therefore strong horizontal gradients in wind speed occurred (see the wind speed trace in Figure 3.12)

In the second storm comparison (Figures 3.15 to 3.17) both hindcasts overpredict the significant wave height during most of the storm but the fine grid leads to values closer to the observation by about half meter (bias 0.6 m versus 1.03 m). This storm developed less rapidly and was less compact than the first storm. The storm was stalled over the Grand Banks for over 30 hours and the winds remained relatively steady for long periods of time. The spatial gradients of wind speed were not as great as in the first storm (see Figure 3.15) and consequently both hindcast grid points were representative of the measurement site. The mean errors in peak period are comparable (bias and RMS errors approximately 2 s for both grids) but the mean wave directions differ by about 30° between the two grids.

The standard and the fine grids differ in their representation of the land boundary. Since the comparison grid

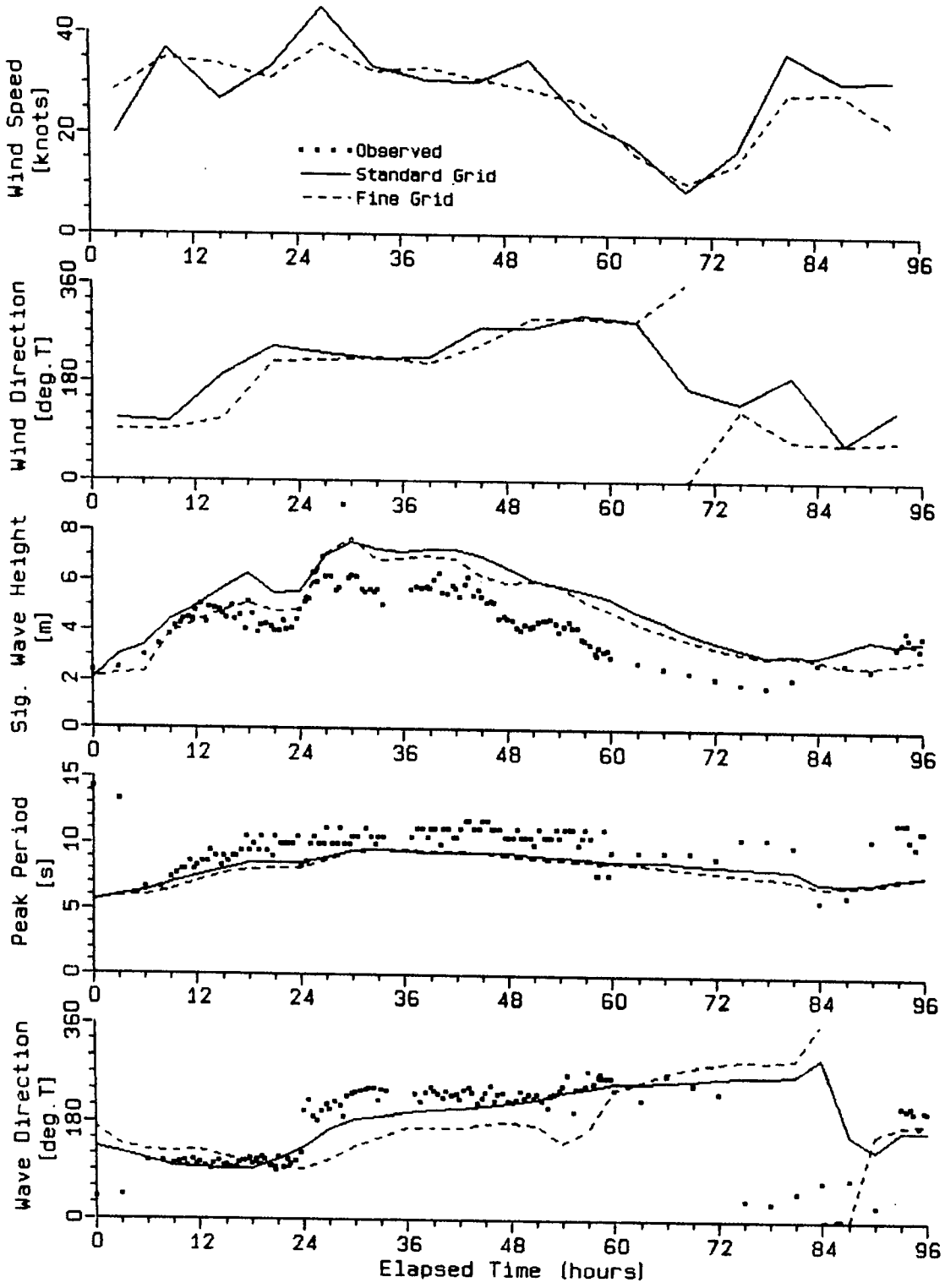

FIGURE 3.15 SENSITIVITY TO GRID SPACING. REAL EVENT HINDCAST: STORM 2.

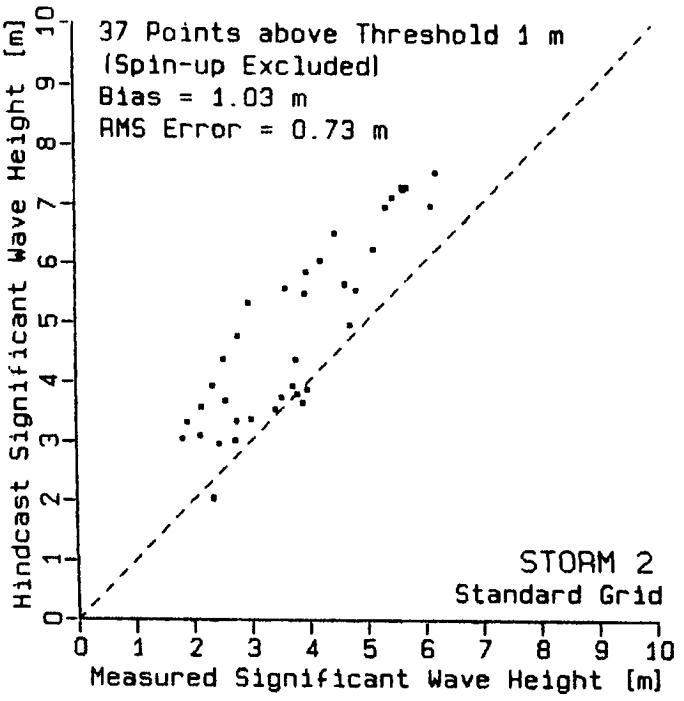

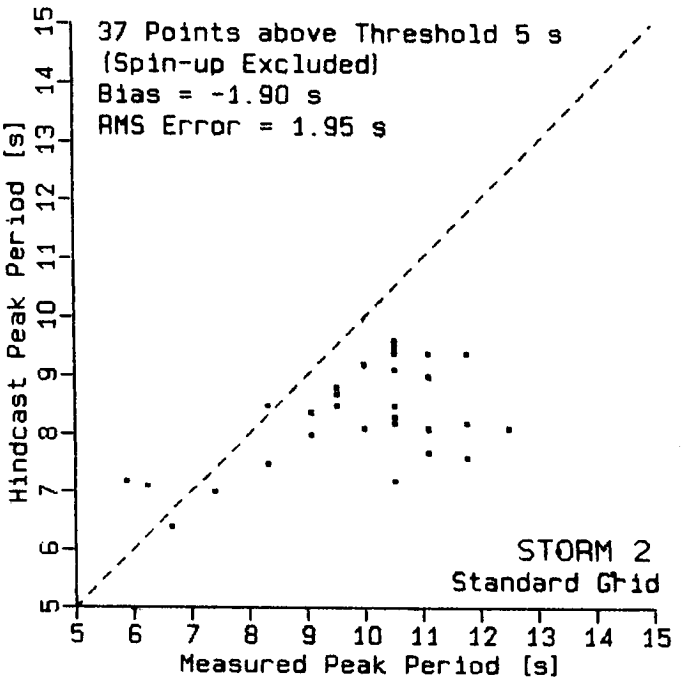

FIGURE 3.16 COMPARISON OF HINDCAST VERSUS MEASURED WAVE PARAMETERS FOR STANDARD GRID - STORM 2.

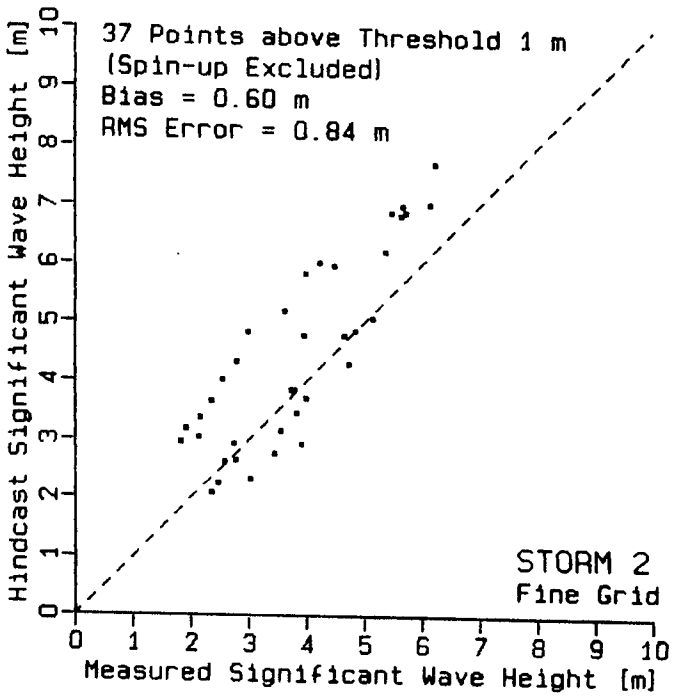

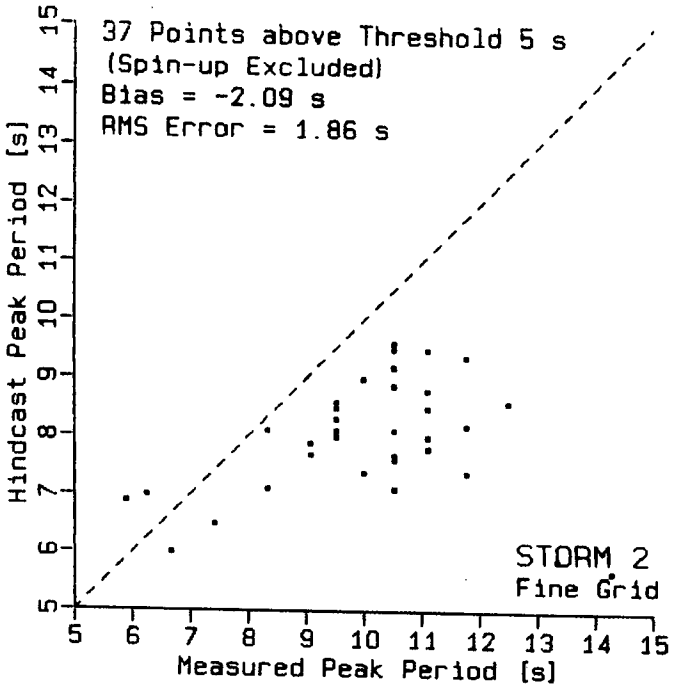

FIGURE 3.17 COMPARISON OF HINDCAST VERSUS MEASURED WAVE PARAMETERS FOR FINE GRID - STORM 2.

points are adjacent to the boundary the fetch for offshore winds somewhat differs between the two cases. As a first approximation, based on the JONSWAP measurements (Hasselmann et al., 1973), the dependencies of windsea significant wave height and peak period on fetch, x, are given by

$$H_s \sim x^{0.50}$$

$$T_p \sim x^{0.33}$$

According to this a 100% increase in fetch should lead to about 41% increase in significant wave height and about 26% increase in peak period. However, in a real storm event the wind direction is not likely to remain unchanged for a long period of time and the occurrence of fetch limited conditions is likely to be limited.

In order to clarify how a change in the boundary resolution may affect the hindcast wave parameters for a real storm both the standard and the fine grids were modified to include additional sea grid points along the Newfoundland and Labrador coastlines. In Figure 3.18 the additional grid points are circled; a typical change in fetch is one grid spacing.

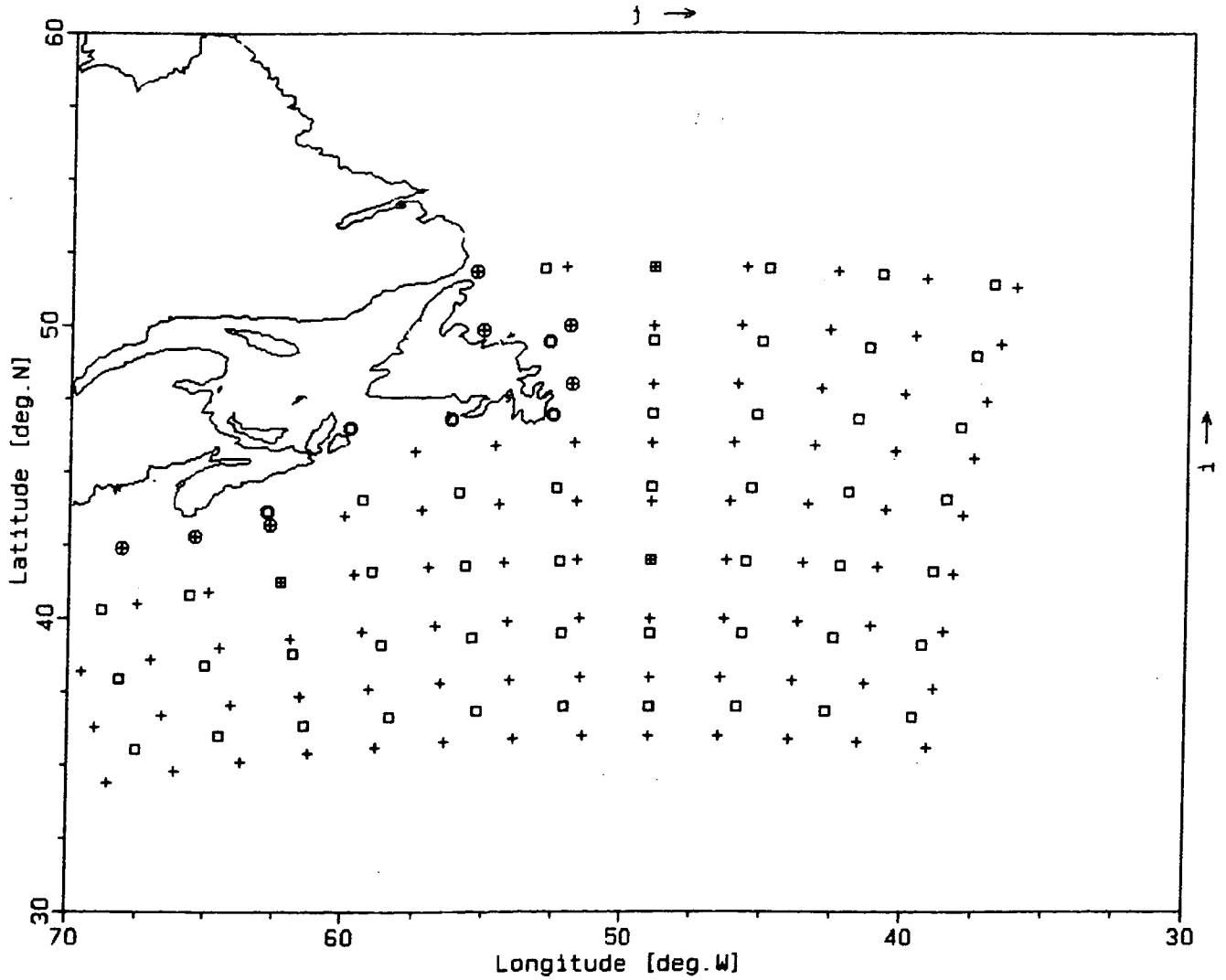

FIGURE 3.18 MODIFIED STANDARD AND FINE GRIDS.

Figures 3.19 and 3.20 show the difference in the hindcast significant wave height between the modified and unmodified standard grids for the first storm. Since the grid spacing and the input winds are the same in both hindcasts the differences should be due mainly to the change in fetch (or possibly due to a smoothing effect of the advective term, suggested in Section 2.3.2). Over the whole storm the increase in fetch leads to a mean difference in H_s of 0.34 m and RMS difference of 0.29 m (Figure 3.20). However, the differences are distributed unevenly. They are negligible during the growth when the seas are limited by duration, and at the peak of the storm, but they increase to about 1 m as the storm abates. Comparison with the wind direction plot indicates that before the storm peaks, the wind direction at Station 71 is onshore and therefore the wave growth is not limited by fetch (note that in the real data plots the directions are in degrees true, i. e. measured clockwise from the north, in order to facilitate comparison with observational data). However, during the abatement of the storm the wind direction gradually changes from southwest to northwest where the fetch is limited by the presence of land boundary. The extension of the grid leads to an insignificant change in the peak period and in the mean direction. The small change in peak period may be due to the

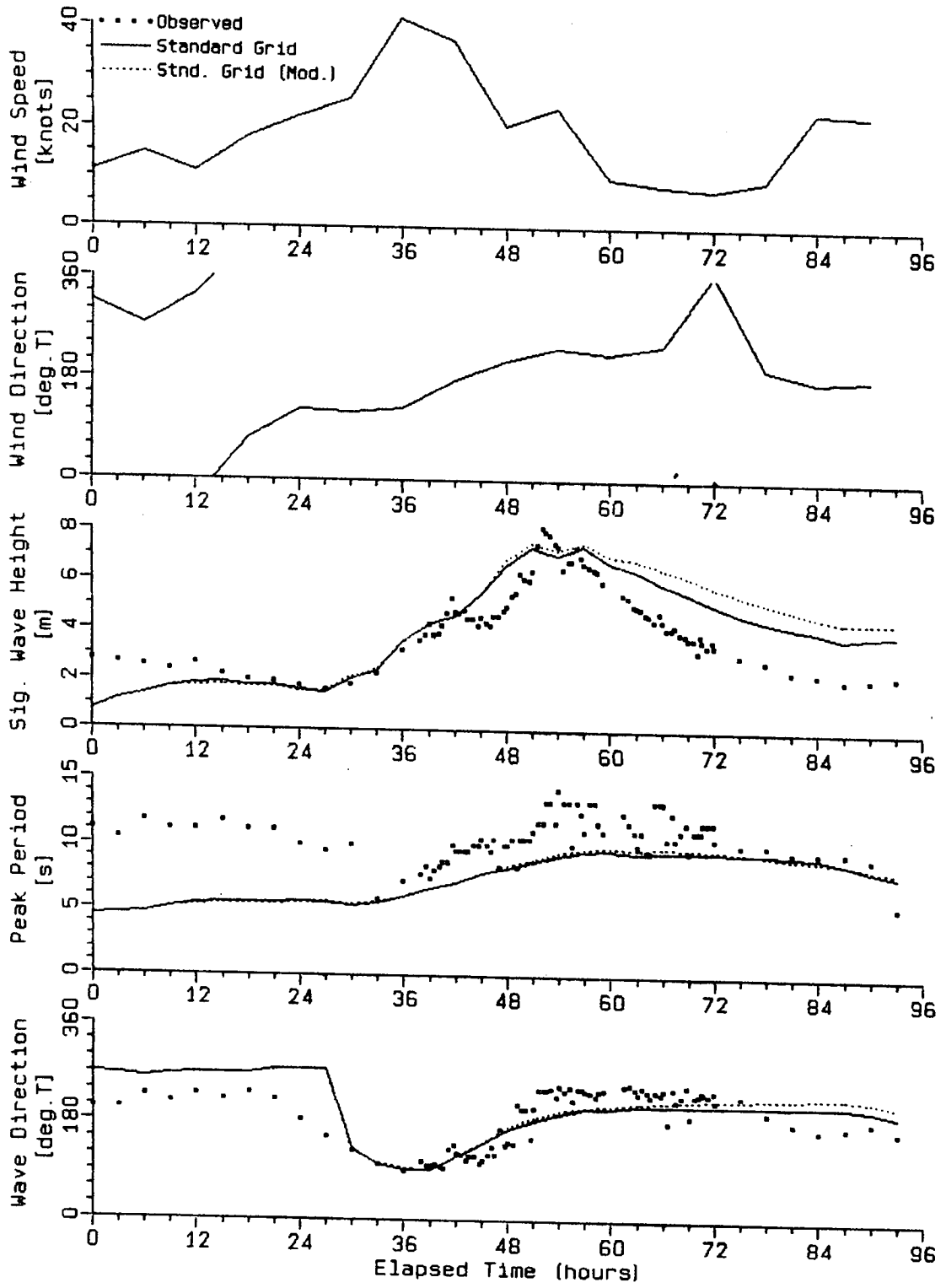

FIGURE 3.19 SENSITIVITY TO SHIFT IN LAND BOUNDARY. STANDARD GRID - STORM 1.

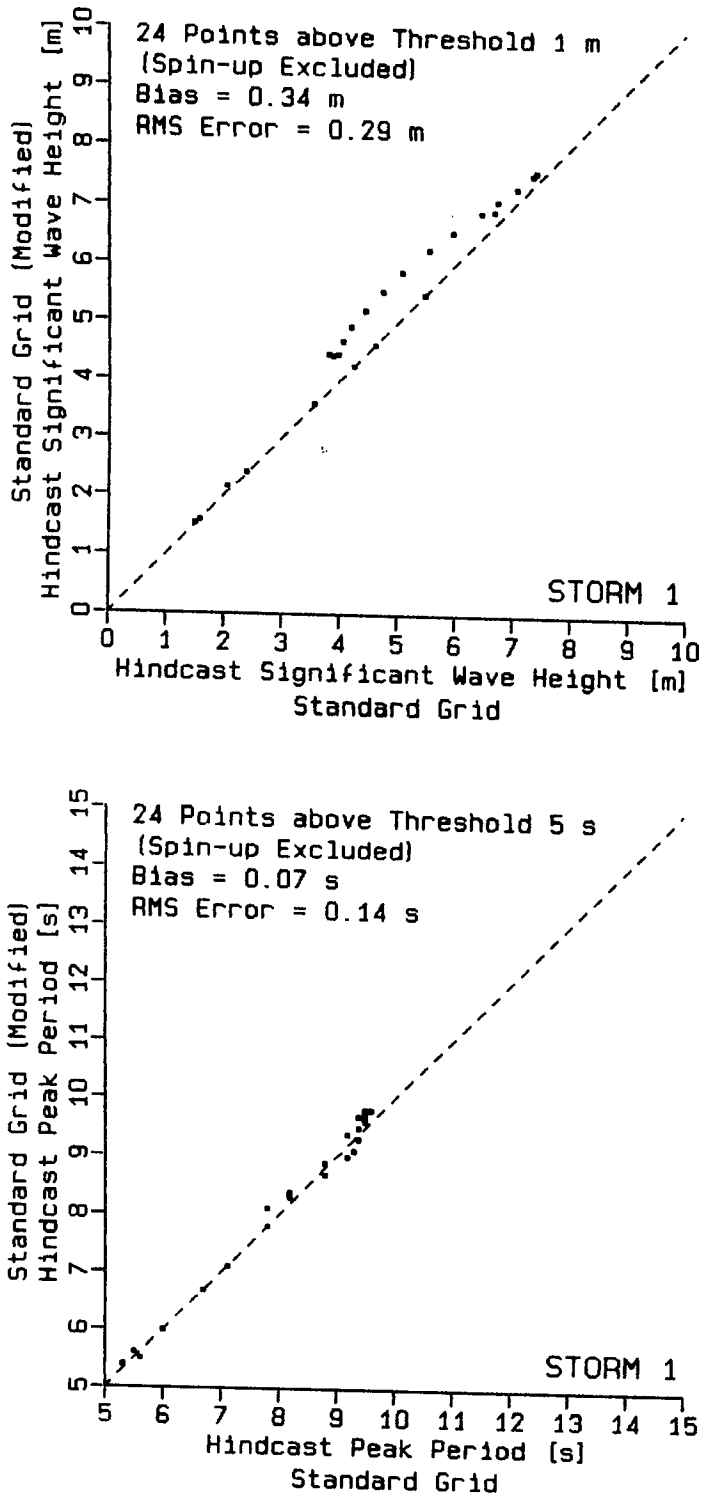

FIGURE 3.20 COMPARISON OF HINDCAST WAVE PARAMETERS FOR STORM 1: MODIFIED VERSUS UNMODIFIED STANDARD GRID.

discrete nature (and therefore a finite resolution) of the peak period.

The extension of the fine grid (Figures 3.21 and 3.22) leads to a much smaller change in the significant wave height: mean difference of 0.16 m and RMS difference of 0.15 m. There are two reasons for this: first, the grid spacing, and therefore the potential increase in fetch, are 20% smaller; second, the comparison grid point (Station 114f) is further south than in the previous case (see Figure 3.18) and for westerly winds the minimum fetch, limited by the land boundary, is several grid spacings.

Wave hindcasts for the second storm (at Station 71) for the modified and unmodified standard grids are presented in Figures 3.23 and 3.24. The results are similar to those from the first storm. Over the whole storm the shift in grid boundary leads to mean increase in significant wave height equal 0.26 m and RMS difference equal 0.21 m. The differences are small when the winds are on shore but they increase for offshore winds. Due to a large proportion of swell the difference in H_s persists even after the winds swung back on shore.

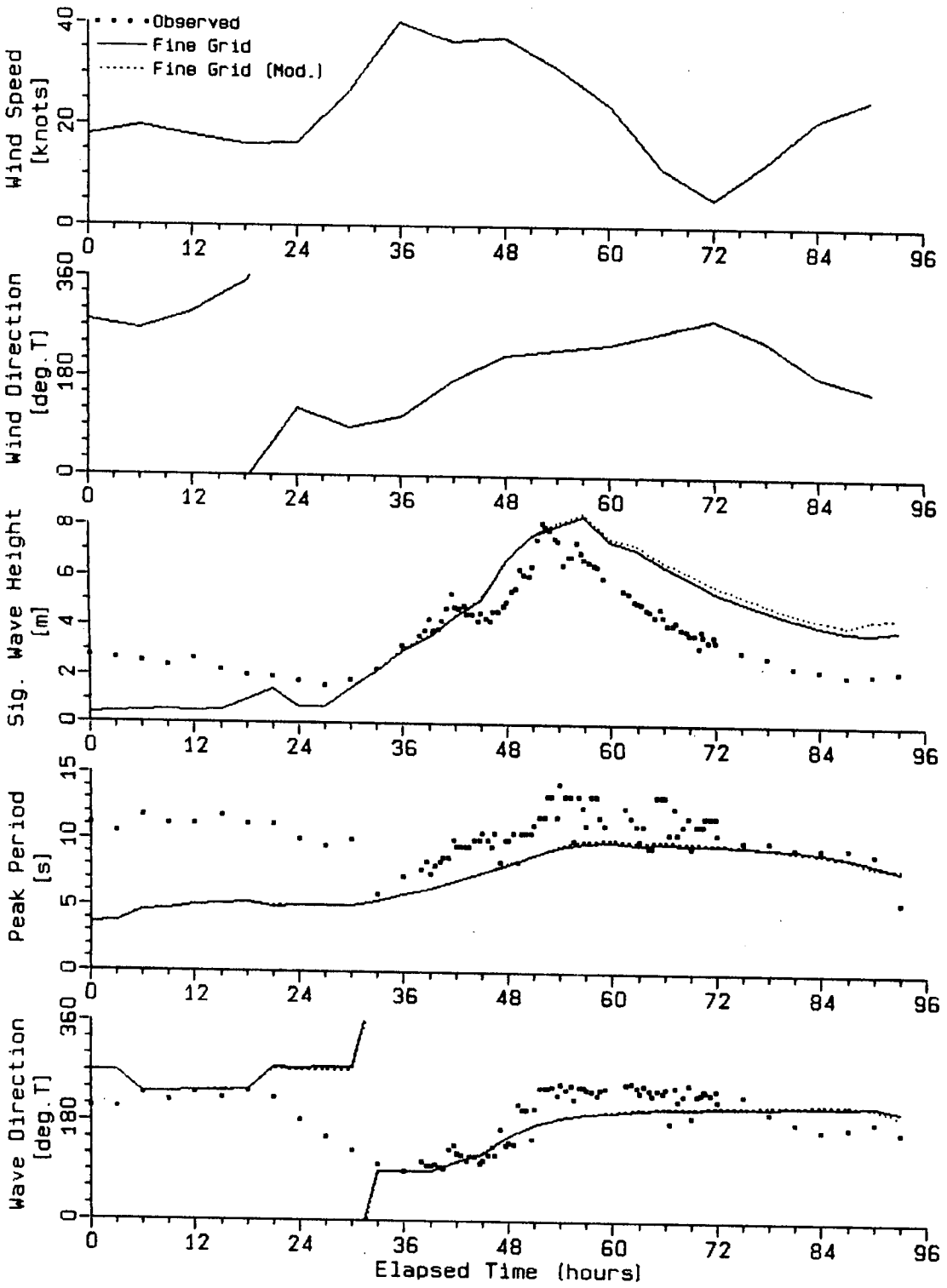

FIGURE 3.21 HINDCAST SENSITIVITY TO SHIFT IN LAND BOUNDARY. FINE GRID - STORM 1.

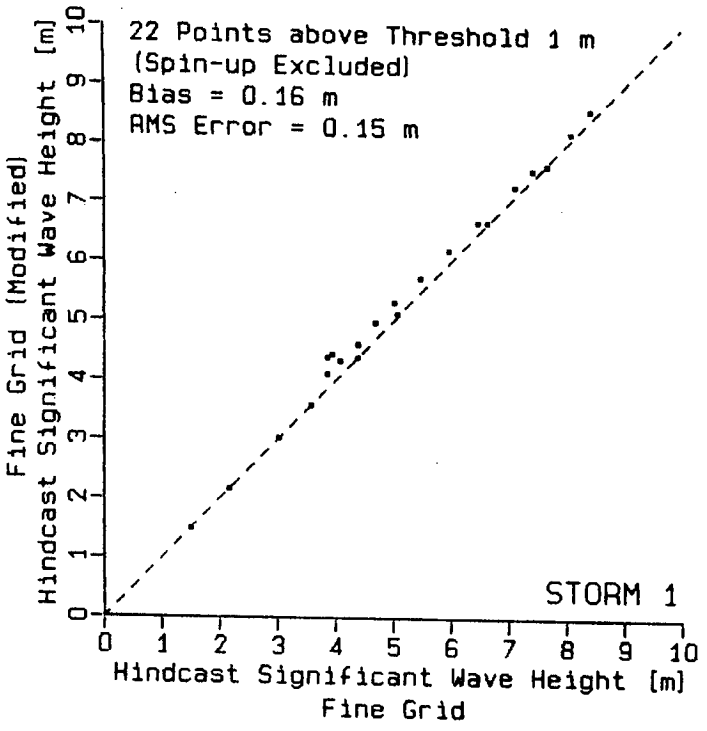

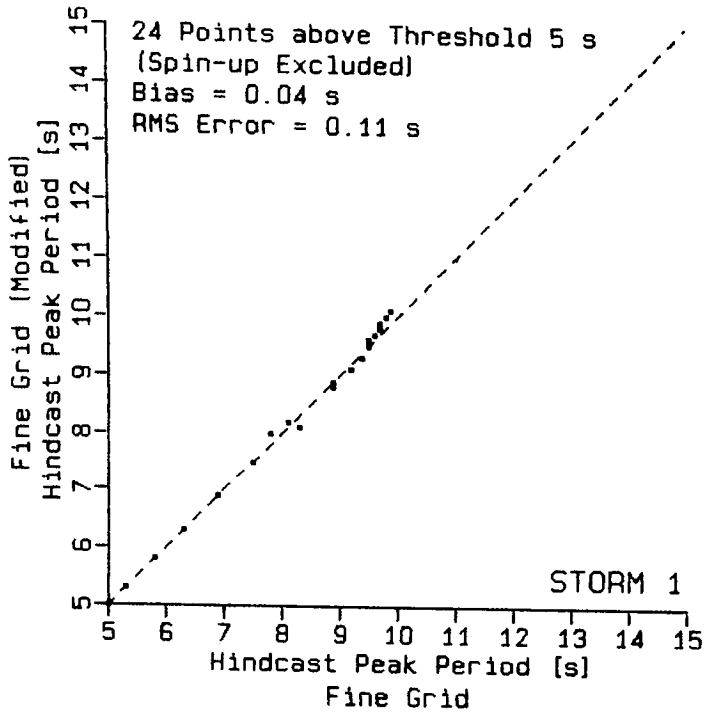

FIGURE 3.22 COMPARISON OF HINDCAST WAVE PARAMETERS FOR STORM 1: MODIFIED VERSUS UNMODIFIED FINE GRID.

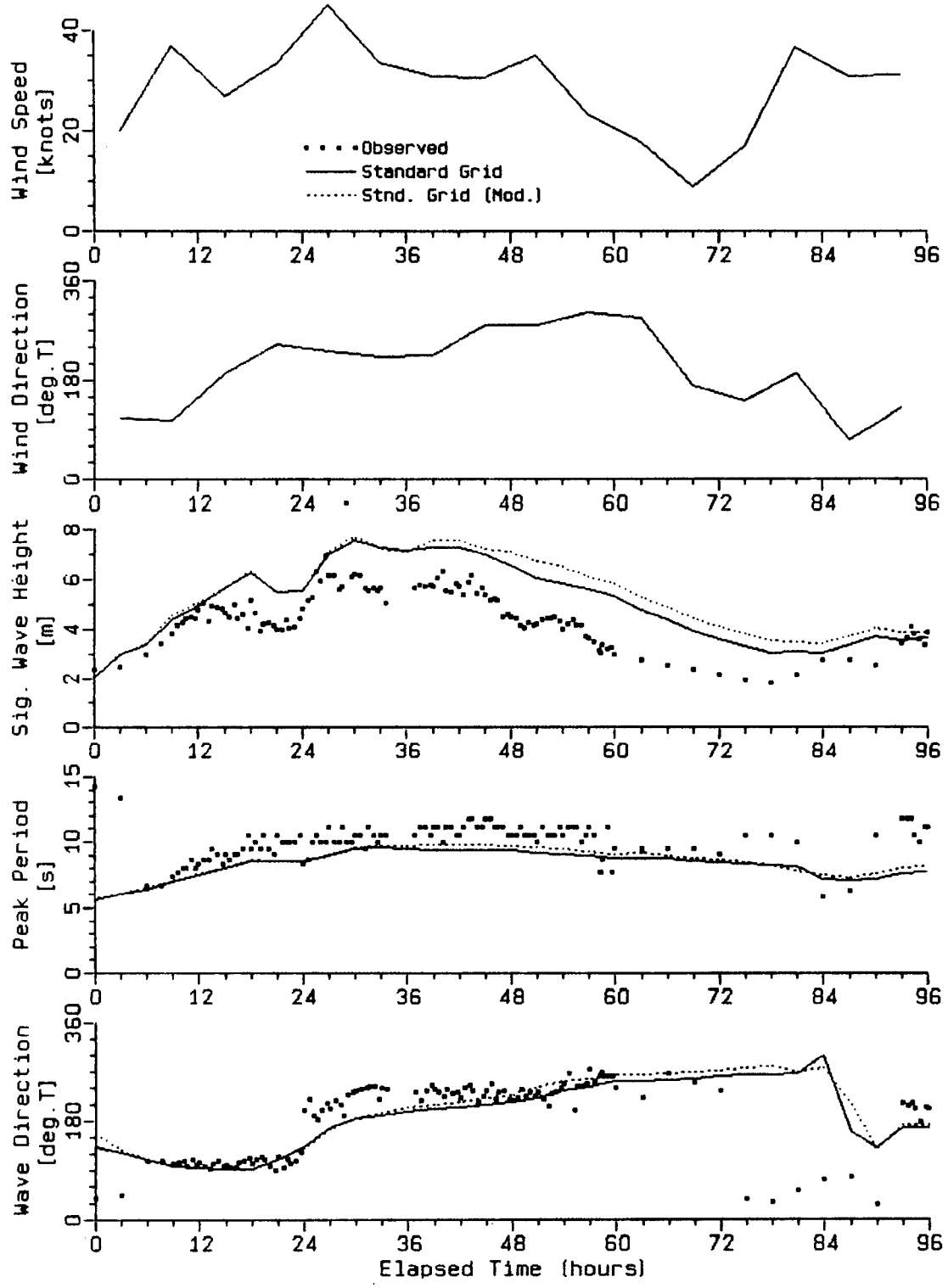

FIGURE 3.23 HINDCAST SENSITIVITY TO SHIFT IN LAND BOUNDARY. STANDARD GRID - STORM 2.

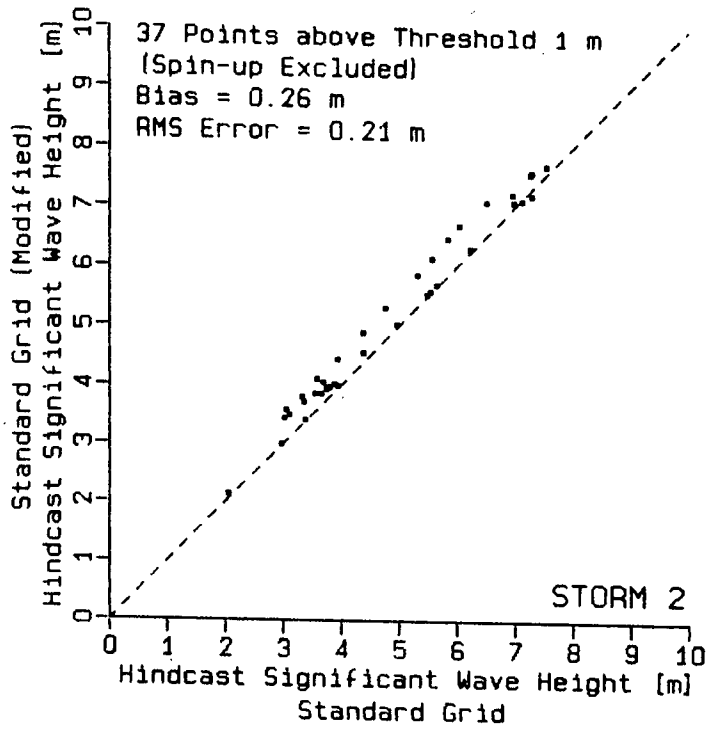

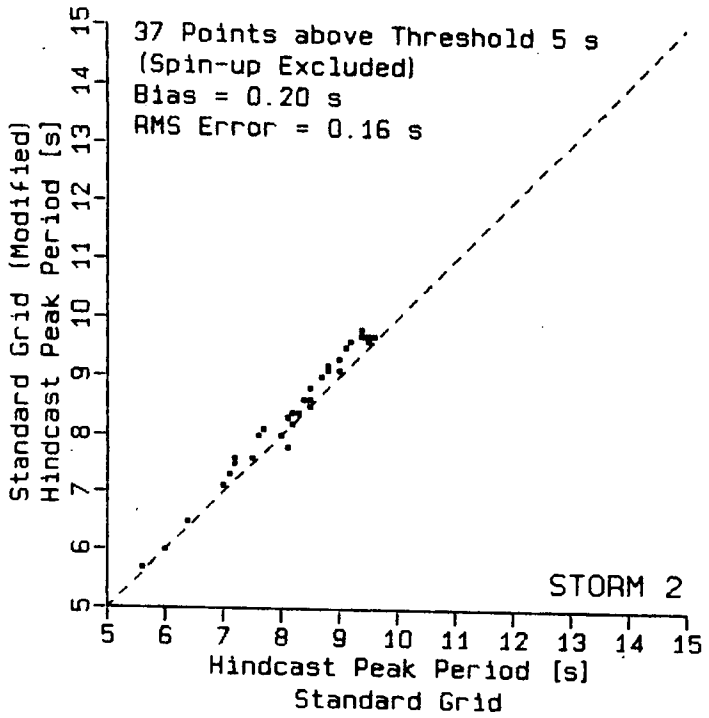

FIGURE 3.24 COMPARISON OF HINDCAST WAVE PARAMETERS FOR STORM 2: MODIFIED VERSUS UNMODIFIED STANDARD GRID.

3.3 SENSITIVITY TO TIME STEP

Figures 3.25 to 3.45 show the sensitivity of the hindcast wave parameters to model time step for a number of stations and various grid spacings. The comparison grid points were selected to have different distances from the land boundary and from the storm track (see Figures 2.6 and 2.23). The input winds were obtained by digitizing the analytical expression for the synthetic winds (Equation 13) at the appropriate intervals. As a consequence the local winds differ somewhat for the different time step hindcasts. With one exception (Station 71, 4 h time step) the hindcast significant wave heights and peak periods increase with decreasing time step. This suggests a need for a recalibration should a time step be modified. The average change in significant wave height over the whole storm for the decrease in time step from 3 h to 2 h ranges between 0.16 m and 0.32 m, the RMS difference is between 0.16 m and 0.38 m. The changes in peak period are smaller than the period resolution. Increasing the time step to 4 h has a greater effect: up to -0.65 m in the mean and 0.46 m in the RMS difference.

There is an indication in some of the time series plots that the wave growth is more rapid for shorter time steps and

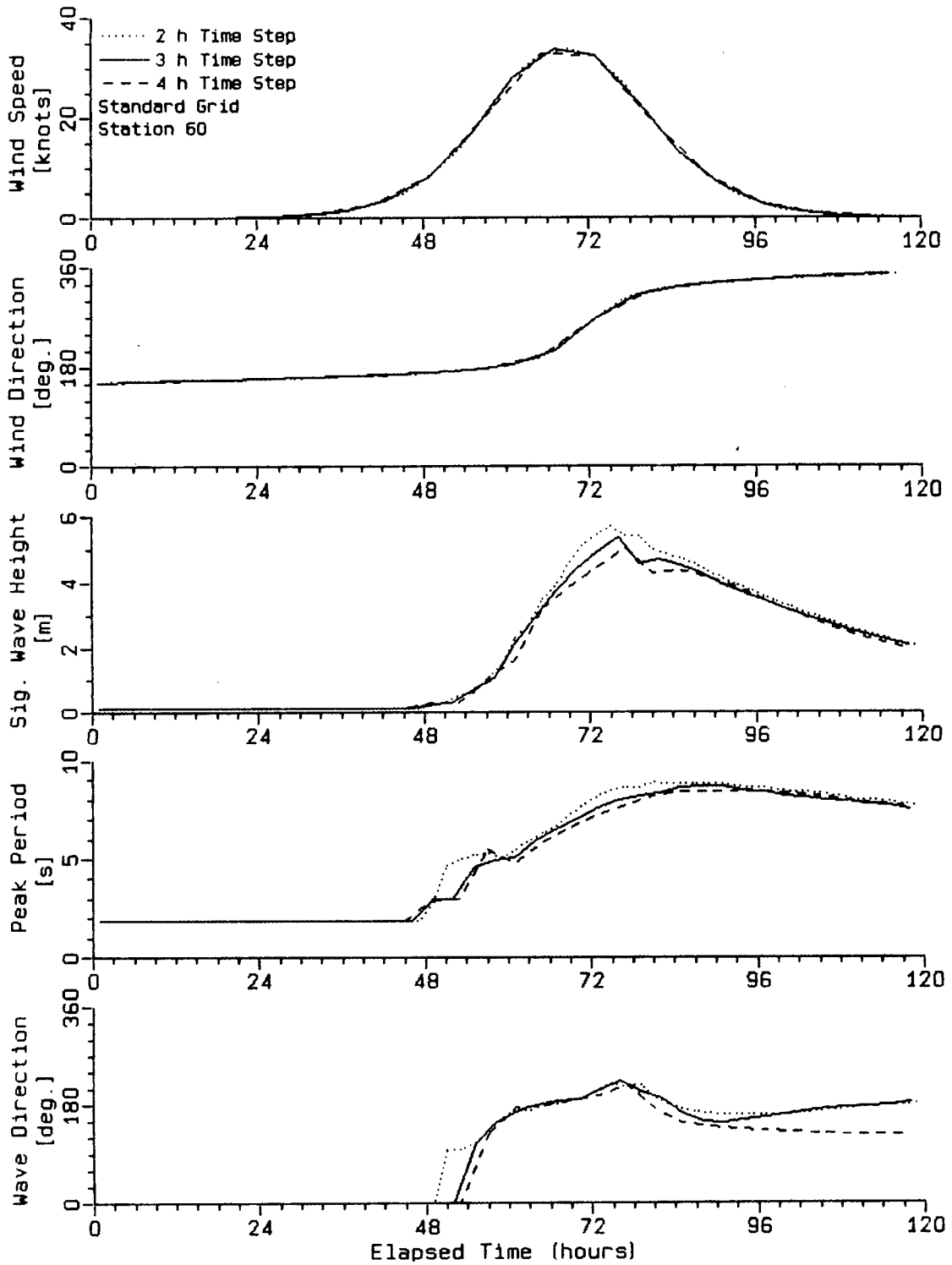

FIGURE 3.25 SENSITIVITY TO TIME STEP. SYNTHETIC INPUT HINDCASTS AT STATION 60.

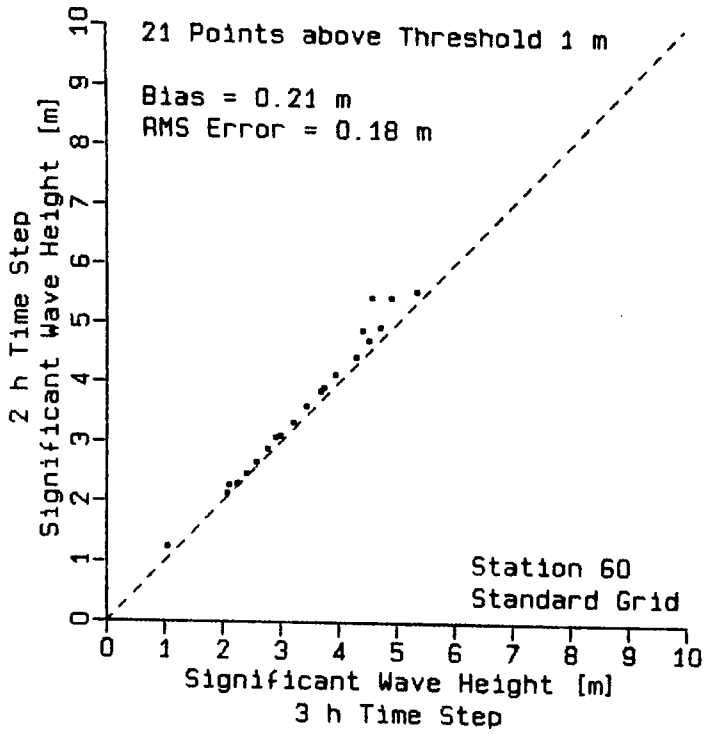

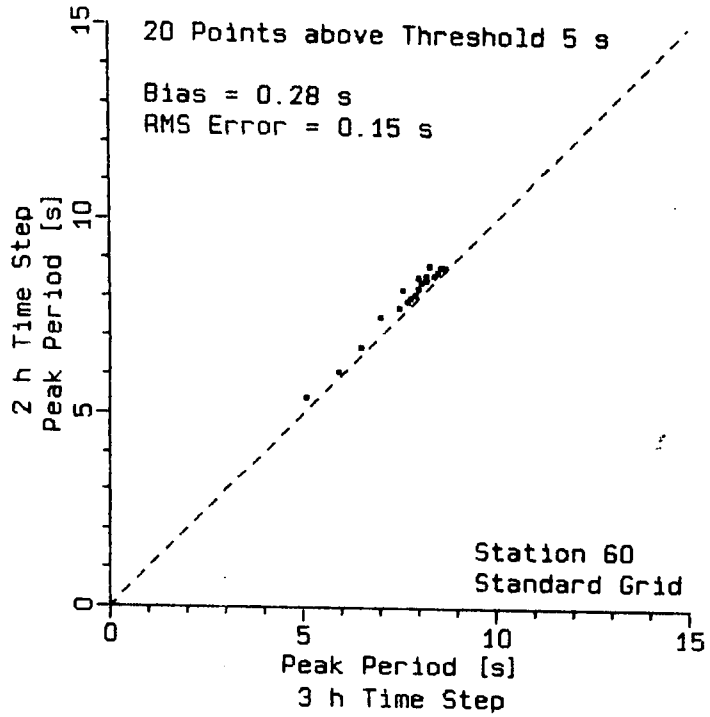

FIGURE 3.26 COMPARISON OF HINDCAST WAVE PARAMETERS AT STATION 60: 2 H VERSUS 3 H TIME STEP.

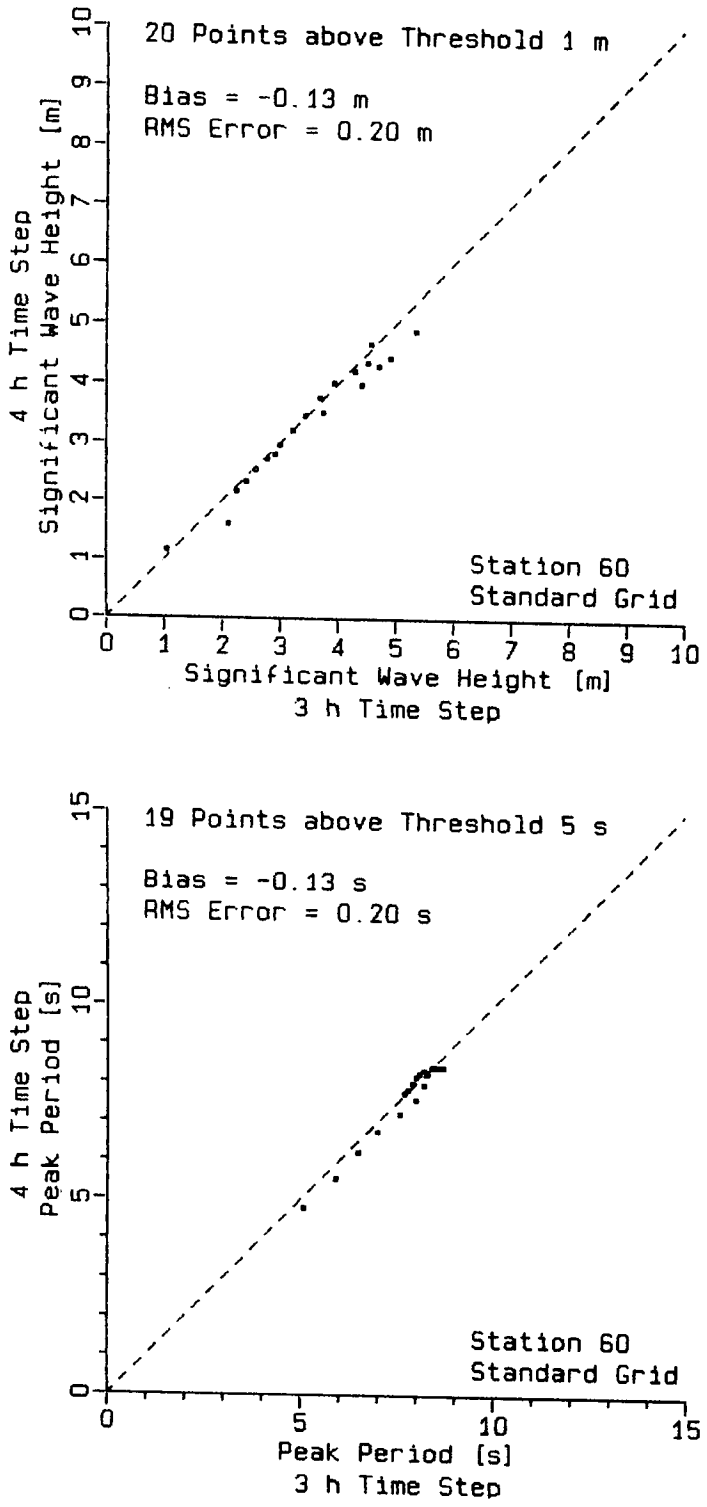

FIGURE 3.27 COMPARISON OF HINDCAST WAVE PARAMETERS AT STATION 60: 4 H VERSUS 3 H TIME STEP.

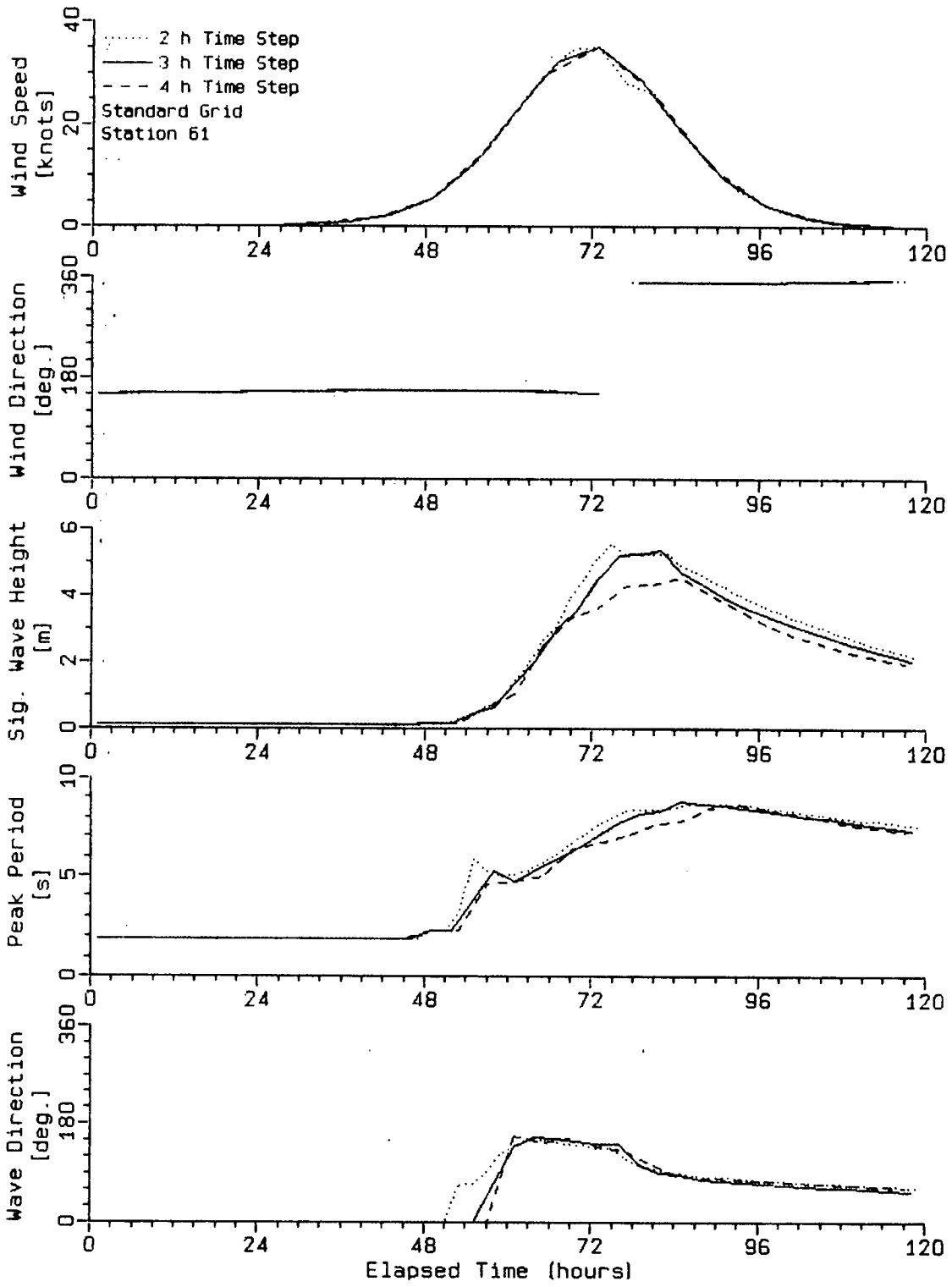

FIGURE 3.28 SENSITIVITY TO TIME STEP. SYNTHETIC INPUT HINDCASTS AT STATION 61.

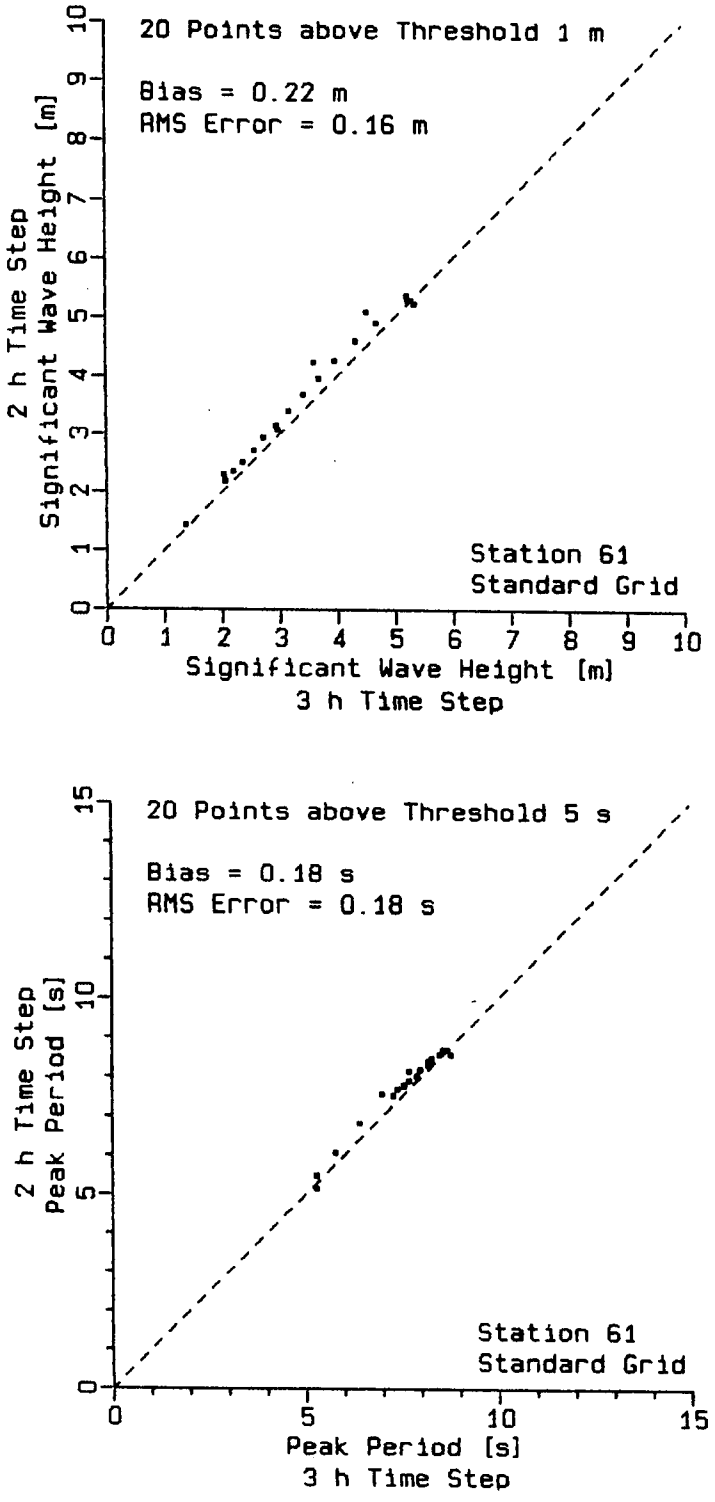

FIGURE 3.29 COMPARISON OF HINDCAST WAVE PARAMETERS AT STATION 61: 2 H VERSUS 3 H TIME STEP.

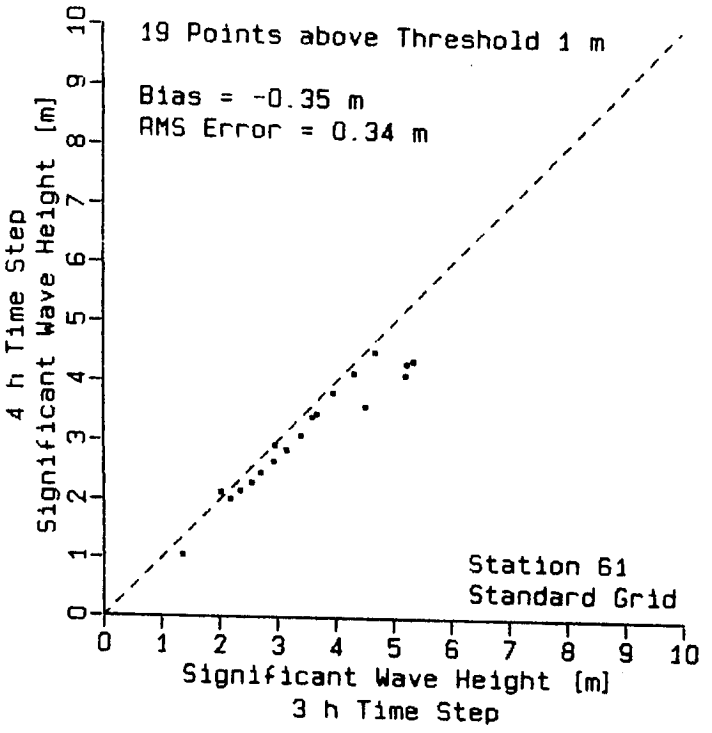

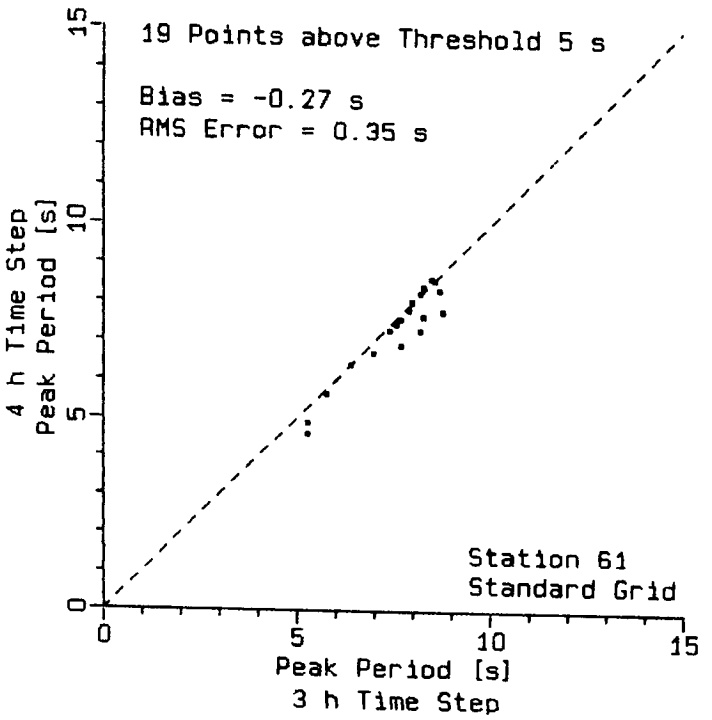

FIGURE 3.30 COMPARISON OF HINDCAST WAVE PARAMETERS AT STATION 61: 4 H VERSUS 3 H TIME STEP.

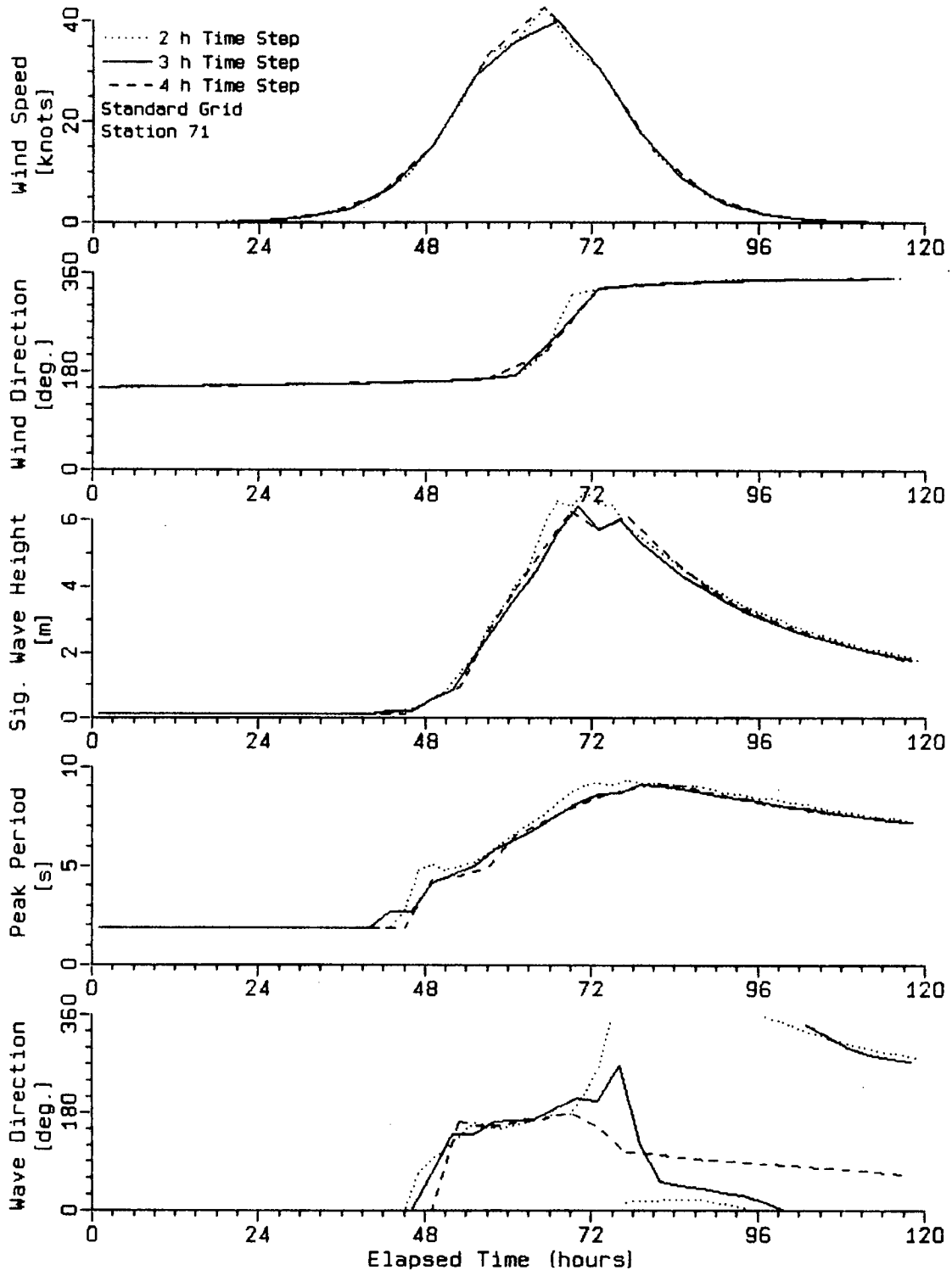

FIGURE 3.31 SENSITIVITY TO TIME STEP. SYNTHETIC INPUT HINDCASTS AT STATION 71.

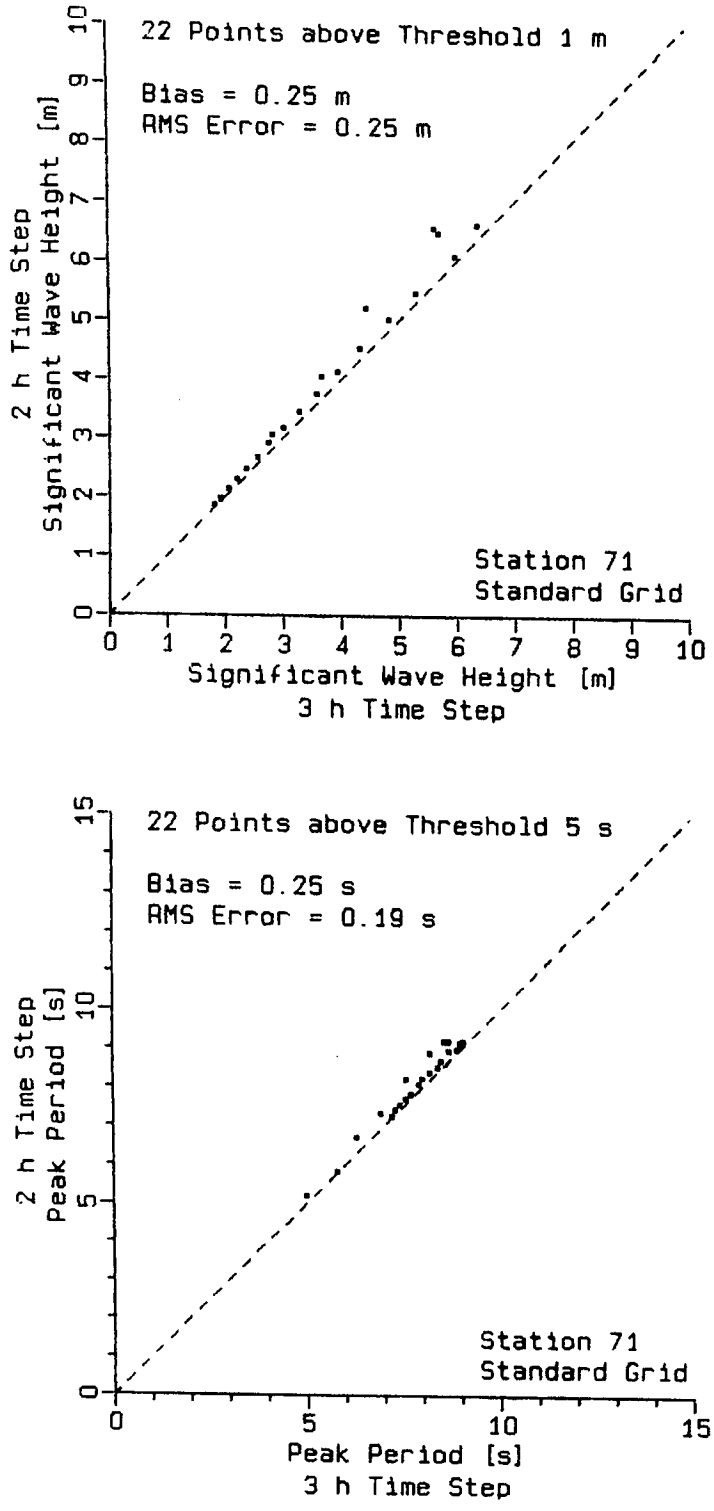

FIGURE 3.32 COMPARISON OF HINDCAST WAVE PARAMETERS AT STATION 71: 2 H VERSUS 3 H TIME STEP.

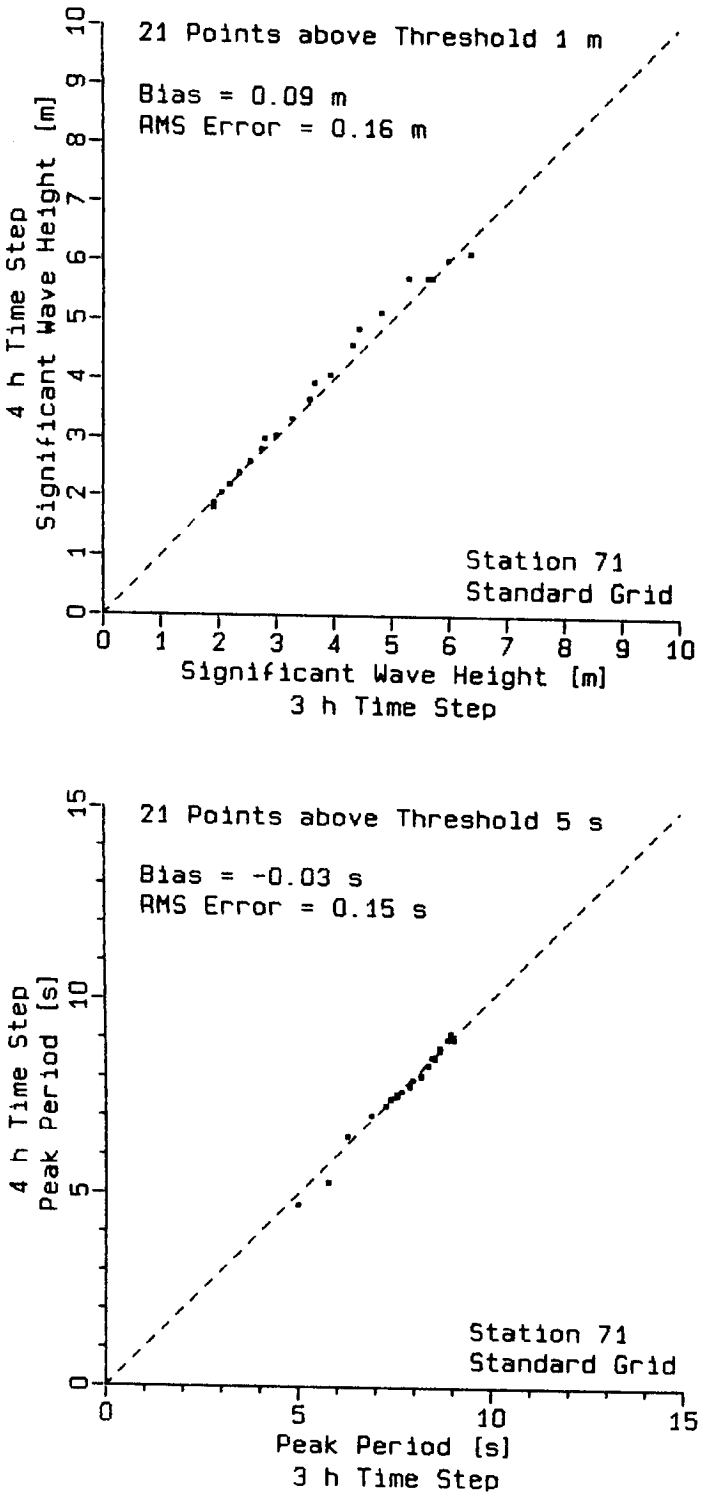

FIGURE 3.33 COMPARISON OF HINDCAST WAVE PARAMETERS AT STATION 71: 4 H VERSUS 3 H TIME STEP.

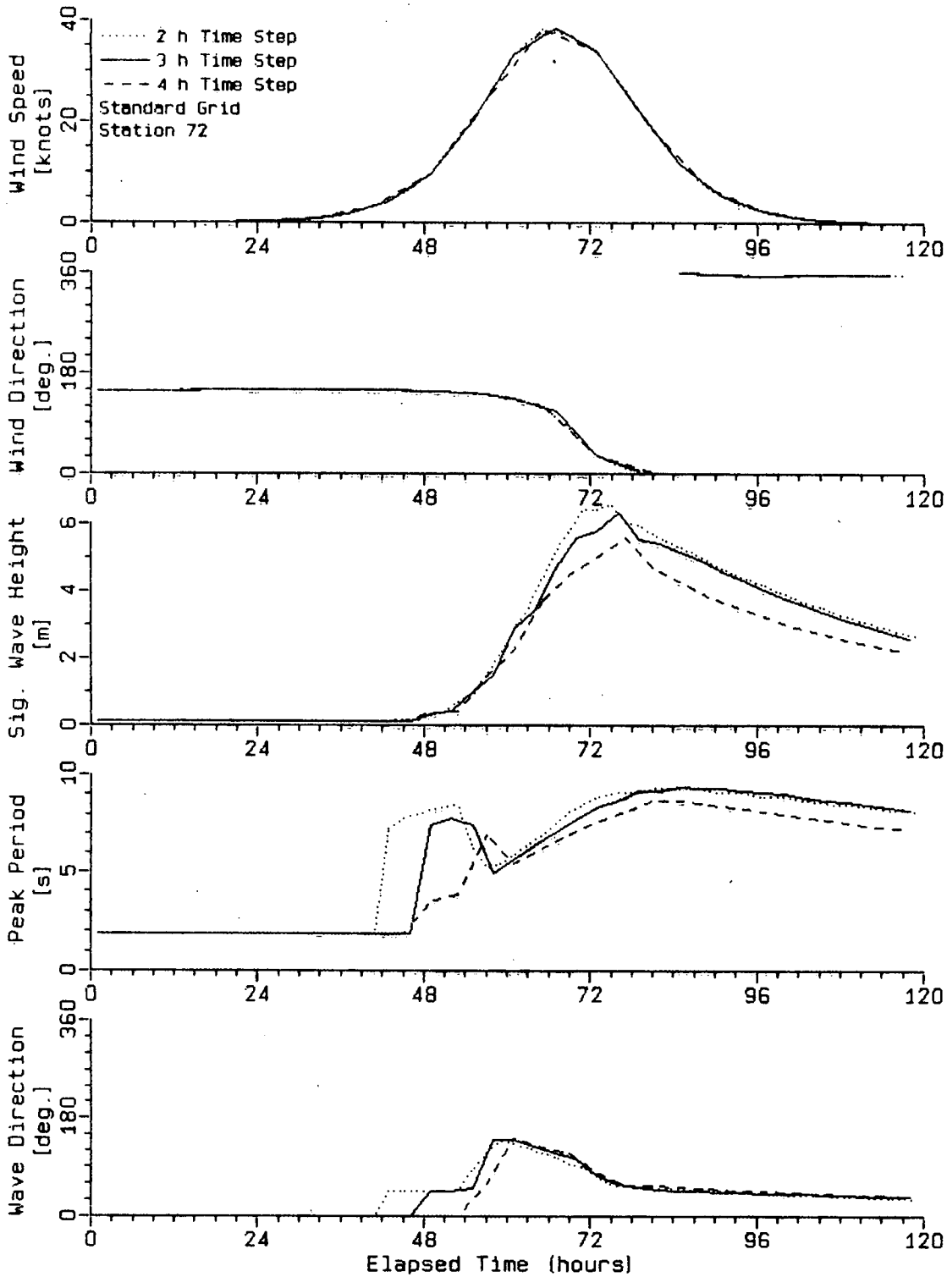

FIGURE 3.34 SENSITIVITY TO TIME STEP. SYNTHETIC INPUT HINDCASTS AT STATION 72.

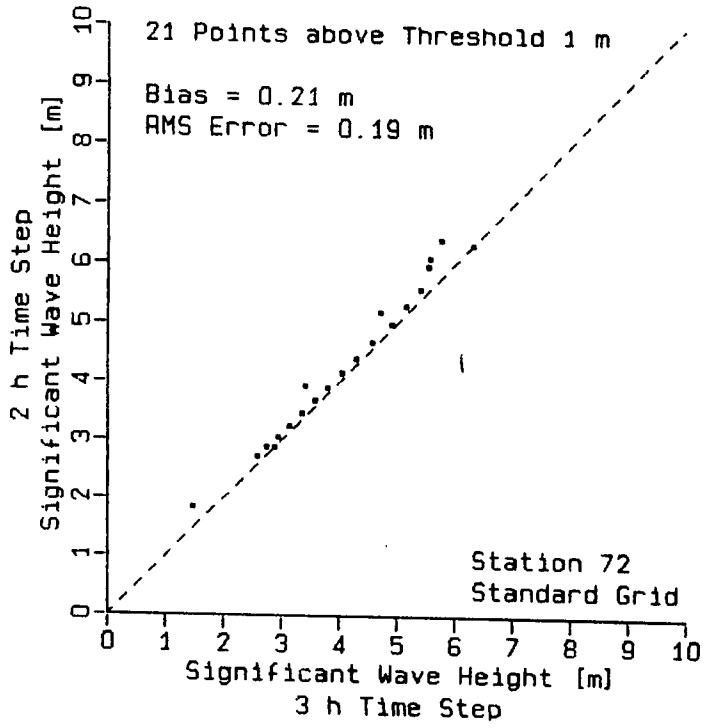

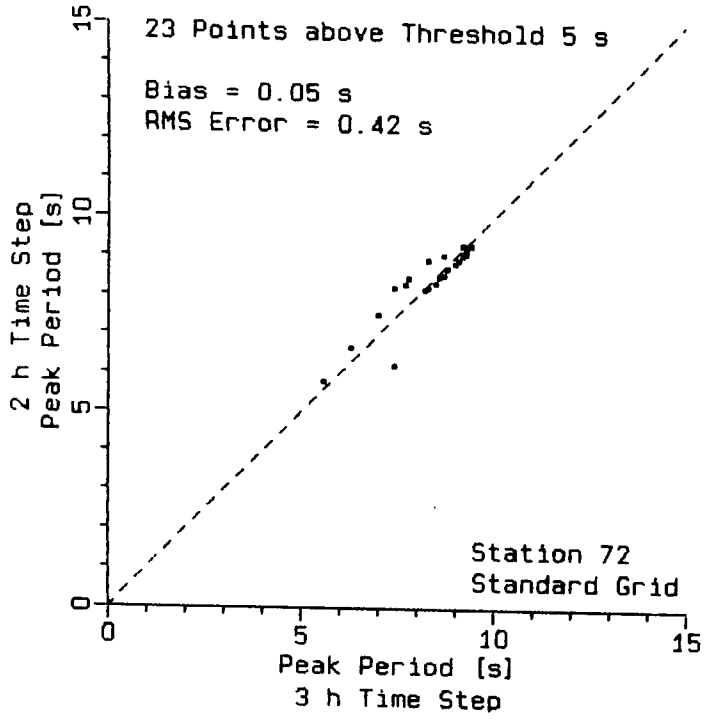

FIGURE 3.35 COMPARISON OF HINDCAST WAVE PARAMETERS AT STATION 72: 2 H VERSUS 3 H TIME STEP.

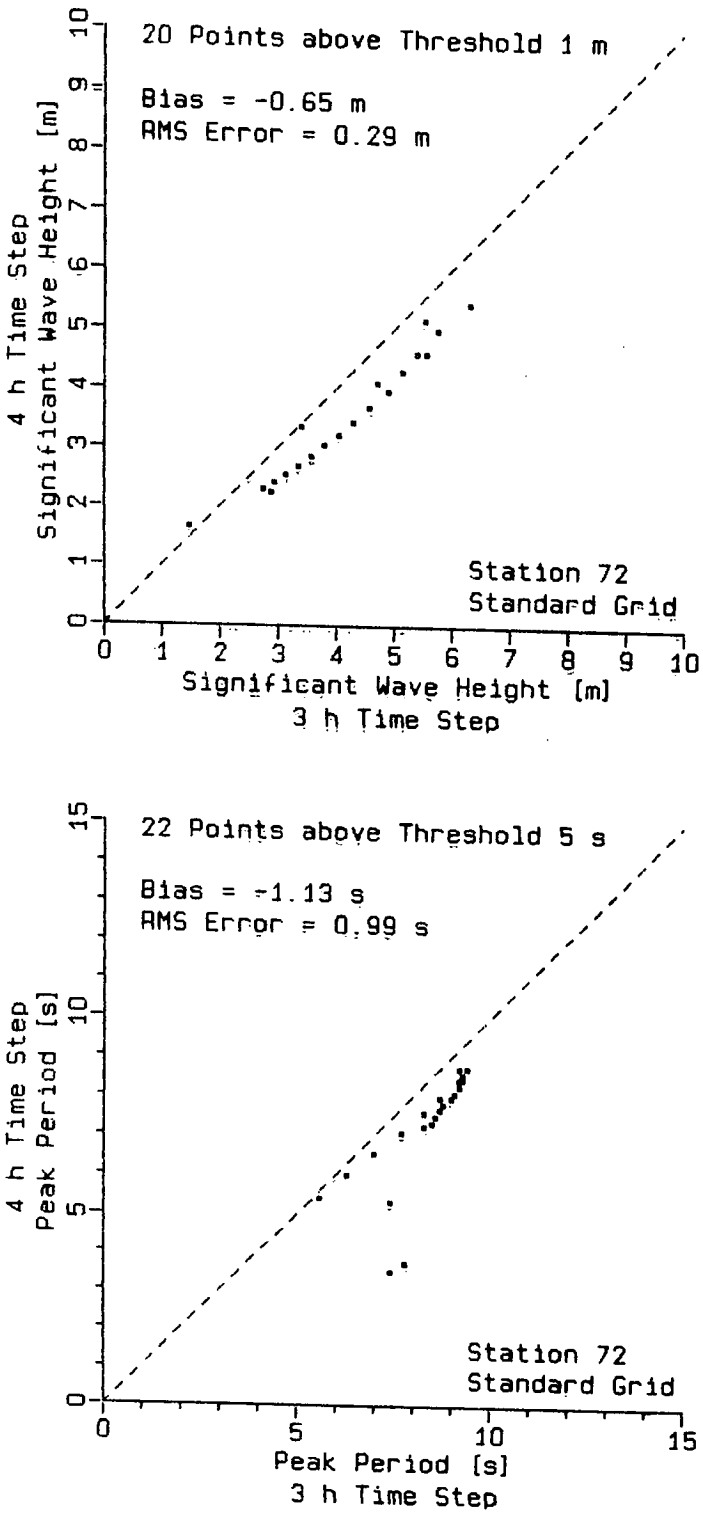

FIGURE 3.36 COMPARISON OF HINDCAST WAVE PARAMETERS AT STATION 72: 4 H VERSUS 3 H TIME STEP.

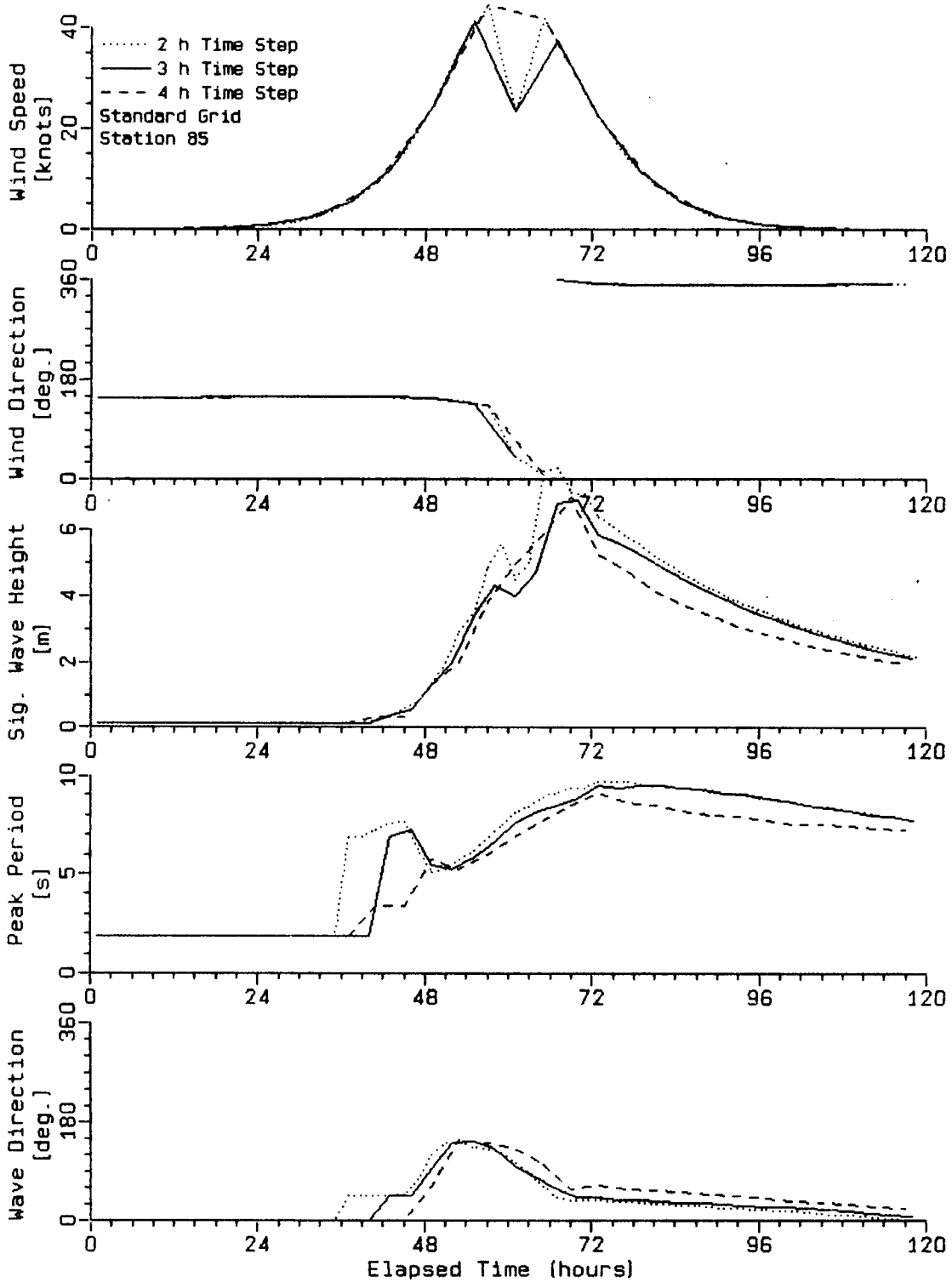

FIGURE 3.37 SENSITIVITY TO TIME STEP. SYNTHETIC INPUT HINDCASTS AT STATION 85.

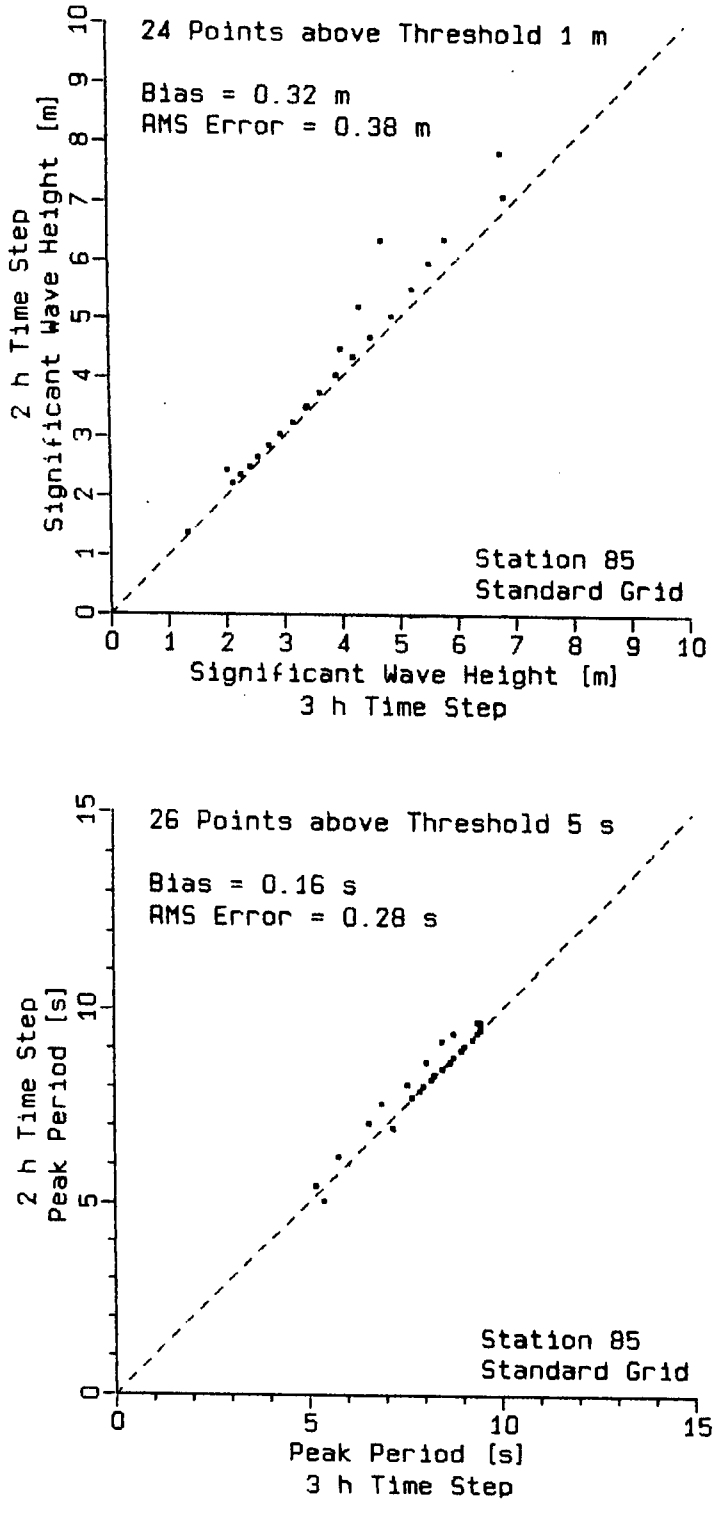

FIGURE 3.38 COMPARISON OF HINDCAST WAVE PARAMETERS AT STATION 85: 2 H VERSUS 3 H TIME STEP.

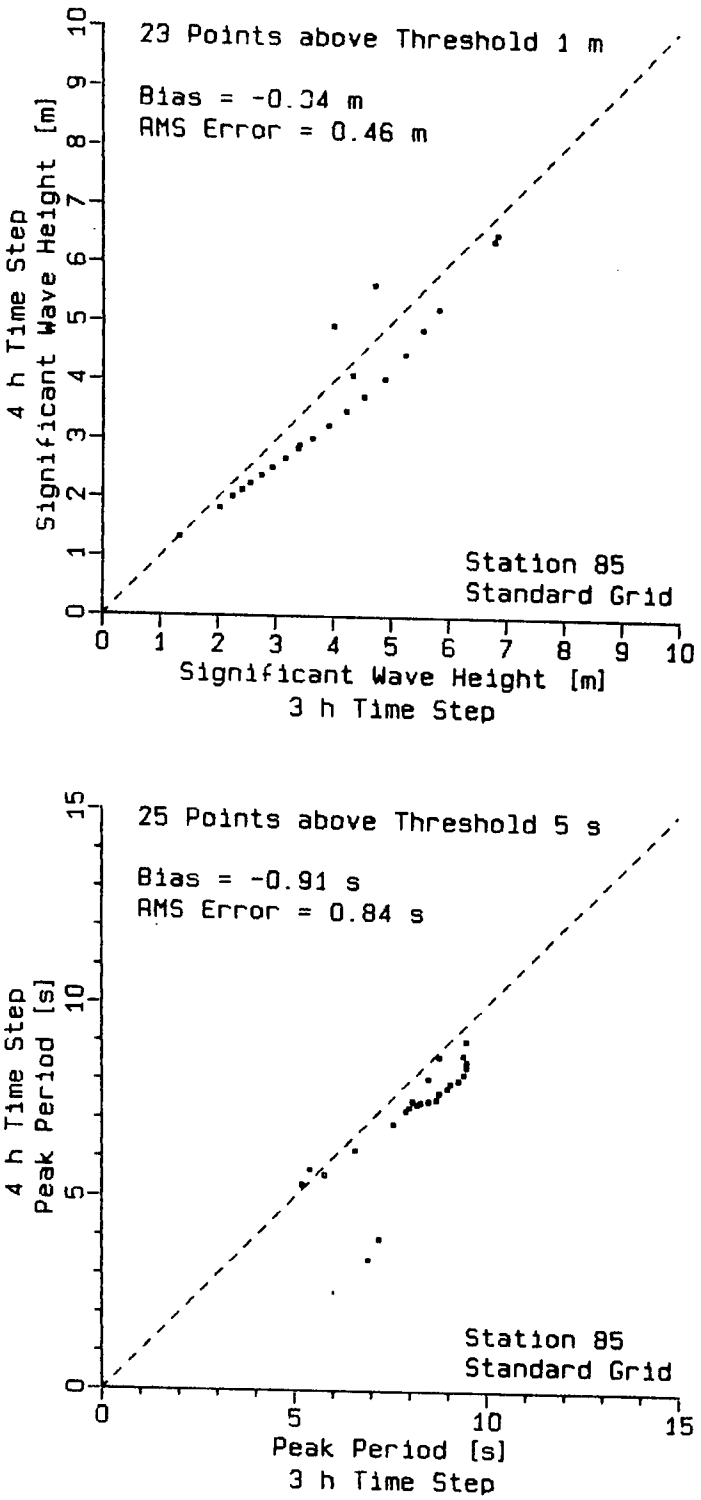

FIGURE 3.39 COMPARISON OF HINDCAST WAVE PARAMETERS AT STATION 85: 4 H VERSUS 3 H TIME STEP.

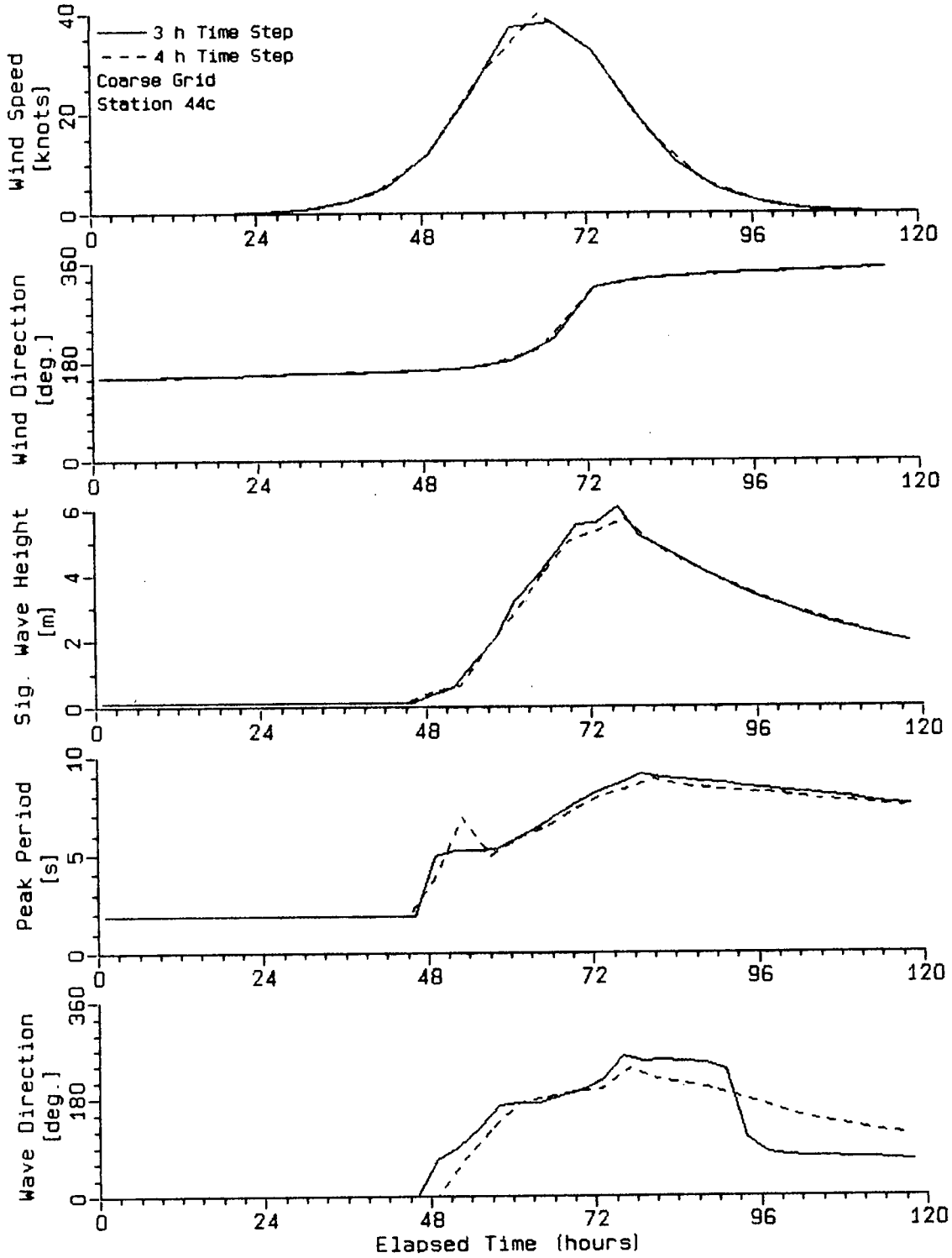

FIGURE 3.40 SENSITIVITY TO TIME STEP. SYNTHETIC INPUT HINDCASTS AT STATION 44C - COARSE GRID.

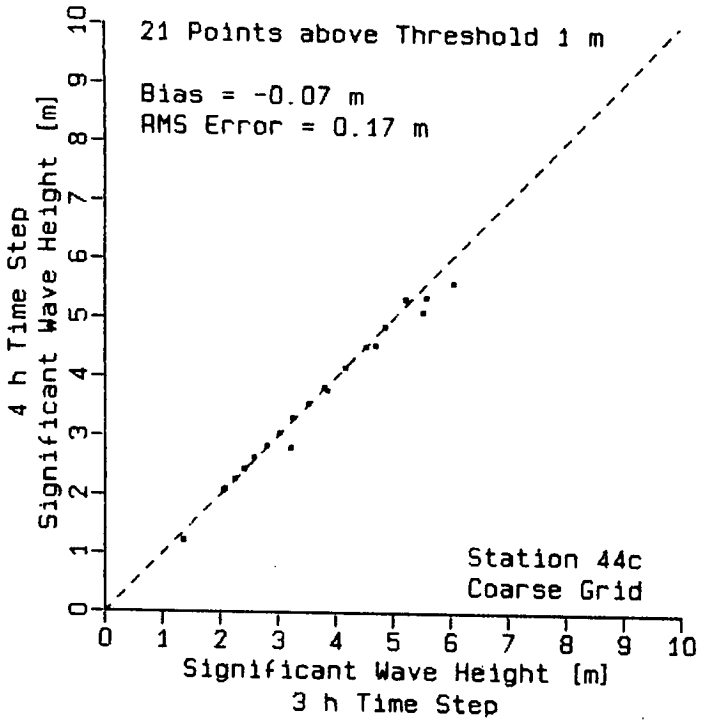

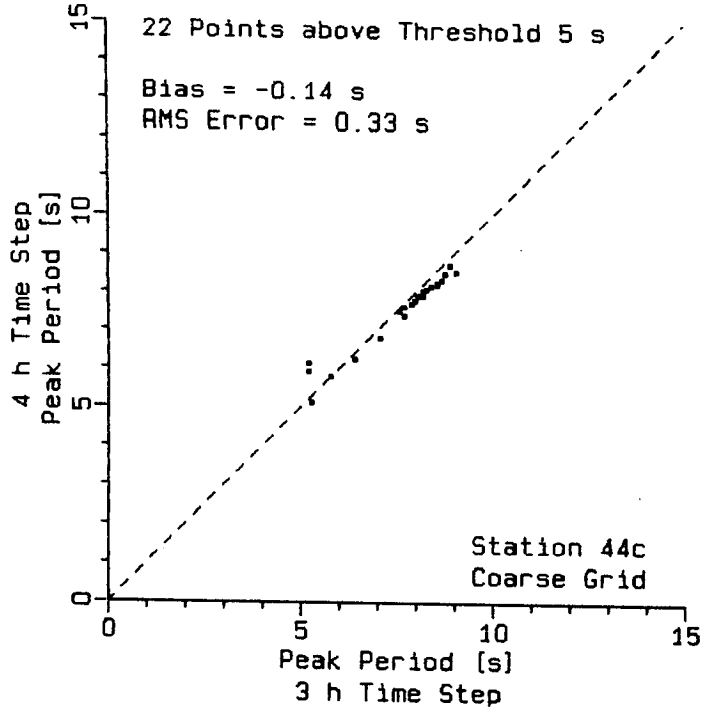

FIGURE 3.41 COMPARISON OF HINDCAST WAVE PARAMETERS AT STATION 44C: 4 H VERSUS 3 H TIME STEP.

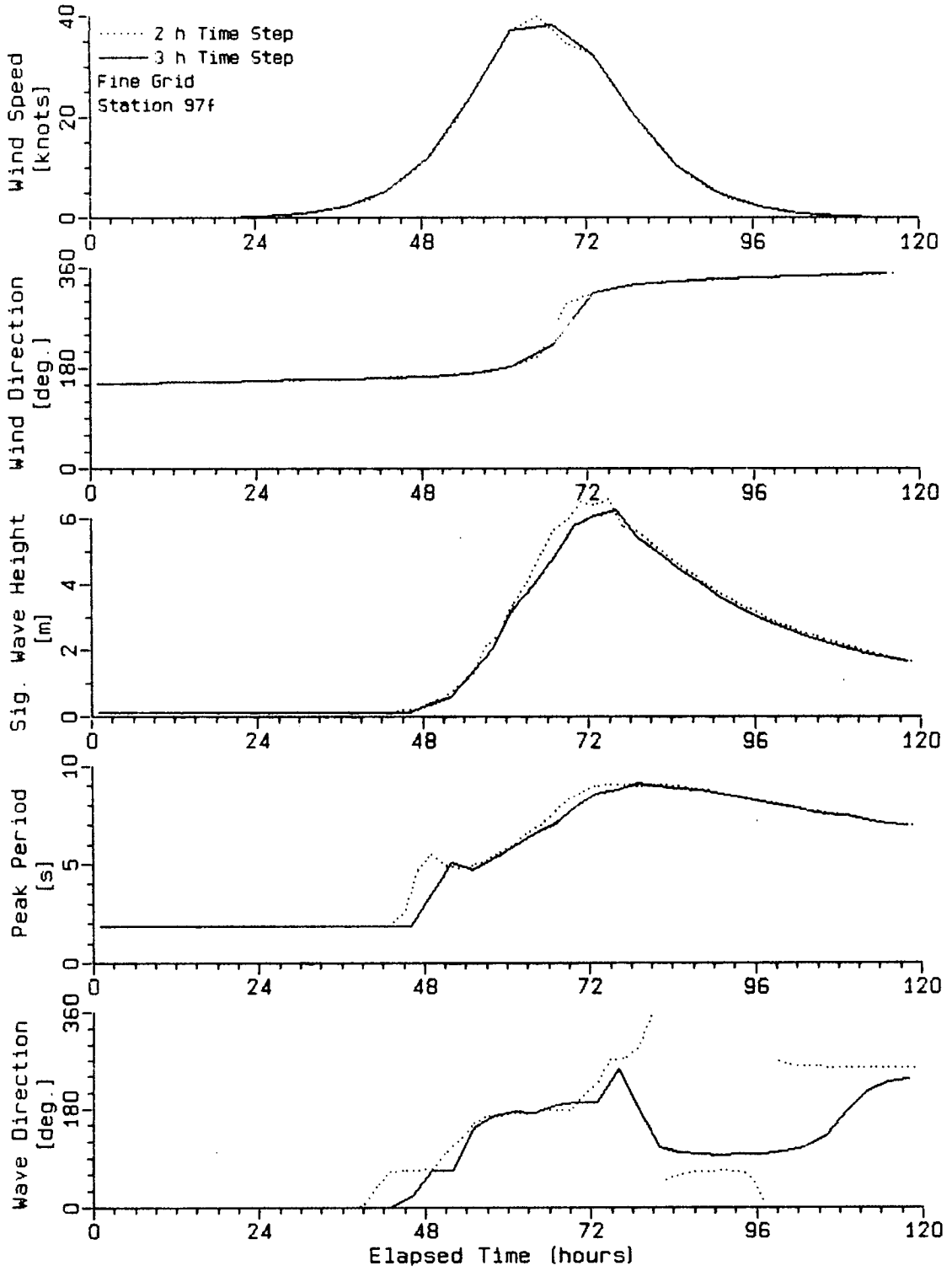

FIGURE 3.42 SENSITIVITY TO TIME STEP. SYNTHETIC INPUT HINDCASTS AT STATION 97F - FINE GRID.

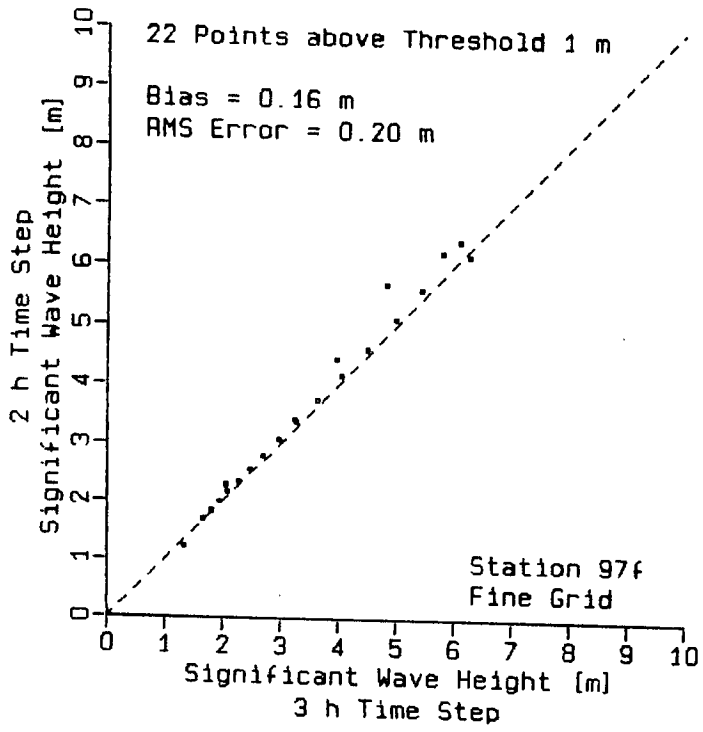

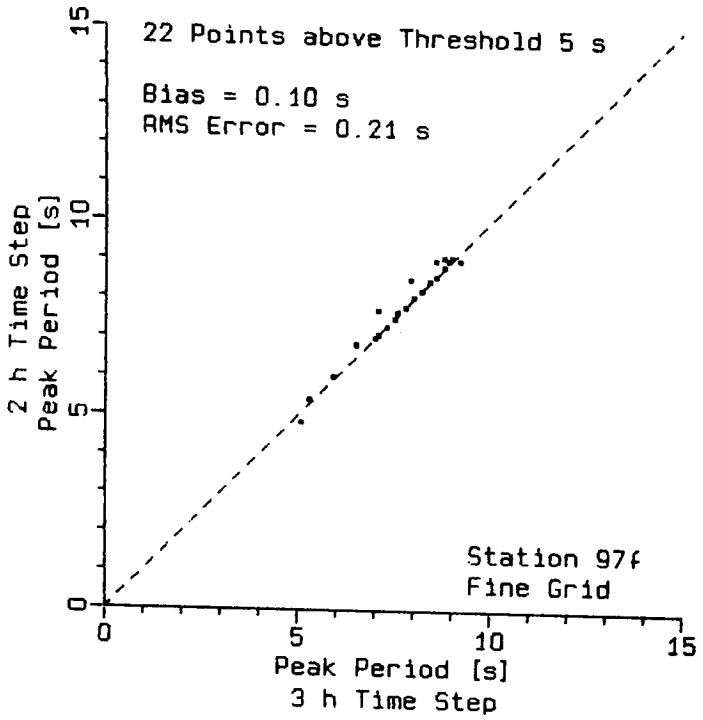

FIGURE 3.43 COMPARISON OF HINDCAST WAVE PARAMETERS AT STATION 97F: 2 H VERSUS 3 H TIME STEP.

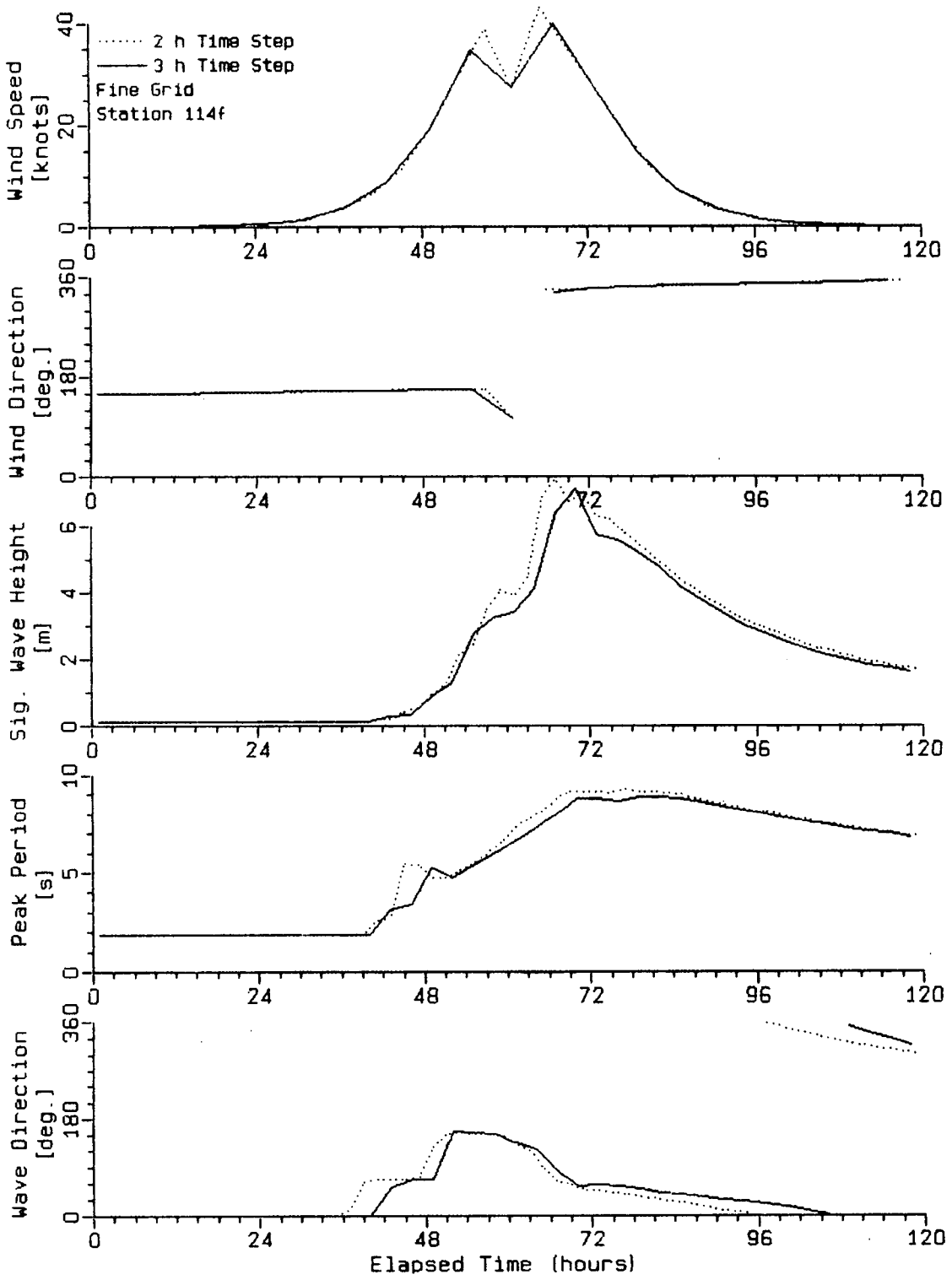

FIGURE 3.44 SENSITIVITY TO TIME STEP. SYNTHETIC INPUT HINDCASTS AT STATION 114F - FINE GRID.

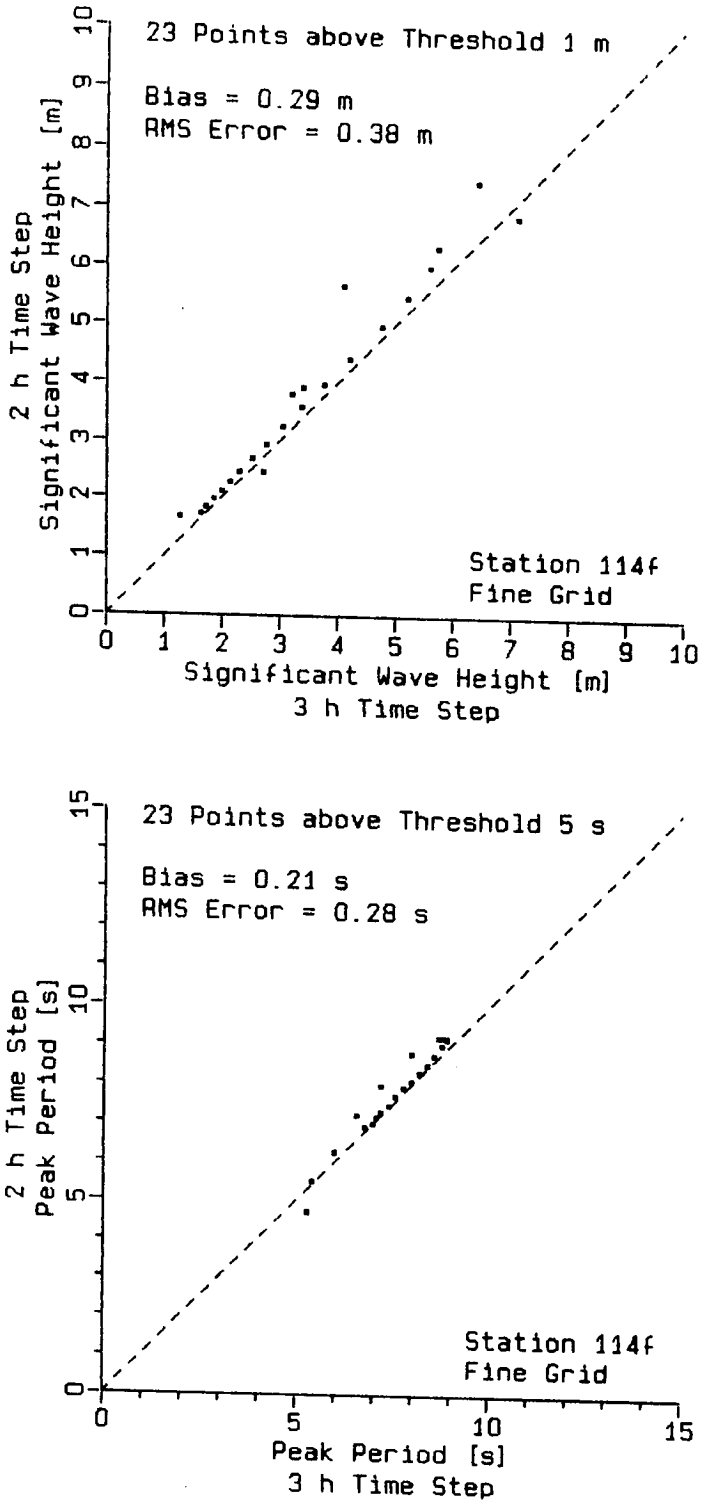

FIGURE 3.45 COMPARISON OF HINDCAST WAVE PARAMETERS AT STATION 114F: 2 H VERSUS 3 H TIME STEP.

that the peak in significant wave height is reached earlier. There is no corresponding shift in the maximum local wind speed therefore the shift is most likely due to a change in the accuracy of the time-wise integration of the governing energy equation. For a shorter time step the significant wave heights also fall off slightly more rapidly with the decreasing wind. In view of the insufficient wave decay noted in the real event hindcasts it can be expected that a shorter time step would lead, after a proper calibration, to an improved agreement with observation. Peak periods are somewhat higher for hindcasts with shorter time steps. Since in both real event hindcasts (Figures 3.12 to 3.17) the peak periods were underpredicted a shorter time step may also lead to a slightly better agreement with observation for this parameter.

Figure 3.37 shows how a decrease in time step may lead to an improved resolution in the input wind fields. In most practical situations input wind fields are derived from synoptic weather maps which are available only at 6 hourly intervals. For shorter time steps the wind data must be interpolated and an improvement in time-wise resolution is not realized. In principle, however, where a very high accuracy is required, an increased resolution could be

achieved by a careful post-analysis, and by incorporating additional wind data collected at non-synoptic times, in place of the time-wise interpolation.

3.4 CONCLUSIONS AND RECOMMENDATIONS

The tests presented here do not show a clear advantage in using a grid finer than the standard MEDS SOG. This seems to indicate that the numerical solution of the governing equation is not sensitive to a further decrease in grid spacing, and that a possible improvement may be masked by other factors. In particular the tests suggest that at least for some storms it is important to carefully match the grid to the location for which the hindcast (or comparison) is required. The standard grid seems to be optimized for hindcasts at Hibernia and a change in grid spacing would have to be accompanied by a shift in the grid, if the hindcasts were to be made for the same location.

The wave simulations are sensitive to boundary resolution during episodes containing offshore winds. For some applications (such as for example general wave forecasting) the simulation results may be required over certain area

rather than at a specific site. In such cases smaller grid spacing should lead to a better boundary resolution and a more accurate representation of fetch. Obviously, in the case of site specific hindcasts the distance of the hindcast site from land limits the possible choices of grid spacing that will improve the fetch representation.

Finally, the resolution of input wind fields is limited by the wind analysis method and by the 2.5° x 2.5° spacing of the input grid rather than by the wave model grid. Therefore, should the wave model grid spacing be decreased it should be accompanied by a corresponding increase in the resolution of the wind fields.

The hindcast results are more sensitive to a change in time step. There are indications that a decrease in time step leads to an emphasis of the peak, and a more rapid fall off, in the significant wave height. This should lead to an improved agreement with observation in the real event hindcasts presented in this report. It is therefore recommended that a shorter, for example 2 h, time step be employed in future hindcasts.

4. EFFECT OF VARIATION IN THE PERCENTAGE OF PRESSURE BASED WINDS VERSUS KINEMATIC ANALYSIS WINDS

4.1 INTRODUCTION

Wind fields used in the MEDS hindcast procedure are a mixture of winds computed from surface pressure fields and winds obtained through kinematic analysis. The pressure fields are produced by interpolating background pressures defined on a 10° latitude x 10° longitude grid, onto a finer mesh (2.5° x 2.5°) grid and than overlaying them with representations of storm systems. The storm systems are specified by the position of their centre and by measurements from the centre to surrounding isobars for each of the 8 points of the compass (i.e. every 45 degrees of azimuth). Only closed isobaric features can be represented in this way.

The kinematic analysis winds are specified on a diamond grid with values given at the corners and in the centre of each 5° latitude by 5° longitude box. The grid may be variable in size but the basic diamond pattern must be maintained. The two wind fields are blended together for later interpolation onto the spherical orthogonal grid. At

present MEDS uses a blend of 20% pressure based winds and 80% kinematic analysis winds.

In designing this set of tests it was realized that there is a great risk that, rather than evaluating the sensitivity of the hindcast technique, the tests may result in comparison between the skills of the analyst who produced the weather analysis charts and the skills of the analyst responsible for the kinematic analysis. An attempt was therefore made to utilize, as input, data sets as free of subjective influences as possible.

It is believed that the wave hindcasts and observations prepared for the ESRF Wave Directional Spectrum Intercomparison Study provided the means to achieve the above objective. Wave hindcasts for two storm events during March 1984 were prepared for the intercomparison and they showed a good agreement with observation (Juszko, 1985). Kinematic analysis was done by D.T. Resio at Offshore and Coastal Technologies, Inc. for an area from 36°N to 54°N and 38°W to 70°W. Surface pressures were scaled off Atlantic Weather Centre surface analyses, and a planetary boundary layer model was employed to compute wind velocity at 10m height from local pressure gradients. The input wave fields were a mixture of

pressure based winds and kinematic analysis winds with a ratio of 0.2 : 0.8 for all grid points with the exception of the comparison grid point (46°N, 48°W) where winds derived from observations at nearby drilling vessels were used alone without a contribution from the pressure based winds. The difference between the anemometer height of the drilling vessel and the standard 10 m level was accounted for by means of a planetary boundary layer model (for further details of the wind analysis see Penicka et al., 1985).

The good agreement between hindcast and observation suggests that the wind fields assembled for the Intercomparison Study (in the following referred to as OCTI winds) provide a good approximation to the actual winds which occurred during the two storm events. The wind fields consist of 80% kinematic analysis winds (100% at the comparison location) and are believed to be a good representation of kinematic analysis performed by a skilled analyst. In other words, the wind fields are considered, for the purposes of the present study, to be a representative sample drawn from a set of kinematic analyses prepared by a number of skilled analysts. It seems reasonable to assume that the 20% contamination by winds based on surface pressures represents less variability than would be introduced by different analysts.

(Note that the 20% do not refer to an error; the error is most likely much smaller, as indicated by the good hindcast results).

The original OCTI winds were digitized on a 2° latitude x 2° longitude grid and for the present application had to be interpolated to the locations required by the MEDS wind blending program. Quadratic interpolation routine was used to achieve this. Prior to the interpolation winds estimated from weather maps were inserted in place of dummy values over land and on grid boundaries in the original fields. The resulting kinematic analysis winds cover an area from 40°N to 50°N and 40°W to 60°W. The wind speeds and directions were checked against wind observations given on weather maps and for the first storm few of the values were modified where a discrepancy was noticed. (However, this idea was abandoned for the second storm because it was felt that modifying the winds would be inconsistent with the above argument. The discrepancies were few and possibly due to the insertion of replacement values over land and grid boundaries).

The standard MEDS procedure for preparing pressure fields was not followed. Instead, surface pressures on a 2.5° latitude x 2.5° longitude grid were interpolated

directly from CMC pressure analysis data, defined on a polar stereographic grid, which were available on magnetic tape. The CMC analyses are produced by an objective analysis method and therefore are not affected by a subjective judgement of the analyst.

Four blends of pressure based and kinematic analysis winds were compared in these tests: 100% : 0%, 80% : 20%, 50% : 50% and 20% : 80%. The area covered by the kinematic analysis was not sufficiently large for a 0% : 100% hindcast. Therefore separate inputs were prepared by interpolating the OCTI winds over the whole area of their coverage in the same way as described above for the kinematic analysis. In this case the active region of the MEDS wave model grid was reduced to cover the same sea area as the OCTI grid (Figure 4.1). This provided 0% : 100% input consistent with the other blends. In addition, comparison could be made between the MEDS version of the Resio model and the more recent version used by OCTI in which the input and wave propagation terms were modified (Penicka et al., 1985).

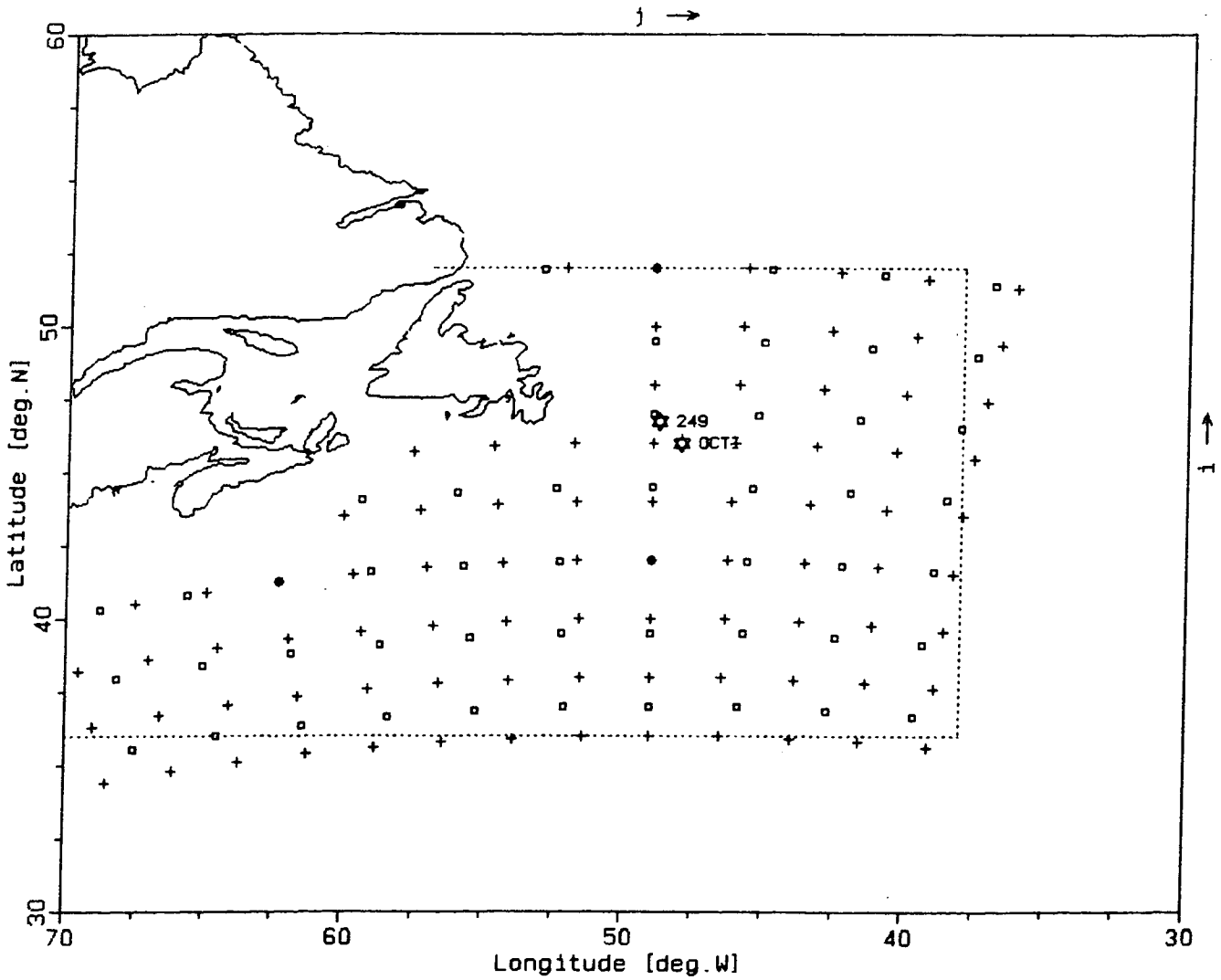

FIGURE 4.1 MODEL GRID AND LOCATIONS OF COMPARISON POINTS. DOTTED LINE MARKS THE EXTENT OF OCTI GRID.

4.2 VARIATION IN THE PERCENTAGE OF PRESSURE BASED AND KINEMATIC ANALYSIS WINDS

Figure 4.2 shows the time series of the wind and wave variables for three combinations of pressure based and kinematic analysis winds for the first storm. Both the observed waves and the OCTI hindcasts are included for reference. The standard MEDS grid and 3 h time step were used in all hindcasts. There is only a small difference between the three estimates of the local winds and an even smaller difference in the hindcast significant wave heights. It is interesting to notice that while the local wind speeds diverge as the wind speed drops the difference in the significant wave heights is the largest at, or immediately after, the peak of the storm, and it becomes quite small towards the end of the storm. The peak wave height is the lowest for the input containing the largest proportion of the pressure based winds (80%) which seems to indicate some smoothing of pressure gradients. The differences in peak period and in the mean wave directions are negligible.

Figures 4.3 to 4.5 show comparison, for the first storm, of the hindcast versus measured wave parameters for various combinations of pressure based winds and kinematic analysis

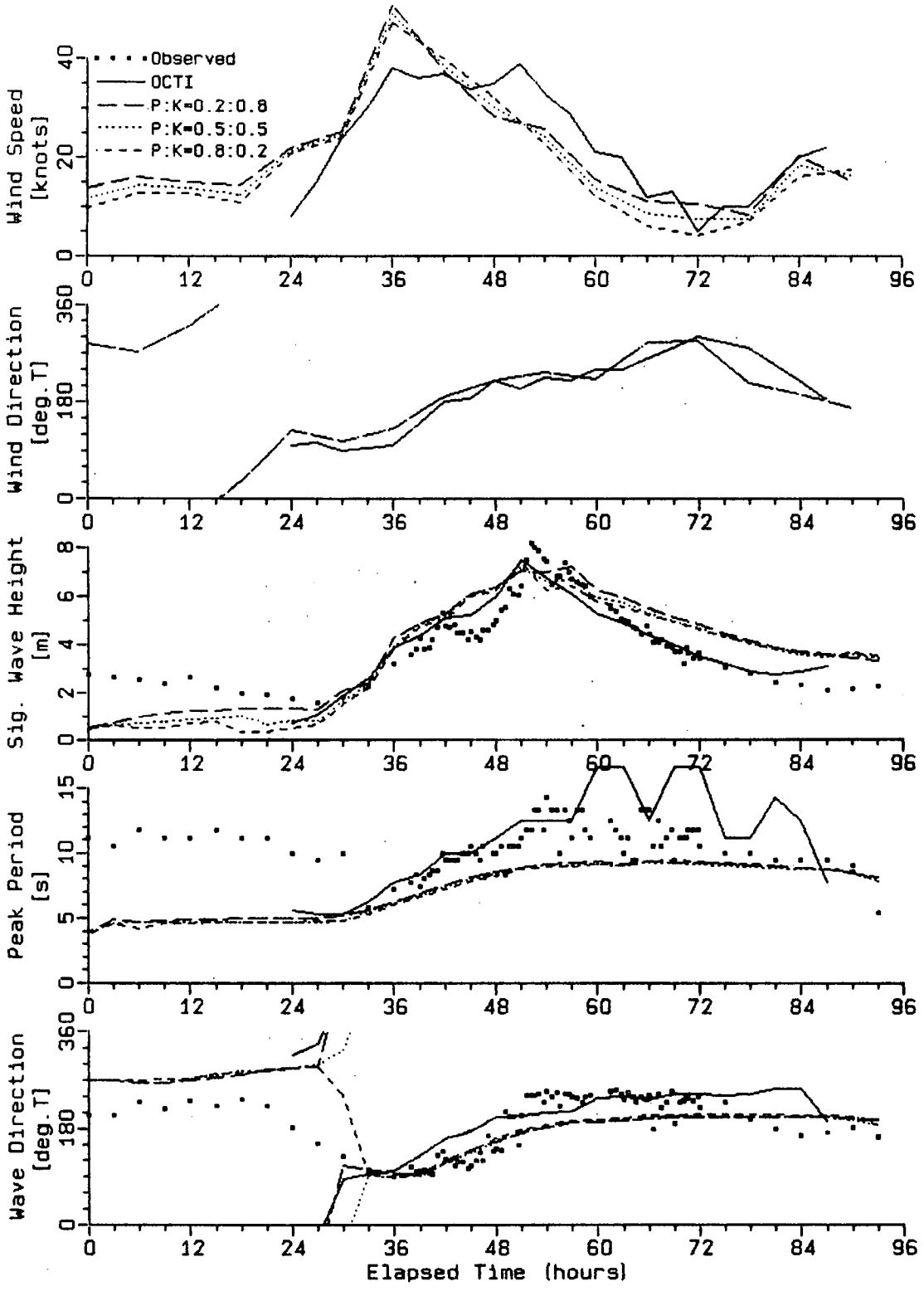

FIGURE 4.2 TIME SERIES OF HINDCAST AND MEASURED WAVE PARAMETERS FOR VARIOUS PROPORTIONS OF PRESSURE BASED WINDS AND KINEMATIC ANALYSIS WINDS - STORM 1.

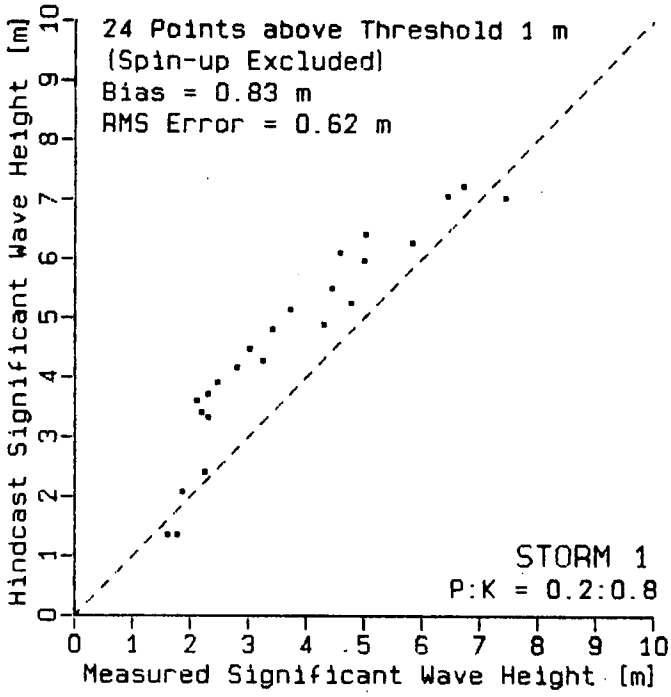

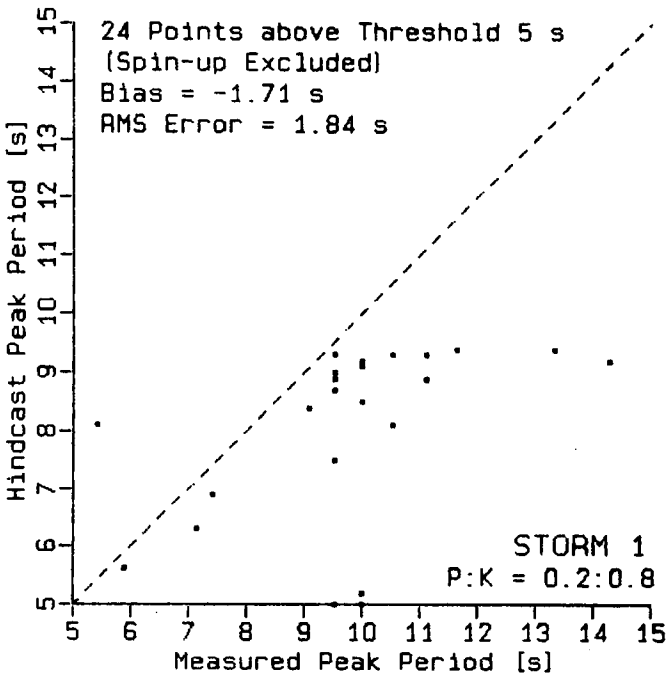

FIGURE 4.3 COMPARISON OF P:K = 20%:80% HINDCAST VERSUS MEASUREMENT FOR STORM 1.

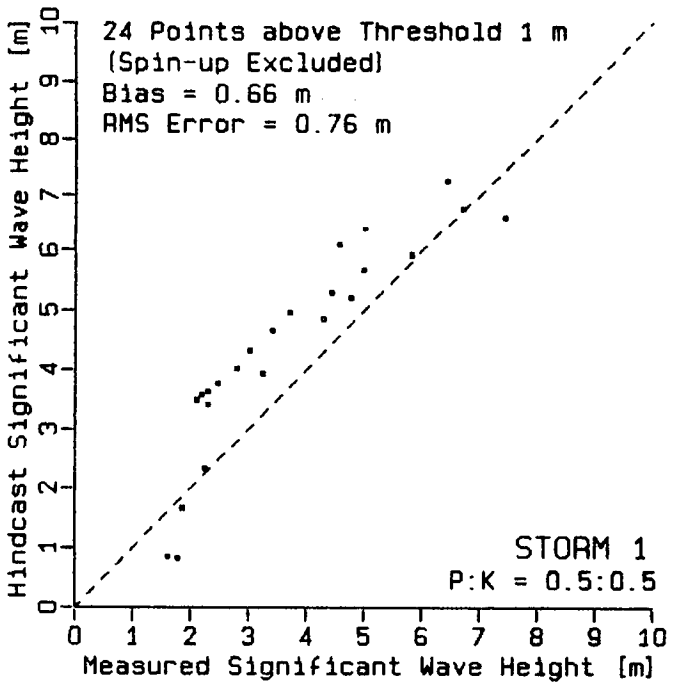

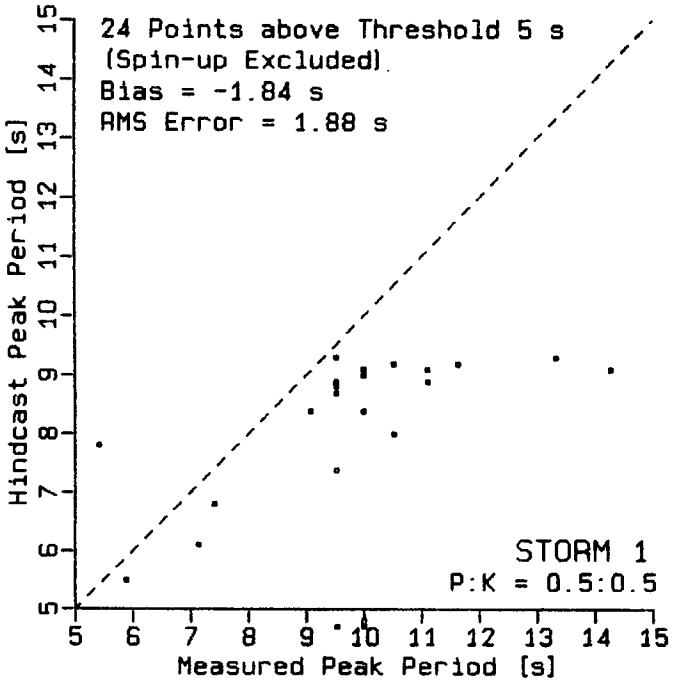

FIGURE 4.4 COMPARISON OF P:K = 50%:50% HINDCAST VERSUS MEASUREMENT FOR STORM 1.

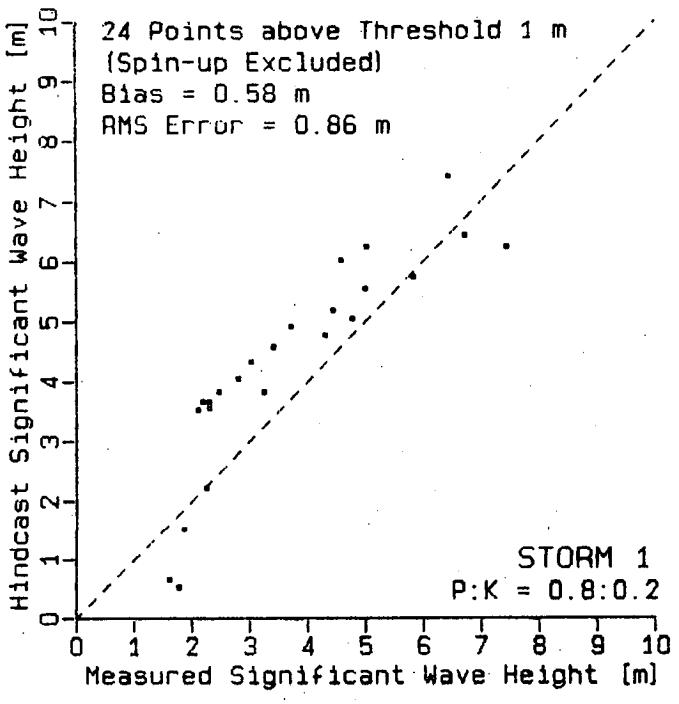

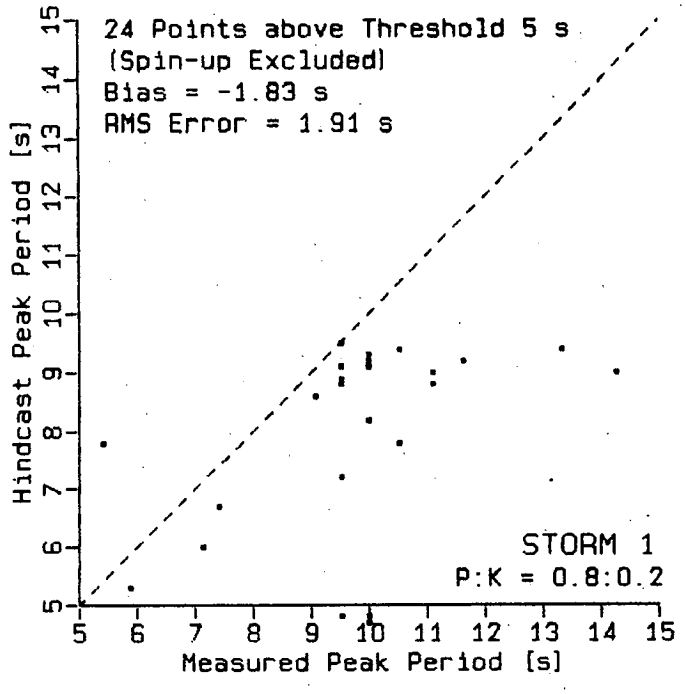

FIGURE 4.5 COMPARISON OF P:K = 80%:20% HINDCAST VERSUS MEASUREMENT FOR STORM 1.

winds. The wind fields containing the largest percentage of the pressure based winds result in wave hindcast with the lowest bias (0.58 m) and the highest RMS error (0.86 m) in significant wave height, and the highest RMS error in peak period (1.91 s). The peak period bias (-1.83 s) is almost the same as that of the 50%:50% blend (-1.84 s) which is the highest. Wind fields containing the largest percentage of kinematic analysis winds lead to significant wave heights with the highest bias (0.83 m) but the lowest RMS error (0.62 m). The peak period also exhibits the lowest bias (-1.71 s) and the lowest RMS error (1.84) for this blend.

Figure 4.6 presents the time series of the wind and wave variables for the second storm. In this case the differences between the hindcasts are much greater particularly after the storm reached its peak. Since the differences in local winds do not follow the same pattern the differences in wave parameters must be due to the advection from surrounding grid points. The divergence from the observed wave parameters is the greatest, more than 4 m during a part of the storm, for the inputs containing a large proportion of pressure based winds (80% and 100%). This suggests an error in the pressure analysis used to derive the winds.

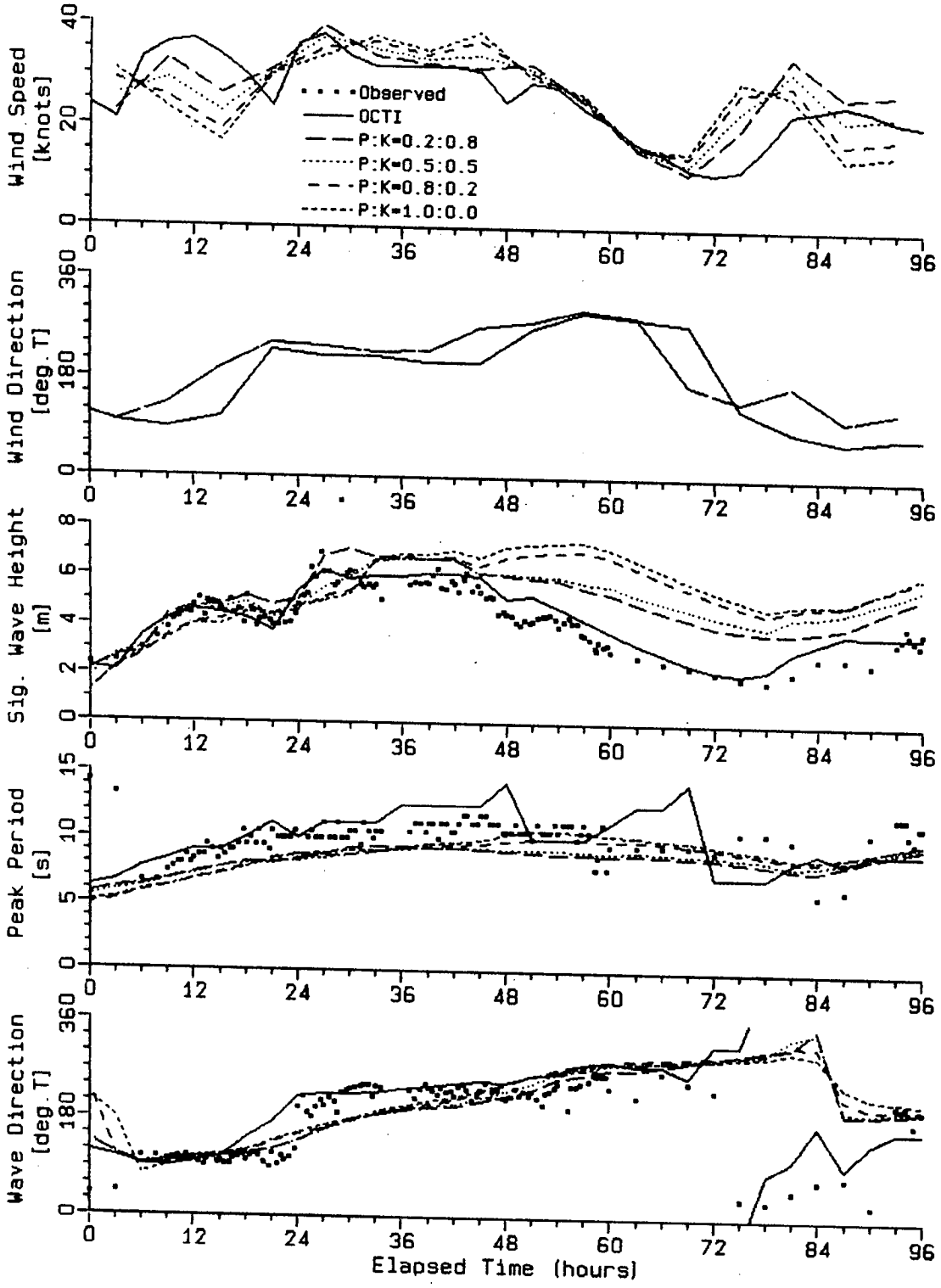

FIGURE 4.6 TIME SERIES OF HINDCAST AND MEASURED WAVE PARAMETERS FOR VARIOUS PROPORTIONS OF PRESSURE BASED WINDS AND KINEMATIC ANALYSIS WINDS - STORM 2.

The comparison of the hindcast versus measured wave parameters for the second storm is shown in Figures 4.7 to 4.10. In this case the blend with the highest percentage of kinematic analysis winds results in a hindcast with the best overall significant wave height error (bias 1.28 m, RMS error 0.8 m) and the lowest RMS error in peak period (1.83 s). However, the peak period bias is larger than that of any other combination (-1.53 s). The peak period bias is the smallest in the hindcast using only pressure based winds (-1.14 s) but the other error statistics in this hindcast are substantially degraded (1.77 m bias and 1.71 m RMS error in significant wave height; and 2.17 s bias in peak period).

4.3 COMPARISON WITH MORE RECENT VERSION OF THE RESIO MODEL

Figure 4.11 shows the time series of the OCTI and the MEDS hindcasts, together with the observed waves, for the first storm. It should be noted that since the two grids are different the hindcasts apply to slightly different locations and that neither of these locations coincides with the site of the measurements (Figure 4.1). In the first storm both hindcasts provide similar wave growth with the exception of a slight dip at around 45 hours (corresponding to a dip in

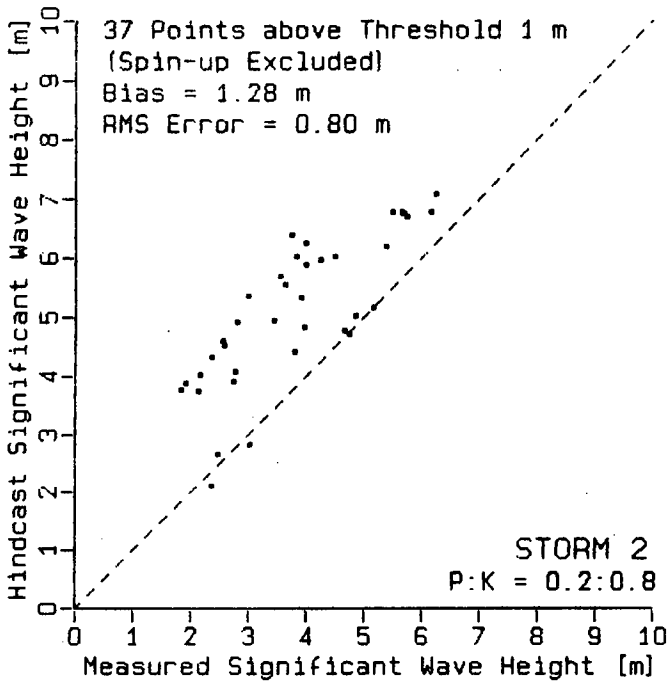

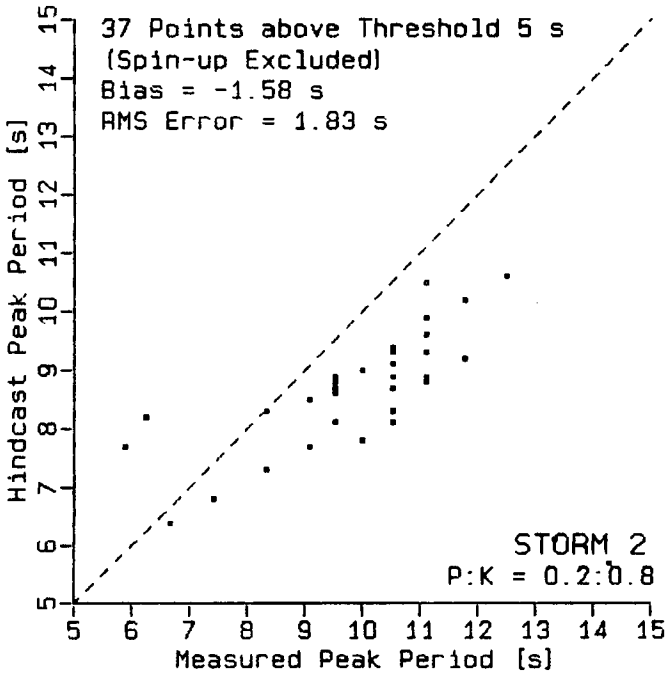

FIGURE 4.7 COMPARISON OF P:K = 20%:80% HINDCAST VERSUS MEASUREMENT FOR STORM 2.

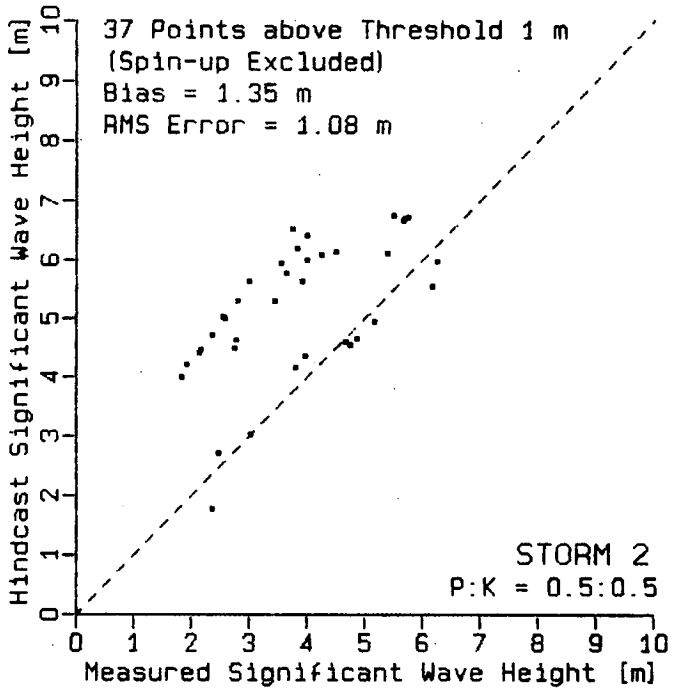

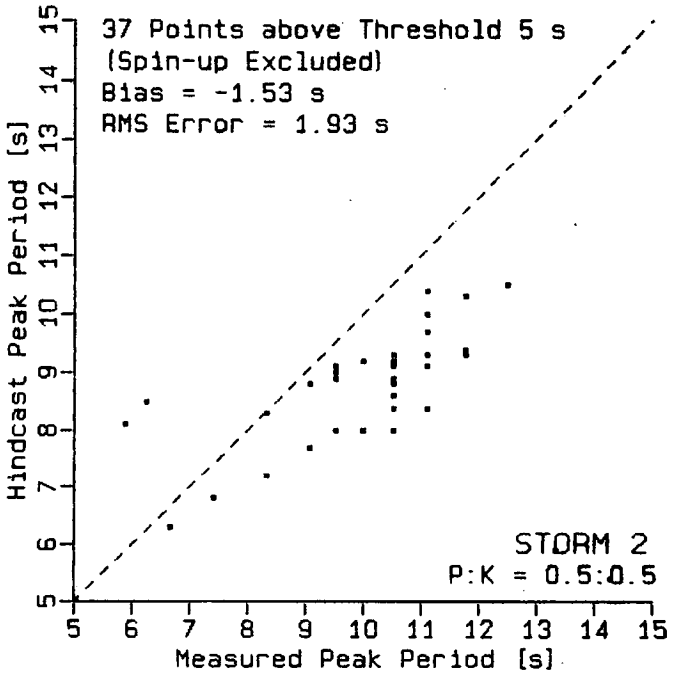

FIGURE 4.8 COMPARISON OF P:K = 50%:50% HINDCAST VERSUS MEASUREMENT FOR STORM 2.

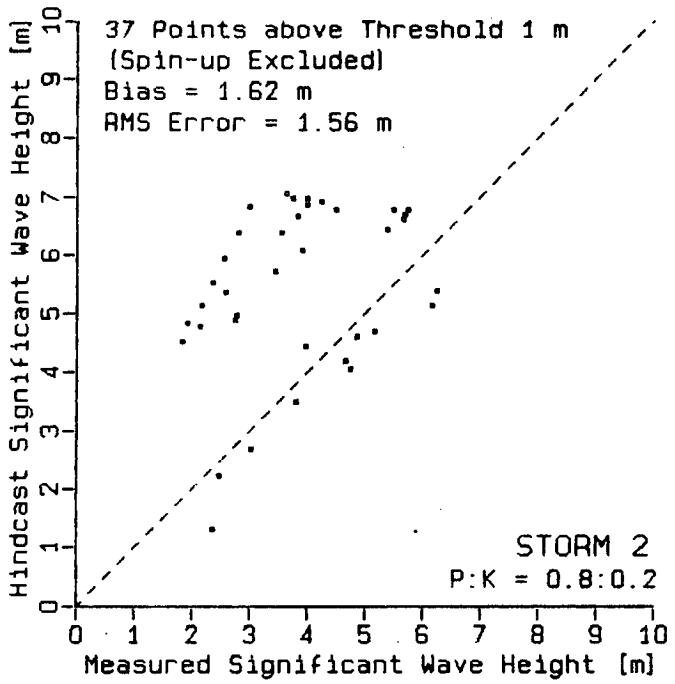

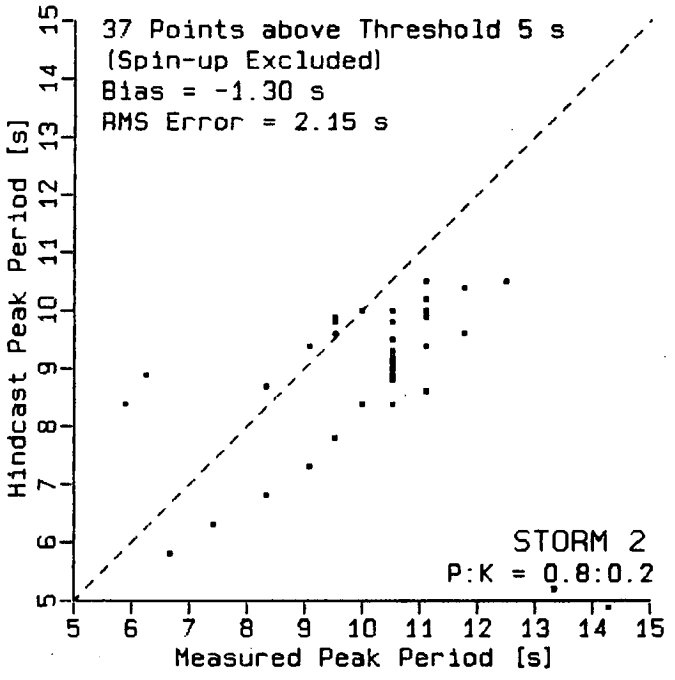

FIGURE 4.9 COMPARISON OF P:K = 80%:20% HINDCAST VERSUS MEASUREMENT FOR STORM 2.

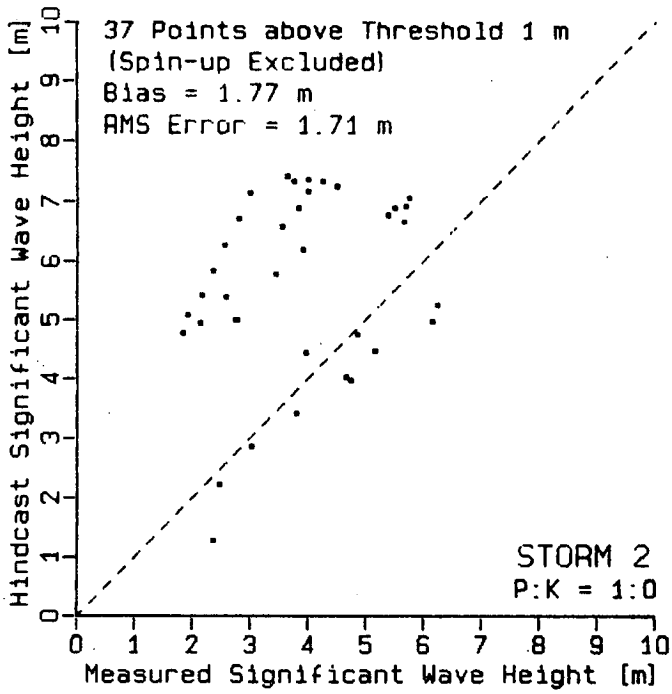

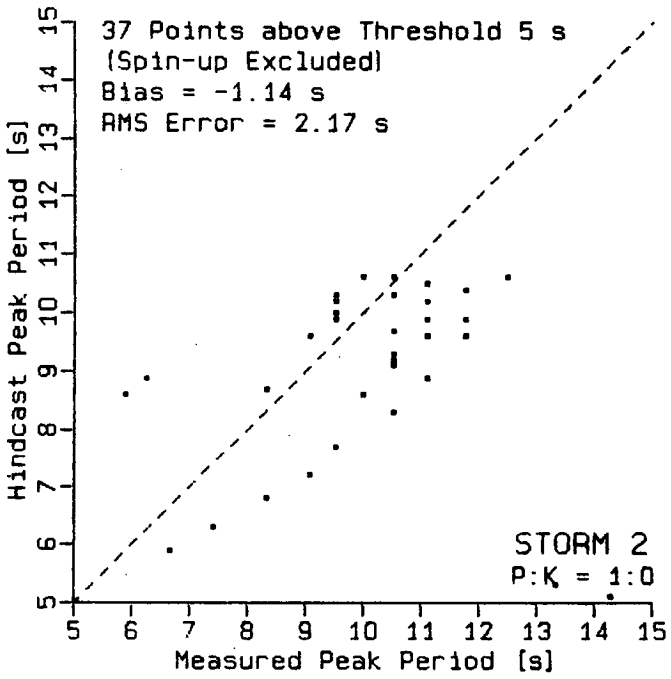

FIGURE 4.10 COMPARISON OF P:K = 100%:0% HINDCAST VERSUS MEASUREMENT FOR STORM 2.

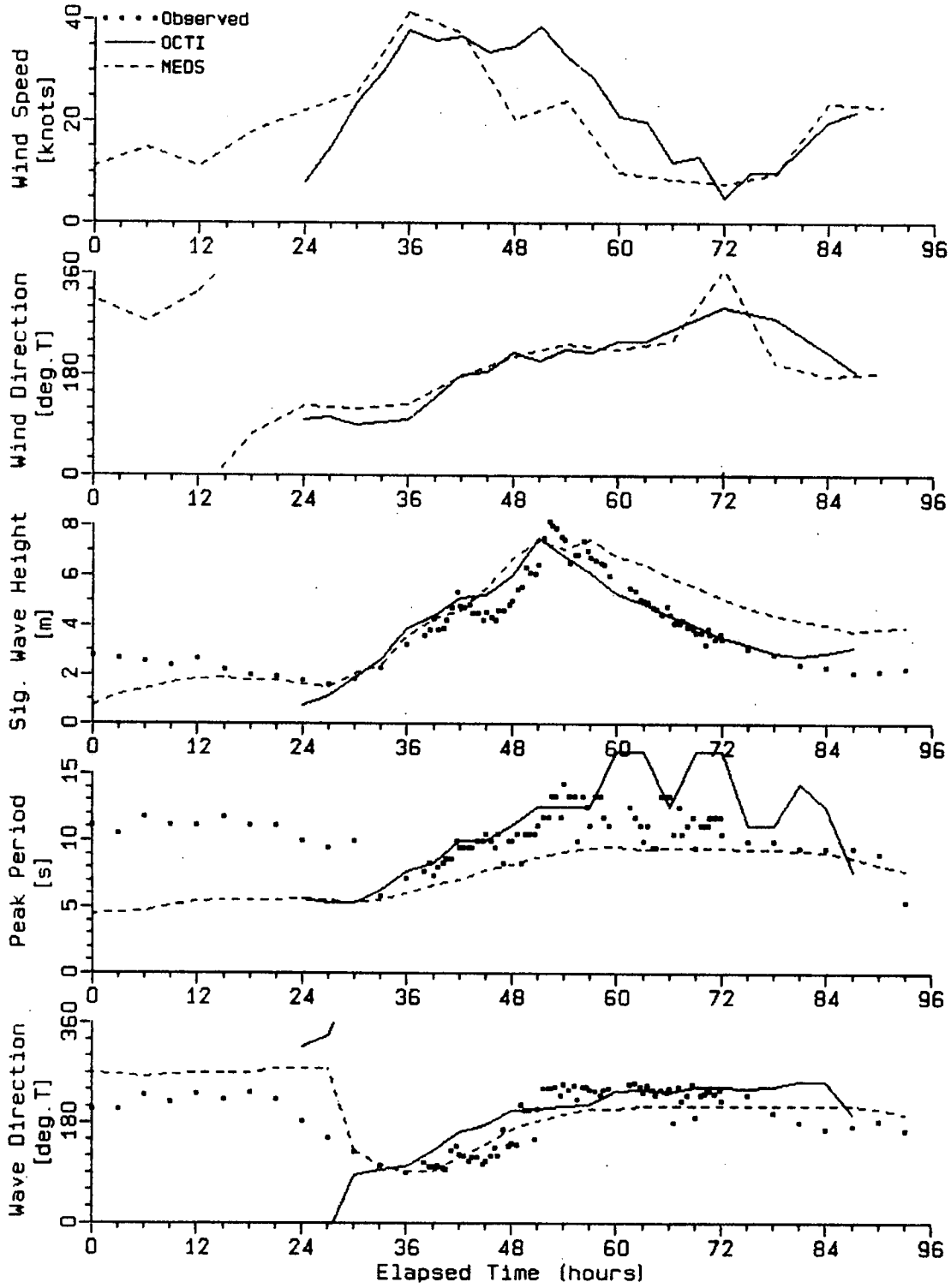

FIGURE 4.11 TIME SERIES OF HINDCAST AND MEASURED WAVE PARAMETERS FOR STORM 1: MEDS AND OCTI VERSIONS OF RESIO MODEL.

observed wave heights) which is almost absent in the MEDS hindcast. Both hindcasts reach approximately the same peak, about 1 m lower than the observed maximum. The MEDS hindcast has a second peak about 6 h later which matches almost exactly a secondary peak in the observed wave heights. However, the two hindcasts diverge markedly as the storm abates. The OCTI hindcast shows a good agreement with the observed wave heights while the MEDS hindcast waves are almost 1.5 m higher. There is a marked difference in the peak periods for the two models. The OCTI hindcast exhibits a good agreement during the growth but after the storm reached its peak the peak period shows a large fluctuation and diverges from the observation. The MEDS hindcast underpredicts the peak periods during growth but matches the observation better during decay. Wave directions between the two hindcasts differ on average by about 30° but both provide a reasonable approximation to the observed wave directions.

The overall bias and RMS errors for the OCTI hindcast are shown in Figure 4.12; the corresponding statistics for the MEDS hindcast were presented in Figure 3.13. The OCTI hindcast has a negligible bias in significant wave height (0.14 m) and a small bias in peak period (1.04 s). The RMS error in significant wave height is also small (0.56 m) but

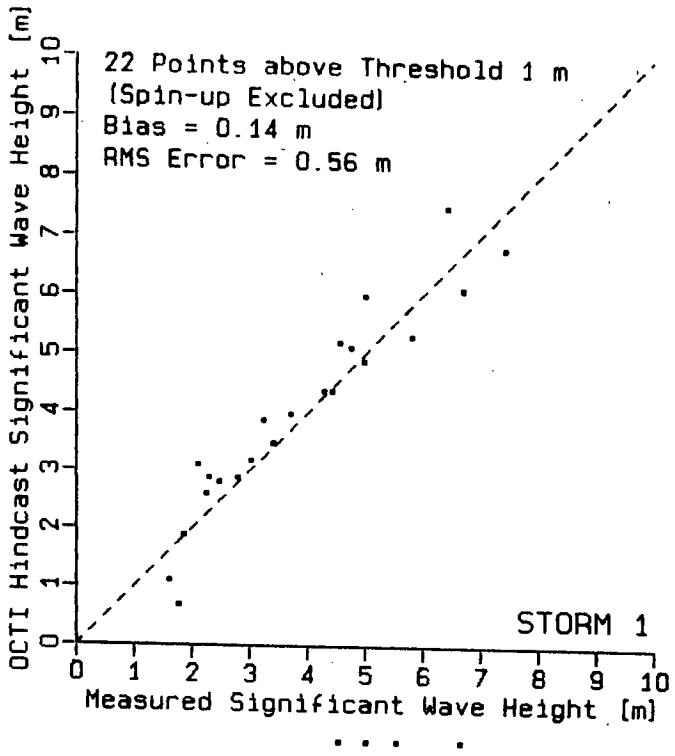

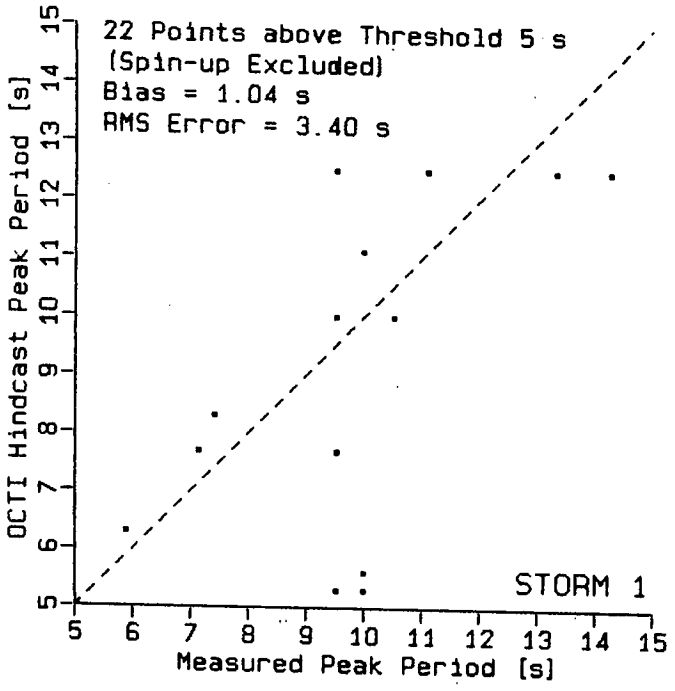

FIGURE 4.12 COMPARISON OF OCTI HINDCAST VERSUS MEASURED WAVE PARAMETERS FOR STORM 1.

relatively large in peak period (3.4 s). The significant wave height bias is much larger in the MEDS hindcast (0.96 m) but the RMS error is similar (0.78 m). The peak period bias is somewhat greater in the MEDS hindcast (-1.65 s), the RMS error is, however, only about one half of the OCTI hindcast.

The differences in hindcast results are greater for the second storm (Figures 4.13, 4.14 and 3.16). Here the significant wave height from the OCTI hindcast provides a good agreement with the observation (bias 0.26 m, RMS error 0.45 m) but in the MEDS hindcast the significant wave heights are overpredicted by more than 1m for almost the entire duration of the storm (bias 1.03 m). The difference in the RMS error is much smaller (0.73 m compared to 0.45 m). As in the previous case the differences are the greatest after the storm reached its peak. The peak periods are underestimated in the MEDS hindcast (bias -1.9 s) while the OCTI hindcasts are remarkably free of bias (0.17 s) but they show a larger scatter (RMS error 2.62 s compared to 1.86 s in the MEDS hindcast).

The large differences between the two hindcasts are probably due to a combination of factors. Figure 4.1 shows the location of the hindcast grid points with respect to the

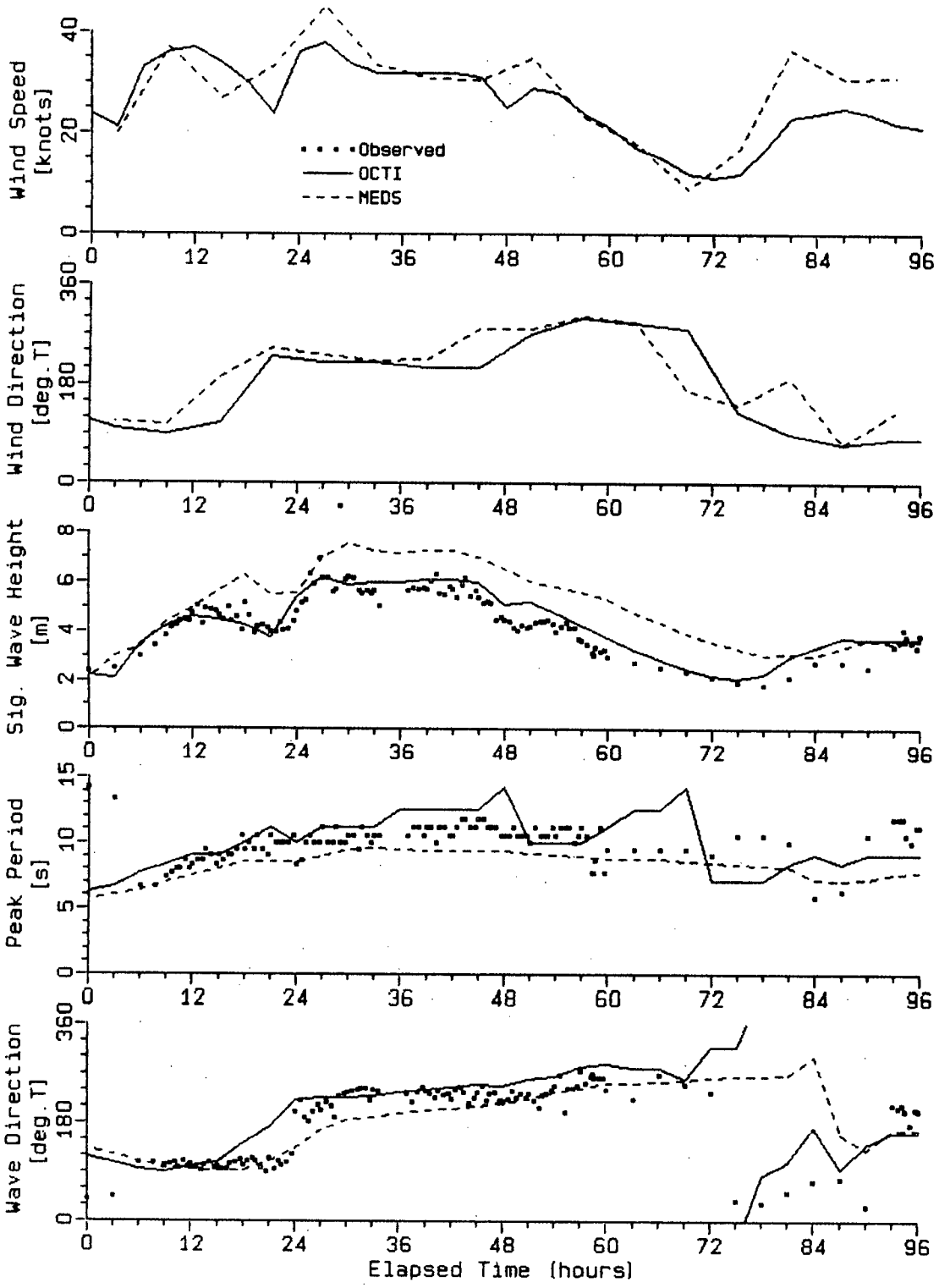

FIGURE 4.13 TIME SERIES OF HINDCAST AND MEASURED WAVE PARAMETERS FOR STORM 2: MEDS AND OCTI VERSIONS OF RESIO MODEL.

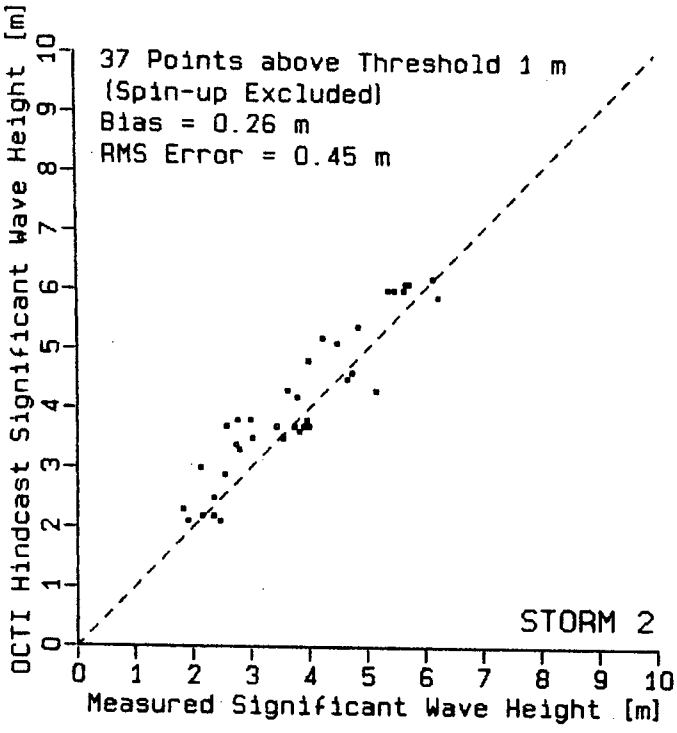

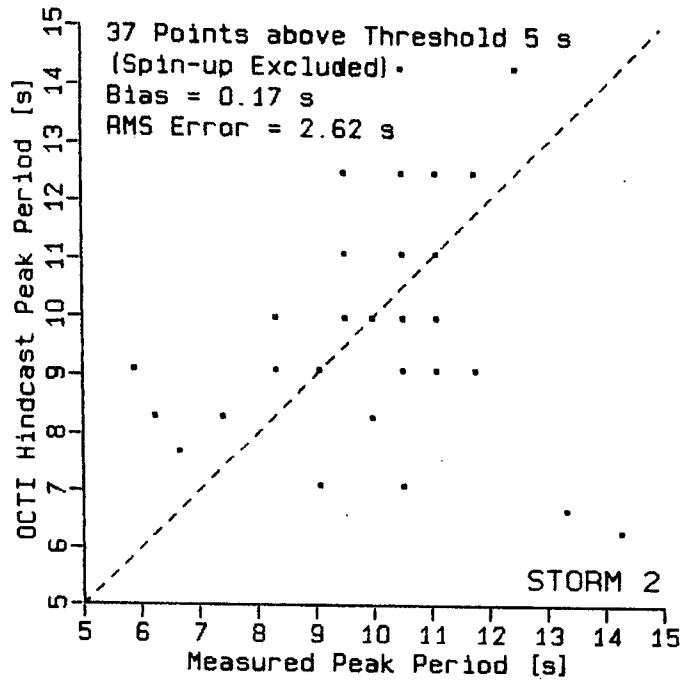

FIGURE 4.14 COMPARISON OF OCTI HINDCAST VERSUS MEASURED WAVE PARAMETERS FOR STORM 2.

location of the wave measuring buoy and the location of nearby drilling rigs (at the scale of the plot the buoy and the rig locations are approximately the same). While the MEDS grid point is closer to the buoy than the OCTI grid point the winds at the OCTI grid point are probably a better approximation to the actual winds at the measurement site because they were set equal to the winds derived from wind observations reported from the drilling rigs. By interpolating the winds to the SOG the local winds at the comparison grid point were shifted in space compared to the winds at the measurement site. In retrospect, it probably would have been better to set the winds at the MEDS comparison grid point equal to the winds at the OCTI comparison grid point. Obviously, from the time series of wind speeds in Figures 4.11 and 4.13 the spatial gradients were sufficiently large to cause relatively large differences in the winds between the two hindcasts but these are only local differences between the two comparison grid points; over an area of several grid points the wind fields should be essentially identical.

The differences in local winds may explain some of the differences in the hindcast waves but they cannot be the main reason. It is seen in Figure 4.11 that the local winds are

actually decreasing much faster in the MEDS hindcast than in the OCTI hindcast while the opposite applies to the wave heights. Furthermore, after the tests were completed it was learnt that the two versions of the Resio model assume the input wind fields to be at different reference levels: 19.5 m for the MEDS version versus 10 m for the OCTI version. This also should have lead to wave heights being lower in the MEDS hindcast. It appears obvious that the difference between the two hindcasts must be due to differences in the wave models rather than to the differences in the input. Perrie and Toulany (1985) found the original MEDS version of the model to exhibit excessive energy growth. They corrected the problem by tuning a drag coefficient, used in the model, for the hindcasts to match fetch limited growth rates observed during JONSWAP. A change in the drag coefficient would affect the hindcast results when energy is input into the wave field but it is not likely that it would reduce the wave energy during times when the input winds actually drop. It is not likely that re-tuning the drag coefficient would improve the results presented here.

To this author's knowledge, the two versions of the Resio model differ in only two respects (apart from some computer code differences): different formulation of the

input source term G_{in} and a different representation of wave propagation.

In the MEDS version of the model the energy from the atmosphere enters the wave field through an exponential growth term (Resio, 1981)

$$G_{in} = BE$$

where B is a coefficient based on the work of Snyder and Cox (1966). According to Resio (personal communication) this formulation was found to result in excessive wave energy growth under certain conditions.

In the OCTI version of the model the G_{in} term is based on the observation that a constant proportion (approximately 20%) of the total momentum flux from the atmosphere enters the wave field. Presumably, the remainder of the momentum is directly input into currents.

In both versions of the model the wind energy enters the central frequencies and is redistributed within the spectrum by the non linear wave-wave interactions. As the spectrum approaches saturated condition a negative lobe of the

wave-wave interaction term (i.e. the range of frequencies which lose energy due to the non linear interaction) moves progressively into lower frequencies until it approaches the so-called wind frequency ($f = g/2\pi u$). At this point the exponential term G_{in} goes to zero and the growth of the spectrum is stopped (Resio, 1981).

The significant wave height plots in Figures 4.11 and 4.13 seem to suggest a difference in the way energy is dissipated in the two versions of the model. However, there is no explicit dissipation term in the Resio model. Wave energy dissipation takes place primarily in the high frequency equilibrium range of the spectrum and it is responsible for the f^{-5} dependence at the tail of the spectrum. In the model, wave dissipation is included implicitly by forcing the tail of the spectrum to conform to the f^{-5} dependence in the high frequency parametric domain.

The two versions of the Resio model also differ in the propagation term. In the MEDS version of the model propagation is achieved for all spectral components lower than the parametric high frequency domain by using a modified Lax-Wendroff scheme

$$E?^{j+1} = \sum_{k=1}^{5} \mu_k \; E?_{j,k}$$

where the superscript, n, denotes the time step and the subscripts i, j, and k refer to frequency, direction and space counters respectively; μ_k are multipliers representing a one step version of a modified Lax-Wendroff scheme. This scheme was superseded in the OCTI version of the model by an explicit finite difference formula

$$E_{i,j}^{n+1} = \sum_{k=1}^{2} \mu_k \, E_{i,j,k}^{n}$$

after a study of the dispersion effects and angular spreading effects in long distance swell propagation.

It is not obvious which of the changes is responsible for the improvement in the prediction of the significant wave height. The OCTI version of the model gives somewhat larger RMS error in estimates of the peak period. However, since the significant wave height is the more critical wave parameter in most applications it seems that the OCTI version is an improvement over the MEDS version of the model.

4.4 CONCLUSIONS AND RECOMMENDATIONS

Caution must be exercised when drawing any conclusions from these comparisons. Obviously, if a wave model simulates

correctly the physics of wave generation and propagation, a more accurate representation of input winds will result in a more accurate hindcast of waves. In the computation of winds from pressure fields a number of simplifying assumptions are made, some processes in the balance of forces are neglected and small scale features are not resolved. The purpose of blending in kinematic analysis winds is to correct for those factors which are not represented in the pressure based winds (such as for example atmospheric stability, frontal features etc.). The degree to which the wind estimates actually are improved by blending in kinematic analysis winds crucially depends on the skill of the analyst. An attempt was made to introduce some degree of objectivity into the tests described here. However, this does not mean that comparable results would necessarily be achieved in hindcasts prepared by different analysts or in those applying to different meteorological conditions.

Comparison with a more recent version of the Resio model indicates that a new formulation of the atmospheric input source term and of the wave propagation term may lead to more accurate hindcasts. It is recommended that the MEDS version of the model be revised to take advantage of the improvements in the more recent version of the model.

5. COMPARISON BETWEEN BI-LINEAR AND QUADRATIC INTERPOLATION OF INPUT WIND FIELDS

5.1 QUADRATIC INTERPOLATION ALGORITHM

In the present MEDS hindcast system the wind fields defined on the 2.5° latitude x 2.5° longitude grid (in the following called the input grid) are interpolated to the SOG using a bi-linear interpolation from the surrounding four input grid points. For this sensitivity test the original interpolation program was replaced by a new program incorporating a quadratic interpolation routine. The interpolation algorithm is a straightforward finite difference transcription of the first six terms of the Taylor series

$$\begin{aligned} F(x,y) = {} & F(a,b) + (x-a)F_x(a,b) + (y-b)F_y(a,b) \\ & + (x-a)(y-b)F_{xy}(a,b) \\ & + \frac{1}{2}\{(x-a)^2F_{xx}(a,b) + (y-b)^2F_{yy}(a,b)\} \end{aligned}$$

where x and y are the longitude and latitude of the SOG point; a and b are the longitude and latitude of the closest input grid point (Figure 5.1); and the subscripts x and y denote partial derivatives evaluated as follows:

$$F_x = \{F(a_{+1},b) - F(a_{-1},b)\}/2\delta x$$

$$F_y = \{F(a, b_{+1}) - F(a, b_{-1})\}/2\delta y$$

$$F_{xx} = \{F(a_{+1}, b) - 2F(a, b) + F(a_{-1}, b)\}/\delta x^2$$

$$F_{yy} = \{F(a, b_{+1}) - 2F(a, b) + F(a, b_{-1})\}/\delta y^2$$

$$F_{xy} = \{F(a_{+1}, b_{+1}) - F(a_{-1}, b_{+1}) - F(a_{+1}, b_{-1}) + F(a_{-1}, b_{-1})\}/4\delta x\delta y$$

$$\delta x = a_{+1} - a = a - a_{-1}$$

$$\delta y = b_{+1} - b = b - b_{-1}$$

The interpolation cell consists of nine grid points as shown in Figure 5.1. The program interpolates wind speeds and their u and v components. Wind directions are computed from the components.

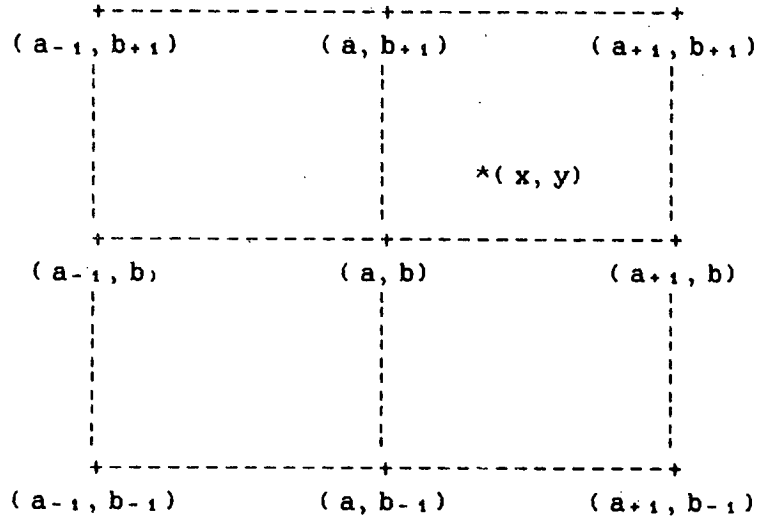

FIGURE 5.1 QUADRATIC INTERPOLATION CELL

The quadratic interpolation program does not include any rotation of wind directions to correct for the curvature of the SOG. This omission introduces an error in the test results. However, at the comparison grid point the error is believed to be small. Figure 3.2 shows that the comparison point (buoy Station 249, hindcast Station 71) lies on a line of grid points coinciding with a meridian. At this line the SOG directions are the same as the input grid directions, and the deviation from the correct direction is also small at the surrounding grid points which contribute most of the wave energy at the comparison point.

5.2 TEST RESULTS AND CONCLUSIONS

Figures 5.2 to 5.5 show the comparison between the quadratic and bi-linear interpolation results for the two March 1984 storms. In all cases the input was a blend of 80% kinematic winds and 20% pressure based winds. The plots indicate negligible differences both in local winds and in the hindcast wave parameters. The quadratic interpolation leads to a slight emphasis of the peak significant wave height and consequently to a slight increase in the overall bias. However, the differences are insignificant and they

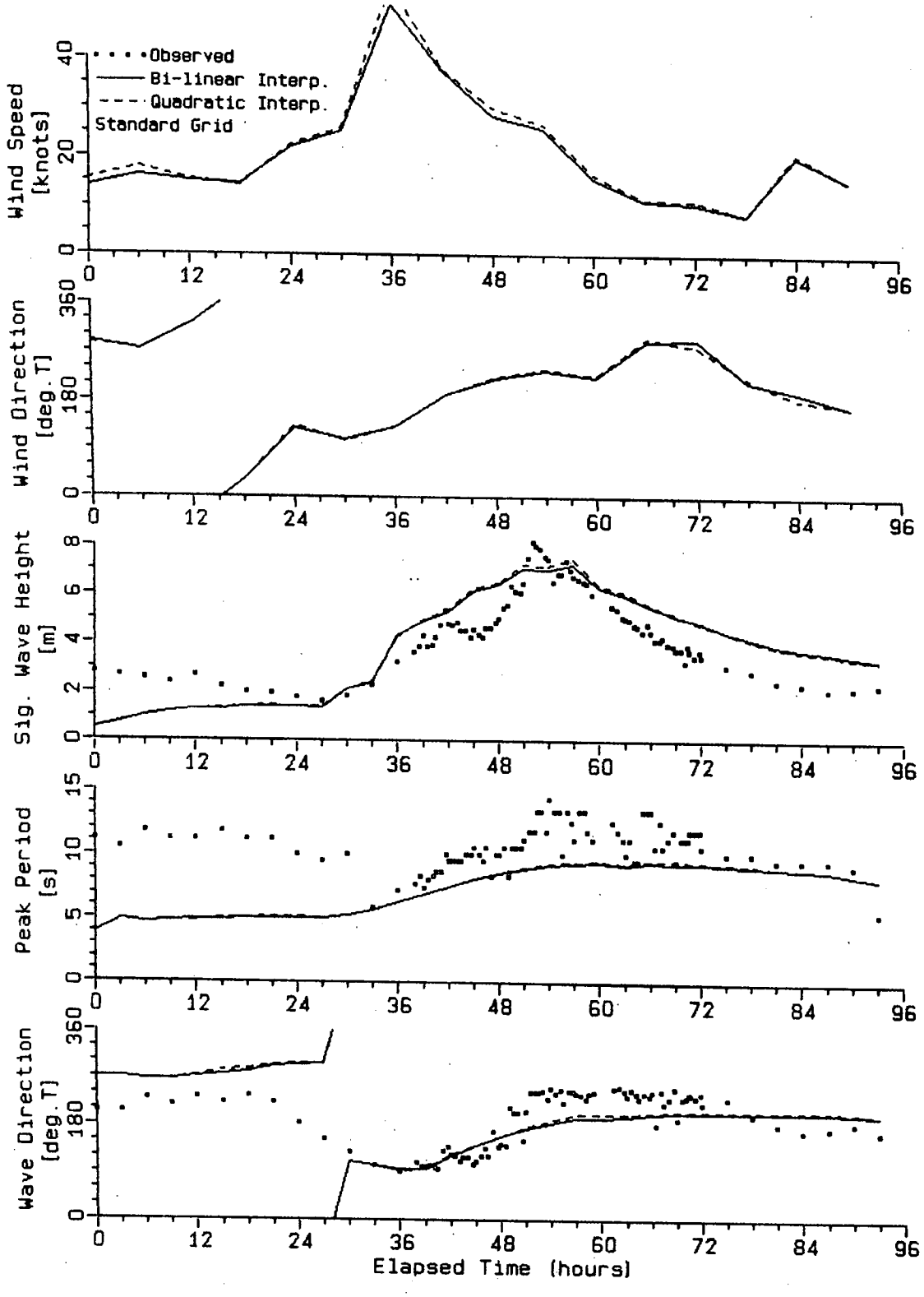

FIGURE 5.2 TIME SERIES OF HINDCAST AND MEASURED WAVE PARAMETERS FOR BI-LINEAR AND QUADRATIC INTERPOLATION OF INPUT WIND FIELDS - STORM 1.

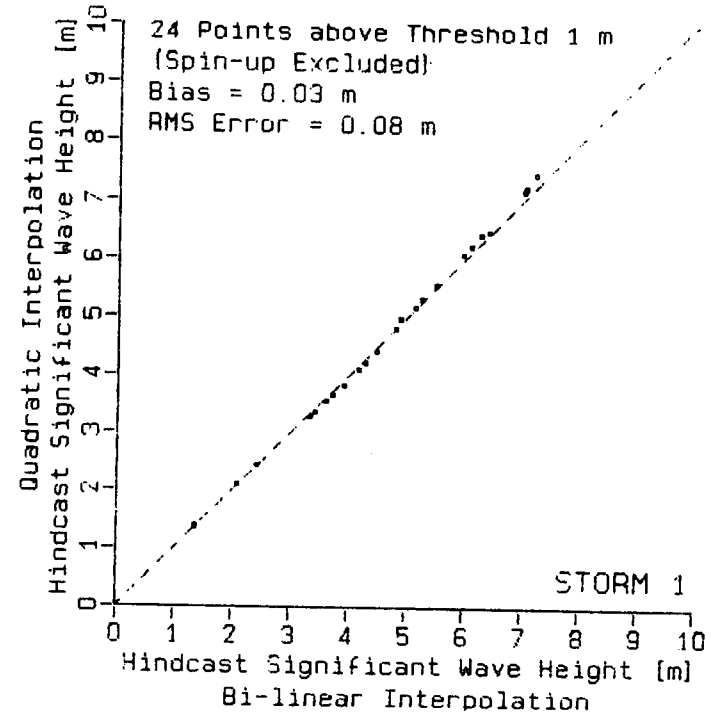

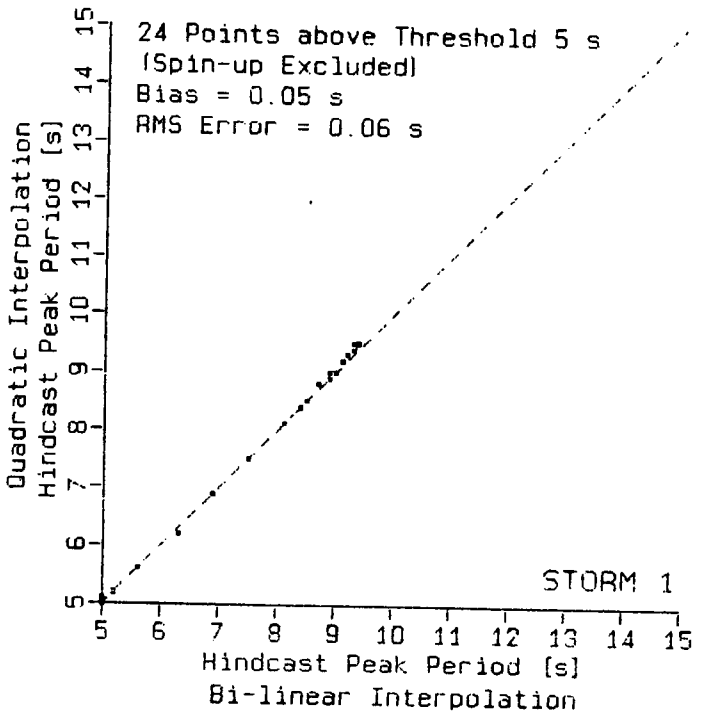

FIGURE 5.3 COMPARISON OF QUADRATIC VERSUS BI-LINEAR INTERPOLATION OF INPUT WIND FIELDS FOR STORM 1.

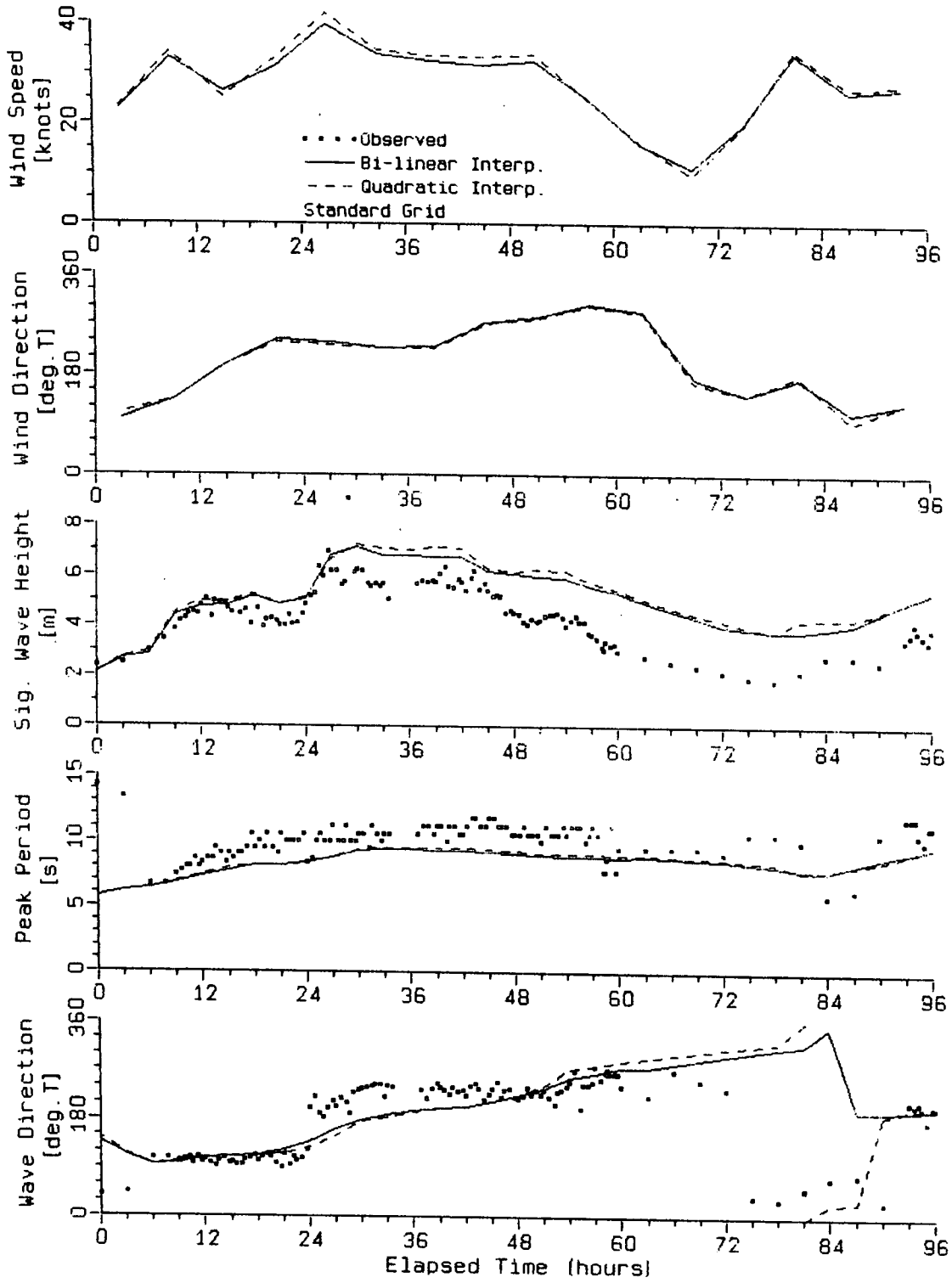

FIGURE 5.4 TIME SERIES OF HINDCAST AND MEASURED WAVE PARAMETERS FOR BI-LINEAR AND QUADRATIC INTERPOLATION OF INPUT WIND FIELDS - STORM 2.

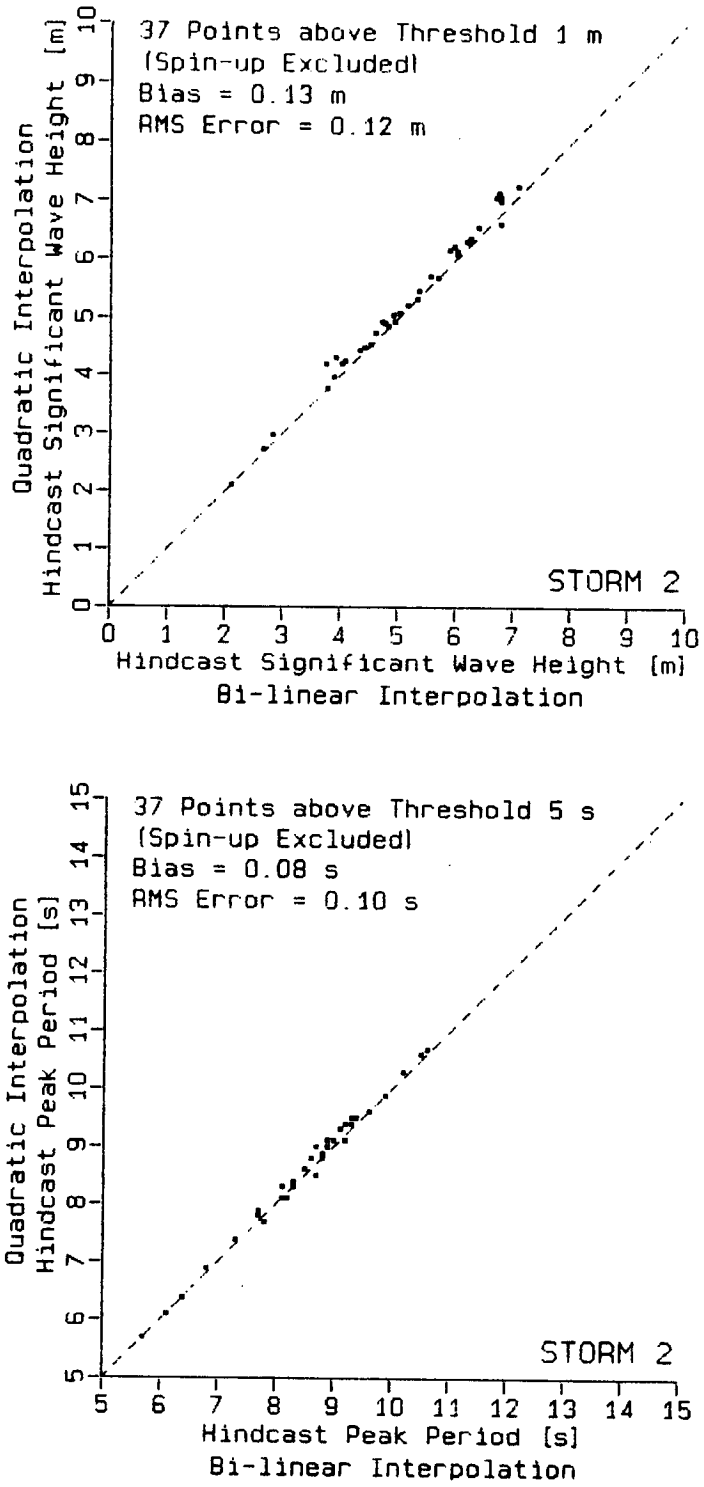

FIGURE 5.5 COMPARISON OF QUADRATIC VERSUS BI-LINEAR INTERPOLATION OF INPUT WIND FIELDS FOR STORM 2.

do not justify replacing the simple and computationally fast bi-linear interpolation with the slower quadratic interpolation.

No comparison between linear and non-linear time-wise interpolation could be made. This interpolation is a part of the wave model computer code and therefore an access to the code would be required to make the appropriate changes and to interface them with the rest of the program.

6. ADDITIONAL STORM HINDCASTS.

6.1 STORM SELECTION

As a part of this study additional hindcasts were to be made, from a list of severe storms prepared for the ESRF, in order to test the performance of the model under a variety of storm conditions and types. Inspection of the ESRF report on the climatology of severe storms affecting Canadian East Coast areas (Brown et al., 1984) revealed that the number of storms for which adequate wave measurements are available for comparison is rather limited. Storm wave measurements made in shallow or nearshore areas were not considered

suitable for this study since the MEDS version of the Resio model does not simulate processes affecting wave generation and propagation in shallow water, and the resolution of the grid is not sufficient to resolve the sheltering effect of complex coastlines. Prior to 1980 the wave time series recorded during severe storms were too short to be of much use in hindcast verification. An exception is a storm which occurred in October 1975 on the Labrador Shelf and was ranked 2 in the classification by Brown et al. (1984). For this storm Waverider measurements of several days duration are available at three sites. This storm was selected here to test the performance of the MEDS hindcast procedure when applied to a Labrador Shelf storm.

The second storm selected for these tests was a storm which occurred in January 1982 on the Grand Banks and was ranked 4 by Brown et al. (1984). Wave measurements for the whole duration of the storms are available for two locations at Hibernia. The only other storm for which long time series of measured wave heights were available was a storm which occurred in February 1982 and was ranked 7. However, this storm was similar in type to the January 1982 storm, and therefore it was not hindcast in the present study.

6.2 INPUT PREPARATION AND MODEL GRID

Two sets of weather maps were obtained for the study: one prepared by the Atlantic Weather Centre (AWC) in Bedford, N.S.; the other prepared by the Canadian Meteorological Centre (CMC) in Montreal. Both sets were photocopies of the original maps and their legibility was somewhat limited, particularly in the case of the 1975 storm. For this reason a kinematic analysis was performed only for the 1982 storm and only within a small area (typically 20° by 20°) in the vicinity of the comparison site. The photocopies of Atlantic Weather Centre weather maps did not cover the whole area for which surface pressure data were required, and therefore the CMC maps were selected as the primary data set while the AWC analyses were used only to fill in missing information.

The standard MEDS procedure for the derivation of input wind fields was followed. Surface pressures were scaled off the weather maps at 10° latitude x 10° longitude intervals to form a background pressure field, and distances of selected closed isobars were measured from the storm centre along rays 45° apart, to represent the storm systems. This information was processed by MEDS into pressure based wind fields. In addition, for the January 1982 storm, kinematic analysis was

done for a small area in the vicinity of the grid point closest to the wave observation site. This consisted from approximately fitting the wind speed vectors plotted on the weather maps with a set of streamlines and isotachs and reading off the interpolated wind vectors at the locations required by the MEDS blending procedure. No reference level correction was applied to the ships observations plotted on the weather maps (90% of these observations are estimates based on the state of the sea). For some synoptic times the number of wind vectors plotted on the weather maps was not sufficient to draw the streamlines and isotachs. In such cases subjective interpolation was done from the patterns on preceding and following weather maps and from the shape and location of isobars. Because of the poor legibility of the wind vector symbols on many of the weather maps the kinematic analysis was not considered to be reliable and therefore a combination of 50% pressure based winds and 50% kinematic analysis winds was used in the wave hindcast. A hindcast using 100% pressure based winds was also done for a comparison with the 50/50 blend.

The standard MEDS grid does not provide a sufficient resolution for wave hindcasting on the Labrador Shelf, particularly at the locations of the October 1975 wave

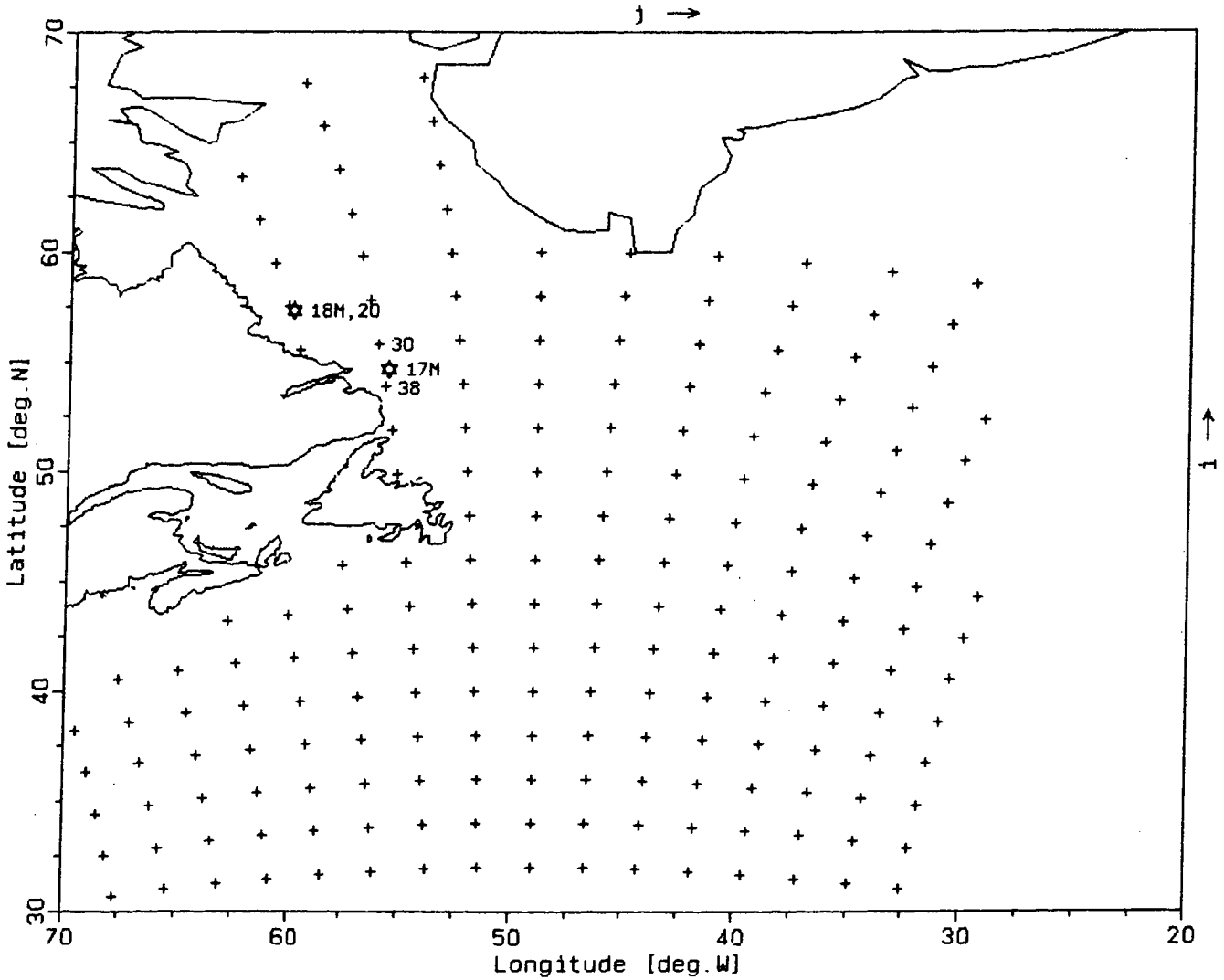

FIGURE 6.1 MODEL GRID AND MEASUREMENT LOCATIONS FOR OCTOBER 1975 STORM.

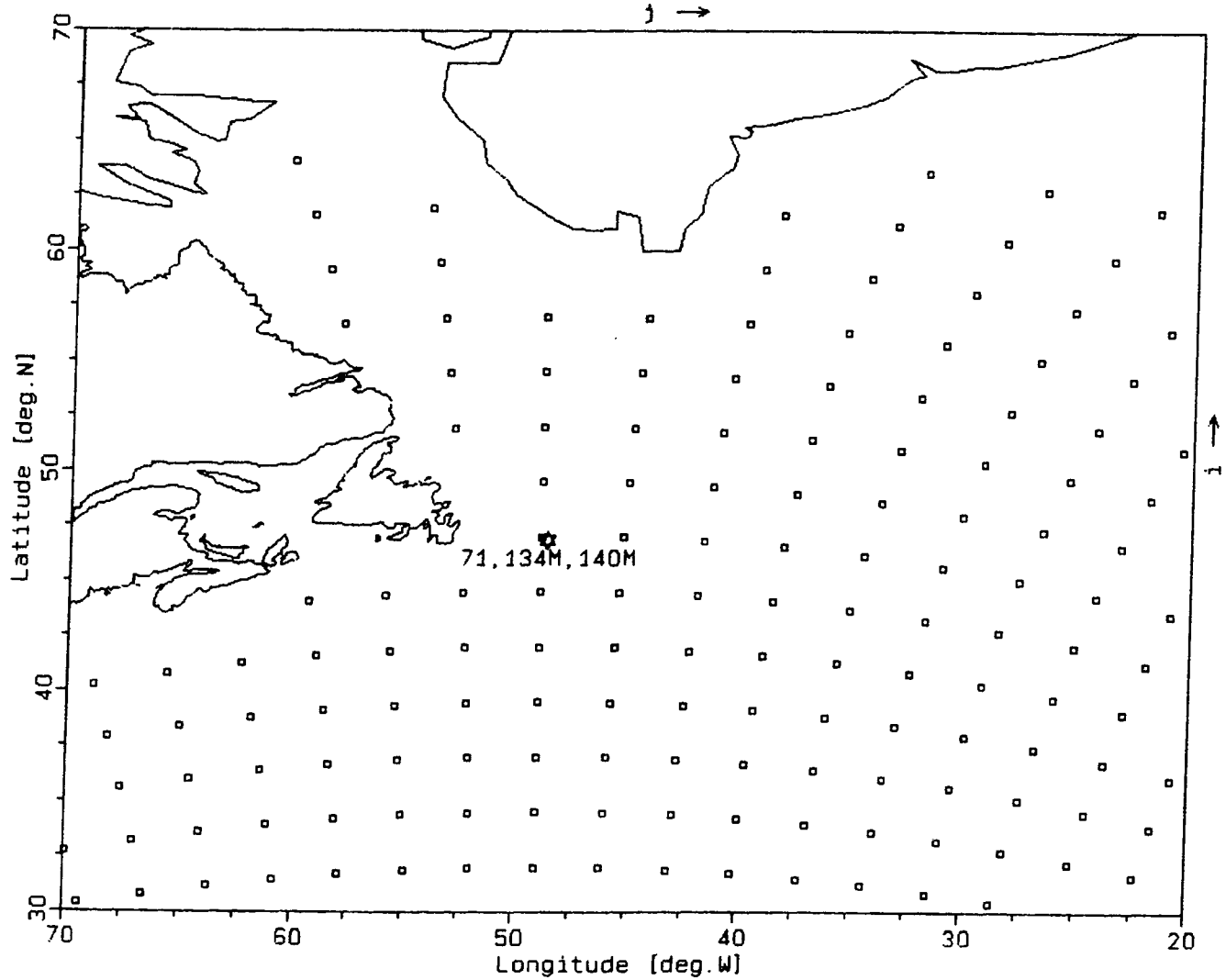

FIGURE 6.2 MODEL GRID AND MEASUREMENT LOCATIONS FOR JANUARY 1982 STORM.

measurements. These measurements took place close to the shore and for this reason the fine (120 nautical mile spacing) grid was selected, and modified to include additional grid points along the coastlines. Figure 6.1 shows the grid together with locations of the wave measurements. The modified grid potentially increased fetch for some wind directions above what would be a correct representation of actual conditions but since the prevailing wind direction during the storm was from the north it is believed that the hindcast was not adversely affected by the grid modification. The same grid was originally employed for the January 1982 storm hindcast. In this case, however, the wind was offshore during a large part of the storm and the increased fetch contributed to excessive hindcast wave energy compared to observations. Consequently, for this storm, a new hindcast was made using the standard MEDS grid. The measurement locations superimposed on the grid are shown in Figure 6.2.

No grid adjustments were made for the presence of sea ice. Some ice presence along the Labrador Coast during the January 1982 storm was indicated on the Canadian Forces Meteorological and Oceanographic Centre (METOC) wave analysis charts but its extent was not sufficient to be resolved by the model grid.

6.3 OCTOBER 1975 STORM

The October 1975 storm appears to have been due to a sequence of two or three weather systems. On October 7, 1975 a low pressure system (central pressure about 982 mb) was located over the Baffin Island just north of Frobisher Bay causing northwesterly to southwesterly winds over the Labrador Shelf. A cold front associated with the system was projecting into the Labrador Sea north of Lake Melville. At the same time another cyclonic system of similar intensity was lying south of Greenland, centered at the latitude of approximately 52°N and a new low was forming off the Atlantic seaboard of the United States at the latitude of about 42°N. The Baffin Island low was slowly moving north and gradually weakening while the two Atlantic lows by October 8 appear to have merged into a single trough. The southwestern part of the trough gradually intensified moving north-northeast until on October 9, 06Z the central pressure dropped to its lowest point, 970 mb. At that time the storm centre was located at about 54°N, 47°W and the winds over the Labrador Sea were from the north to north-northwest reaching on average 30 to 40 knots. The system remained stalled in the area south of Greenland for more than two days until, by the end of October 11, the central pressure weakened to about

996 mb. During this time the winds in the area of interest were blowing steadily from the north along almost the whole length of Davis Strait and Labrador Sea. The tracks of the two dominant lows are shown in Figure 6.3.

The time series of hindcast winds at three locations together with the hindcast and observed (Waverider) wave parameters are shown in Figure 6.4 (observations at MEDS Station 17) and in Figure 6.7 (observations at MEDS Station 18). The corresponding comparison of hindcast versus observed significant wave heights and peak periods is presented in the scatter diagrams in Figures 6.5, 6.6, and 6.8. At both stations the significant wave heights and the peak periods are strongly underpredicted with the exception of the last 12 hours during which the hindcast significant wave heights at Stations 30 and 31 exceed the observed values by 3.5 to 6 m. Apart from the first 12 hours, when there is a rapid growth from 2 to about 5 m, the observed significant wave heights and peak periods, at least at Station 17, change very slowly during the three days shown in Figure 6.3. This suggests relatively steady winds and fully developed seas. However, the plot of hindcast wind speeds shows an increase at a rate (reflected in the hindcast wave parameters) which is not entirely consistent with the slow observed wave

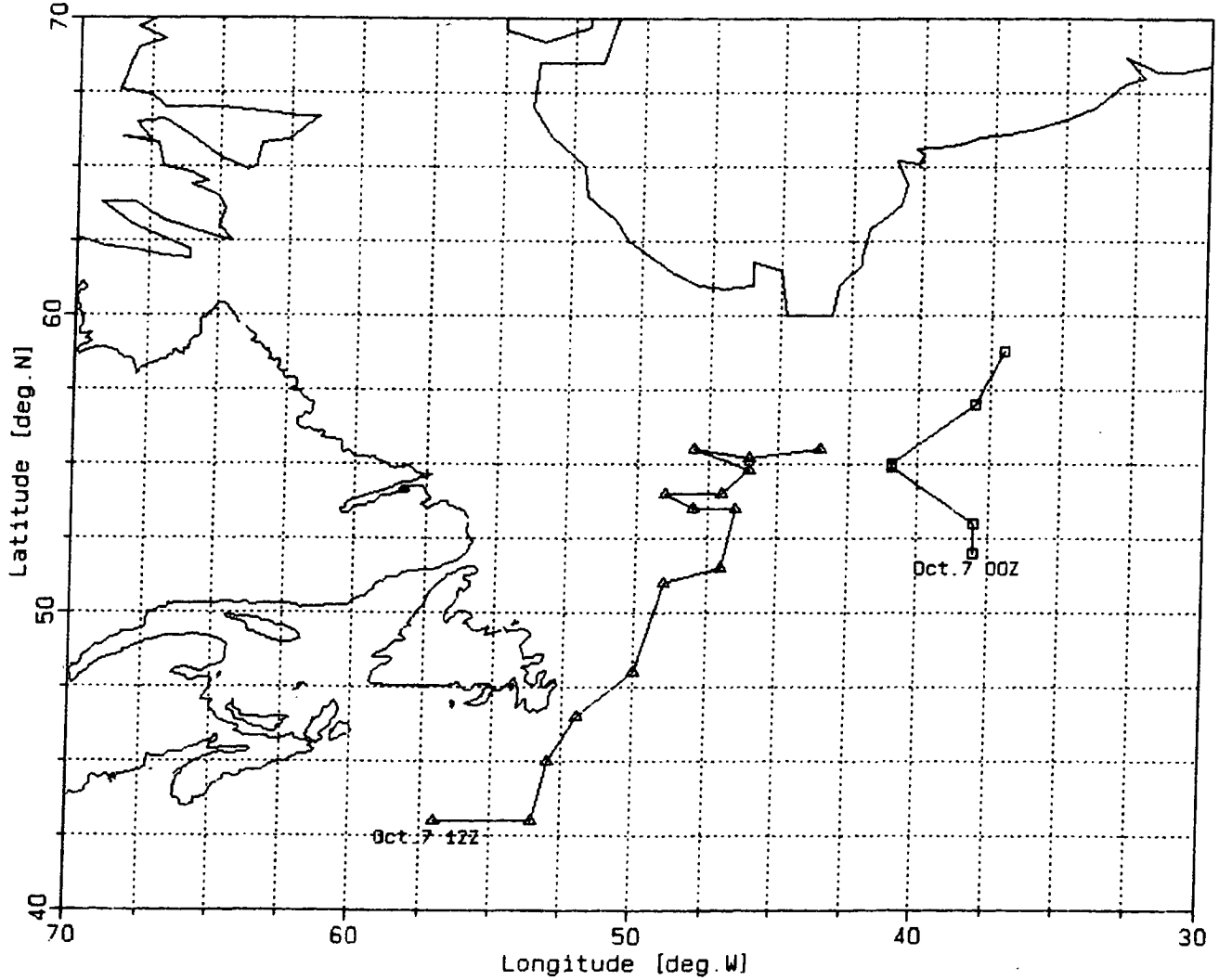

FIGURE 6.3 TRACKS OF LOW PRESSURE SYSTEMS DURING OCTOBER 1975 STORM. (FROM CMC SURFACE ANALYSIS MAPS.)

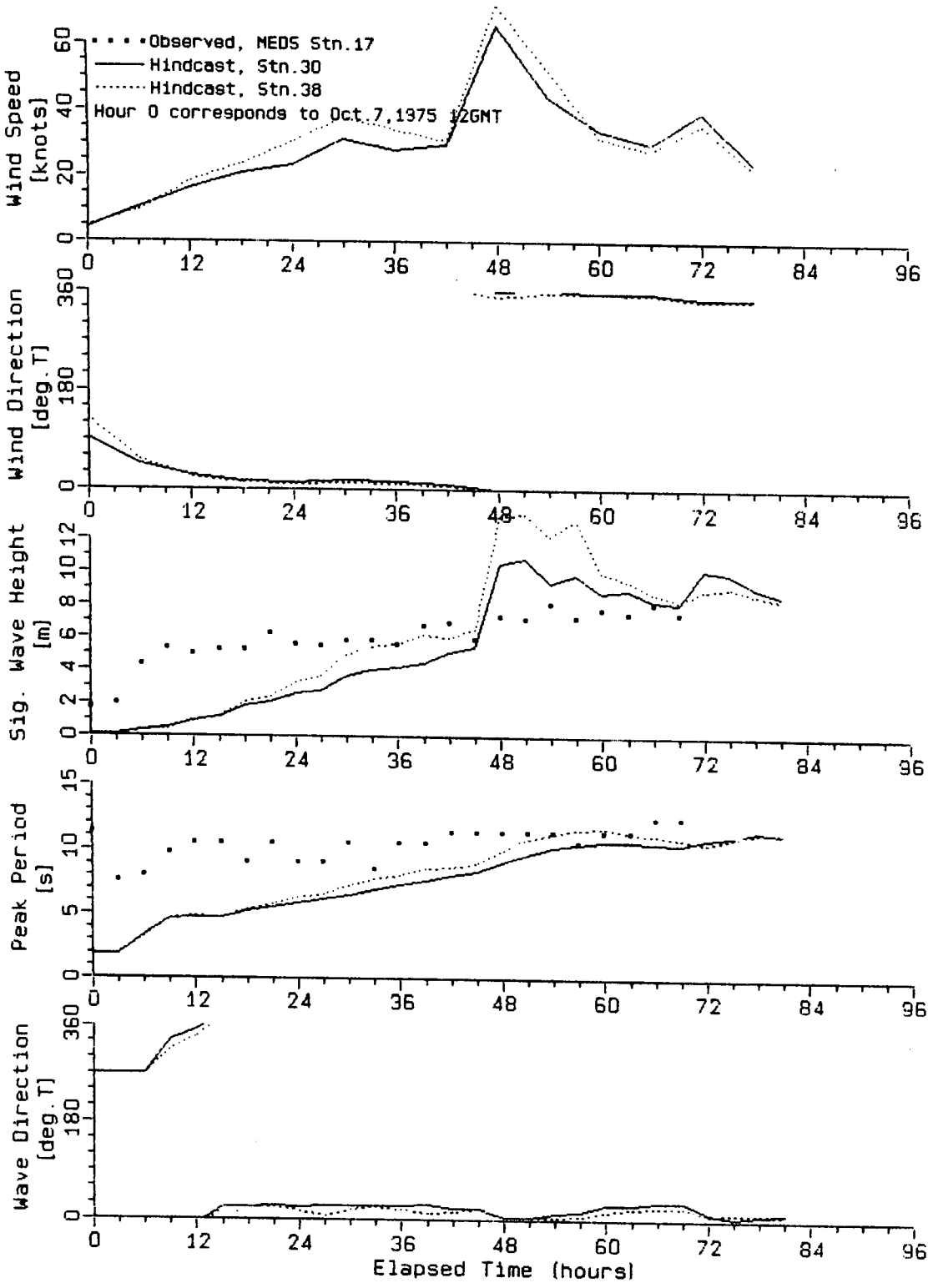

FIGURE 6.4 TIME SERIES OF HINDCAST AND MEASURED WAVE PARAMETERS FOR OCTOBER 1975 STORM (MEDS STATION 17).

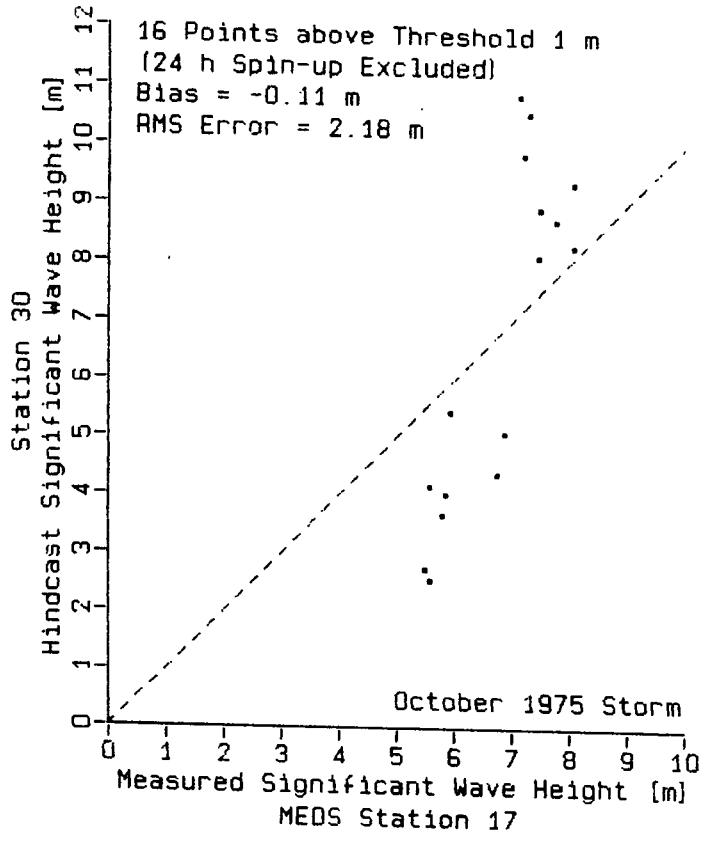

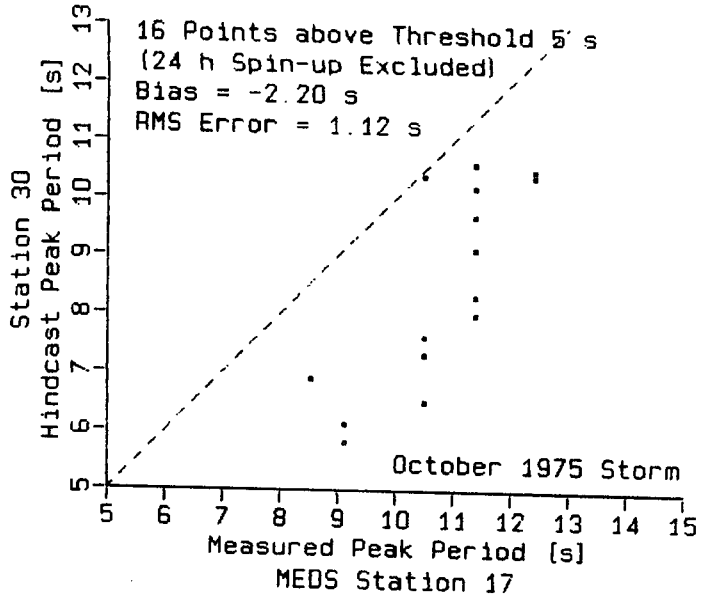

FIGURE 6.5 COMPARISON OF HINDCAST (STN. 30) VERSUS MEASURED (MEDS STN. 17) WAVE PARAMETERS FOR OCTOBER 1975 STORM.

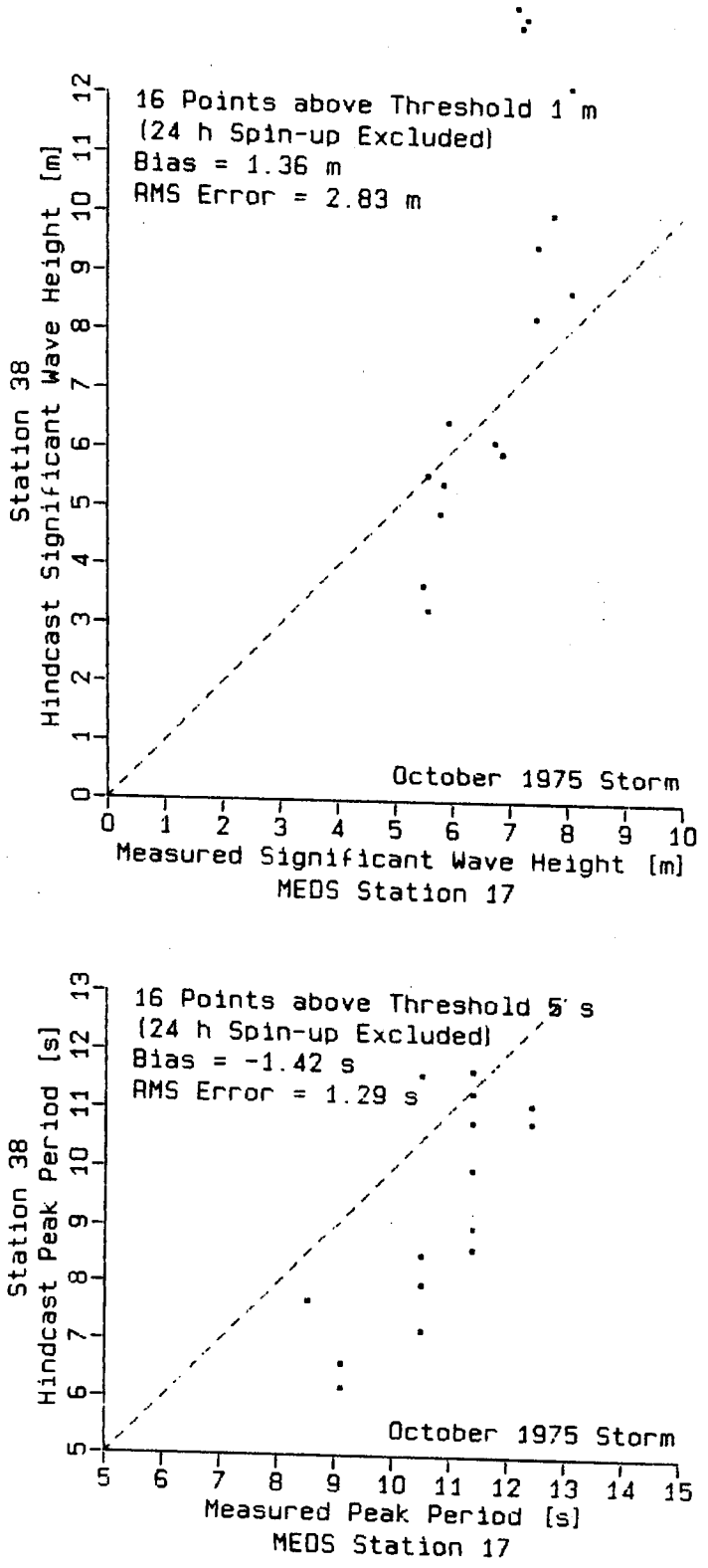

FIGURE 6.6 COMPARISON OF HINDCAST (STN. 38) VERSUS MEASURED (MEDS STN. 17) WAVE PARAMETERS FOR OCTOBER 1975 STORM.

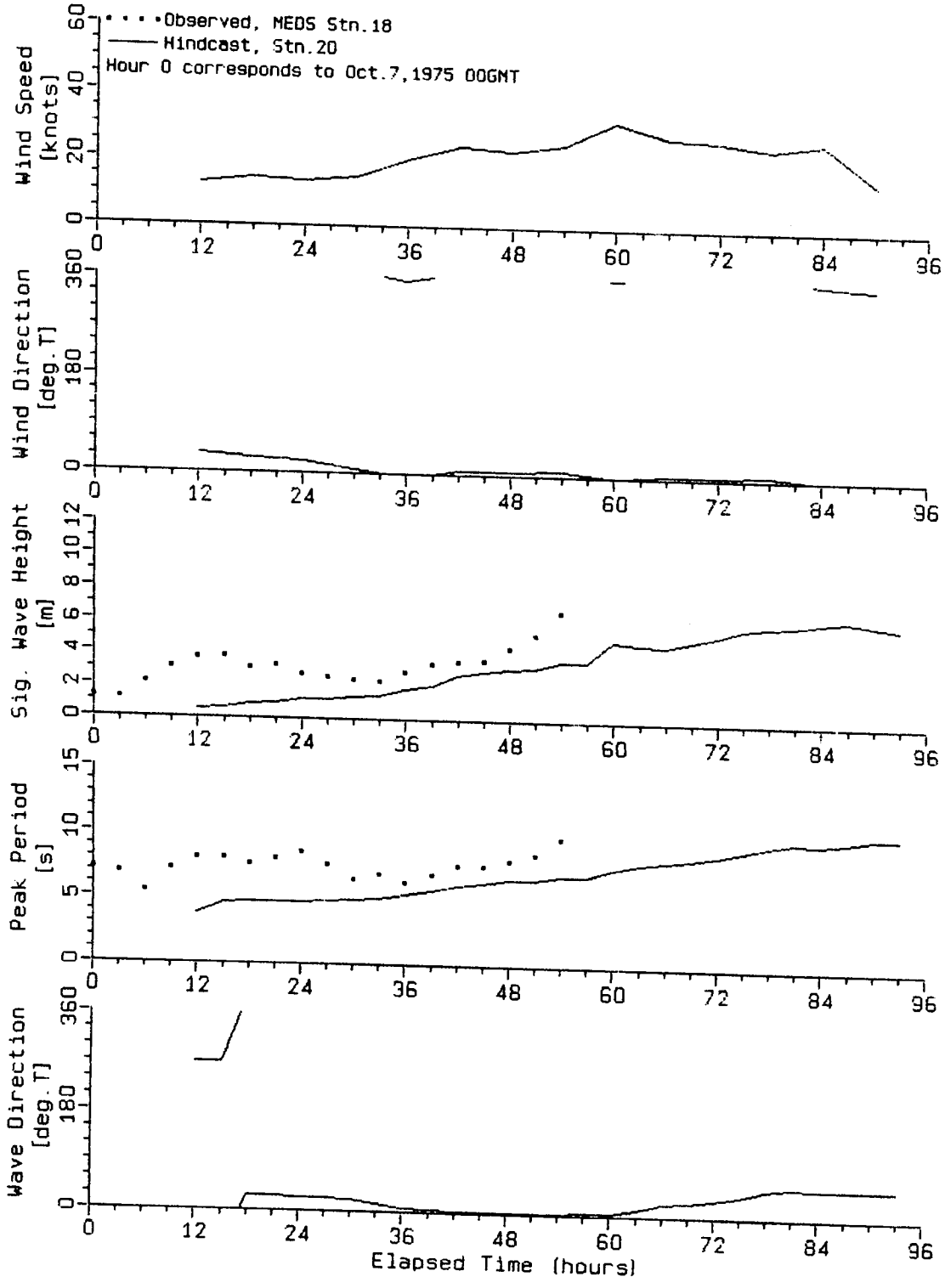

FIGURE 6.7 TIME SERIES OF HINDCAST AND MEASURED WAVE PARAMETERS FOR OCTOBER 1975 STORM (MEDS STATION 18).

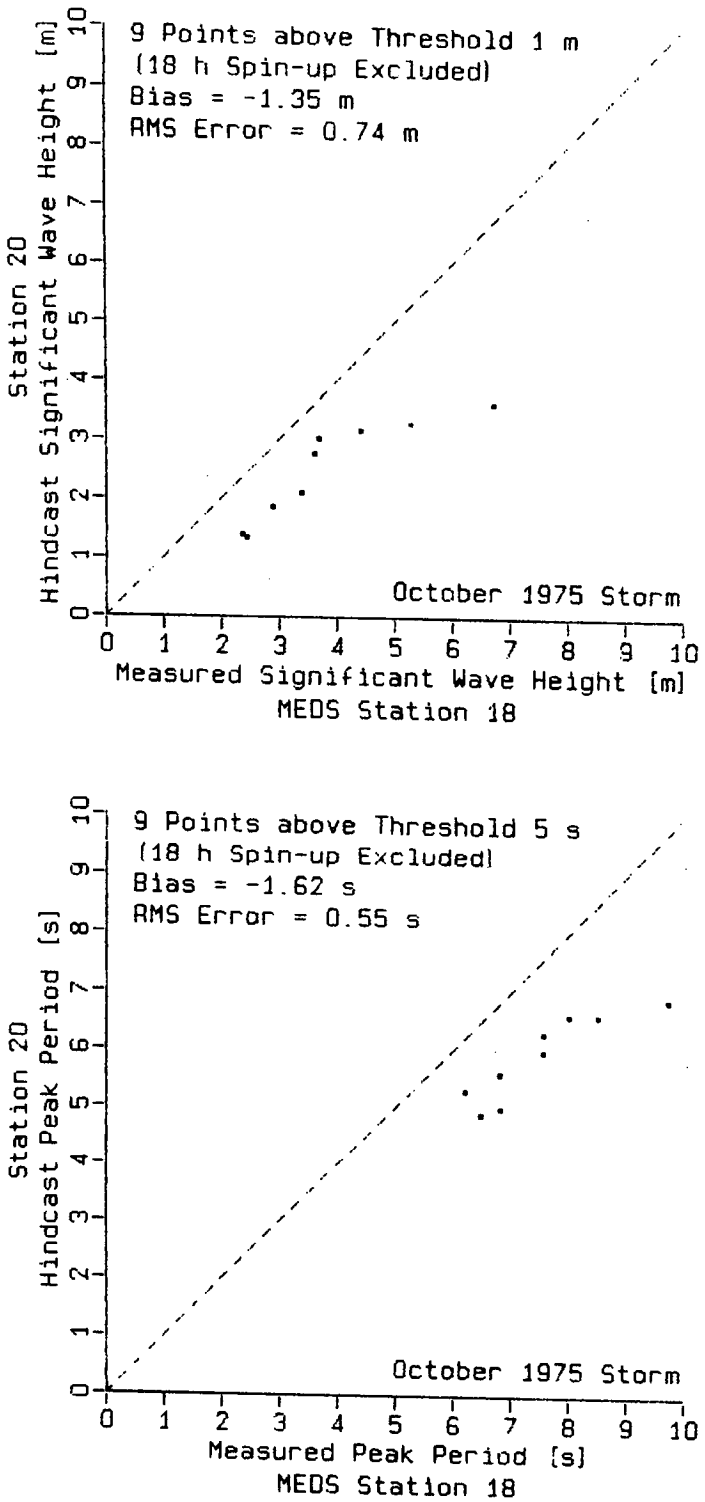

FIGURE 6.8 COMPARISON OF HINDCAST VERSUS MEASURED WAVE PARAMETERS FOR OCTOBER 1975 STOPM (MEDS STATION 18).

growth. The most likely explanation for this discrepancy is that the 10° x 10° background pressures and the polar representation of the closed isobaric features could not adequately resolve the full details of a rather complex situation during the initial stages of the storm. At that time the three low pressure systems did not form three distinct cyclonic systems but rather a single large three-lobed system with relatively strong pressure gradients weaving around the three centers.

During October 8 a single cyclonic system gradually became dominant. On October 9 12Z the central pressure was the lowest, 967 mb, and the pressure gradients the steepest. At that time wind velocity at Goose Bay, and at two sea locations less than 100 nautical miles off the Labrador and Newfoundland coasts, reached about 25 knots, considerably less than the over 60 knots shown in Figure 6.3. A data entry error was suspected but checking the polar representation of the isobars supplied to MEDS did not reveal any discrepancies. It is concluded that the most likely reason for the excessive wind speeds is an error in the pressure analysis.

It is interesting to note that the values of maximum significant wave heights for this storm over the Labrador Shelf and adjacent part of the Labrador Sea, listed by Brown et al. (1984), vary widely between data sets. The lowest maximum significant wave height, 6.9 m, was estimated in the Waterways Experiment Station (WES) hindcast (using the Resio model) while the highest, 14.6 m, was produced in a Spectral Ocean Wave Model (SOWM) hindcast. The METOC wave analysis charts gave the maximum significant wave height of 10 m. The maximum measured significant wave height was 8.1 m while 12.7 m was reported from a ship. For the purposes of ranking the severity of the storm Brown et al. (1984) used a Bretschneider (U.S. Army Coastal Engineering Research Center, 1977) nomogram with the Atmospheric Environment Service geostrophic wind data to estimate storm wave heights. This resulted in an estimate of 20.4 m which gave the storm rank 2. (As pointed out by the authors this estimate should not be considered accurate representation of actual wave conditions but rather a relative measure of storm severity). The above estimates do not apply to the same location and therefore some scatter is to be expected. However, the large differences probably also reflect a large uncertainty in the input wind data.

6.4 JANUARY 1982 STORM

The January 1982 storm was caused by a sequence of two intense low pressure systems. The first one developed off the United States East Coast south of Cape Hatteras and it deepened fast as it tracked north-northeastward. On January 16, 00GMT the central pressure dropped to its lowest point, 950 mb, and it remained there for almost 12 hours while the storm centre was crossing over the Island of Newfoundland. Ship reports plotted on the weather maps in the vicinity of Hibernia indicate wind speeds at that time in the range of 40 to 60 knots. The wind directions changed from approximately west on January 14 through south on January 15 back to south-west or west during January 16. The winds on the Grand Banks eased somewhat during January 17 as the low dissipated and moved east into the North Atlantic but they increased again to about 50 knots as a new low intensified over Northern Labrador. The second system reached a low of 952 mb at 12GMT on January 18 when the centre was located over the Labrador coast at the latitude of approximately 55°N. At that time the winds at Hibernia were reaching 50 knots from the west. The winds remained relatively steady as the low tracked east into the Atlantic.

Large differences were noticed between the storm tracks and central pressures as represented in the two sets of weather maps. Figure 6.9 shows the track of the January 1982 storm as determined from the CMC analyses (solid line) and from the AWC analyses (dashed line). The dotted coordinate lines are 2.5° apart. Positions of the storm centre differ possibly by as much as 200 nautical miles between the two sets in the case of the later, more northerly storm. The locations of the storm centers together with the central pressures are listed in Table 6.1. Differences in central pressure up to 6 mb are seen in the table. The copies of the AWC weather maps were somewhat more legible than the CMC copies but they did not cover the whole area for which the data were required. Therefore, the CMC analyses were primarily used to scale off pressure data while the AWC maps were used for the kinematic analysis. In both cases information from the alternate set was used where it seemed appropriate. The large differences occur at times when the real time data from ship observations are sparse (as evidenced by a lack of plotted meteorological reports on the weather maps), particularly during the most severe stages of the storms. This points out to the need for post analysis of all available data where a high hindcast accuracy is required.

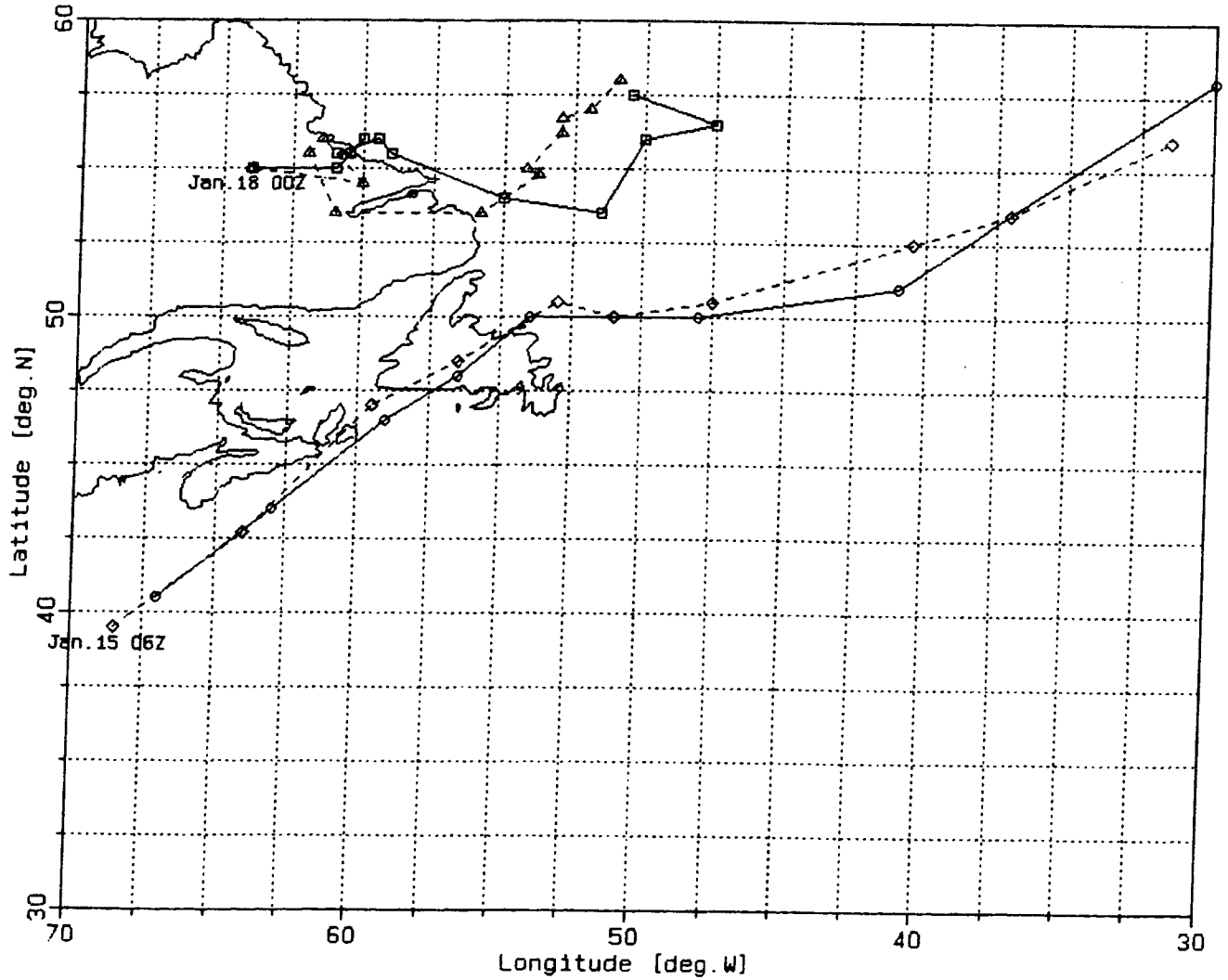

FIGURE 6.9 TRACKS OF LOW PRESSURE SYSTEMS DURING JANUARY 1982 STORM. (—— CMC SURFACE ANALYSIS; --- AWC SURFACE ANALYSIS)

Two hindcasts were prepared for this storm: one using only pressure based winds, the other using a blend of 50% pressure based winds and 50% kinematic analysis winds. The time series of hindcast winds and wave parameters for the two blends are shown in Figures 6.10 and 6.11 plotted against observations at two nearby locations. The two blends provide virtually the same results during the initial wave growth,

TABLE 6.1

LOCATIONS OF STORM CENTERS AND CENTRAL PRESSURES FOR JANUARY 1982 STORM AS REPRESENTED IN CMC AND AWC WEATHER MAPS.

Time Day/Hour	Center Location CMC	Center Location AWC	Central pressure [mb] CMC	Central pressure [mb] AWC
14/06Z	38.5N, 71.0W		996	
12Z	41.5N, 68.0W	41.5N, 68.5W	995	996
18Z	43.0N, 66.0W	42.5N, 65.0W	992	990
15/00Z	43.0N, 63.5W	43.3N, 64.0W	990	990
06Z	40.5N, 67.0W	39.5N, 68.5W	972	972
12Z	43.5N, 63.0W	42.7N, 64.0W	968	961
18Z	46.5N, 59.0W	47.0N, 59.5W	960	944
16/00Z	48.0N, 56.5W	48.5N, 56.5W	952	952
06Z	50.0N, 54.0W	50.5N, 53.0W	950	950
12Z	50.0N, 51.0W	50.0N, 51.0W	952	954
18Z	50.0N, 48.0W	50.5N, 47.5W	960	956
17/00Z	51.0N, 41.0W	52.5N, 40.5W	968	964
06Z	58.0N, 30.0W	53.5N, 37.0W	971	968
12Z	58.0N, 29.0W	56.0N, 31.5W	969	970
18Z	60.0N, 26.5W		970	
17/06Z	53.0N, 70.5W		990	
12Z	53.5N, 67.0W		988	
18Z	53.0N, 65.0W		980	
18/00Z	55.0N, 64.0W		975	
06Z	55.0N, 61.0W	54.5N, 60.0W	965	964
12Z	56.0N, 60.0W	56.0N, 61.5W	952	950
18Z	55.5N, 61.0W	55.5N, 62.0W	954	948
19 00Z	55.5N, 61.0W	53.5N, 61.0W	954	956
06Z	56.0N, 59.0W	53.5N, 55.8W	964	967
12Z	55.5N, 59.0W	54.8N, 53.8W	970	968
18Z	54.0N, 55.0W	55.0N, 54.2W	973	968
20 00Z	53.5N, 51.5W	56.2N, 53.0W	978	970
06Z	56.0N, 50.0W	56.7N, 53.0W	980	972
12Z	56.5N, 47.5W	57.0N, 52.0W	979	976
18Z	57.5N, 50.5W	58.0N, 51.0W	978	979

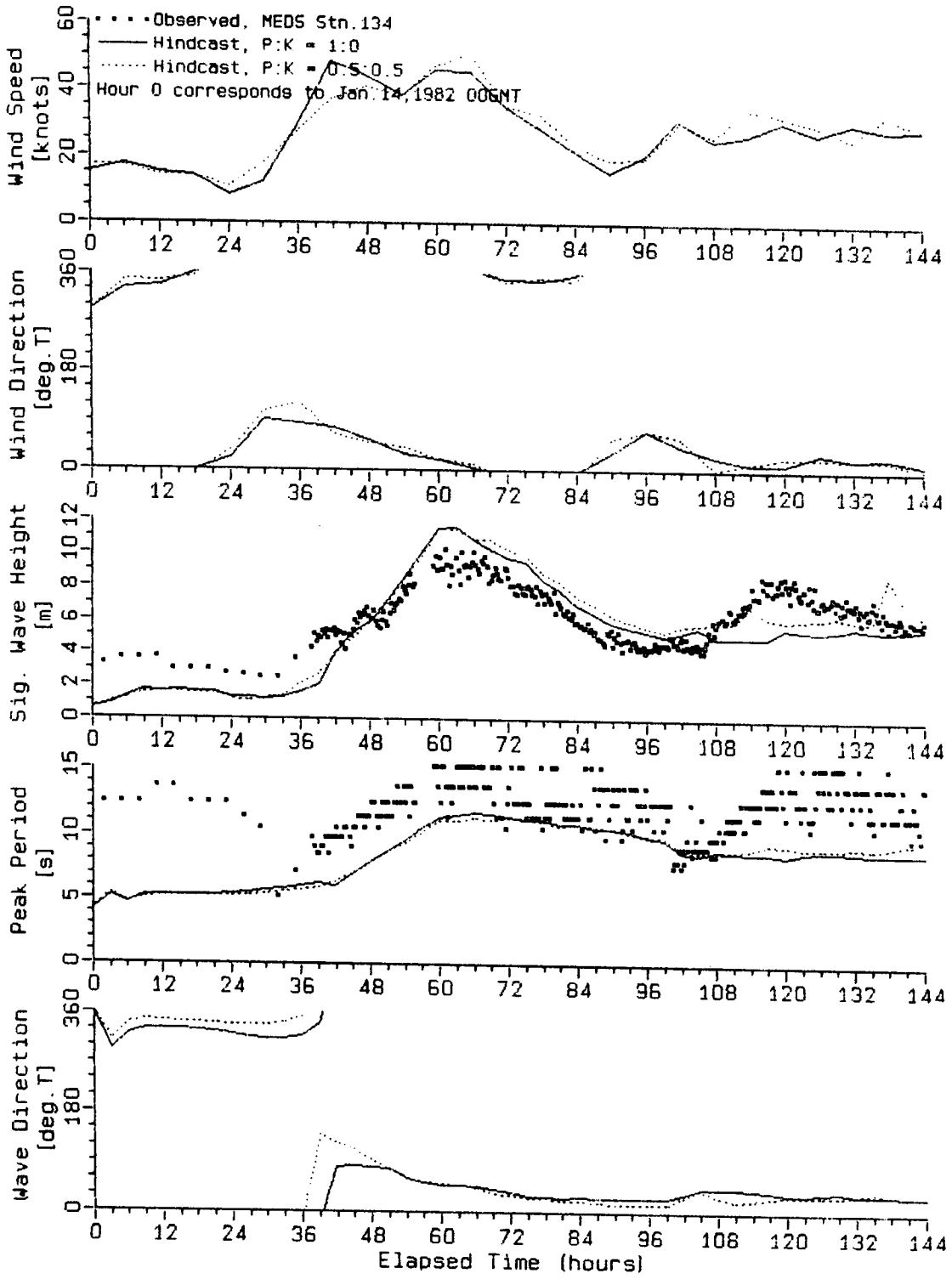

FIGURE 6.10 TIME SERIES OF HINDCAST AND MEASURED WAVE PARAMETERS FOR JANUARY 1982 STORM (MEDS STATION 134).

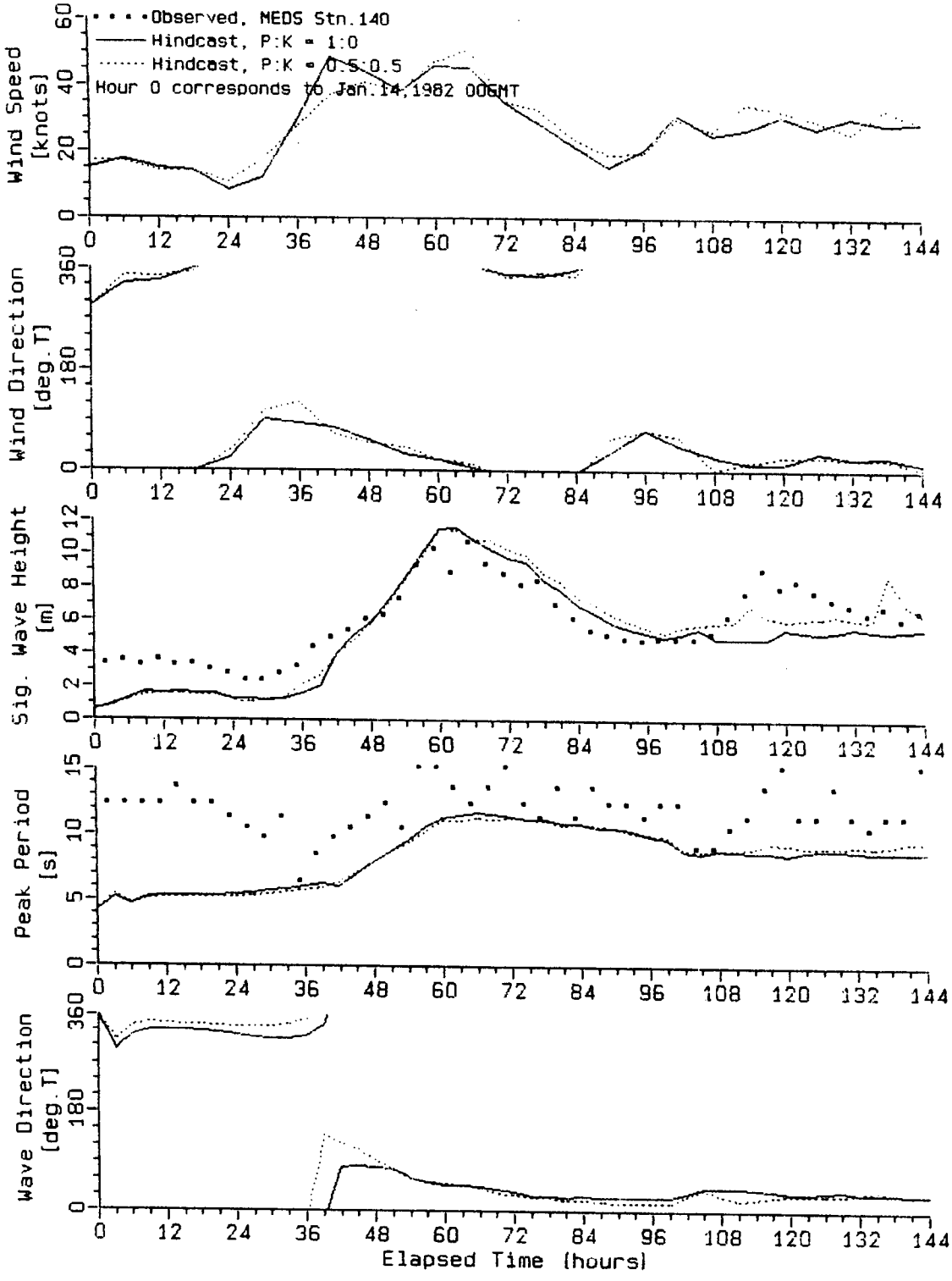

FIGURE 6.11 TIME SERIES OF HINDCAST AND MEASURED WAVE PARAMETERS FOR JANUARY 1982 STORM (MEDS STATION 140).

and only slightly different results during most of the remaining time. The hindcast using the 50%/50% blend shows some increase in significant wave height during the second peak of the storm (hour 108 to 132), which is completely missed by the hindcast using pressure based winds only, however, this increase is not sufficient to match the observed wave heights. In both cases the hindcast waves exhibit more rapid growth than the observations and the peak is overpredicted by about 1.5 m. Peak periods are underpredicted on average by about 2 to 3 s throughout the storm.

The overall statistics are given in Figures 6.12 to 6.15. The hindcast significant wave heights exhibit the lowest bias, 0.06 m, and RMS error, 1.25 m, when compared to measurements at Station 140, for the case using the 50%/50% blend (Figure 6.15). This case also has the lowest error in peak period: bias -2.53 s and RMS error 1.14 s. Comparison with measurements at Station 134 shows the lowest errors in significant wave height (bias -0.16 m and RMS error 1.48 m) for the hindcast using pressure based winds only (Figure 6.11). Peak period hindcast is, however, slightly better in the case of the 50%/50% blend (Figure 6.12).

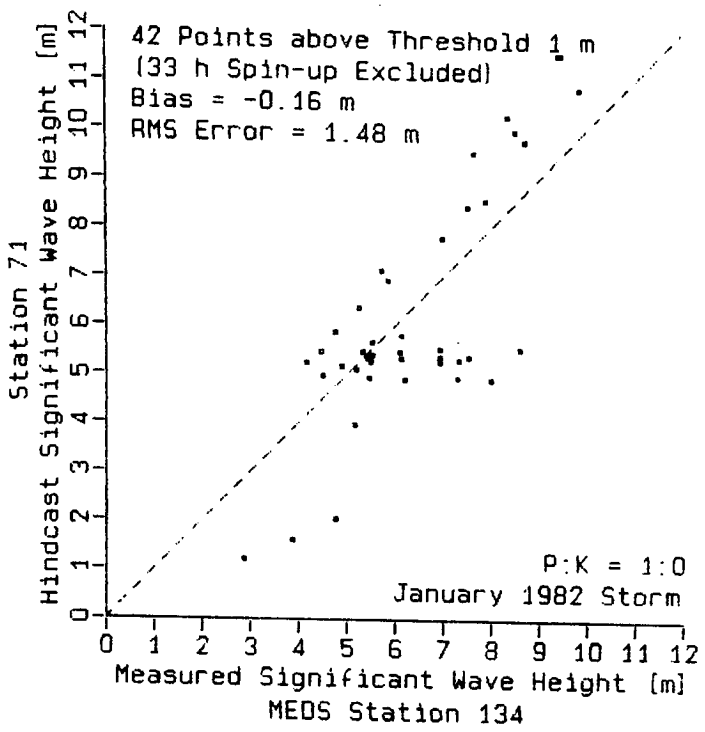

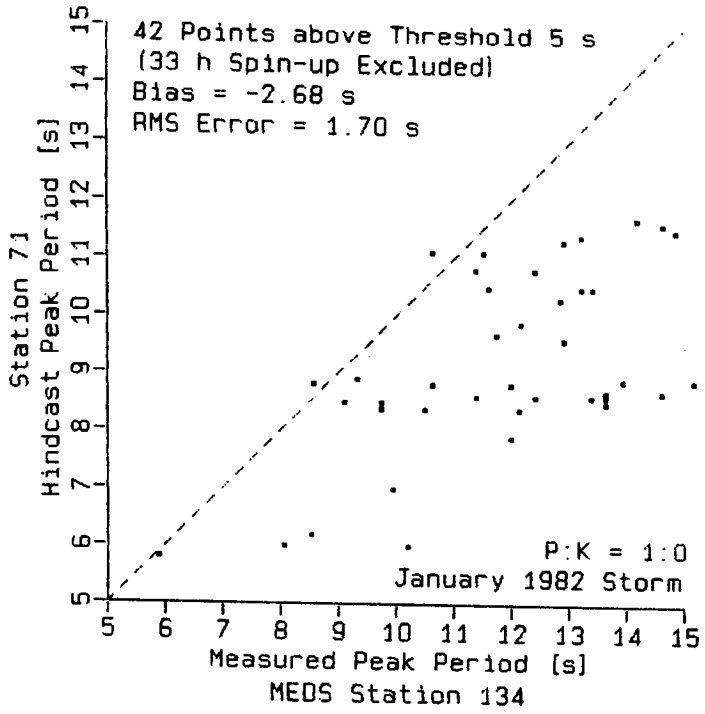

FIGURE 6.12 COMPARISON OF HINDCAST (P:K = 100%:0%) VERSUS MEASURED WAVE PARAMETERS FOR JANUARY 1982 STORM (MEDS STATION 134).

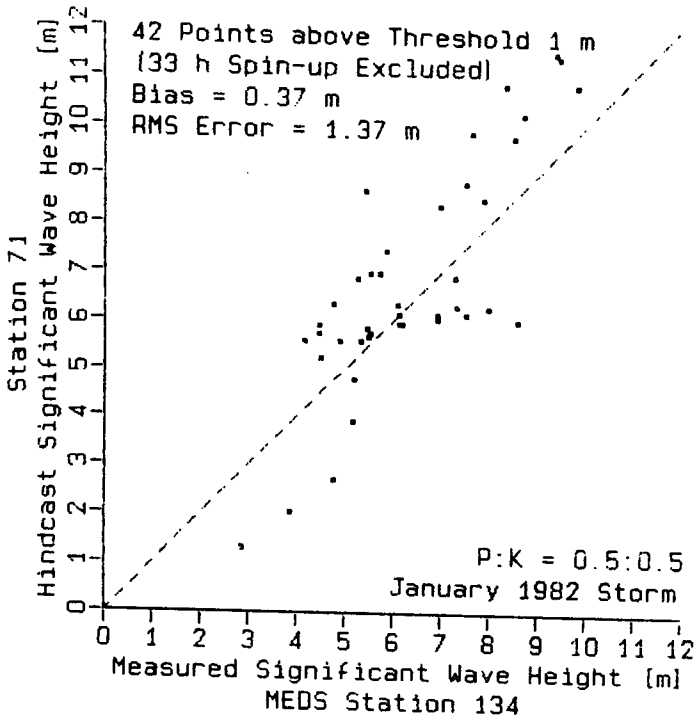

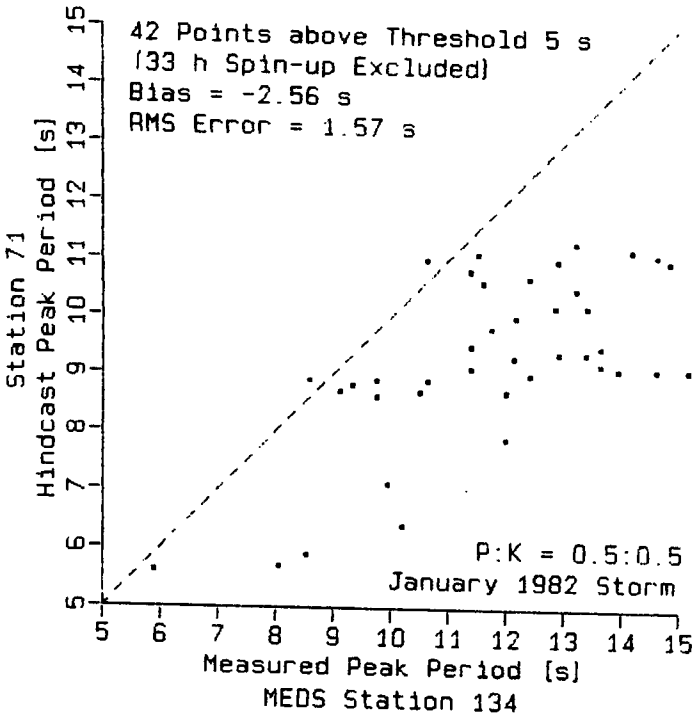

FIGURE 6.13 COMPARISON OF HINDCAST (P:K = 50%:50%) VERSUS MEASURED WAVE PARAMETERS FOR JANUARY 1982 STORM (MEDS STATION 134).

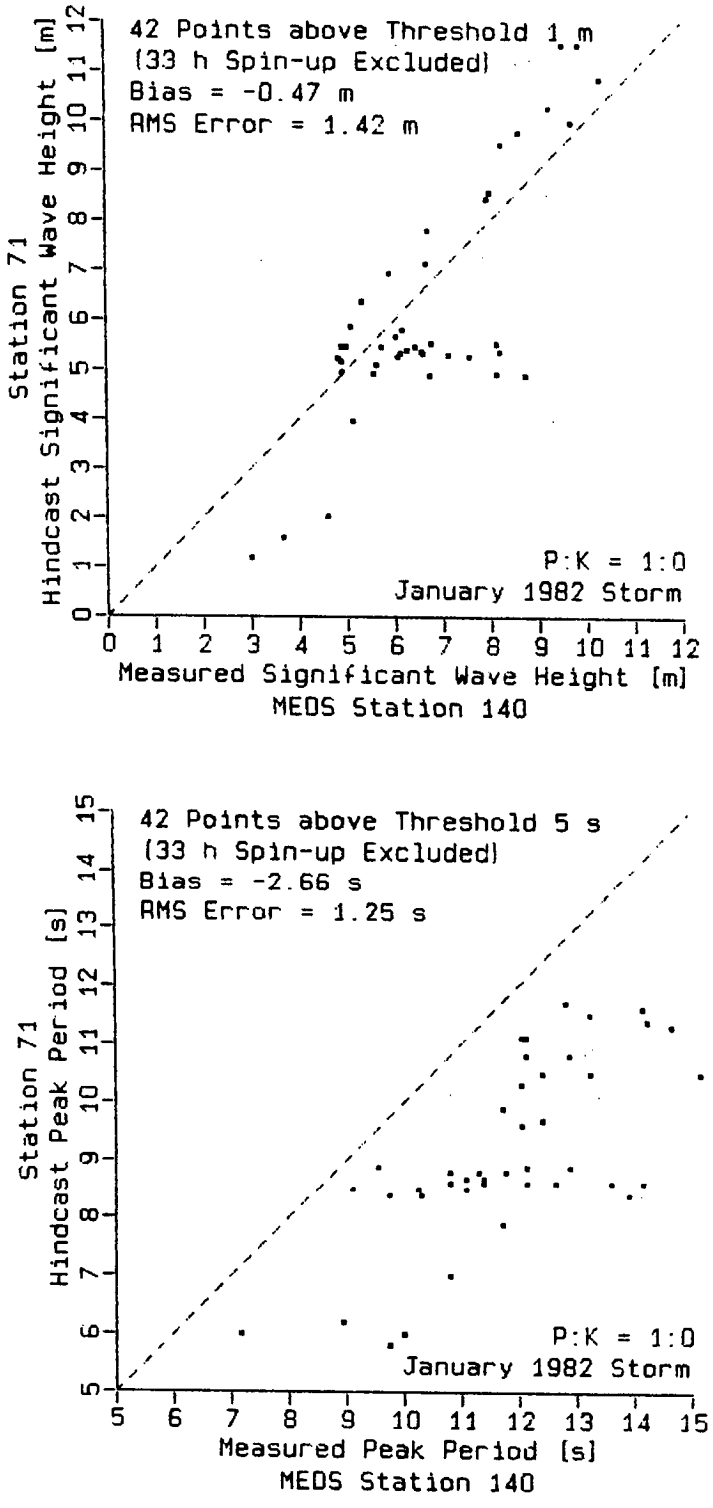

FIGURE 6.14 COMPARISON OF HINDCAST (P:K = 100%:0%) VERSUS MEASURED WAVE PARAMETERS FOR JANUARY 1982 STORM (MEDS STATION 140).

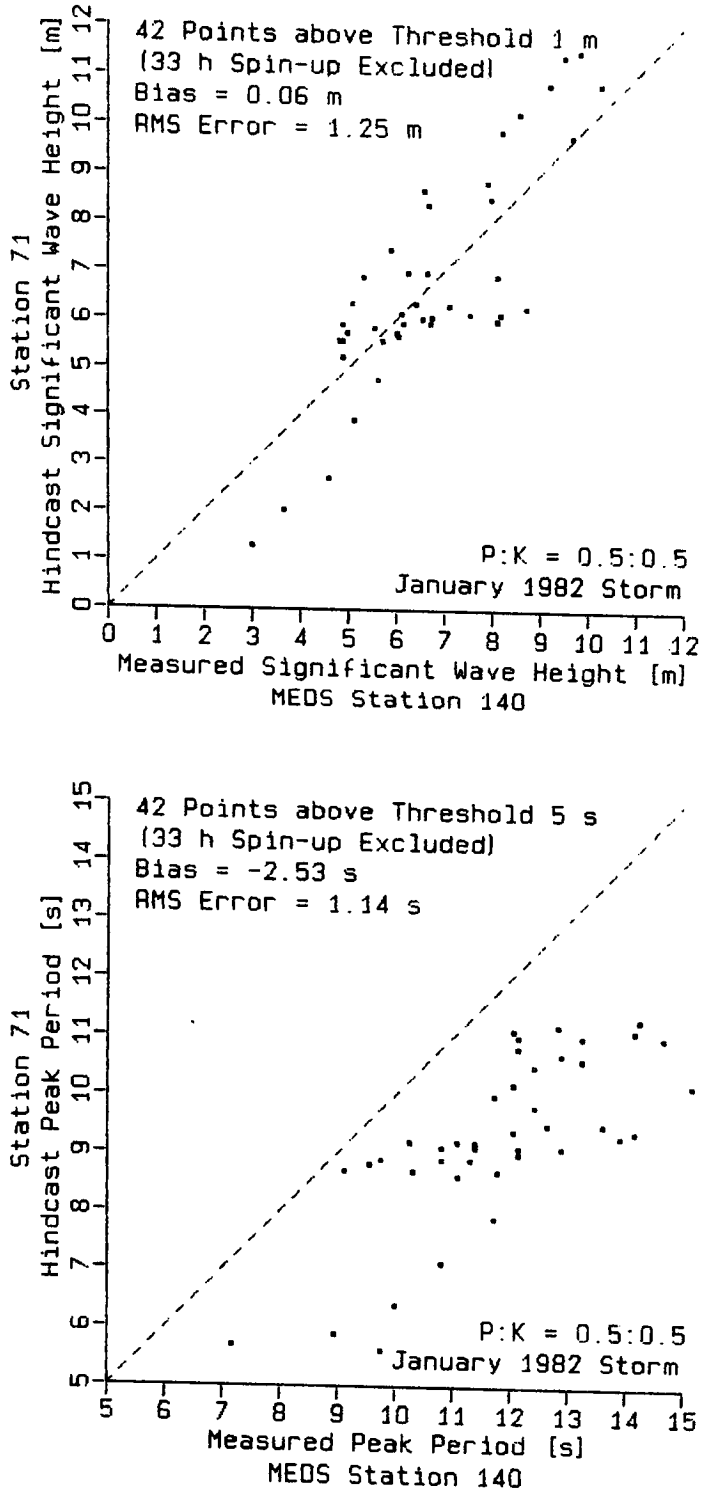

FIGURE 6.15 COMPARISON OF HINDCAST (P:K = 50%:50%) VERSUS MEASURED WAVE PARAMETERS FOR JANUARY 1982 STORM (MEDS STATION 140).

6.5 CONCLUSIONS AND RECOMMENDATIONS

Of the two events presented in this section one hindcast showed good agreement with wave observations while in the other the agreement was unsatisfactory. It is believed that the poor results of the October 1975 storm hindcast were not due to a failure of the wave model itself but rather due to incorrect wind input. It is suggested that the way in which the surface pressures are digitized cannot provide correct representation of pressure fields under the conditions that occurred during that storm, namely a situation when the isobars have a relatively complex shape. Even relatively common features, such as a trough or a ridge of high pressure, cannot be accurately specified on the 10° x 10° grid or by the polar representation of closed isobars. In some cases kinematic analysis could compensate for the deficiencies of the pressure based winds but this is not always possible where direct wind observations are scarce.

7. SUMMARY CONCLUSIONS AND RECOMMENDATIONS

Four sets of sensitivity tests have been performed on the numerical wave model developed by D.T. Resio and acquired by the Marine Environmental Data Service in Ottawa for wave climate hindcasting in Canadian offshore areas. In addition to the sensitivity tests two events from the ESRF list of severe storms were hindcast in order to test the overall performance of the model.

In the first set of tests an indication of the basic accuracy of the model simulations was obtained by running the model with constant wind as input. Sensitivity of the model to errors in input wind fields was determined using synthetic input subject to three types of perturbations.

In the first test the model was forced with a constant 40 knot wind blowing from the west. The errors in significant wave height were the largest (of the order of 1/2 m) at grid points adjacent to the upwind boundary and they diminished rapidly with distance away from the boundary. It is therefore recommended that the model grid should be designed in such a way that the grid points for which a hindcast is

required should not be immediately adjacent to the boundary. The errors in peak period in this test were small and less then the period resolution of the discrete spectrum. The errors in mean wave direction were in general the largest close to the model boundaries and they decreased towards the interior. In the Grand Banks area this error reached 14° for the 40 knot westerly wind which is smaller than the directional resolution of the discrete spectrum.

Three types of input wind field errors were considered: errors in wind speed and wind direction random in space and in time; errors in pressure at the centre of a low pressure system which cause weakening or intensification of the storm; and errors in storm track which result in a displacement of the storm from its correct location.

On the basis of published information typical errors in wind speed were assumed to have a bias in the range of 2 to 6 knots and root mean square (RMS) error in the range of 4 to 10 knots. Errors in wind direction were assumed to have a bias of 25 to 40 degrees and RMS errors in the range of 25 to 50 degrees. Uniform stationary wind field with a random perturbation in speed and direction was used to drive the wave model and the fluctuations in the hindcast significant wave

heights, peak periods and mean directions were compared against the input perturbations. Site specific correlation was found to have a large scatter due to advection of energy from neighbouring grid points. Where local input predominated, the error in significant wave height, expressed as percentage of the mean, was found to be approximately equal to the percent error in wind speed in accordance with empirical relationships for fetch limited windseas.

Errors in central pressure resulted in a bias in the input wind speeds and consequently in a bias in the computed wave parameters. The relative bias in the significant wave height was larger than the relative bias in the wind speed, their ratio ranging from approximately 1 in areas of strong winds to 1.8 in areas containing a large proportion of swell.

Errors in the position of the storm track lead to errors in both wind speed and wind direction. The response of the model was, therefore, more complex. In general there was a shift in the time evolution of the wave parameters as well as an increase or decrease in their magnitude. The response depended strongly on the relative position of the hindcast site with respect to the unperturbed and perturbed storm

track with the greatest differences occurring when the track passed close to the hindcast site.

In the second set of tests sensitivity of the model to grid spacing and time step was evaluated. Synthetic and real event inputs were employed in these tests. The model was found to be relatively insensitive to a decrease in grid spacing from the grid presently used by MEDS; increase in grid spacing lead to a larger change in the hindcast wave parameters. The tests suggest that at least for some storms it is important to carefully match the grid to the location for which the hindcast is required. The standard grid seems to be optimized for hindcasts at Hibernia and a change in grid spacing would have to be accompanied by a shift in the grid, if the hindcasts were to be made for the same location. The wave simulations were sensitive to boundary resolution during episodes containing offshore winds. For some applications (such as for example general wave forecasting) the simulation results may be required over certain area rather than at a specific site. In such cases smaller grid spacing should lead to a better boundary resolution and a more accurate representation of fetch.

The model results were quite sensitive to time step, with a shorter time step leading to higher estimates of the significant wave height, particularly at the peak of the storm. It is suggested that a decrease of the time step from the present 3 h to 2 h would improve the accuracy of the hindcasts, however, the model would require recalibration.

The input wind fields used to drive numerical wave models are determined from surface atmospheric pressure distributions, using a planetary boundary layer model, and/or from observed wind speeds and directions, using the technique of kinematic analysis. The input to the wave model may be a blend of pressure based winds and kinematic analysis winds. In the third set of tests hindcasts using various percentages of pressure based winds and kinematic analysis winds were compared using two storm events. In the case of one storm the hindcast accuracy increased with increasing proportion of pressure based winds while the opposite was true in the case of the second storm. This test is not objective and the results cannot be generalized because they depend on the relative accuracy of the pressure based winds and the kinematic winds which in turn are affected by the amount of available data, meteorological conditions and skill of the analysts.

Comparison with a more recent version of the Resio model indicated that a new formulation of the atmospheric input source term and of the wave propagation term may lead to more accurate hindcasts. It is recommended that the MEDS version of the model be revised to take advantage of the improvements in the more recent version of the model.

In the MEDS hindcast procedure wind fields are initially specified on a 2.5° latitude x 2.5° longitude grid. For the use by the wave model they have to be interpolated onto the wave model spherical orthogonal grid. In the forth set of tests quadratic interpolation was compared with the presently used bi-linear interpolation. The differences in the hindcast wave parameters were found to be negligible.

In addition to the sensitivity tests two events from the ESRF list of severe storms were hindcast in order to test the performance of the model. The results of one hindcast compared well with measured wave parameters while in the second case the correspondence was unsatisfactory. It is suggested that the poor results of the second hindcast were not caused by a failure of the wave model itself but by a poor resolution of pressure fields which did not adequately represent rather complex conditions occurring during the storm.

REFERENCES

Brown, R. D., P. Roebber, and K. Walsh. 1984: Climatology of severe storms affecting Canadian East Coast areas. Draft report submitted to the Environmental Studies Revolving Funds.

Cardone, V. J. 1969: Specification of the wind distribution in the marine boundary layer for wave forecasting. Tech. Rep. 69-1, Geophys. Sci. Lab., New York University, 137 pp.

Cardone, V. J., A. J. Broccoli, C. V. Greenwood, and J. A. Greenwood. 1979: Error characteristics of extratropical storm wind fields specified from historical data. Proc. Offshore Tech. Conf., Houston, Paper No. OTC 3598.

Carter, D. J. T. 1982: Prediction of wave height and period for a constant wind velocity using the JONSWAP results. Ocean Engng., Vol. 9, 17-33.

Donelan, M. A., J. Hamilton, and W. H. Hui. 1985: Directional spectra of wind-generated waves. Phil. Trans. R. Soc. Lond. A 315, 509-562.

Hasselmann, K., T. P. Barnett, E. Bouws, H. Carlson, D. E. Cartwright, K. Enke, J. A. Ewing, H. Gienapp, D. E. Hassel-

mann, P. Kruseman, A. Meerburg, P. Muller, D.J. Olbers, K. Richter, W. Sell, and H. Walden. 1973: Measurements of wind-wave growth and swell decay during the Joint North Sea Wave Project (JONSWAP). Dtsch. Hydrogr. Z., A8 (Suppl.), No.12, 95pp.

Hasselmann, S., K. Hasselmann, J.H. Allender, and T.P. Barnett. 1985: Computations and parameterizations of the nonlinear energy transfer in a gravity-wave spectrum. Part II: Parameterizations of the nonlinear Energy transfer for application in wave models. J. Phys. Oceanogr., Vol.15, 1378-1391.

Hodgins, D.O., P.H. LeBlond, and D.A. Huntley. 1985: Shallow water wave calculations. Can. Contract. Rep. Hydrogr. Ocean Sci. 10, 75 p.

Juszko, B.A. 1985: Directional wave spectrum intercomparison study. Phase 4 - intercomparison of results. Draft report submitted to the Environmental Studies Revolving Funds.

Lazanoff, S.M., and N.M. Stevenson. 1975: An evaluation of a hemispheric operational wave spectral model. U.S. Navy Fleet Numerical Weather Central, Tech. Note 75-3, 103pp.

Overland, J.E., and Gemmill, W.H. 1977: Marine winds in the New York Bight. Mon. Wea. Rev., 105, 1003-1008.

Penicka, F.X., D.T. Resio, and R.D. Worsfold. 1985: Wave directional spectrum hindcasts for the ESRF Wave Directional Spectrum Intercomparison Study. Report submitted to the Environmental Studies Revolving Funds.

Perrie, W., and Toulany, B. 1985: Assessing a wave model à la SWAMP. Can. Tech. Rep. Hydrogr. Ocean Sci. 61, vi+78 p.

Pierson, W.J. and L. Moskowitz. 1964: A proposed spectral form for fully developed wind seas based on the similarity theory of S.A. Kitaigorodskii. J. Geophys. Res., Vol. 69, 5181-5190.

Resio, D.T. 1981: The estimation of wind-wave generation in a discrete spectral model. J. Phys. Oceanogr., Vol 11, 510-525.

Resio, D.T. 1982: Assessment of wave hindcast methodologies in the Scotian Shelf, Grand Banks and Labrador Sea areas. Can. Contract. Rep. Hydrogr. Ocean Sci. 4, 128 p.

Resio, D.T., A.W. Garcia, and C.L. Vincent. 1978: Preliminary investigation of numerical wave models. Proc. Coastal Zone '78, 2085-2104.

Resio, D.T., C.L. Vincent, and W.D. Corson. 1982: Objective specification of Atlantic Ocean wind fields from historical data. WIS Report 4, U.S. Army Engineer Waterways Experiment Station, Vicksburg, Miss.

Snyder, R., and C.S. Cox. 1966: A field study of the wind generation of ocean waves. J. Mar. Res., Vol. 24, 141-177.

U.S. Army Coastal Engineering Research Center.. 1977: Shore protection manual, Vol. I. U.S. Govt. Printing Office, Washington.

Vincent, C.L., and D.T. Resio. 1979: A discussion of wave prediction in the Northwest Atlantic Ocean. Marine Forecasting, Predictability and Modeling in Ocean Hydrodynamics. Elsevier Oceanography Series, Ed. Jacques C.J. Nihoul.

World Meteorological Organization. 1976: Handbook on wave analysis and forecasting. WMO - No. 446.